# A Fundamental Study of Flow Characteristics and Heat Transfer in Multiple Burner Oil Fired Marine Boilers

A Thesis presented for the degree of
Doctor of Philosophy
of the University of Sheffield
by Horace Whaley, B.Sc.(Tech.)

Department of Fuel Technology
and Chemical Engineering.
June 1965.

## SUMMARY

This study has shown that the main characteristics of axial velocity decay and recirculation in multiple enclosed jets can be related to those of single enclosed jets. This is achieved by considering each jet to be bounded by an imaginary duct whose dimensions can be related to the nozzle spacing parameters. If the nozzles are close together compared with the surrounding chamber, the above treatment is only valid near to the nozzles. Further downstream the jets coalesce and their behaviour can be related to that of a single jet by an equivalent nozzle radius.

Recirculation in both single and multiple enclosed jets has been related to the Thring-Newby parameter $\theta$ by the equation:-

$$0.6 + \frac{M_r}{M_o} = \frac{0.66}{\theta}$$

where $M_r/M_o$ is the recirculated flux in relation to the total nozzle mass flow. The value of $\theta$ (i.e. $\frac{r}{L'}$) is calculated from the equation:-

$$\frac{L'}{L} = 2 \left\{ 0.389 + \frac{0.611}{\exp 0.396n} \right\} \frac{R}{L}$$

where $L'$ = radius of imaginary duct (average value when $\frac{R}{L} > 0.5$)

$L$ = true radius of duct

$n$ = number of outer jets in configuration

$R$ = pitch radius of outer jets

This equation can only be applied near to the nozzles when $\frac{R}{L} < 0.5$. Further downstream the equivalent nozzle radius of the combined jet is used to calculate $\theta$ ($= \frac{r'}{L}$) from the relationship $r' = \sqrt{n+1}\, r$.

The introduction of a mesh grid to simulate the tube banks of a boiler causes greater recirculation due to back deflection of part of the main jet flow. A changeover of the main recirculation flux from the outer zone bounded by the duct to the inner zone between the jets is observed as the grid is moved upstream. The magnitude of grid resistance is shown to have little influence on the flow patterns.

Water model studies have revealed that recirculation through the grid can occur, although this was not observed in the air model due to measuring difficulties. Photographs and visual observations confirm the air model flow patterns.

Simple tube bank heat transfer calculations indicate that the temperature of recirculated gases re-entering the combustion chamber will only be slightly above that of the tubes. In practice this dilution with colder gases would certainly be detrimental to the efficient operation of a marine boiler.

INDEX


| | | Page No. |
|---|---|---|
| | Summary | i |
| | Index | iii |
| | Acknowledgements | vi |
| | List of Figures | vii |
| | List of Plates | xi |
| | Nomenclature | xii |
| CHAPTER 1 | Introduction | 1 |
| 1.1. | Scope of Research | 1 |
| 1.2. | Literature Survey | 1 |
| 1.2.1. | Combustion Model Studies | 2 |
| 1.2.2. | Single Jets - Theoretical and Experimental | 3 |
| 1.2.3. | Annular and Concentric Jets | 10 |
| 1.2.4. | Multiple Jet Systems | 12 |
| 1.2.5. | Conclusions from the Literature | 15 |
| CHAPTER 2 | Apparatus and Experimental Techniques | 17 |
| 2.1. | Air Models Laboratory | 17 |
| 2.1.1. | The Perspex Models | 17 |
| 2.1.2. | The Nozzles | 18 |
| 2.1.3. | The End Plates | 18 |
| 2.1.4. | The Grids | 19 |
| 2.1.5. | The Air Supply | 19 |
| 2.2. | The Velocity Measuring Technique | 20 |
| 2.2.1. | The Beaudouin Pressure Transducer | 20 |
| 2.2.2. | The "T" Shaped Velocity Probe | 20 |
| 2.2.3. | The Traversing Rig | 21 |

Page No.

2.3. The Water Models Laboratory 22

2.3.1. The Perspex Model 22

2.3.2. The Nozzles 22

2.3.3. The Grid 22

2.3.4. The Water Supply 23

2.4. The Photographic Technique 23

CHAPTER 3 Aerodynamic Studies of Enclosed Jets 24

3.1. Single Enclosed Jets 24

3.1.1. The Effect of $r_o/L$ on Axial Velocity Decay 24

3.1.2. The Effect of $r_o/L = 0$ on Recirculation 26

3.2. Multiple Enclosed Jets 26

3.2.1. The Effect of Reynolds Number 26

3.2.2. The Effect of Nozzle Diameter 27

3.2.3. The Effect of Pitch Circle Radius of Outer Nozzles 27

3.2.4. The Effect of reducing the number of Outer Jets 28

3.3. The Study of the Introduction of a Downstream Resistance 29

3.3.1. The Effect of Grid Position 30

3.3.2. The Effect of Grid Resistance Magnitude 31

3.3.3. The Effect of Nozzle Diameter 31

3.3.4. The Effect of Pitch Circle Radius of Outer Nozzles 32

3.4. Water Model Studies of Enclosed Multiple Jets 33

3.4.1. The Effect of Pitch Circle Radius of Outer Nozzles 34

3.4.2. The Effect of Grid Position 34

Page No.

CHAPTER 4 Analysis of Results 36

4.1. Single Enclosed Jet Studies 36

4.1.1. Calculation and Correlation of Single Enclosed Jet Recirculation 36

4.2. Multiple Enclosed Jet Studies 40

4.2.1. Determination of the Radius of the Imaginary Enclosing Duct 41

4.2.2. Calculation and Correlation of Recirculation in Multiple Enclosed Jet Systems 45

CHAPTER 5 Conclusions 50

5.1. Single Enclosed Jets 50

5.2. Multiple Enclosed Jets 50

5.3. The Introduction of a Grid into Multiple Enclosed Jet Systems 52

5.4. Suggestions for Further Work 52

CHAPTER 6 Simple Calculation of the Heat Transfer in Marine Boiler Tube Banks 54

6.1. Introduction 54

6.2. Heat Transfer Calculations 54

6.3. Conclusions 59

APPENDICES

1. The Study of a Single Enclosed Swirling Jet 60

2. Calibration of Flow Measuring Devices 63

3. Design Calculations and Operating Conditions 66

4. Estimation of Errors due to Turbulence 77

List of References 80

Figures Nos. 1 - 32

Plates Nos. 1 - 10

ACKNOWLEDGEMENTS

The author wishes to express his gratitude to Professor M. W. Thring and Dr. C. Hulse under whose guidance this research has been conducted. He would also like to thank Dr. A. M. Brown and Mr. M. A. Patrick for invaluable advice and time spent in checking the author's work. He is also grateful to his former academic and technical colleagues for help and many suggestions which were useful. Finally he records his thanks to those Admiralty Departments under whose direction and sponsorship these studies were carried out.

## LIST OF FIGURES


| Fig.No. | Title |
|---|---|
| 1 | Comparison of Multiple Free Jet Data with Free Jet Data of Hinze |
| 2 | Diagram of Perspex Model |
| 3 | Axial Decay of Velocity in Single Jets for $\theta$ from 0.063 to 0.446 |
| 4 | Axial Decay of Velocity in Single Jets for $\theta$ from 0.486 to 0.669 |
| 5 | Recirculation in Single Jet Systems |
| 6 | Variation of Nozzle Velocity in Multiple Jets. Effect on axial velocity decay when R = 2", n = 6, $r_o$ = 0.375" |
| 7 | Velocity Contours when R = 2", n = 6, $r_o$ = 0.375" |
| | (a) $U_o$ = 106 ft./sec. Re = 31900 |
| | (b) $U_o$ = 84.5 ft./sec. Re = 27900 |
| | (c) $U_o$ = 71.5 ft./sec. Re = 23900 |
| | (d) $U_o$ = 57.6 ft./sec. Re = 19900 |
| | (e) $U_o$ = 46.4 ft./sec. Re = 15950 |
| | (f) $U_o$ = 33.4 ft./sec. Re = 11950 |
| 8 | Velocity Contours when R = 2", n = 6, $r_o$ = 0.25" |
| | (a) $U_o$ = 150 ft./sec. Re = 31900 |
| | (b) $U_o$ = 106 ft./sec. Re = 21300 |
| | (c) $U_o$ = 86 ft./sec. Re = 18600 |
| | (d) $U_o$ = 71 ft./sec. Re = 15950 |
| | (e) $U_o$ = 52 ft./sec. Re = 13300 |
| | (f) $U_o$ = 42 ft./sec. Re = 10620 |
| 9 | Effect of Pitch Circle Radius of Outer Nozzles n = 6, $r_o$ = 0.375" |
| | (a) R = 2.625" $U_o$ = 89 ft./sec. |
| | (b) R = 2.375" $U_o$ = 81.5 ft./sec. |
| | (c) R = 1.75" $U_o$ = 89 ft./sec. |
| | (d) R = 1.5" $U_o$ = 89 ft./sec. |
| 10 | Velocity Contours when R = 2.625", n = 6, $r_o$ = 0.25" |

| Fig.No. | Title |
|---|---|
| 11 | Effect of reduction of number of outer nozzles, n = 3<br>(a) R = 2.625" $r_o$ = 0.375" $U_o$ = 88 ft./sec.<br>(b) R = 2.625" $r_o$ = 0.25" $U_o$ = 150 ft./sec.<br>(c) R = 2" $r_o$ = 0.375" $U_o$ = 88 ft./sec.<br>(d) R = 1.5" $r_o$ = 0.375" $U_o$ = 93 ft./sec. |
| 12 | Effect of Grid 1 on Flow Patterns when R = 2", $r_o$ = 0.375", n = 6, $U_o$ = 84.5 ft./sec.<br>(a) Grid Position $x/L$ = 1.75<br>(b) Grid Position $x/L$ = 1.5<br>(c) Grid Positions $x/L$ = 1.25 and 1<br>(d) Grid Positions $x/L$ = 0.75 and 0.5 |
| 13 | Initial Effect of Grid 1 on Axial Velocity Decay<br>Grid Position $x/L$ = 1.75, $U_o$ = 84.5 ft./sec.<br>R = 2", $r_o$ = 0.375", n = 6 |
| 14 | Effect of Increased Grid Resistance on Flow Patterns when<br>(a) Grid Position $x/L$ = 1.75 $U_o$ = 84.5, R = 2" $r_o$ = 0.375", n = 6<br>(b) Grid Position $x/L$ = 1.25 and $x/L$ = 1 |
| 15 | Effect of decreased Grid Resistance on Flow Patterns<br>(a) Grid Position $x/L$ = 1.75 R = 2", $r_o$ = 0.375" $U_o$ = 84.5 ft./sec. n = 6<br>(b) Grid Positions $x/L$ = 1 and 0.75 |
| 16 | Effect of Grid Resistance on Axial Velocity Decay when R = 2", $r_o$ = 0.375", $U_o$ = 84.5 ft./sec.<br>Grid Position $x/L$ = 1.25, n = 6 |
| 17 | Effect of Grid 1 on Flow Patterns when R = 2", $r_o$ = 0.25", n = 6, $U_o$ = 150 ft./sec.<br>(a) Grid Position $x/L$ = 1.75<br>(b) Grid Position $x/L$ = 1.5<br>(c) Grid Positions $x/L$ = 1.25 and 1 |
| 18 | Effect of Grid 1 on Flow Patterns when R = 2.625", $r_o$ = 0.375", n = 6, $U_o$ = 89 ft./sec.<br>(a) Grid Position $x/L$ = 1.75<br>(b) Grid Position $x/L$ = 1.5<br>(c) Grid Positions $x/L$ = 1.25 and 1 |

| Fig.No. | Title |
|---|---|
| 19 | Effect of Grid 1 on axial velocity decay when $R = 2.625"$, $r_o = 0.375"$, $U_o = 89$ ft./sec. Grid Position $x/L = 1.25$, $n = 6$ |
| 20 | Comparison of axial velocity decay of single and Multiple Jets<br>(a) $n = 6$ $\theta$ from 0.14 to 0.23<br>(b) $n = 6$ $\theta$ from 0.093 to 0.29 |
| 21 | Comparison of axial velocity decay of single and multiple jets when $n = 3$, $\theta$ from 0.08 to 0.22 |
| 22 | Comparison of axial velocity decay of single and multiple jets when $n = 2$, $\theta = 0.1$ and 0.15 |
| 23 | Comparison of Recirculation in Single and Multiple Jet Systems |
| 24 | Water Model Flow Patterns when $U_o = 3.32$ ft./sec. $Re = 14700$<br>(a) $R = 2.625"$ $r_o = 0.375"$ $n = 6$<br>(b) $R = 2"$ $r_o = 0.375"$ $n = 6$<br>(c) $R = 1.5"$ $r_o = 0.375"$ $n = 6$<br>(d) Effect of Grid 3 when $R = 2"$ $r_o = 0.375"$ $n = 6$ Grid Position $x/L = 1.5$<br>(e) Effect of Grid 3 when $R = 2"$ $r_o = 0.375"$ $n = 6$ Grid Position $x/L = 1.0$ |
| 25 | Temperature Profiles at Exit from Tube Banks based on Flow Pattern Studies<br>(a) $R = 2.625"$ $r_o = 0.375"$ $n = 6$<br>(b) $R = 2.625"$ $r_o = 0.375"$ $n = 3$<br>(c) $R = 2"$ $r_o = 0.375"$ $n = 6$<br>(d) $R = 2"$ $r_o = 0.375"$ $n = 3$<br>(e) $R = 1.5"$ $r_o = 0.375"$ $n = 6$<br>(f) $R = 1.5"$ $r_o = 0.375"$ $n = 3$ |
| 26 | Effect of Increased Swirl on a Single Enclosed Jet Flow Pattern, $r_o = 0.375"$<br>(a) Tangential Air = 0<br>and " " = 13.7% of total nozzle fluid<br>(b) " " = 21.5% " " " "<br>and " " = 29.1% " " " "<br>(c) " " = 35.4% " " " "<br>" " = 40.6% " " " "<br>" " = 45.1% " " " "<br>(d) Effect of increased swirl on axial velocity decay of single jets |

| Fig.No. | Title |
|---|---|
| 27 | Calibration Characteristics of the "T" shaped Probe. Comparison with standard pitot tube. |
| 28 | Calibration Characteristics of the "T" shaped Probe. Pitching and Yawing Characteristics. |
| 29 | Calibration of Nozzles |
| 30 | Calibration of Pressure Transducer |
| 31 | Comparison of Resistance Characteristics of the Grids with typical Marine Boiler Tube Banks |
| 32 | Simplified Diagram of Marine Boiler of the Selectable Superheat type. |

## LIST OF PLATES


| Plate No. | Title |
|---|---|
| 1 | End View of Small Model assembled for calibration of probe |
| 2a. | General View of Large Perspex Model |
| b. | View along axis of model |
| 3a. | Sleeves used for nozzle radius variation |
| b. | Modified central nozzle used for swirl studies showing tangential injection ports |
| 4 | Low Resistance Grid (Grid 3) |
| 5 | Medium and High Resistance Grids (Grids 1 and 2) |
| 6 | Traversing Rig and Probe Assembly |
| 7 | Water Model Photograph illustrating flow patterns when $R = 2"$, $r_o = 0.375"$, $n = 6$ $Re = 14700$, $U_o = 3.32$ ft./sec. |
| 8 | Water Model Photograph illustrating flow patterns when $R = 2"$, $r_o = 0.375"$, $n = 6$ $Re = 14700$, $U_o = 3.32$ ft./sec. Grid Position $x/L = 1.5$ |
| 9 | Water Model Photograph illustrating flow patterns when $R = 2"$, $r_o = 0.375"$, $n = 6$, $Re = 14700$, $U_o = 3.32$ ft./sec. Grid Position $x/L = 1.0$ |
| 10 | Selectable Superheat type Marine Boiler |

## NOMENCLATURE

| | | | |
|---|---|---|---|
| $A$ | = | Constant in Recirculation Equation | |
| $A_f$ | = | Area of forward flow region | ins.$^2$ |
| $A_r$ | = | Area of recirculation flow region | ins.$^2$ |
| $B$ | = | Constant in Recirculation Equation | |
| $C_p$ | = | Specific heat at constant pressure | B.Th.U./lb.$^\circ$F |
| $d$ | = | Diameter of nozzle | ins. |
| $d_e$ | = | Equivalent diameter of nozzle | ft. or ins. |
| $D_o$ | = | Diameter of tubes in bank | ins. |
| $f$ | = | Friction factor in Modified Fannings Equation for tube banks | |
| $F_r$ | = | Froude Number (Modified) $= \frac{U_o^2}{g\ d_e}\ \frac{Ta}{To}$ | |
| $g$ | = | Gravitational acceleration constant | ft./sec.$^2$ |
| $G_o$ | = | Momentum of jets $= \frac{M_o^2}{\rho \pi r}$ | poundals |
| $G_m$ | = | Maximum Specific Mass flow rate | lb./ft.$^2$ sec. |
| $h_m$ | = | Surface heat transfer coefficient | B.Th.U./ft.$^2$ hr.$^\circ$F. |
| $\Delta_h$ | = | Pressure differential across jets | ins. w.g. |
| $K$ }<br>$K'$ } | = | Constants for entrinment equation of free jets (Ricou[20]) | |
| $K''$ | = | Constant for probe in equation $U = K'' \sqrt{\Delta p}$ | |
| $K_f$ | = | Thermal conductivity of gas at film temperature $T_f$ | B.Th.U./hr. ft.$^\circ$F. |
| $L$ | = | Duct radius | ft. or ins. |
| $L'$ | = | Equivalent duct radius of imaginary cylinder | ft. or ins. |

| | | | |
|---|---|---|---|
| $L_1$ | = | Smallest Radius of a conical chamber or $\frac{1}{2}$ shortest side of rectangular cross section | ft. or ins. |
| $L_2$ | = | Largest radius of conical chamber or $\frac{1}{2}$ longest side of rectangular cross section | ft. or ins. |
| $M_o$ | = | Mass flow rate in nozzle (x = 0) | lb./sec. or lb./hr. |
| $M_a$ | = | Ambient air mass flow rate | lb./sec. or lb./hr. |
| $M_e$ | = | Entrained air mass flow at downstream distance x | lb./sec. |
| $M_j$ | = | Total mass flow rate of air in jet at downstream distance x | lb./sec. |
| $M_f$ | = | Forward mass flow rate occurring in area $A_f$ at downstream distance x | lb./sec. or lb./hr. |
| $M_r$ | = | Recirculation mass flow rate occurring in area $A_r$ at downstream distance x | lb./sec. or lb./hr. |
| $M_s$ | = | Mass flow rate on superheater side of tube banks | lb./sec. |
| n | = | Number of outer jets surrounding central jet in multiple nozzle assembly | |
| N | = | Number of rows of tubes over which fluid flows | |
| $\Delta_p$ | = | Pressure differential across probe corresponding to mean velocity | ins. w.g. |
| $\Delta_{pt}$ | = | Pressure differential corresponding to turbulence fluctuations | ins. w.g. |
| R | = | Pitch radius of the outer ring of nozzles | ins. |
| Re | = | Reynolds Number $= \frac{U_d \rho}{\mu} = \frac{2Ur_o \rho}{\mu}$ | |
| $r_o$ | = | Radius of nozzles $= \frac{d}{2}$ | ins. |

| | | | |
|---|---|---|---|
| $t_f$ | = | Temperature under film conditions, arithmetic mean of surface temperature and bulk fluid temperature | $^{o}F.$ |
| $T_f$ | = | Absolute Temperature of Gas under film Conditions = $t_f + 460$ | $^{o}R.$ |
| $T_e$ | = | Local Temperature after passage through tube banks | $^{o}F.$ |
| $\Delta T$ | = | Temperature drop of gases between inlet and exit of tube banks | $^{o}F.$ |
| $\Delta Tm$ | = | Logarithmic mean temperature difference between bulk fluid temperature and tube surface | $^{o}F.$ |
| $T$ | = | Turbulence Intensity at any location | |
| $T_m$ | = | Momentum flux turbulence intensity at same location | |
| $U$ | = | Local velocity at any point | ft./sec. |
| $U_o$ | = | Maximum nozzle discharge velocity | ft./sec. |
| $U_a$ | = | Average nozzle discharge velocity | ft./sec. |
| $U_f$ | = | Mean forward flow velocity at downstream point x corresponding to maximum $M_r$ | ft./sec. |
| $U_r$ | = | Mean recirculation velocity at downstream point x corresponding to maximum value of $M_r$ | ft./sec. |
| $\bar{U}$ | = | Mean velocity at any point | ft./sec. |
| $\sqrt{\bar{U}^2}$ | = | Momentum flux velocity at same point | ft./sec. |
| $U'$ | = | Turbulent fluctuation velocity | ft./sec. |
| $U_m$ | = | Maximum velocity at downstream point x | ft./sec. |
| $U_{m_o}$ | = | Maximum velocity at downstream point x when no swirl is applied to jet | ft./sec. |
| $x$ | = | Downstream distance from nozzle | ft. or ins. |
| $x_T$ | = | Pitch to tube diameter ratio for banks of tubes | |

Greek Symbols

| | | | |
|---|---|---|---|
| $\theta$ | = | Thring-Newby Parameter = $\frac{M_o + M_a}{M_o} \times \frac{r_o}{L}$ | |
| $\lambda$ | = | blockage ratio of mesh grids | |
| | = | covered area/total area for flow | |
| $\mu$ | = | absolute viscosity of fluid | lb./hr.ft. |
| $\mu_f$, $\mu_c$, $\mu_h$ | = | absolute viscosities of fluid under film, cold and hot conditions respectively | lb./ft.hr. |
| $\rho$ | = | density of fluid | lb./ft.$^3$ |
| $\rho_o$, $\rho_h$ | = | densities of fluid under cold and hot conditions respectively | lb./ft.$^3$ |

# CHAPTER 1

## INTRODUCTION

### 1.1. Scope of Research

This work is the second stage of a research programme aimed at the improvement of heat transfer and combustion conditions in oil fired multiple burner marine boilers. The first stage was an aerodynamic study of a twelfth scale model of a "D" shaped marine boiler[1]. Although this was generally useful, the data obtained can only be applied to other marine boilers systems of the same basic shape. It did not yield data on the behaviour of groups of enclosed burners. The present study uses a fundamental approach to obtain data about the factors affecting burner performance and the subsequent effect of tube banks in marine boiler systems. This poses certain problems since boilers vary greatly in size, shape, number and type of burners, as well as tube bank characteristics.

It was proposed to study a system of parallel axi-symmetrical jets inside a circular cross sectioned duct, representing a much simplified marine boiler system. The variables to be investigated were nozzle spacing, diameter and Reynolds number. The subsequent introduction of a mesh grid at various downstream positions was to simulate boiler tube banks. Finally, heat transfer calculations based on the data obtained, were to be made in order to afford some comparison with practical conditions.

### 1.2. Literature Survey

The literature is presented in the form which led to the choice of experimental programme, and subsequent interpretation of the results.

### 1.2.1. Combustion Model Studies

One of the earliest studies of combustion aerodynamics was by Rosin[2]. Rosin's study showed the recirculation eddies set up by a two dimensional multiple burner arrangement in which the burner separation distance could be varied. One of the techniques employed by Rosin was to study the erosion patterns of lumps of rock salt, when water was used to simulate the gas flow.

The combustion model work which provided the basis for many later studies was begun by Chesters and his associates in 1949[3]. This team worked on various enclosed jet systems, and also operated a scale model of an open hearth steel making furnace. This work is one of the earliest which reports the existence of recirculation in enclosed jet flow, and predicts that recirculation might be expected whenever jets are confined within walls.

In 1951, Chesters[4] published a report of the agreement obtained between a model and an open-hearth furnace. The prototype (with single uptake and sloping ends) was probably the first furnace to be designed aerodynamically. Later Chesters[5] stressed the need for a more fundamental approach to combustion model studies, citing recirculation as an example of a phenomenon which might otherwise remain unexplained and therefore uncontrolled.

The work was extended from two dimensional slice models[3] to three dimensional models[6]. The three-dimensional flow patterns (presented in the form of isometric drawings) were very similar to those in the two dimensional slice models with the same basic shape. One of the main differences between two and three dimensional models of the same basic

shape, was the frequent occurrence of swirl in the latter. An excellent review of the fundamental aerodynamics of jet systems was presented by Chesters[7] in which he progressed from free jet studies to simple enclosures and eventually to scale models of furnaces.

So far mainly water model studies, of fundamental jet systems and actual combustion systems have been considered. Winter and Deterding[8] advocated the use of water rather than air models as allowing better flow visualisation. Simultaneous observation of the whole flow field can be made and thus the effect of any changes rapidly assessed. There are also advantages due to the absence of probing instruments, and also the lower velocities required for similarity purposes. If accurate quantitative data is required, the use of air models becomes desirable. The basic principles of combustion model studies have been dealt with by Putnam and Ungar[9] and Curtis and Johnson[10]. A condensed treatment covering the modelling criteria relevant to marine boilers is contained in a text by Johnstone and Thring[11].

1.2.2. Single Jets - Theoretical and Experimental

There has been a considerable amount of work on the theoretical and experimental aspects of single free jets. Notable studies have been made by Tollmien[12], Reichardt[18] and Hinze and Van der Hegge Zijnen[22]. The theoretical analyses of Tollmien[12], Howarth[13], Tomotika[14] and Abramovich[15] were based on the turbulent transfer theories of either Prandlt[16] or Taylor[17] and each shows some disagreement with experimental data. Hinze's[22] solution was based on an eddy viscosity term which was independent of radial position and good agreement was obtained. The solution of Reichardt[18] was based on the correlation of the radial

distribution of momentum with the Gaussian error curve. Although there was no theoretical basis for this assumption, good agreement with practice was observed by Baron and Alexander[19] who conducted experiments which confirmed Reichardts hypothesis. A later treatment of entrainment in turbulent free jets was conducted by Ricou[20]. The experimental technique involved the use of a porous cylinder, which surrounded the jet, but was of a sufficient size not to restrict the free expansion. The static pressure inside the porous cylinder was kept at atmospheric, and it was assumed that in this condition the jet was entraining freely. The rate of supply of entrainment air could then be measured accurately. Ricou concluded that the entrainment of a free jet could be represented by an equation of the form

$$\frac{M_e}{M_o} = K \frac{x}{d_e} \qquad \ldots\ldots\ldots\ldots\ldots 1$$

where $M_e$ is the entrained air mass at x

$M_o$ is the nozzle air mass ($x = 0$)

$x$ - axial distance from nozzle

$d_e$ - effective diameter of nozzle (after Thring and Newby[21])

$K$ - constant

The value of K for all free jets was found to be 0.246, with the exception of some of the special multiple nozzles used, which will be described later in section 1.2.4. An alternative way of expressing Ricou's entrainment data was

$$M_j = K' (G_o \rho_a)^{\frac{1}{2}} x \qquad \ldots\ldots\ldots\ldots\ldots 2$$

where $M_j$ is mass of air in jet at x

$G_o$ - momentum of jet

$\rho_a$ - density of surrounding fluid

x - axial distance

K' - constant

In this equation, which is independent of jet diameter, the ability of a jet to "forget" its origin can be seen. K' was found to be 0.28 for an isothermal round jet. Ricou correlated burning jets by plotting $\frac{M_e}{M_o} Fr^{\frac{1}{2}}$ against $\frac{x}{d_e} Fr^{\frac{1}{2}}$ where

$$Fr = \text{(Modified) Froude Number} = \frac{U_o^2}{g\, d_e} \frac{T_a}{T_o} \qquad \text{.....3}$$

$U_o$ = exit velocity of jet

g = gravity constant

$T_o$ = nozzle temperature

$T_a$ = ambient temperature

Ricou noted an important discrepancy between Hinze's[22] measurement of a full jet andle of $20^o$ and his own value of $30^o$ for an unburning jet. He attributed this to the infinitesimally small velocities existing in the outer jet regions and the inability of normal velocity and concentration techniques to measure these flows.

Using the entrainment equation of Hinze and Van der Hegge Zijnen[22], Thring and Newby[21] predicted the recirculation in an enclosed single jet.

The assumption was that the free jet entrainment appetite was equal to the total of the recirculation flow rate and the ambient air flow rate. The most important feature of this treatment was the derivation of the parameter $\Theta$ which has been used to correlate recirculation in most of the subsequent enclosed jet studies.

$$\Theta = \frac{M_o + M_a}{M_o} \cdot \frac{r_o}{L} \qquad \ldots\ldots\ldots\ldots\ldots 4$$

$\Theta$ is the Thring-Newby Parameter

$M_a$ is the ambient air flow rate supplied around the nozzle

$r_o$ is the nozzle radius

L is the chamber radius

Their introduction of an equivalent nozzle diameter concept enabled isothermal model studies to be applied to practical systems involving combustion. The equivalent nozzle radius $r_o' = \frac{d_e}{2}$ was given by

$$r_o' = \frac{M}{\sqrt{\rho_f \pi G_o}} \qquad \ldots\ldots\ldots\ldots\ldots 5$$

$\rho_f$ = density of nozzle fluid at flame temperature

$G_o$ = momentum of nozzle fluid

It can also be seen that

$$\frac{r_o'}{r_o} = \sqrt{\frac{\rho_o}{\rho_f}} \qquad \ldots\ldots\ldots\ldots\ldots 6$$

The equation given by Thring and Newby to predict recirculation was

$$1 + \frac{M_r}{M_o + M_a} = \frac{0.9}{\theta} \quad \ldots\ldots\ldots\ldots\ldots 7$$

where $M_r$ is the recirculation mass flow rate. It was also shown that dynamic similarity could be obtained between model and combustion system making the parameter $\theta$ equal in both.

$$\theta = \left[\frac{M_o + M_a}{M_o}\right] \frac{r_o}{L_{(model)}} = \left[\frac{M_o + M_a}{M_o}\right] \frac{r_o'}{L_{(combustion\ system)}} \quad \ldots\ldots\ldots\ldots\ldots 8$$

Confirmation of the use of Equation 6 was made by Sunavala, Hulse and Thring,[23] who used tracer techniques to study free and enclosed turbulent jets. They found substantial agreement between cold and hot non-combusting jets. In cases where combustion occurred, the axial concentration decay was found to be 30% greater than in the non-combusting case.

Since 1955 experimental work on confined jets has been conducted at Grenoble, arising from theoretical treatment of Craya and Curtet[24]. Curtet's[25] experiments give the equation

$$\frac{M_r}{M_o + M_a} + 0.88 = \frac{0.44}{\theta} \quad \ldots\ldots\ldots\ldots\ldots 9$$

when presented in the same form as equation 7 and when $\theta >> \frac{r_o}{L}$. Later studies by Cohen de Lara et.al.[26] have been summarised by Hubbard[27]. The recirculation mass flow rate was found as a function of inlet conditions for both cylindrical and conical chambers. The results could be represented

by the equation

$$\frac{M_r}{M_o + M_a} + 0.9 = \frac{0.62}{\theta} \quad \ldots\ldots\ldots\ldots\ldots 10$$

when $\frac{r_o}{L} > 0.15$. When $r_o$ was small such that $\frac{r_o}{L} < 0.02$ the experimental points tended towards the Craya-Curtet prediction of Equation 9.

As well as recirculation data, the variation of axial decay of velocity with distance from the nozzle was given for several low values of $\frac{r_o}{L}$, but the higher values of $\theta$ were obtained by variation of the ambient air mass flow rate $M_a$. When there was no surrounding air flow, increasing nozzle radius had the effect of accelerating axial velocity decay. Obviously this could only occur up to a certain limiting value of $\frac{r_o}{L}$ since as $r_o$ tends towards L the conditions approached pipe flow. Although no axial velocity decay data were given, recirculation measurements were made on enclosed jets when the burner radius was large in comparison with the chamber dimensions. It was found that the position of maximum recirculation moved upstream towards the nozzle as $\frac{r_o}{L}$ was increased. The variation of the magnitudes of recirculation velocities with position was given for various small values of $\theta$. These are fairly similar increasing to a maximum value of $\frac{U_r}{U_o}\frac{L}{r_o} = 0.68 \pm 6\%$ at $\frac{x}{L} = 4$. An attempt to give a unique dimensionless plot of the radial velocity distribution was made, but the scatter of points was too great to give meaningful results. Little difference in recirculation flux and axial velocity decay was found when the combustion air was supplied uniformly, axially and peripherally. Although restriction of the exit did not alter

the recirculation flow rate, it did cause the recirculation to take place entirely within the model, rather than from outside the model, as was the case without an exit venturi section.

When the chamber was of conical shape, it could still be treated as equivalent to a cylindrical chamber. The characteristic dimension L' used to correlate recirculation was found to be the radius of the chamber where the maximum recirculation occurred.

Research into recirculation in cylindrical, conical, square and rectangular shaped models has been conducted by Ibiricu[28].

He also used the Thring-Newby parameter $\Theta$ for the correlation of recirculation data with chamber characteristics and operating conditions. He gives the experimental equation:-

$$1 + \frac{M_r}{M_o + M_a} = \frac{0.73}{\Theta} \quad \ldots\ldots\ldots\ldots\ldots 11$$

for the correlation of recirculation made from the analysis of velocity profile data, and:-

$$1 + \frac{M_r}{M_o + M_a} = \frac{1}{\Theta^{0.82}} \quad \ldots\ldots\ldots\ldots\ldots 12$$

obtained from the use of concentration data. The latter equation gives substantially lower values of $\frac{M_r}{M_o + M_a}$ at low values of $\Theta$, and is in good agreement with the Craya-Curtet Theory expressed in Equation 9. Above a value of $\Theta = 0.1$ there is better agreement between the two Equations 11 and 12, than between either and the Craya-Curtet theory. An important result of this work was the definition of a characteristic dimension for non-cylindrical

chambers given by an equation of the form:-

$$L' = \frac{2L_1 L_2}{L_1 + L_2} \qquad \ldots\ldots\ldots\ldots 13$$

where $L_1$ is the smallest radius of a conical chamber, or half the shortest side of a rectangular cross section

$L_2$ is the largest radius of a conical chamber, or half the largest side of a rectangular cross section

$L'$ is the characteristic dimension of the chamber used to calculate Q.

It can be seen that this equation is based on the hydraulic mean radius of the chamber, a characteristic dimension used by engineers for the calculation of the Reynolds Number[29].

1.2.3. Annular and Concentric Jets

These jets are not thought sufficiently relevant to this study to include an exhaustive survey. There are, however, points of similarity between the double concentric jet, in which a central jet is surrounded by an outer annular jet, and the multiple jet systems studied in this research. Consequently the more important papers on this topic are reviewed here.

Research into concentric jets was probably initiated by Squire and Trouncer[30] who analysed the expansion of a jet in a parallel stream and Forstall and Shapiro[31] who investigated the mixing of two parallel co-axial streams of fluid. The latter case differs from the double concentric jet in which the surrounding stream also behaves as an expanding jet. Research into the velocity fields of double concentric jets has been carried out by Chigier and Beér[32]. The results of these aerodynamic studies are

particularly interesting due to comparison with the hot pulverised fuel trials employing the same type of burner. When the velocity ratio between the annular jet and the central jet was almost unity, the axial velocity decay could be characterised in three regions. An initial period of velocity decay unaffected by the outer jet, was followed by a jet mixing zone in which the velocity increased. When the outer and central jets have combined into a single jet, normal axial velocity decay then occurred, which could be related to a free jet by use of the equivalent nozzle diameter. In this region which occurred eight nozzle diameters downstream, agreement with the axial velocity decay observed during the combustion trials was noted. When the annular jet velocity was much smaller than that of the central jet, the effect on axial decay was negligible and direct comparison with a free jet, could be made. Later work by Beér and Chigier[33] showed the effect of velocity ratio for a double concentric jet. In the developed region of flow, each condition could be related to the single free jet case by means of the axial velocity decay, and the position of apparent origin of the jet was found to vary with velocity ratio. A similar effect has been found by Patrick[34] in a study of the pure annular jet, where the apparent origin of the equivalent free jet depends on the diameter ratio of the nozzle. An important feature both of the annular jet and the double concentric jet was the existence of a recirculating vortex between the inside boundaries of the jets. In the case of the annular jet there is a return flow on the axis due to the lack of entrainable fluid inside the annulus. With the introduction of a weak central jet, its fluid was immediately 'dragged' outwards to satisfy the entrainment appetite of the annular jet, with a consequent weakening of the recirculation vortex. As the momentum of the central jet

was increased the vortex was deflected into the region between the two interfaces. As yet there is no theoretical treatment of the non-developed flow regions near to the nozzle due to the influence of pressure fields which make the problem very complex.

1.2.4. Multiple Jet Systems

Very little relevant information on multiple jets was found in the literature, the most useful being reports of boiler combustion trials, and rocket motor studies, in which multiple injection was utilised. The boiler studies were concerned mainly with steam raising efficiency but the work on rocket motors was more useful since some velocity measurements were made during experiments on blow-off conditions and flame stability. Wright[35], working on jet interactions in rocket motor systems, obtained Schlieren photographs of the flow patterns existing when disc type stabilisers were placed in a single plane across a duct, in either a vertical or staggered array. When using two disc stabilisers, one above the other, he obtained a fluctuating condition in which the flames passed from an assymetric flow pattern, through the symmetrical to the opposite assymetric flow pattern. When several discs were used distortion and pinching together of adjacent jets was observed, with fluctuations from side to side as before. A drastic reduction in flame blow-off velocity occurred due to the crowding together of the jets, with consequent difficulty in flame stabilisation. Wright suggested that each flameholder appeared to behave as if it were "a single flameholder in a smaller duct". This not only accounts for the reduction in flame blow-off velocity but also explains the shorter combustion chamber length required for multiple flame arrays. Single flameholder tests appear to corroborate this theory. When the disc stabilisers were staggered,

pinching together of the jets was again observed, but blow-off velocities were generally much higher than the single row case. The precise blow-off conditions were found to be related to the type of staggered array employed.

Corrsin[36] investigated the flow of gases through grids, during a study of the flow patterns and stability of several parallel two dimensional jets. The system was made two dimensional by the use of side screening plates, and the jets were of high aspect ratio. He found that when the blockage ratio $\lambda = \frac{\text{covered area}}{\text{Total area}} = 0.83$ instability of flow resulted, but this could be remedied by the use of a fine wire mesh of low density, which did not otherwise affect the flow. The stablising effect of the grid was reduced by increasing distance from the nozzles, or placing the grid too near to the nozzles. The ranges given were:

Complete stabilisation 1.25 - 7.5 jet widths

Partial stabilisation 7.5 - 10.6 jet widths

Outside these limits instability was recorded. The instability was in the form of fluctuating velocity profiles, with unequal peaks and troughs, which moved from one specific jet to another. Corrsin attributed this instability to the rapid amalgamation of the separate jets adjacent to each other. Earlier work on similar systems was referred to by Corrsin, notably Gran Ollsen[37] and Cordes[38] both of whom discovered no instability when the blockage ratio was smaller ( $\lambda \simeq 0.25$). Side Screening plates were not used by either author, and hence an influx of air into the zones between the jets was permitted thus eliminating the recirculation zone. This has been shown to remove instability in such systems, although in this case it was probable that the blockage ratio would fall outside the range of instability

deduced by Corrsin. It was concluded that the physical mechanism of multiple jet systems hinged on the entrainment of air by the individual jets from the dead air spaces between them which resulted in recirculation. The reduced static pressure in the recirculation zone tended to pull the jets together. For a given air jet, wider spacing of the jets required a greater diffusion angle before adjacent jets could impinge to form stable flow. When the spacing became large enough the diffusion angle was prohibitively large and breakdown of flow occurred. Corrsin discovered that increased turbulence had no effect on the stability of the systems studied. He concluded that the instability must occur over a range of blockage ratios, whose limiting values depend on conditions such as nozzle Reynolds Number and nozzle shape.

Ricou[20] measured the total entrainment of five parallel $\frac{1}{8}$" diameter jets, arranged with one central and four on a pitch circle of radius $\frac{1}{2}$". He found this compared favourably with a single jet with the same total mass flow rate and nozzle area, after a certain downstream distance. Inclination of the outer jets towards the axis, and removal of the central jet, had the effect of increasing the jet angle, giving higher entrainment rates with increasing angle of inclination. For given inlet conditions, inclination of the outer jets at $45^{\circ}$ to the aerodynamic axis almost doubled the entrainment rate.

Investigations into free multiple jets have been made by Laurence and Benninghoff[39]. Turbulence and mean flow characteristics were determined for a linear array of slots with different spacings, and also for a circular nozzle, in which three $60^{\circ}$ sectors were blanked, thus dividing the flow into the three remaining sectors. The flow patterns were obtained by velocity traverses and turbulence intensities were measured using a hot wire

anemometer. Assymetric flow patterns were observed for both systems, probably due to structural irregularities. As the jets were unconfined no recirculation was found for either nozzle assembly. An interesting feature of the linear array of slot jets was that all jets behaved as free jets (Fig.1). The end jets showed good agreement when the axial velocity decay was compared with that of Hinze[22] but the middle jets seemed to behave as a free jet which originated two diameters downstream of the ideal free jet of Hinze. In both cases the rate of decay of velocity was the same. The maximum turbulence intensity occurred at the outer fringes of the end jets, indicating that jet interactions in the between jet zones causes a reduction in the turbulence.

1.2.5 Conclusions from the Literature

No systematic study has been made of three dimensional multiple jets, either unconfined or enclosed. Models of marine boilers[1] give results that can only be directly useful to the particular type of boiler studied, although some trends are observed which can be applicable to all multiple burner systems. It might be argued that the logical first step in obtaining fundamental knowledge of multiple jet systems is the study of an array of nozzles discharging into free space. However, since much of the confined single jet data has yet to be related to the single free jet, it is improbable that relationships can be found between free and confined multiple jets. It was concluded that a fundamental study of confined multiple jets would provide a basis from which work on more practical systems employing swirl and complex aerodynamic arrangements could proceed, and to provide knowledge regarding the existing flow patterns and heat transfer characteristics of marine boilers. Useful ideas were obtained from the literature about the

type of flow patterns expected in multiple jet systems. Particularly useful was Wright's[35] concept suggesting that each jet would behave as if confined in a smaller separate duct, although this appeared to contradict Ricou's[20] work suggesting the combination of jets. However, when the jets are close together in relation to the size of the enclosure, combination of the jets into a single jet probably occurs but if the jets are widely spaced then it would be impossible for them to coalesce with each other before hitting the wall of the duct. Here, Wright's theory is likely to apply, and recirculation would be expected around each jet. Double concentric jet studies[32, 33] indicate that recirculation between the jets occurs, due to low static pressure regions caused by jet entrainment. Laurence and Benninghoff[39] also found that multiple free jets behaved as single free jets when the separation distance was sufficiently large (Fig.1).

## CHAPTER 2

## APPARATUS AND EXPERIMENTAL TECHNIQUES

### 2.1. The Air Models Laboratory

Facilities were provided for operation with air over a suitable range of flow rates. Local velocities could be measured at desired points within the models.

#### 2.1.1. The Perspex Models

The apparatus used for the bulk of the single enclosed jet studies consisted of a 4.2 inches outside diameter 3.7 inches inside diameter perspex duct of length 3 feet (Plate 1). The duct was provided with 7 inches square, $\frac{1}{2}$ inch thick perspex flanges, which were glued on to each end so that various nozzle and exit assemblies could be changed fairly easily. A matching end plate was made with a detachable section so that the radius of the nozzle could be varied. The duct was drilled, tapped and plugged at 2 inch intervals along its length to give access for probes. The same duct was also utilised for the calibration of the "T" shaped pitot-probe.

The rest of the single jet studies and all of the multiple jet studies were effected in the second model which represented a simplified 1/12th scale marine boiler as shown in Appendix 3 (Plate 10 and Fig. 32). It consisted of a perspex duct 9" outside diameter, 8" inside diameter and 3 feet in length, which was mounted with two 16" square $\frac{1}{2}$" thick perspex flanges at each end. Holes were drilled along the sides of the cylinder in two lines separated by one quarter of the circumference to enable traverses both through and between the axes of the outer jets. These ports

were situated at 1" intervals for the first 6", 2" intervals for the next 14" and 4" intervals for the remainder of the length of the duct. Each hole was tapped with $\frac{1}{4}$" Enots thread, and a removable blocking plug inserted. The model is shown in Plates 2a and b and Fig. 2.

2.1.2. The Nozzles

Each of the seven nozzles consisted of an 18" length of 7/8" outside diameter, $\frac{3}{4}$" inside diameter brass tubing. Half-way along each tube was placed a tight-fitting brass sleeve 2" long, and $\frac{3}{4}$" outside diameter and 5/8" inside diameter. Pressure tappings were located $\frac{3}{4}$" upstream and 3/8" downstream of the constriction. A brass flange $1\frac{1}{2}$" diameter 1/16" thick was soldered 1" from the discharge end of the tube, so that each nozzle could be secured to the end plate of the model. To vary the jet diameter, a removeable brass sleeve could be fitted into the end of each nozzle. Each sleeve was $1\frac{1}{2}$" long and $\frac{3}{4}$" outside diameter, $\frac{1}{2}$" inside diameter and was bevelled at $45^{\circ}$ on the leading edge. The sleeves are shown in Plate 3a and the nozzles in Plates 2 and 3 and Figs. 2.
A modification of the central nozzle with two $\frac{1}{4}$" inside diameter tangential air intakes situated $1\frac{1}{2}$" from the nozzle discharge, enabled a swirling single jet to be studied (Appendix 1). This modification can be seen in Plate 3b.

2.1.3. The End Plates

Several end plates were used to enable different nozzle arrangements to be studied. Each plate was a 16" diameter 1" thick perspex disc drilled with eight 3/8" diameter holes on a pitch circle diameter of 12".

These were used for bolting the plate to the perspex model. Each end plate was drilled with a central hole, and six other holes, equally

spaced on a pitch circle around the central hole. The holes were 7/8" diameter to accommodate the nozzles, which could then be fastened to the end plates by means of self tapping screws, or countersunk bolts. The pitch circle radius of the outer nozzles was one of the variables studied in this research and consequently the value was different for each end plate.

At the exit end of the model, a 16" square ½" thick perspex plate was used with a central 6" diameter hole. It was also drilled with 3/8" diameter holes matching the flange of the model. The grid resistances used in the later studies were secured to the ends of three lengths of ¼ B.S.F. screwed rod, and these were attached to the end plate by means of ¼ B.S.F. nuts. For this purpose three 3/8" diameter holes were drilled on a 7" diameter pitch circle about the centre of the end plate. The position of the grid could then be varied by altering the position clamping nuts.

2.1.4. The Grids

Three types of grid were used in the experimental work which studied the effect on the flow pattern of resistances placed inside the model. The first grid was of a course mesh of low resistance, consisting of perforated aluminium sheet, secured to an 8" outside diameter 7" inside diameter ½" thick perspex ring (Plate 4). The second grid was a finer mesh brass gauze and was secured to a perspex strengthening ring of 8" outside diameter 7½" inside diameter, and ¼" thick. This grid is shown in Plate 5 together with the fibre pad which could be added to make the third high resistance grid.

2.1.5. The Air Supply

Air was supplied by an Alldays and Onions 30 h.p. fan along an 18 inch diameter overhead duct. The supply was regulated by a gate-valve

and metered with an orifice plate prior to passing into a manifold for distribution to the individual nozzles. Each offtake on the manifold was fitted with a valve for exact control of the air flow to the nozzles. The valves were connected to the nozzles by suitable lengths of 7/8" outside diameter colourless polythene tubing.

## 2.2. The Velocity Measuring Technique

### 2.2.1. The Beaudouin Pressure Transducer

The fluctuating pressure signals from the primary sensing element were rectified into a d.c. millivoltage output suitable for chart recording, using the Beaudouin Pressure Transducer and ancillary 1000 c.p.s. generator and bridge circuit. This equipment has been described fully by Pengelly[40].

The output from the transducer circuit was recorded on a high speed Honeywell Brown single-pen recorder. The recorder had three ranges, and when used in conjunction with the three ranges of output from the transducer bridge unit enabled a wide range of differential pressures to be recorded.

### 2.2.2. The "T" Shaped Velocity Probe

The primary sensing element consisted of a "T" shaped probe mounted in a motor driven traversing rig (Plate 6). The probe was one foot long with a ¼" long measuring head, at right angles to the longitudinal axis of the probe. The stem was made from two, eleven inch, lengths of 1/16" bore brass tube which were soldered together for strength. Into one end of each brass tube, a length of 1/16" outside diameter stainless steel hypodermic tube was secured with one inch protruding. These ends were bevelled to seal the dynamic head from the suction head of the probe. The head consisted of a ¼" length of 1/16" bore 1/8" outside diameter brass tube

which was drilled with two 1/16" diameter holes on one side only, to accommodate the stainless steel tubes. Two ¼" outside diameter copper tubes were soldered on to each pressure tapping in order that ¼" bore rubber tubing could be used to transmit the pressure signals to the transducer. This arrangement was later modified, so that 1/16" bore pressure tubing could be used. This gave a constant 1/16" bore from the probe head to the transducer, and in view of the reduction of the total volume of the connecting tubing, a faster response time was anticipated. Atmospheric venting was allowed by suitable three way valves and the arrangement is seen in Plate 1.

2.2.3. The Traversing Rig

The framework for the motor driven traversing mechanism was made from slotted metal angle. The base was formed from four 18" lengths of dexion fitted with ½" diameter meccano wheels which could run along rails above the model. At right angles to the plane of the framework were mounted two 18" lengths of ¼" B.S.F. screwed rod driven by co-ordinated gears from a small 1/50 h.p. Edwards motor. A piece of threaded perspex 2" x 1" x 3" was driven by the threaded rod, and mounted between four guiding surfaces to prevent lateral movement. A ½" diameter holder rod attached to the perspex block could be moved up or down through a ½" diameter guiding hole at the base of the traversing rig. The "T" shaped velocity probe was secured to the rod by means of a perspex clamp. With this arrangement it was possible to traverse for distances up to 10". Various speeds could be arranged by manipulation of the driving gears, the fastest being 2" per minute and the slowest being 1" per minute. These speeds proved to be quite adequate for use in conjunction with the transducer, the slowest being

preferred as this gave less error when measuring up the traces for conversion to velocity profiles. A view of the traversing element is shown in Plate 6.

## 2.3. The Water Models Laboratory

Facilities were provided for operation of the water model, and for photographs recording the flow patterns.

### 2.3.1. The Perspex Model

The perspex model used for the air model studies was modified for use with water flows. In order to expel all the air from the duct it was necessary to increase the upstream pressure by constricting the outlet of the system. This was achieved by securing a $90^{\circ}$ elbow of 2" internal diameter pipe and control valve to the exit flange. Any remaining air was removed through a small bleed valve. The sampling ports were sealed with fibre washers and blocking screws. To obtain photographs with minimum distortion due to the curved perspex surface, the duct was surrounded with a water jacket, contained in a flat-sided box fitted to the end flanges. The whole arrangement was temporarily sealed with a mastic compound.

### 2.3.2. The Nozzles

The nozzles were identical with those used for the air model studies. Pressure tappings were not utilised for flow metering and were thus blanked-off with short lengths of $\frac{1}{4}$" plastic hose, secured by wire. Uniform water flow to each jet from the manifold was assumed.

### 2.3.3. The Grid

The low resistance grid was used to indicate the effect of a downstream resistance on the system. The mesh size of the higher resistance grids was smaller than the polystyrene particles used for flow visualisation.

For part of these studies, the perspex strengthening ring was moved 6" further downstream, to minimise its effect on the flow pattern in the immediate vicinity of the grid.

2.3.4. The Water Supply

The water supply was provided by a Worthington-Simpson $1\frac{1}{2}$ horse power recirculation pump using a large reservoir, into which the water from the model was discharged. The water from the pump passed into the manifold through $1\frac{1}{4}$" inside diameter strengthened rubber hoses. Each line included a 0-1500 gallons/hour rotameter to meter the flow to the nozzles. The manifold consisted of a drum 6 inches diameter and 12 inches long. At one end two inlet sections of $1\frac{1}{4}$" outside diameter pipe were welded, on to which the strengthened hoses were fastened with "jubilee" clips. The $\frac{3}{4}$" diameter offtakes to the seven nozzles on the opposite end of the cylinder were secured with $\frac{3}{4}$" diameter hose to the nozzles in the model end plate. The geometrical arrangement of the offtakes was identical with that of the nozzles so that they could be joined with the minimum difficulty. The top of the manifold was fitted with a tap to vent the trapped air inside the chamber during the initial operation of the model.

2.4. The Photographic Technique

Photographs of the flow patterns inside the model were obtained using the standard technique of slit lighting and polystyrene tracer. Light was provided by two, two kilowatt lamps housed in an air cooled chamber. The slit was formed by suitable metal screens, whose width could be varied. The 1 millimetre diameter polystyrene particles were introduced into the water supply at the reservoir. Photographs and visual observations of the flow patterns were obtained at sections corresponding to the position of the light slit, and these can be seen in Plates 7, 8, 9 and Figs. 24 a-e.

# CHAPTER 3

## AERODYNAMIC STUDIES OF ENCLOSED JETS

### 3.1. Single Enclosed Jets

It was found necessary to obtain more complete data than that available for a single jet issuing into a duct in the absence of an ambient air stream. In an attempt to become familiar with the measuring techniques several measurements on single jets were made, and it was found that there was a difference between these results and those obtained by the French Team at Grenoble[26]. The differences were only slight and could be attributed to a number of possible factors such as presence of a front wall, nozzle type or model exit conditions. In view of this, it was decided to study single jets over a range of $\frac{r_o}{L}$ from 0.0625 to 0.669. In view of the later comparison between single and multiple jet data, care was taken that the inlet and exit conditions in both investigations were similar. In the absence of an ambient air stream the only variables possible were the inlet nozzle velocity, and the ratio of the nozzle dimensions to those of the duct $\frac{r_o}{L}$. In this case $\frac{r_o}{L}$ was equal to the Thring-Newby parameter $\theta$. The purpose of these experiments was to obtain axial velocity decays, especially for high values of $\theta$, and to correlate recirculation in terms of $\theta$.

#### 3.1.1. The Effect of $r_o/L$ on axial velocity decay

There are two extreme cases, that of the free jet when $\frac{r_o}{L}$ is extremely small, so that the walls do not hinder the jet expansion, and ordinary pipe flow in which $\frac{r_o}{L}$ reaches its maximum value of unity, and there is no axial velocity decay. In the former case the well established equation of Hinze[22]

will describe the axial velocity decay

$$\frac{U_o}{U_m} = 0.077 \sqrt{\frac{x}{r_o}} \quad \text{.....3.1}$$

where $U_o$ is maximum nozzle exit velocity

and $U_m$ is axial velocity at point x.

This equation becomes applicable after the potential core region which is normally presumed to extend about 6 jet diameters downstream. The equation for pipe flow is simply $U_o/U_m = 1$. As expected, all intermediate values of $\frac{r_o}{L}$ produce axial velocity decay graphs which lie between these two extremes, (shown in Figs. 3 and 4). Since a free jet cannot be represented when $U_o/U_m$ is plotted against $\frac{x}{L}$ because L is infinite, another means of indicating the effect of $\frac{r_o}{L}$ between the two extremes would be a plot of $U_o/U_m$ against $\frac{x}{2r_o}$. In this case a simple fall from Hinze's free jet equation (Equation 3.1) down to the $U_o/U_m = 1$ of pipe flow does not occur. An initial increase of $\frac{r_o}{L}$ from zero is accompanied by an increase in $U_o/U_m$ at the same value of $\frac{x}{2r_o}$. This trend continues until a critical value of $\frac{r_o}{L}$ is reached, when values of $U_o/U_m$ begin to fall again at the same value of $\frac{x}{2r_o}$. The value of the critical $\Theta$ was 0.5 in the present case, but it appears to depend on the experimental conditions prevailing. The maximum value given by Cohen de Lara et al[26] in the absence of ambient air flow was $\Theta = 0.089$, although it is not certain that this was the inversion value, since no higher values of $\Theta$ when $M_a = 0$, were published. After inversion the values of $U_o/U_m$ fall for the same value of $\frac{x}{2r_o}$, when $\Theta$ is further increased. There was also a flattening of the curve to an assymptotic value of $U_o/U_m$ at higher values of axial distance which was to be expected

since there will be a tendency towards pipe flow conditions as $\Theta$ tends to unity.

3.1.2. Effect of $r_o/L = \Theta$ on Recirculation

The recirculation was computed from the velocity profiles, both by integrating the forward flow profile, and the reverse flow, the difference between these two being the nozzle inlet mass flow rate $M_o$. A correlation between $\frac{M_r}{M_o}$ where $M_r$ was the recirculation mass flow rate, and $\frac{1}{\Theta}$ was found and is shown in Fig.5. Very close agreement was observed at high values of $\frac{r_o}{L}$ with both Cohen de Lara[26] and Ibiricu[28], although as $\frac{r_o}{L}$ decreased, the values of $\frac{M_r}{M_o}$ were found to lie between these studies. The recirculation data are given in table No.4.3. in Chapter 4.

3.2. Multiple Enclosed Jets

In this study, the situation was made more complex than that of the single enclosed jet, by surrounding the single jet with other jets in a parallel uniform configuration. Many extra variables are introduced by such an arrangement, although some of these were not investigated in the present research. The radii and velocities and consequently momenta of the outer jets were maintained the same as the central jet, as in the marine boiler case. The ambient air supply was ommitted as the pressure jet burner employed in marine boilers is of the swirling concentric jet type, which can be replaced in the first instance by a simple jet.

3.2.1. The Effect of Reynolds Number

The Reynolds Number was varied over a range 1.19 - 3.19 x $10^4$, which was less than those of practice but it has been shown[11] that for fully turbulent conditions ($R_e > 10^4$), similarity should result. In order to achieve the same Reynolds Numbers as in practice, (approximately 117 x $10^4$)

prohibitively large supersonic nozzle velocities would have to have been used. The first arrangement studied was that of six $\frac{3}{4}$" diameter nozzles equally spaced on a pitch circle of radius 2", and one $\frac{3}{4}$" diameter nozzle placed centrally. Velocity traverses were made in two planes, through and between the axes of the outer jets. It was thought that these would yield sufficient information about the flow patterns. A general feature of the variation of flow rate, in which the Reynolds Number was almost trebled, was the basic similarity of all the flow patterns. These are shown in Figs. 7a-f. The recirculation zone between the central and outer jets is seen to extend about $2\frac{1}{2}$" downstream in all cases, and this can be compared with the stagnation point in double concentric jet studies. The outer recirculation zone was observed to diminish fairly uniformly as the outer jets expanded. The axial velocity decay curves shown in Fig.6 fall on a smooth curve at all Reynolds Numbers.

3.2.2. Effect of Nozzle Diameter

In these experiments the same nozzle configuration was used as in the previous section but the nozzle diameter was $\frac{1}{2}$". The Reynolds Number varied over a range 1.06 - 3.19 x $10^4$ but there was no corresponding change in flow pattern (see Figs. 8a-f). Good agreement was found between $\frac{3}{4}$ and $\frac{1}{2}$ diameter nozzles in terms of basic flow pattern, the only differences being in the axial velocity decay, and the magnitudes of recirculation velocities.

3.2.3. The Effect of Pitch Circle Radius of the Outer Nozzles

The pitch circle radius of the outer nozzles was varied for five values of $\frac{R}{L}$ from 0.375 to 0.656. As in section 3.2.1. the nozzle diameters were $\frac{3}{4}$" and six outer jets were used. For this study the Reynolds Number

was maintained constant in each jet at a value of $2.87 \times 10^4$. It was thought that the lower values of $\frac{R}{L}$ would show considerably more jet interference, and consequently turbulence, due to the closer proximity of the jets. This proved to be the case, and when $\frac{R}{L} < 0.5$ the jets rapidly combined with a loss of individual profile. Above this value the jets maintained their individuality. An interesting feature at large $\frac{R}{L}$ was the difference in axial velocity decay between inner and outer jets, indicating crowding of the outer jets by each other and by the walls of the duct. The flow patterns are shown in Figs. 9 and the axial decay of velocities in Figs. 20. Recirculation velocities were found to be higher when the jets were further apart.

Two other experiments were performed with $\frac{1}{2}$" nozzles for $\frac{R}{L}$ of 0.5 and 0.656, but the flow patterns were basically similar to those when the diameter was $\frac{3}{4}$" (Fig. 10).

3.2.4. The Effect of reduction of Number of Outer Jets

A further configuration of three outer nozzles uniformly spaced about the central jet was studied. The pitch circle radius was varied over the range of $\frac{R}{L}$ from 0.375 to 0.656 and the nozzle diameter was $\frac{3}{4}$". The Reynolds Number was again maintained constant at $2.87 \times 10^4$. Additional experiments were conducted at $\frac{R}{L} = 0.5$ and 0.656 when the nozzle diameters were $\frac{1}{2}$". In this case the Reynolds Number was $3.19 \times 10^4$. The flow patterns are shown in Figs. 11 and the axial decay of velocity in Fig. 21. The recirculation velocities were lower, probably due to the increased area available for flow, as well as the decreased nozzle total mass flow rate. There was a complete absence of mixing between outer jets at all pitch circle radii because of their wide spacing. This is shown in the traverses between the

axes of the outer jets, which indicate a smooth jet expansion, with none of the irregular peaks observed with six outer jets, when, due to their mutual proximity some turbulent mixing was observed between the outer jets. For the higher pitch circle radius, the axial decay of velocity of both central and outer jets was the same, contrary to the observations with six outer jets. A possible explanation of this is the fact that the outer jets are less crowded, and hence are able to expand as freely as the central jet.

A further investigation of two outer $\frac{3}{4}$" diameter jets on a pitch circle radius $\frac{R}{L}$ = 0.5 was made, (i.e. in the same plane as the centre jet) obtaining point values of the axial velocity. The axial velocity decay is shown in Fig. 22.

3.3. The Study of the Introduction of a Downstream Resistance

An investigation was made of the effects of placing a downstream resistance, in some of the multiple jet arrangements studied above. This was intended to take account of the tube banks in practical boiler installations, and also to discover the effects of decreasing combustion chamber length. In prototype boilers (Plate 10 and Fig. 32), the tube banks are situated alongside the flames, so that the combustion gases must turn through a right angle prior to entry. Thus combustion at the outer wing burners may not be completed before the gases are swept into the tube banks. The grids were placed at various points inside the jet expansion zone, where in practice combustion would still be taking place. Although the data obtained in this study cannot be directly applied to marine boilers, the results give a qualitative picture of the probable effects of tube banks upon flow.

### 3.3.1. The Effect of Grid Position

The first investigation was made on the seven jet system when $\frac{R}{L} = 0.5$. The grid was moved successively from downstream to a point $\frac{x}{L} = 0.375$ and the flow patterns are shown in Figs. 12. When the grid was placed at $\frac{x}{L} = 1.75$, a reduction in the size of the inner jet recirculation zone was noticed. Without the grid in position the zone extended some $2\frac{1}{2}$" downstream, but with the grid in place the zone was barely detectable 1" downstream from the nozzles. This recirculation appeared to be displaced into the outer zones, and a corresponding 50% increase in velocity was observed. This effect was also indicated by the more rapid axial velocity decay of the outer jets when compared with the centre. This effect was only observed at higher values of $\frac{R}{L}$ when no resistance was introduced. When the grid was moved nearer to the nozzles, a "compression" effect was noticed, with the outer jets spreading out to the wall prior to the grid. The flow patterns between $\frac{x}{L} = 1.75$ and 1.25 were all similar, with the main recirculation occurring in the outer zone. Movement of the grid to $\frac{x}{L} = 1$ revealed a drastic change in the flow pattern (seen in Fig.12c). A recirculation zone extending to the grid was now established between the jets. It appeared that this recirculation had been produced at the expense of the outer zone, because the recirculation velocities were drastically reduced in the latter. The axial velocity decay was the same in all jets, as had been the case with no grid present. Further upstream, movement of the grid increased recirculation between the jets, and further reduced it outside. In all cases, movement of the grid towards the nozzles accelerated the axial velocity decay. This can be seen in Figs. 13, 16. The initial effect of the grid introduction was to deflect the outer jets into the outer recirculation zone.

Recirculation from behind the grid may also have occurred but the velocities involved were too small to be measured. Also a high turbulence level was present downstream of the grid, with the fluctuations often exceeding the mean pressure reading from the probe. In contrast to this the turbulence level before the grid was much less than with no grid at all, resulting in better velocity traces. This result agreed with Corrsin's observations[36].

3.3.2. The Effect of Grid Resistance Magnitude

The same arrangement of jets as in the previous section were investigated using grids of higher and lower resistance respectively. The resistance calibrations of the grids are given in Appendix 3. The high resistance grid did not alter the basic flow patterns as can be seen in Fig. 14 a and b, although slightly more rapid axial velocity decays were noticed. The boundaries of the recirculation zones in each grid position were not altered by increased grid resistance. The low resistance grid initially had a less drastic effect on the system, the flow patterns (shown in Figs. 15 a and b) falling between those without a grid, and those with the medium resistance grid. The initial grid placings from $\frac{x}{L}$ = 1.75 to 1.25 showed an inner recirculation zone extending $1\frac{1}{2}$" downstream compared with $2\frac{1}{2}$" in the open system and 1" with the medium resistance grid. The change over of maximum recirculation flow occurred at $\frac{x}{L}$ = 1 as before, but in general all recirculation velocities were lower than with the medium resistance grid. The effect of each grid on the axial velocity decay can be seen in Fig. 16.

3.3.3. The Effect of Nozzle Diameter

In this study with the same pitch circle radius of the outer jets $\frac{R}{L}$ = 0.5, the nozzle diameters were reduced to $\frac{1}{2}$". The flow patterns (Fig. 17 a-c) have the same recirculation zone limits as those for the same

$\frac{3}{4}$" diameter nozzle configuration and this result compared well with the variation of diameter when no grid was present (Figs. 7 and 8). The changeover of the main recirculation flow which was observed at $\frac{X}{L} = 1$ with $\frac{3}{4}$" diameter nozzles was observed here at $\frac{X}{L} = 1.25$, although some reverse flow was noticed near to the grid when it was positioned at $\frac{X}{L} = 1.5$. As before, after the changeover, the outer zone recirculation velocities were reduced almost to zero.

3.3.4. The Effect of Pitch Circle Radius of Outer Nozzles

The main effect of the grid in the previous sections, (where $\frac{R}{L}$ was constant at 0.5) was to increase outer zone recirculation at the expense of that between the jets, but as the grid was moved towards the nozzles, a changeover was observed. At a grid position of $\frac{X}{L} \simeq 1$, the main recirculation flow changed from the outer recirculation zone to the inner zone between the jets. It was also apparent that in these cases ( $\frac{R}{L} = 0.5$), when studied without a grid the between jet recirculation zone was the minor one. A study was thus made of the effect of the grid introduction when $\frac{R}{L} = 0.656$, where even without the grid the major recirculation zone was between the central and outer jets. Seven $\frac{3}{4}$" diameter nozzles and the medium resistance grid (Grid 2) were used. An immediate effect of the grid introduction at $\frac{X}{L} = 1.75$ (shown in Fig. 18a) was a reduction in smaller outer recirculation zone velocities. In the between jet zones, the recirculation took the form of a reversed jet, an effect which had also been noticed in the above studies where the inner zone of recirculation was predominant. This phenomenon was not observed in any of the systems prior to the grid studies. A movement of the grid upstream, (shown in Figs. 18 b, c) caused increased recirculation in both zones, and some jet interaction was observed in the form of regions

of isolated forward flow in the plane between the outer jets. In the present case, no changeover of recirculation flow was noticed, only a gradual strengthening of all the zones as the grid was moved upstream. The effect of the grid on axial velocity decay can be seen in Fig. 19.

Let each grid have a limiting velocity which depends on the pressure drop across it. As the grid is moved upstream, it encounters velocities which exceed the limiting value, and consequently jet fluid will be deflected back into the recirculation zones. It can be seen that this effect will be more pronounced as the grid is moved further upstream. For closer jet configurations ( $\frac{R}{L} \leq 0.5$), the changeover of recirculation flows can be explained by the same reasoning. Upstream of the changeover point each jet behaves separately, and so recirculation is deflected back into both zones. This effect is more pronounced in the inner recirculation zones because of the smaller cross sectional area available for return flow. Downstream of the changeover point the grid causes the jets to coalesce into a single jet. Since no inner recirculation zones would then exist, all the deflected flow of this "jet" would be to the outer zone.

In the widely spaced jet systems ( $\frac{R}{L} > 0.5$), where both recirculation zones persist to greater downstream distances, all the studies made were upstream of the changeover point, and enhancement of both recirculation zones resulted from introduction and movement of the grid upstream.

### 3.4. Water Model Studies of Enclosed Multiple Jets

The main objective of the water model work was to obtain qualitative confirmation of the flow patterns obtained in the air model studies. Although quantitative measurements from flow pattern photographs are possible, these would have proved extremely tedious since they involve measurement of particle trace lengths. The photographs were marred by the presence of minute air

bubbles which adhered to the inside surface of the perspex and were not easily removed. It was felt that the visual observations made during the operation of the water model could be best represented as line drawings and these, in conjunction with the photographs, would present a fairly clear picture of the various flow patterns. These are shown in Figs. 24 a-e and Plates 7, 8, 9.

3.4.1. The Effect of Pitch Circle Radius of Outer Nozzles

Since the pitch radius of the outer nozzles proved to be an important parameter in the air model studies three values of $\frac{R}{L}$ were chosen to represent normal and extreme cases. The values were $\frac{R}{L}$ = 0.375, 0.5 and 0.656 and corresponding water flow patterns can be seen in Figs. 24 a, b, c.

For $\frac{R}{L}$ = 0.375 the combination of the jets was clearly seen, with pronounced areas of recirculation occurring around the outside. The combined jet flow appeared to have some instability as the "jet" oscillated very slowly from top to bottom of the section. When $\frac{R}{L}$ = 0.5, close agreement with the air model studies was observed, with the size of recirculation zones comparing favourably with the values recorded previously (Figs. 8 and 9). The outer recirculation zone extended 10" downstream ($\frac{X}{L}$ = 2.5) and a general forward flow indicating amalgamation of the jets was observed 6" downstream ($\frac{X}{L}$ = 1.5). The inner recirculation zone was poorly defined but the extension downstream was about $\frac{X}{L}$ = 0.375 (in good agreement with air model studies). The higher value of $\frac{R}{L}$ = 0.656, as expected, showed the individual nature of the jets, which persisted beyond $\frac{X}{L}$ = 3, and the recirculation zones were very similar in size to those of the air model studies(Fig. 9a).

3.4.2. The Effect of Grid Position

An immediate observation was the distortion of the flow pattern near the grid caused by the perspex strengthening ring so it was located downstream of

the grid. Some recirculation through the grid was then noticed, a feature which had not been noticed in the air model studies. The flow patterns shown in Figs. 24 d, e are similar to the air model observations (Figs. 12, 14 and 15). The change over of recirculation flow from the outer zone to the inner zone as the grid was moved upstream, was observed.

## ANALYSIS OF RESULTS

### 4.1. Single Enclosed Jet Studies

The basis for the correlation of recirculation in single enclosed jets has been provided by Thring and Newby[21]. In an attempt to predict the recirculation of a single enclosed jet from the entrainment of a free jet they arrived at the equation

$$1 + \frac{M_r}{M_o + M_a} = \frac{0.9}{\theta} \qquad \ldots\ldots\ldots\ldots\ldots 4.1$$

To obtain this they used an entrainment equation derived from Hinze's free jet velocity decay data[22]. Enclosed jets do not behave like free jets[26, 28] and thus discrepancies arise between Equation 4.1. and practice. The general form of the equation has been retained with some success by Cohen de Lara et al[26] and Ibiricu[28]. The general form of the equation is:-

$$A + \frac{M_r}{M_o + M_a} = \frac{B}{\theta} \qquad \ldots\ldots\ldots\ldots\ldots 4.2$$

In order to correlate recirculation where $M_a = 0$, it was decided to plot $M_r/M_o$ against $\frac{1}{\theta}$ and compare the results of the present studies with those of the above mentioned workers.

#### 4.1.1. Calculation and Correlation of Single Enclosed Jet Recirculation

The recirculation mass flow rate was computed from the velocity profiles. A simple integration of the forward and reverse flows at any section of the duct gave a double check of the recirculation value at that distance downstream

Values of the maximum recirculation mass flow rates are given in Table 4.1. A plot of $M_r/M_o$ versus $\frac{1}{\theta}$ is shown in Fig. 5 and the results compared with the data of Cohen de Lara et al[26], and Ibiricu[28]. Table 4.2. shows comparative values of A and B in Equation 4.2. due to various workers.

Nomenclature used in Table 4.1.

| | | | |
|---|---|---|---|
| $\left(\frac{x}{L}\right)_c$ | = | axial position of maximum recirculation mass flow rate | |
| $A_r$ | = | Recirculation Area | (Square Inches) |
| $U_r$ | = | Average Recirculation velocity | (ft./sec.) |
| $M_{r_1}$ | = | Recirculation mass flow rate | (lb./hr.) |
| $A_f$ | = | Area of forward flow | (Square Inches) |
| $U_f$ | = | Average Velocity of forward flow | (ft./sec.) |
| $M_f$ | = | Mass of forward flow | (lb./hr.) |
| $M_o$ | = | Mass flow rate in nozzle | (lb./hr.) |
| $M_{r_2}$ | = | Recirculation mass flow rate based on integration of forward flow | |
| | = | $(M_f - M_o)$ | (lb./hr.) |
| $M_r$ | = | Average recirculation mass flow rate | (lb./hr.) |
| | = | $(M_{r_1} + M_{r_2})/2$ | |

All the above values are computed from the velocity traverse at $\left(\frac{x}{L}\right)_c$.

TABLE 4.1. Single Jet Recirculation

| $r_o$ | L | $\theta = \frac{r_o}{L}$ | $A_r$ ins.$^2$ | $U_r$ ft/sec. | $M_{r_1}$ lb hr. | $A_f$ ins.$^2$ | $U_f$ ft/sec. | $M_f$ lb/sec. | $M_o$ lb/hr. | $M_{r_2}$ lb./hr. | mean $M_r$ | $\frac{M_r}{M_o}$ | $(\frac{x}{L})_c$ |
|---|---|---|---|---|---|---|---|---|---|---|---|---|---|
| 0.375 | 4 | 0.094 | 33.5 | 6.4 | 418 | 16.8 | 13.0 | 425 | 62 | 364 | 391 | 6.35 | 3.63 |
| 0.25 | 4 | 0.063 | 34.2 | 7.5 | 506 | 16.2 | 16.5 | 521 | 46 | 475 | 491 | 10.7 | 3.13 |
| 0.25 | 1.85 | 0.135 | 8.7 | 7.7 | 131 | 2.0 | 36 | 140 | 27.6 | 112.4 | 121.7 | 4.4 | 2.16 |
| 0.375 | 1.85 | 0.203 | 6.84 | 10.8 | 144 | 4.0 | 28 | 217 | 55.6 | 161.4 | 152.7 | 2.74 | 3.24 |
| 0.5 | 1.85 | 0.27 | 6.1 | 21 | 264 | 4.6 | 45 | 404 | 139 | 265 | 264.5 | 1.9 | 3.24 |
| 0.7 | 1.85 | 0.38 | 6.2 | 12.3 | 148.5 | 4.5 | 40 | 352 | 174.5 | 177.5 | 163 | 0.94 | 2.16 |
| 1.0 | 1.85 | 0.54 | 5.0 | 33.2 | 325 | 5.7 | 72 | 796 | 496 | 300 | 312.5 | 0.63 | 1.08 |
| 1.24 | 1.85 | 0.67 | 5.7 | 18.9 | 210 | 7.0 | 65 | 887 | 674 | 213 | 211.5 | 0.31 | 1.08 |

TABLE 4.2.

Values of the constants in Equation 4.2.

Comparison between various Investigators

| Investigator | Nature of Study | A | B |
|---|---|---|---|
| Thring and Newby | Enclosed Jet Models | 1 | 0.9 |
| Curtet | Enclosed Jet Models — Theoretical | 1 | 0.5 |
| | Enclosed Jet Models — Experimental | 1 | 0.6 |
| Riviere | Combustion System (Gas analysis) | 1 | 0.45 |
| Cohen de Lara et al | Enclosed Jet Models above $\frac{r_o}{L} = 0.15$ | 0.9 | 0.62 |
| Craya and Curtet | Enclosed Jet (Theoretical) below $\frac{r_o}{L} = 0.02$ | 0.88 | 0.44 |
| Ibiricu | Circular, Square and rectangular cross-section models (velocity profiles) | 1 | 0.73 |
| Whaley | Circular, cross-section, no ambient air stream. | 0.6 | 0.66 |

It can be seen from Table 4.2. that the slopes of the experimental lines (B) from the results of the later single jet studies are very similar (approximately 0.65). The lines originate from different points, (different values of constant A), which are functions of the inlet conditions of both the nozzle and the ambient air stream.

4.2. Multiple Enclosed Jet Studies

A theoretical analysis of the non fully developed regions of turbulent multiple jet flows, near to the nozzles, where there is considerable influence from pressure fields would be extrmely complex. The Wright concept[35] that each jet behaves as though it were enclosed in its own separate duct allows a considerable simplification of the system. This enables direct comparison to be made with the single enclosed jet results of previous sections. In order to compare single and multiple jet data it was necessary to assign a value to the radius of the imaginary enclosing duct (L'), in order to calculate the value of the Thring-Newby Parameter $\Theta\left(\frac{r_o}{L'}\right)$. This was achieved by relating the axial velocity decay graphs of the multiple jet arrangements to those for single jets. It was only possible to do this over the downstream distance where the multiple jets remain separate from each other. Good agreement between multiple jet and single jet axial velocity decay plots ($U_o/U_m$ versus $\frac{x}{L}$ or $\frac{x}{L'}$) was observed for a greater downstream distance when the nozzles were further apart (i.e. $\frac{R}{L} > 0.5$). When the nozzles were closer together, it was impossible to compare the axial velocity decay graphs except in the immediate vicinity of the nozzles where the jets were still separate. Further downstream the graphs flattened towards an assymptotic value of $U_o/U_m$ which was much

smaller than that expected for the single jet as predicted from the upstream characteristics. This indicated an interaction between the jets, resulting in the formation of a single equivalent jet, which meant that the "separate duct" theory of Wright was inapplicable. Consequently an alternative treatment was required in which the upstream flow pattern could be described by considering each jet individually and the downstream flow pattern could be regarded as that of a single combined enclosed jet. The coalesced jet conditions were treated using the theory demonstrated by Ricou[20] that a multiple nozzle behaves downstream as a single jet with the same total nozzle mass flow rate and velocity.

4.2.1. Determination of the Radius of the Imaginary Enclosing Duct

The values of L' the radius of the ficticious enclosing duct, were determined by comparison with the single jet axial velocity decay plots shown in Figs. 3, 4. Here we had values of $U_o/U_m$ versus $\frac{x}{L}$ for single jets with various values of $\theta$, and in order to compare, it was necessary to interpolate for intermediate values of $\theta$. The comparisons are shown in Figs. 20 a, b, 21, 22 and the values of L' for the various multiple jet systems are given in Table 4.3. These values were precise, since small errors in the value of L' chosen could result in large deviations in $U_o/U_m$ for that particular location, due to the rapid rate of axial velocity decay at downstream positions. The effect of closer spacing of the jets can also be seen in Figs. 20 a, b, 21, 22 where departure from single jet data was observed after the initial zone of jet development. The ranges over which the values of L' describe the axial velocity decay of the multiple jet systems are also given in Table 4.3.

It was found that the nozzle dimensions had no effect on L', the value of this depending solely on the nozzles spacing parameters ($\frac{R}{L}$ and n).

TABLE 4.3.

Experimental Values of L'

| | $r_o$ ins. | R ins. | n | L' ins. | centre or outer jets | $(\frac{x}{L})_c$ |
|---|---|---|---|---|---|---|
| | 0.375 | 2.625 | 6 | 2.70 | centre | 2.125 |
| | 0.375 | 2.625 | 6 | 2.30 | outer | 2.125 |
| | 0.25 | 2.625 | 6 | 2.70 | centre | 2.125 |
| | 0.25 | 2.625 | 6 | 2.30 | outer | 2.125 |
| | 0.375 | 2.625 | 3 | 3.10 | both | 2.125 |
| | 0.25 | 2.625 | 3 | 3.10 | both | 2.125 |
| | 0.375 | 2.375 | 6 | 2.50 | centre | 2.125 |
| | 0.375 | 2.375 | 6 | 2.00 | outer | 2.125 |
| | 0.375 | 2.0 | 6 | 1.79 | both | 1.625 |
| | 0.25 | 2.0 | 6 | 1.79 | both | 1.625 |
| | 0.375 | 2.0 | 3 | 2.30 | both | 1.625 |
| | 0.25 | 2.0 | 3 | 2.30 | both | 1.625 |
| † | 0.375 | 2.0 | 2 | 2.50 | both | 1.875 |
| † | 0.25 | 2.0 | 2 | 2.50 | both | 1.875 |
| | 0.375 | 1.75 | 6 | 1.60 | both | 1.125 |
| | 0.375 | 1.5 | 6 | 1.30 | both | 0.625 |
| | 0.375 | 1.5 | 3 | 1.70 | both | 0.875 |

† indicates only axial velocity measurements taken

n = no. of outer jets

$(\frac{x}{L})_c$ = axial downstream distance over which L' applies

For a fixed number of outer jets the relationship between the parameter $\frac{L'}{L}$ and $\frac{R}{L}$ was linear. When n = 6 the equation was

$$\frac{L'}{L} = 0.895 \frac{R}{L} \qquad \ldots\ldots\ldots 4.3$$

and when n = 3 the equation was

$$\frac{L'}{L} = 1.15 \frac{R}{L} \qquad \ldots\ldots\ldots 4.4$$

Although insufficient points were obtained for n = 2, if it is assumed that the lines pass through the origin as in the previous equations the following equation can be obtained.

$$\frac{L'}{L} = 1.25 \frac{R}{L} \qquad \ldots\ldots\ldots 4.5$$

Average values of L' were used to obtain the above equations as in some cases ($\frac{R}{L} > 0.5$, n = 6) the outer jets behaved differently to the central jet.

In order to relate all these equations into a single equation involving n, the number of outer jets, an additional point can be utilised. The single jet case when n = 0, gives L' = L. It is seen that plotting $\frac{L'}{L}$ against n would yield a family of graphs for different values of $\frac{R}{L}$, all passing through the point n = 0, $\frac{L'}{L}$ = 1, suggesting an exponential form of equation. The following equation was deduced from the experimental values for uniform configurations of nozzles.

$$\frac{L'}{L} = 2\left(0.389 + \frac{0.611}{\exp.0.396\ n}\right)\frac{R}{L} \qquad \ldots\ldots\ldots 4.6$$

where obviously R $\nmid$ L and R has no meaning when n = 0. This equation fitted all the results with a maximum error of $\pm$ 6.5%. At higher values of $\frac{R}{L}$ when the outer jets were closely spaced (i.e. for large n), the proximity of the outer jets to each other and the wall of the duct caused a more rapid axial velocity decay than the centre jet, and consequently a lower value of L'. Since this did not occur at the same value of $\frac{R}{L}$, when n = 2 and 3 it was concluded that wall effects were accentuated by increasing the number of outer jets.

The critical separation distance between the outer jets, and the duct wall was half the duct radius ($\frac{L}{2}$). In the present case, this meant that when $\frac{R}{L} > 0.5$ and $n \geq 6$ the outer jets will restrict each other, and hence behave differently to the central jet. By decreasing the number of outer jets the central jet was no longer fully bounded and could "see" beyond the outer jets to the wall of the duct. This was proved since when there were only two or three outer jets, the values of L' were greater than R. In order to assess the values of L' for the central and outer jets where these were different, the hydraulic mean diameter was used (see Ibiricu[28]). This diameter was that used for the calculation of Reynolds Number for fluids flowing in irregular shaped ducts or open channels[29]. In the calculation for multiple jet systems, the distances between the jets and the duct wall were used. When $\frac{R}{L} < 0.5$, the distance between the jets was small and was the limiting value in the calculation of the hydraulic mean diameter. When $\frac{R}{L} > 0.5$ the distance between outer jets and the duct wall was smaller than the distance between the jets and thus became the limiting value. Two stages were involved in the computation. Initially the central jet was

bounded by the outer jets and the duct wall, and so the initial hydraulic m mean diameter of the imaginary duct was thus harmonic mean of the pitch diameter of the jets and the duct diameter.

$$\text{Initial hydraulic mean diameter at } x = 0 \quad = \frac{4.LR}{L + R} \qquad \ldots\ldots\ldots\ldots 4.7$$

Further downstream, the jets were still separate when $\frac{R}{L} > 0.5$, and the value of the effective diameter of the duct was given by the average value of equation 4.3.

$$\text{Downstream Diameter} \quad = \quad 1.79\ R \qquad \ldots\ldots\ldots\ldots 4.8$$

The central jet can now be regarded as entering a conical section, of which the equivalent cylindrical radius can be computed as follows:-

$$L' \text{ central jet} \quad = \left[ \frac{\frac{4.LR}{L+R} \cdot 1.79R}{\frac{4.LR}{L+R} + 1.79R} \right] \qquad \ldots\ldots\ldots\ldots 4.9$$

this being half the hydraulic mean diameter. The value of L' for the outer jet can be calculated from this value and the average value from Equation 4.3. For the two cases in the present investigation when $\frac{R}{L} > 0.5$ and n = 6 and different characteristics were observed for the central and outer jets, the calculated value agreed with the experimental value, the maximum error being 3%.

### 4.2.2. Calculation and Correlation of Recirculation in Multiple Enclosed Jet Studies

The recirculation mass flow rate at any cross-section in the enclosed multiple jet arrangements studied, was calculated from the velocity profiles

obtained by traversing through and between the axes of the outer ring of jets. In the absence of a complete radial analysis at each section, the reverse flow was calculated by finding the average recirculation velocity and the area over which this velocity applied. The average recirculation velocity was found by integration of the velocity profiles, and the area for recirculation by subtracting the area for forward flow from the total duct cross-section. The double check of integration of the forward flow could not be applied to the multiple jet studies without a complete radial analysis. However, since the recirculation velocities were generally greater than those encountered in the single enclosed jet studies, their measurement was made more accurately. The turbulence intensities were quite small in the recirculation regions and so it was considered satisfactory to use the momentum flux velocity values rather than the mean velocity, since the latter would have involved the measurement of turbulence intensity. It has been shown in Appendix 4 that unless the system is highly turbulent with intensities of the order of 0.75 the error involved in this assumption will be less than 4.5%.

The values for the recirculation mass flow rate are given in Table 4.4. These are maximum values except when $\frac{R}{L} < 0.5$, where the values given are the recirculation mass flow rates in the region where L' applies. A comparison between the values of Table 4.4 and those for single jets given previously in Table 4.1. is given in Fig.23.

In the case of the downstream regions of the single equivalent jets ($\frac{R}{L} < 0.5$) the maximum recirculation was computed as before and the value of $\theta$ calculated from Ricou's theory. This assumed that the combined jet

TABLE 4.4. Recirculation in Multiple Jet Systems

| $(\frac{x}{L})_c$ | n | $r_o$ ins. | L' mean ins. | $\theta = \frac{r_o}{L'}$ | $A_r$ sq.ins. | $U_r$ ft/sec. | $M_r$ lb/hr. | $U_a$ ft/sec. | $M_o$ lb/hr. | $M_r/M_o$ | R ins. |
|---|---|---|---|---|---|---|---|---|---|---|---|
| 0.625 | 6 | 0.375 | 1.79 | 0.210 | 43.6 | 13.0 | 1105 | 70 | 421 | 2.625 | 2 |
| 0.375 | 6 | 0.25 | 1.79 | 0.140 | 43.1 | 10.6 | 891 | 80 | 214.2 | 4.16 | 2 |
| 0.625 | 6 | 0.375 | 2.35 | 0.160 | 46.2 | 17.9 | 1567 | 72 | 434 | 3.61 | 2.625 |
| 0.825 | 6 | 0.375 | 2.12 | 0.183 | 38.5 | 16.0 | 1200 | 68 | 410 | 2.93 | 2.375 |
| 0.825 | 6 | 0.25 | 2.35 | 0.107 | 45.4 | 19.9 | 1770 | 120 | 322 | 5.5 | 2.625 |
| 0.625 | 6 | 0.375 | 1.6 | 0.234 | 40.0 | 11.1 | 868 | 68 | 410 | 2.12 | 1.75 |
| 0.625 | 6 | 0.375 | 1.3 | 0.289 | 42.0 | 9.8 | 804 | 72 | 434 | 1.85 | 1.5 |
| 0.625 | 3 | 0.375 | 2.3 | 0.163 | 46.9 | 9.0 | 821 | 72 | 248 | 3.32 | 2 |
| 0.625 | 3 | 0.375 | 3.1 | 0.121 | 47.0 | 13.1 | 1205 | 71.5 | 246 | 4.9 | 2.625 |
| 0.625 | 3 | 0.25 | 3.1 | 0.081 | 47.0 | 15.5 | 1425 | 120 | 184 | 7.75 | 2.625 |
| 0.375 | 3 | 0.375 | 1.7 | 0.220 | 46.0 | 6.85 | 615 | 72 | 248 | 2.48 | 1.5 |

Where $U_a$ is average nozzle velocity

TABLE 4.5 Downstream Recirculation Mass flow rates when $R/L < 0.5$

| $(\frac{x}{L})_c$ | n | $r_o$ ins. | R | $r_o'$ ins. | $\Theta = \frac{r_o'}{L}$ | $A_r$ sq.ins. | $U_r$ ft/sec. | $M_r$ lb/hr. | $U_a$ ft/sec. | $M_o$ lb/hr. | $M_r/M_o$ |
|---|---|---|---|---|---|---|---|---|---|---|---|
| 1.625 | 6 | 0.375 | 1.5 | 0.99 | 0.247 | 35 | 15 | 1025 | 72 | 434 | 2.36 |
| 1.625 | 6 | 0.375 | 1.75 | 0.99 | 0.247 | 35.5 | 13 | 900 | 68 | 410 | 2.19 |
| 1.625 | 3 | 0.375 | 1.5 | 0.75 | 0.187 | 41 | 9 | 700 | 72 | 248 | 2.83 |

Where $r_o'$ is the equivalent radius of the combined jet $r_o' = \sqrt{(n+1)\, r_o^2}$

might have issued from a single nozzle of the same total cross-sectional area. The values of maximum recirculation mass flow rates are given in Table 4.5. The comparison between these values and thos of Table 4.1. are also shown in Fig.23.

The recirculation mass flow rates given in Table 4.5 were higher than those given for the same arrangement of jets in Table 4.5, since the maximum recirculation flow occurred after the jets had coalesced. In order to describe such systems it was better to use the equivalent nozzle radius to calculate $\theta$, since the equivalent duct radius L' would only apply for a limited distance downstream. When $\frac{R}{L} \geq 0.5$, L' was used since the jets retained their individuality and could be treated separately.

# CHAPTER 5

## CONCLUSIONS FROM THE ENCLOSED JET STUDIES

### 5.1. Single Enclosed Jets

The studies of single enclosed jets are simplified by the absence of an ambient air stream. The axial velocity decay characteristics are found to lie between the free jet and pipe flow cases as the relative nozzle size is increased. The axial decay of velocity is accelerated as $\theta$ is decreased from unity (pipe flow) to zero (free jet) (Figs. 3 and 4). It is also possible to correlate the recirculation of such systems by the use of the Thring-Newby parameter $\theta$. The equation calculated from the experimental data of Fig. 5 is:-

$$0.6 + \frac{M_r}{M_o} = \frac{0.66}{\theta} \qquad \ldots\ldots\ldots 5.1$$

This equation fits the experimental values with a maximum deviation of $\pm$ 5%.

### 5.2. Multiple Enclosed Jets

The recirculation and axial velocity decay characteristics of multiple enclosed jet systems can be related to those of single enclosed jets. This is achieved by considering each jet to be enclosed by an imaginary duct of radius L', obtained by comparison of the axial velocity decay curves with those of single jets (Figs. 21, 22 and 23). The obtained values of L' were then related to the nozzle configuration by the following empirical equation:-

$$\frac{L'}{L} = 2 \left\{ 0.389 + \frac{0.611}{\exp 0.396n} \right\} \frac{R}{L} \qquad \ldots\ldots\ldots 5.2$$

(where $\frac{R}{L} \gg 1$).

When $\frac{R}{L} > 0.5$ and $n = 6$, due to the proximity of each outer jet and the duct wall, the outer jets are observed to decay more rapidly than the central jet, resulting in different values of L'. The mean value is used for correlation in Equation 5.2. The value of L' for the central jet of such systems is obtained by initially reducing the aerodynamic network around the jet to a conical and then to a cylindrical chamber. This results in the equation:-

$$\frac{L'}{L} \text{ central} = \frac{7.16\,R}{4L + 1.79\,(R + L)} \qquad \ldots\ldots\ldots\ldots 5.3$$

for the central jet. $(\frac{R}{L} > 0.5 \quad n = 6)$. The value of L' from the outer jets can then be found from Equation 5.2. and 5.3.

When $\frac{R}{L} < 0.5$ the values of L' given by Equation 5.2 only apply in the vicinity of the nozzles. Further downstream the jets coalesce and thus the "separate duct" concept is invalid. The equivalent radius of the combined jet is calculated to give the same mass flow and nozzle exit velocity.

It is also possible to relate the recirculation of multiple jet systems to that of single jets by use of the parameter $\Theta$ (where $\Theta = \frac{r_o}{L}$ or $\frac{r_o'}{L}$ and L' = value in Equation 5.2). Comparison of multiple and single jet recirculation is good, (Fig. 23) the maximum error being $\pm$ 8% in Equation 5.2.

Photographs and visual observations of some multiple jet water flow patterns are shown to be in good agreement with those of air jets (Figs. 24 and Plate 7).

## 5.3. The Introduction of a Grid into Enclosed Multiple Jet Systems

The main effect of the grid is the deflection of the jets back into the recirculation zones. Each nozzle configuration has a critical downstream location, beyond which the grid causes outer recirculation prominence. Upstream of this location the recirculation to both zones is increased as the grid is moved towards the nozzles. In the two configurations studied ($n = 6$, $\frac{R}{L} = 0.5$ and $0.656$) when the jets are widely spaced ($\frac{R}{L} = 0.656$) the critical point is not observed and is assumed to be downstream of the experimental section ($\frac{x}{L} = 0$ to $\frac{x}{L} = 1.625$). For closer jet spacing ($\frac{R}{L} = 0.5$) the critical point can be observed at $\frac{x}{L} \simeq 1$. The critical point can be explained by the interference of the grid with the complex pressure fields of the multiple jet systems at the point when the jets are tending to coalesce. Obviously this point will be further downstream as $\frac{R}{L}$ is increased.

The variation of the grid resistance characteristics to cover a range comparable with marine boiler tube bank resistances had little effect on the flow patterns or axial velocity decay (Figs. 12 to 17).

Operation of the multiple jet systems with water shows that recirculation can occur back through the grid (Fig. 24 d and e, and Plates 8 and 9). This is not observed in air model studies due to measuring difficulties in the proximity of the grid.

## 5.4. Suggestions for further work

This study of multiple enclosed jets provides a basis for work on more practical systems. Such studies would include swirling jets, irregular

shaped enclosures, and side offtakes, as well as actual and novel boiler models. This would then enable more pertinent heat transfer studies to be made both from the steam raising and combustion aspects.

## CHAPTER 6

## SIMPLE CALCULATION OF THE HEAT TRANSFER IN MARINE BOILER TUBE BANKS

### 6.1. Introduction

Cohen and Fritz[41] have studied heat transfer in D-shaped marine boilers. The main purpose of this investigation was to investigate the control of superheat temperature without the use of dampers or attemperators. This was achieved by "turn off" of suitable burners and although the influence on final steam temperature was small, adverse operating efficiencies.were noticed. A complete temperature traverse at the inlet to the tube banks under overload conditions gave a maximum gas temperature of 3200°F at the centre, falling to 2300°F at the rear wall. The average gas temperature was 2950°F and the steam production at 120% of full power (overload conditions) was 314,000 lbs. per hour. An important result of the gas temperature traverses was that flow patterns are not affected subtantially by the right angle bend through which they have to pass to enter the tube banks. Under the same loading the average gas temperature was reduced to 2100°F at the inlet to the main generating tube banks and 1200°F at the exit.

The "shut down" of groups of burners to give 45% of full power conditions, showed that by using burners further away from the tube banks there was a decrease in superheater heat transfer and an increase in furnace heat absorption. This emphasised the importance of burner combinations for control of superheater temperatures.

### 6.2. Heat Transfer Calculations

It is shown in Appendix 3 that the tube banks of a selectable superheat boiler can be regarded for pressure drop calculations as equivalent to 29 staggered rows of 1" diameter tubes on a pitch of $1\frac{5}{8}$ inches.

Heat transfer calculations were made on this simple equivalent bank of tubes. The boiler model chosen was that described in Appendix 3, but the effect of the right angle gas offtake was not considered. The boiler was therefore 4' in equivalent chamber radius, and each burner diameter was $\frac{3}{4}$'.

Calculations of the heat transfer coefficient to banks of staggered tubes are based on the following equation recommended by McAdams[42].

$$\frac{h_m D_o}{K_f} = 0.3 \left(\frac{D_o G_m}{\mu_f}\right)^{0.6} \qquad \text{.....6.1}$$

where $D_o$ = outside diameter of tubes (feet)

$h_m$ is the heat transfer coefficient (B.Th.U./hr.ft.$^2$.$^\circ$F.)

$G_m$ is specific mass velocity between the tubes, based on the minimum area between the tubes (lb./hr.ft.$^2$)

$K_f$ is thermal conductivity of fluid at the film temperature $t_f$

$\mu_f$ is viscosity of fluid at the film temperature

$t_f$ is film temperature or arithmetic mean of surface temperature and bulk fluid temperature.

In the case of the main generating tube banks in the selectable superheat boiler

$D_o$ = $^1/_{12}$ feet = 0.0834 feet

$x$ = transverse pitch = 0.1354 feet

Minimum area for flow per unit area of tube bank $= \frac{0.1354 - 0.0834}{0.1354}$

$= 0.385$ ft.$^2$/ft.$^2$

For 29 rows of tubes in the equivalent tube bank

Heat transfer surface per unit area of tube bank $= \frac{\pi\ 29.}{1.625}$

$= 56\ ft.^2/ft.^2$

Let the steam temperature be 1000°F. and the average gas temperature be 2600°F.

$t_f = \frac{1000 + 2600}{2} = 1800°F$

$\therefore \rho_f = 0.0162$ lb./ft.$^3$ at 1800°F

$\mu_f = 0.1185$ f.p.h. units at 1800°F

$K_f = 0.048$ f.p.h. units at 1800°F

If the local velocity is U.ft./sec. at any point prior to the tube banks

$G_m = \frac{U \times 0.0162 \times 3600}{0.385} = 151.5\ U$ lb./hr.ft.$^2$

$\therefore Re = \frac{D_o G_m}{\mu_f} = \frac{151.5\ U}{12 \times 0.1185}$

$= 106.5\ U$

From equation 6.1.

$\frac{h_m D_o}{K_f} = 0.3\ (106.5\ U)^{0.6}$

$\therefore \frac{h_m D_o}{K_f} = 4.94\ U^{0.6}$

$h_m = \frac{0.048 \times 4.94\ U^{0.6}}{0.0834}$ B.Th.U./ft.$^2$hr.°F.

$= 2.84\ U^{0.6}$ B.Th.U./ft.$^2$hr.°F.

let us consider an element of tube bank in which the velocity is U.

Heat lost by convection = $h_m\ A\ \Delta T_m$

where A is the surface area of tubes

$\Delta T_m$ is the logarithmic mean temperature difference between surface and fluid

$\therefore$ Heat lost by convection = $2.84\ U^{0.6}\ 56\ \Delta T_m$ B.Th.U/hr.ft.$^2$ tube bank area

Heat lost by convection = $159.0\ U^{0.6}\ \Delta T_m$

Sensible heat lost by gases = $U.\ \rho_f.\ C_p.\ \Delta T\ 3600$ B.Th.U/hr.ft.$^2$ tube bank area

where $C_p$ = specific heat of gas = 0.31 B.Th.U/lb.$^\circ$F at 2600$^\circ$F

$\rho_f$ = density of combustion gases = 0.013 lb./ft.$^3$ at 2600$^\circ$F

Sensible Heat lost by gases = U x 0.013 x 0.31 x 3600 $\Delta$T

= 14.5 U. $\Delta$T. B.Th.U/hr.ft.$^2$

$\Delta T$ = temperature drop of waste gases

However, the heat lost by convection and the sensible heat losses by the gas are the same if tranverse heat transfer is neglected.

$$\therefore \quad 159.0\,U^{0.6}\ \Delta T_m = 14.5\ U.\ \Delta T$$

$$\frac{\Delta T_m}{\Delta T} = \frac{U^{0.4}}{11.0}$$

Substitute values of temperatures in equation

$$\log_e\left(\frac{2600 - 1000}{T_e - 1000}\right) = \frac{11.0}{U^{0.4}}$$

$$\therefore \quad \log_e\left(\frac{1600}{T_e - 1000}\right) = \frac{11.0}{U^{0.4}} \qquad \ldots\ldots\ldots\ 6.2$$

where $T_e$ is the temperature after passage through the tube banks.

Equation 6.2 indicates that for each velocity profile, a temperature profile can be plotted for the gas exit from the tube banks. Two calculations have been made, based on different gas inlet temperature assumptions.

(a) The gases were assumed to have a uniform temperature equal to the average value of 2600°F at the inlet to the tube banks.

(b) The gases were assumed to have a temperature proportional to their velocity. At the maximum velocity, the temperature was assumed to be 2950°F, and at zero velocity the temperature assumed was 1000°C. It was thought that the practical case might lie somewhere between these two extremes. The calculations were performed for six cases of burner spacings, and the cross-section chosen corresponded to the downstream average path length of the gases in a marine boiler. Reynolds similarity between the theoretical model and an actual marine boiler under operating conditions was observed.

From Appendix 3 for each burner the Reynolds Number under operating conditions is $3.47 \times 10^8$.

∴ Velocity in $\frac{3}{4}$" diameter burners = 1610 ft./sec. at 2900°F.

In the boiler average path length of gases = 8 ft. (half length and width)

∴ Downstream distance in $1/12$ scale model = 8".

Velocity maps at the inlet to the tube banks were plotted for each burner spacing, and the corresponding temperatures at the exit from the tube banks can be seen in Figs. 25 a-f for the two temperature assumptions. In general the main difference between the two temperature assumptions was that a more uniform exit temperature distribution was observed for the assumption

of uniform temperature at the inlet. For the calculation of recirculation temperatures, the gases were assumed to return through the full tube bank having been cooled to an average temperature of 1200°F by the first pass.

6.3. Conclusions

The calculations of heat transfer in marine boiler tube banks, based on the flow patterns observed in a simplified model, have indicated that tube bank exit temperatures in the region of 1900°F can be expected in regions of highest velocity caused by closer grouping of the burners. Calculations of probable recirculation temperatures have indicated that gases may re-enter the combustion chamber at temperatures in the region of 1060°F. On mixing with the hot combustion gases which are recirculated to the flames, these gases cause a reduction in flame temperature. Since one of the advantages of recirculation in pressure jet burner systems is flame stability caused by preheating the oil droplets before combustion, then adverse operating conditions can be expected if this preheat temperature is lowered by colder recirculated gases.

## APPENDIX 1

### THE STUDY OF A SINGLE ENCLOSED SWIRLING JET

The pressure jet oil burner is a complex system in which angular momentum is imparted to the combustion air, by passing it through an annulus around the oil atomiser which contains a mechanical swirling device. This consists of a circular arrangement of vanes inclined at an angle to the direction of flow, which is placed in the throat of the burner. There are two types of swirl, of which only one can be regarded as stable. This is the "free vortex" swirl system where the radial static pressure gradient is balanced by the centrifugal forces of rotation. In this condition there is no tendency for the jet to spread, other than by the normal entrainment process at the jet periphery. In common practice the unstable "forced vortex" swirl system is utilised in which the centrifugal forces are not balanced and so the jet diverges from the burner mouth. This gives a region of low static pressure on the jet axis, producing a recirculation zone which assists flame stabilisation by the recirculation of hot combustion products to both inside and outside fringes of the oil spray.

It is possible to achieve a similar flow pattern without swirl and investigation is required to decide whether it is the best means of achieving the desired characteristics of flame stability and high combustion intensity.

A preliminary study is made here of the effect of increased swirl on a single jet, using the simple T-pitot probe measuring technique. Although the effect of rotational flow on the probe is not known, it is possible to distinguish between the two types of swirl mentioned previously and also to detect the transition from one condition to the other (Fig. 26). The swirl

is characterized by taking the ratio of tangentially injected air to the total nozzle mass flow. Measurements of mass flows from the velocity traces were not attempted due to the uncertainty of the measuring technique. The results are plotted as velocity contours showing the effects of increasing degrees of swirl in Fig. 26. In these studies the nozzle diameter was $\frac{3}{4}$" and the radius of the duct 4". The relative quantity of tangentially injected air covers the range from 0 to 45% of the total flow. The results are compared with similar studies at the International Flame Research Foundation[47] carried out on an annular swirling free jet of outside diameter 25 centimeters in which the ratio of tangentially injected air varies from 0 to 67% of the total flow. To enable comparison, each swirling jet is related to the non swirling case by the parameter $U_m/U_{m_o}$.

$U_m$ = maximum forward velocity component in swirling jet at downstream point x

$U_{m_o}$ = maximum (i.e. axial) velocity in non-swirling jet of same diameter at downstream point x.

Similar trends are shown for each case in Fig. 26d, as the swirl characteristics of each jet were increased.

From the flow patterns shown in Fig. 26 it can be seen that increased swirl increases the angle of spread of the jet, finally resulting in forced vortex conditions at 35.4% tangential air input. At the maximum degree of swirl studied (45% of tangential air), wall jet conditions are observed with very low forward velocities occurring along the walls of the duct, and recirculation along the axis. Since the nozzle diameter is not varied, it is not possible to make a more detailed analysis of the results.

Conclusions

Increasing the proportion of tangential air flow in a swirling jet caused accelerated maximum velocity decay (Fig. 26d). Below a value of 35.4% tangential air, the conditions corresponded to free vortex swirl for a $\frac{3}{4}$" diameter nozzle and the jet did not spread from the axis other than by a normal jet entrainment and slight angular damping (Figs. 26 a and b). At 40.6% tangential air, the onset of forced vortex swirl was observed. Here the maximum velocity was not on the axis and symmetrical twin peaks were noted in velocity traverses. An axial recirculation zone was formed under forced vortex conditions and for the wall jet which occurred with 45% of tangential air, this was the only recirculation zone.

These results suggest the possibility of relating single and multiple swirling jets for the free vortex condition. At higher degrees of swirl, when the jet spread is greater, considerably more interaction between multiple jets is expected, and they are not expected to behave as separate enclosed single jets.

## APPENDIX 2

### CALIBRATION OF FLOW MEASURING DEVICES

(2a) The T shaped velocity probe

The T shaped velocity probe was calibrated by comparison with a standard N.P.L. pitot tube placed in the same stream. The calibration rig was built from a small perspex duct (Plate 1). The linear calibration (fig. 27) resulted in the equation

$$\text{Velocity at } 60^{\circ}F = 60.6\sqrt{\Delta p}$$

where $\Delta p$ = pressure differential (inches w.g.)

The probe was inclined at an angle to the gas flow to obtain the pitching and yawing characteristics (Figs. 28) . An angle of acceptance up to $45^{\circ}$ was observed from the yawing characteristic. This was useful, since much of the recirculation near the burners was non-axial in direction. The pitching characteristic in which the probe was turned about its own longitudinal axis, gave an angle of acceptance of $25^{\circ}$. Here the acceptance angle is defined as the maximum angle between the probe axis and the velocity vector at which the probe gives 95% of the true velocity reading.

(2b) The Nozzles

The calibration of the constrictions inside the nozzles was double-checked using orifice metering and a rotameter. The calibrations are given in Fig. 29. Although all nozzles except the central one (No.3) had the same sleeve inserted, different characteristics are observed, possibly due to the difficulty of exact positioning of the sleeve within the nozzle body.

(2c) The Pressure Transducer

The Beaudouin Pressure Transducer was calibrated with reference to the static pressure differential across a Prandtl micromanometer. The applied pressure differential could be read accurately to ± 0.0005" w.g. The calibration of the transducer for the various output ranges is given in Fig. 30.

(2d) The Supply Line Orifice

The diameter of the orifice used to meter the flow to the apparatus was calculated according to B.S.1042 Flow Measurement[43]. A flow sufficient to give a nozzle exit velocity of 100 feet per second in seven $\frac{3}{4}$" diameter jets, would also give a 10" water gauge pressure differential for a $1\frac{3}{4}$" diameter orifice in a 4" diameter pipe. The overall flow rate could be checked by summing the individual jet flows. The final equation calculated for the above orifice with air flow at 60°F was

$$Q = 2439 \sqrt{\Delta h}$$

where $Q$ = Volumetric flow rate (cu.ft./hr.)

$\Delta h$ = Pressure differential across orifice (ins. w.g.)

Table A.1. gives calculated and experimental values of $\Delta h$ from the equation calculated from the value of the volumetric flow rate Q.

TABLE A.1. Calibration data for Orifice Plate

| Mean Velocity in $\frac{3}{4}$" dia. nozzles ft./sec. | Q ft.$^3$/hr. | $\Delta h$ calc. ins. wg. | $\Delta h$ exp. ins. wg. |
|---|---|---|---|
| 80 | 6190 | 6.44 | 6.45 |
| 70 | 5410 | 4.94 | 4.90 |
| 60 | 4640 | 3.61 | 3.65 |
| 50 | 3870 | 2.51 | 2.5 |
| 40 | 3090 | 1.605 | 1.6 |
| 30 | 2320 | 0.9 | 0.9 |

## APPENDIX 3

## MODEL DESIGN CALCULATIONS AND OPERATING CONDITIONS

### (3a) Model Design Calculations

The duct used for the multiple jet investigations was one twelfth of the equivalent diameter of a typical marine boiler. Since a marine boiler front wall is not circular, the hydraulic mean diameter was calculated. The compact D shaped boiler shown in Plate 10 and Fig. 32 has a hydraulic mean diameter of 8'. Burner diameters of 1' were used in this boiler, although the operating dimension is smaller due to the blockage effect of the air register and atomiser.

It has been shown that the discharge coefficient of such an assembly is 0.65[45]. The equivalent radius is thus $\sqrt{0.65\ r_o^2}$ where $r_o$ is true diameter. This equation is based on mass flow and momentum equivalence. Since $r_o$ is 6", the equivalent radius $r_o'$ will be 4.85". Therefore, for modelling purposes the similarity parameter $\theta \left(\frac{r_o'}{L}\right)$ was 0.101. In the model, using a standard pipe size of $\frac{3}{4}$" inside diameter for the nozzles the parameter $\theta$ was 0.094 giving fair geometric similarity with the marine boiler. It proved impossible to construct a model with $\theta$ comparable to the hot operation of a marine boiler using the equivalent burner diameter suggested by Thring and Newby[21]. This would be approximately 2' in diameter giving $\theta = 0.25$. Since there were seven burners assembled on the front wall of the $^1/_{12}$ scale model, it can be seen that this would have been impossible to construct. It was thus decided to build the model with geometric similarity, and application of the results to operating conditions using an equivalent hot radius would be possible.

(3b) Operating Conditions and Dynamic Similarity

It is instructive to calculate the Reynolds Number in a typical marine boiler burner for both hot and cold conditions of operation.

Cold Operating Conditions

The oil flow to each burner was taken as 2100 lb./hr. which corresponds to a combustion air flow of 33600 lb./hr. (Air : Fuel Ratio 16 : 1). The equivalent unrestricted diameter of the burner was 10".

$$\text{Reynolds Number at } 60^{\circ}F = \frac{U.\ d.\ \rho_c}{\mu_c}$$

$d$ = diameter of burner = 0.834 feet

$U$ = velocity of air in burner

$\mu_c$ = viscosity of air at $60^{\circ}F.$ = $1.209 \times 10^{-5}$ f.p.s. units

$\rho_c$ = density of air at $60^{\circ}F.$ = 0.077 lb./cu.ft.

$$U = \frac{33600 \times 4}{3600 \times 0.077 \times \pi(0.834)^2} = 222 \text{ ft./sec.}$$

$$Re = \frac{222 \times 0.834 \times 0.077}{1.209 \times 10^{-5}} = 1.18 \times 10^{6}$$

Hot Operating Conditions

The temperature of the combustion gases was taken from Cohen and Frtiz's paper(41). The average temperature in the combustion chamber was given as $2900^{\circ}F.$ at full power conditions for a D shaped marine boiler. Assuming that the gases behave like air, and reach the burner throat at $2900^{\circ}F$, the

Reynolds number in the throat is therefore

$$\text{Reynolds Number at } 2900^{\circ}F = \frac{U.\ d.\ \rho_h}{\mu_h}$$

$\mu_h$ = viscosity of air at $2900^{\circ}F$ = $4.1 \times 10^{-5}$ f.p.s. units calculated from Sutherlands Formula(44).

$\rho_h$ = density of air at $2900^{\circ}F$. = 0.0118 lb./cu.ft.

$$U = \frac{33600 \times 4}{3600 \times 0.0118 \times \pi(0.834)^2} = 1450 \text{ ft./sec. at } 2900^{\circ}F.$$

$$Re = \frac{1450 \times 0.834 \times 0.0118}{4.1 \times 10^{-5}} = 3.47 \times 10^{5}$$

The equivalent diameter of the burner is given by:-

$$d' = d_c\sqrt{\frac{\rho_c}{\rho_h}} = 0.834\sqrt{\frac{0.077}{0.0118}} = 2.125 \text{ feet}$$

∴ The Reynolds Number based on this diameter is:-

$$Re = \frac{33600 \times 4 \times 2.125 \times 0.0118}{3600 \times 0.0118 \times \pi(2.125)^2 \times 4.1 \times 10^{-5}} = 1.36 \times 10^{5}$$

(3c) Reynolds Number in Model Studies

The maximum velocity which it was possible to obtain in the model was 80 ft./sec. for a $\frac{3}{4}$" diameter nozzle.

$$R_e \text{ at } 60^{\circ}F. = \frac{80 \times \frac{3}{4} \times 0.077}{12 \times 1.209 \times 10^{-5}} = 3.19 \times 10^{4}$$

The operating range of Reynolds numbers of the cold air model was less than that of operating marine boilers. Since flow patterns and mixing are essentially independent above Reynolds numbers of 10,000, it was considered

justifiable to operate the model at these lower values.

(3d) Grid Similarity and Pressure Drop through Tube Banks

It was necessary to establish some basis of similarity between the grids and a typical set of tube banks. Calculations were made using data giv n in McAdams[42] and it was possible to obtain a pressure drop versus specific mass flow rate characteristic for a tube bank. This can be compared with experimental results for the grid presented in the same form (Fig.31).

Pressure Drop Calculations for a Marine Boiler Tube Bank under full load conditions

Full details of the tube banks of a marine boiler of the selectable superheat type were obtained. A simplified diagram of this boiler is shown in Fig.32. The boiler has five 1' diameter burners and consequently at full load, the same fuel rate for each burner as that mentioned previously can be used. In the selectable superheat boiler, part of the waste gas flow passes down the superheater side of the bank, and part down the saturated steam side. Control of the steam requirements can be obtained by use of dampers which divert gas preferentially through either side of the tube banks. Calculations were made, assuming a uniform flow distribution, except through the superheater, for both hot and cold conditions of operation. The calculated characteristics are shown in Fig.31.

Cold Operating Conditions

The tube banks can be divided into six parts, three on each side of the boiler. The first two sections, which can be regarded as one for the calculation, are the fire tubes, which extend fully across the tube banks.

These are larger tubes than the rest of the bank, and a larger pitch gives radiant heat transfer to tubes other than the first row. Next the superheater section and the saturated steam pass are followed by the main steam generating bank of closely pitched tubes, which also extend across the full width of the furnaces. No effect of the dampers was considered, and in the superheater and saturated sections, the flow was assumed to be distributed so that the pressure drop across each side was equal.

Fire tubes - full width

Overall dimensions of tube bank 8' x 6.67' consisting of a staggered bank of 2" outside diameter tubes in which there are 18 tubes/row for 3 rows, tube pitch = $4\frac{7}{16}$". The total waste gas mass flow rate is 5 x 33600 = $1.68 \times 10^5$ lb./hr. = 46.7 lb./sec. (where 33600 lb./hr. is air requirement per burner as given previously).

Total free area of tubes = $8 \times 6.67 = 53.4$ ft.$^2$

Of this, area available for Flow = $8\left(6.67 - \frac{18 \times 2}{12}\right)$

= 29.3 ft.$^2$

$\therefore$ Specific Mass flow rate G = $\frac{46.7}{29.3}$

G = 1.59 lb./sec.ft.$^2$

Now Re at 60°F. = $\frac{D_o \; G}{\mu}$

where $D_o$ = diameter of tubes (feet)

G = specific mass flow lb./ft.$^2$sec.

$\mu$ = viscosity at 60°F. = $1.209 \times 10^{-5}$ f.p.s. units

Re at $60^{\circ}$F. $= \frac{2 \; 1.59 \; 10^5}{12 \; 1.209} = 2.2 \times 10^4$

Now $\Delta p = \frac{4 \; fN \; G^2}{2g_c \; \rho}$

where $\Delta p$ = pressure drop (lb./ft.)$^2$

$N$ = Number of rows of tubes

$g_c$ = gravity constant = 32.2 ft./sec.$^2$

$\rho$ = density of air at $60^{\circ}$F = 0.077 lb./cu.ft.

$f$ = friction factor $= \left(0.23 + \frac{0.11}{(x-1)^{1.08}}\right) Re^{-0.15}$

$x$ = pitch to tube diameter ratio where $1.5 < x < 4.0$

In this case $x = \frac{4\,7/16}{2} = 2.22$

$\therefore f = \left(0.23 + \frac{0.11}{(1.22)^{1.08}}\right) (2.2 \times 10^4)^{-0.15}$

$\therefore f = 0.0714$

$\therefore \Delta p = \frac{4 \times 0.0714 \times 3 \times 1.59^2}{2 \times 32.2 \times 0.077}$

$= 0.436$ lb./ft.$^2$ = 0.084 inches w.g.

Main Generating Bank - full width

Overall dimensions of tube bank 8' x 6.67' consisting of a staggered bank of 1" outside diameter tubes in which there are 47 tubes/row for 21 rows, tube pitch = $1\,5/8$". Here x will be 1.625. By a similar calculation to that above we obtain

$G = 2.1$ lb./ft.$^2$sec.

$Re = 1.45 \times 10^4$

$f = 0.098$

$\Delta p = 7.31$ lb./ft.$^2$ $= 1.41$ inches w.g.

Superheater and Saturated Bank

Details of superheater:- Free area $= 3.9' \times 8'$. The tubes are horizontal rather than vertical as in the other sections. There are 50 $1\frac{1}{4}$" outside diameter tubes per row in a staggered bank of 20 rows. The tube pitch $= 1.875$" giving $x = 1.5$. If the mass flow through the superheater is $m_s$ lb./sec.

Now area for flow $= 3.9 \left(8 - 50 \frac{1.25}{12}\right) = 10.91$ ft.$^2$

$\therefore$ Specific mass flow rate $= \dfrac{m_s}{10.91}$

$$Re = \frac{1.25 \; m_s \; 10^5}{12 \; 10.91 \; 1.209} = 7.89 \times 10^3 \; m_s$$

Now $$f = \left(0.23 + \frac{0.11}{(1.5 - 1)^{1.08}}\right) Re^{-0.15} = \frac{0.464}{Re^{0.15}}$$

$$\therefore \Delta p = \frac{4 \times 0.464 \times 20 \; m_s^2}{(7.89 \times 10^3)^{0.15} \; (m_s)^{0.15} \cdot 2 \times 32.2 \times 0.077 \; (10.91)^2}$$

$$= 0.0231 \; m_s^{1.85} \text{ in Superheater}$$

Details of Saturated Bank:- Free area $= 2.75' \times 8'$. There are 12 $1\frac{1}{2}$" outside diameter tubes/row in a staggered bank of 3 rows. The tube pitch $= 2\frac{7}{16}$" giving $x = 1.625$.

Now area for flow $= 8 \left(2.75 - \frac{12 \times 1.5}{12}\right) = 10$ ft.$^2$

mass flow rate = $(46.7 - m_s)$ lb./sec.

$\therefore$ Specific mass flow $G = \frac{(46.7 - m_s)}{10}$ lb./sec.ft.$^2$

$$Re = \frac{1.5\,(46.7 - m_s)\ 10^5}{12 \cdot 10 \cdot 1.209}$$

$$= 1.035 \times 10^3\ (46.7 - m_s)$$

$$f = \left(0.23 + \frac{0.11}{(0.625)^{1.08}}\right) Re^{-0.15}$$

$$= \frac{0.413}{Re^{0.15}}$$

$$\therefore \Delta p = \frac{4 \times 0.413 \times 3\ (46.7 - m_s)^2}{(1.035 \times 10^3)^{0.15}\ (46.7 - m_s)^{0.15}\ \ 2 \times 32.2 \times 0.077 \cdot 10^2}$$

$$= 0.00353\ (46.7 - m_s)^{1.85} \quad \text{for the Saturated Bank.}$$

If the mass flow is assumed to be distributed so that there is equal pressure drop across the two banks then:-

$$0.00353\ (46.7 - m_s)^{1.85} = 0.0231\ m_s^{1.85}$$

$$\therefore m_s = 12.4 \text{ lb./sec.}$$

$$\Delta p = 2.45 \text{ lb./ft.}^2 = 0.471 \text{ inches w.g.}$$

Total Pressure Drop across tube banks = 0.084 + 1.41 + 0.471

= 1.965 inches w.g. at $60^\circ$F.

Hot Operating Conditions

Similar calculations were made for the same tube banks but assuming an average gas temperature at the inlet of 2600°F. The pressure drops calculated for each section were as follows:-

| | | |
|---|---|---|
| $\Delta p$ fire tubes | = | 0.69 inches w.g. |
| $\Delta p$ superheater and saturated pass | = | 3.29 inches w.g. |
| $\Delta p$ main bank | = | 9.91 inches w.g. |

Thus the total pressure drop is 13.8 inches w.g. This is in good agreement with a practical value of 13 inches w.g. at full power.

It is also possible to calculate the number of rows of tubes contained in an equivalent bank composed entirely of generating bank tubes.

$$\text{Cold} \quad \frac{\Delta p \text{ total bank}}{\Delta p \text{ generating bank}} = \frac{N}{21} = \frac{1.965}{1.41}$$

$$\therefore \quad N = 29.3 \text{ rows}$$

$$\text{Hot} \quad \frac{\Delta p \text{ total bank}}{\Delta p \text{ generating bank}} = \frac{N}{21} = \frac{13.8}{9.91}$$

$$\therefore \quad N = 29.3 \text{ rows}$$

Since this figure seems independent of temperature it is possible to simplify other temperature calculations of pressure drop.

(3e) Comparison of tube banks with grids

The pressure drop across the tube banks of a marine boiler can be related to the specific mass flow rate, based on the full tube bank area, by an equation of the form

$$\Delta p = k \cdot G^{1.85}$$

$\Delta p$ is pressure drop (inches w.g.)

$G$ is specific mass flow rate based on total tube bank area (lb./sec.ft.$^2$)

$k$ is a constant (inches w.g./(lb./sec.ft.$^2$)$^{1.85}$

Values of k for both hot and cold operation are as follows:-

$k_{(2600^\circ F)}$ = 17.6 ins. w.g./(lb./sec.ft.$^2$)$^{1.85}$

$k_{(60^\circ F)}$ = 2.51 ins. w.g./(lb./sec.ft.$^2$)$^{1.85}$

The lines representing these conditions are compared with those values for the three grids in Fig. 31. The calibrations of the grids are given in Table A.2.

It can be seen from Fig. 31 that for cold flow conditions the values of the grid resistances used in the air model studies are of the same magnitude. The medium resistance grid has almost identical characteristics to the type of marine boiler tube banks analysed in the previous section. Presumably for higher waste gas temperatures, steeper slopes would be observed for all three grids, similar to those calculated for the tube banks for cold and hot operating conditions. It is concluded, therefore, that the range of grids studied covered a range of practical characteristics which can be encountered in marine boilers of both high and low ratings.

TABLE A.2. Grid Calibrations

| n | $r_o$ | $U_a$ | G | Grid 1 | Grid 2 | Grid 3 |
|---|---|---|---|---|---|---|
| | inches | ft./sec. | lb./sec.ft.$^2$ | ins. w.g. | ins. w.g. | ins. w.g. |
| 6 | 0.375 | 80 | 0.382 | 0.650 | 0.44 | 0.110 |
| 6 | 0.375 | 70 | 0.334 | 0.495 | 0.34 | 0.090 |
| 6 | 0.375 | 60 | 0.287 | 0.350 | 0.24 | 0.060 |
| 6 | 0.375 | 50 | 0.239 | 0.235 | 0.18 | 0.055 |
| 6 | 0.375 | 40 | 0.191 | 0.170 | 0.12 | 0.025 |
| 6 | 0.25 | 120 | 0.253 | 0.310 | 0.205 | 0.050 |
| 6 | 0.25 | 80 | 0.169 | 0.140 | 0.100 | 0.035 |
| 6 | 0.25 | 70 | 0.147 | 0.110 | 0.063 | 0.025 |

## APPENDIX 4

### Estimation of Errors due to Turbulence

In the present studies, the velocities measured are momentum flux velocities which are based on the mean line drawn through the pressure differential traces. Since the velocity is proportional to the square root of the differential pressure, the momentum flux velocity $\sqrt{\overline{U^2}}$ will be in error if the turbulence is appreciable. The definition of turbulence intensity given by Corrsin[46] was

$$T = \frac{U'}{\overline{U}}$$

where $T$ = turbulence intensity

$U'$ = turbulence velocity (deviation from mean velocity $\overline{U}$)

It follows that the time mean average of U is zero since

$$U = \overline{U} + U'$$

where $U$ = instantaneous velocity.

In the case of the momentum flux velocity recorded from pressure traces

$$\overline{U^2} = \overline{U}^2 + \overline{U'^2}$$

The time mean of $\overline{U'^2}$ is not zero so $\sqrt{\overline{U^2}}$ will differ from $\overline{U}$. In these error estimations it is assumed that some measure of the turbulence is indicated by the width of the pressure differential trace. If $\Delta p$ is the differential corresponding to the mean line through a trace then

Momentum flux velocity $\sqrt{\overline{U^2}} = K'' \sqrt{\Delta p}$ by definition

where $K''$ = probe constant

Now if $\pm \Delta p_t$ corresponds to the mean pressure differential of the turbulent peaks we can define the momentum flux turbulence intensity $T_m$ as

$$T_m = \sqrt{\frac{\Delta p_t}{\Delta p}}$$

Now the maximum and minimum velocities will therefore, be $K'' \sqrt{\Delta p + \Delta p_t}$ and $K'' \sqrt{\Delta p - \Delta p_t}$ respectively.

$$\therefore \quad \bar{U} = \frac{K''}{2} \left( \sqrt{\Delta p + \Delta p_t} + \sqrt{\Delta p - \Delta p_t} \right) \quad \text{by simple average.}$$

Simplification of this equation gives:-

$$\bar{U} = \sqrt{\frac{U^2}{2}} \left( \sqrt{1 + T_m^2} + \sqrt{1 - T_m^2} \right)$$

providing $T_m < 1$, which is true for the greater part of the pressure trace. At near to zero velocities, the fluctuations often exceed the mean pressure and in this case $T_m > 1$. The corresponding equation then becomes:-

$$\bar{U} = \sqrt{\frac{U^2}{2}} \left( \sqrt{1 + T_m^2} + \sqrt{T_m^2 - 1} \right)$$

When $T >> 1$ this equation reduces to

$$\bar{U} = T_m \sqrt{U^2}$$

This equation indicates that considerable error can be introduced by assuming $\bar{U} = \sqrt{U^2}$ under highly turbulent conditions. In the present studies measurements of velocity were not made under conditions of $T_m > 1$, except to locate the position of zero velocity. Here, where $T = \infty$ ($\bar{U} = 0$) it is assumed that the momentum flux velocity will also be zero.

In a system where $\bar{U}$ is the mean velocity and U' is the turbulent velocity, then the maximum and minimum velocities are $(\bar{U} + U')$ and $(\bar{U} - U')$ respectively. By squaring these velocities and taking the mean we can obtain the momentum flux velocity.

$$\overline{U^2} = \frac{1}{2}\left[(\bar{U} + U')^2 + (\bar{U} - U')^2\right]$$

The definition of the turbulence intensity is $U'/\bar{U}$ and the equation can be simplified to:-

$$\overline{U^2} = \bar{U}^2 (1 + T^2)$$

$$\sqrt{\overline{U^2}} = \bar{U}\sqrt{1 + T^2}$$

Hence from the two values of $\sqrt{\overline{U^2}} / \bar{U}$ we have:-

$$\left(\frac{2T}{1 + T^2}\right) = T_m^2$$

This equation corroborates Corrsin's observation[46] that the maximum error between the momentum flux velocity and the mean velocity in a free jet is 12% which corresponds to a value of $T = 0.57$.

In the present studies, apart from forward flow - recirculation boundaries, the maximum velocity fluctuations were about 75% of the mean pressure differential (i.e. $T_m = 0.75$). This gives a value of $T = 0.31$ which is in accord with Laurence and Benninghoff's[39] conclusion that the turbulence intensity of multiple nozzles is considerably less than in free jets. The error involved in using the momentum flux velocity rather than the mean velocity was therefore 4.5% when $T_m = 0.75$. It was concluded that using the momentum flux velocity in the present research is valid because the errors involved were quite small, and appreciable simplification in the calculations and experimentation were made.

## REFERENCES


1. RIGG C. — Ph.D. Thesis, University of Sheffield (in course of preparation), 1965.

2. ROSIN P.O. — (a) "Fuel in Science and Practice", 15, 136, (1936)
(b) "Aerodynamics as a Basis of Modern Fuel Practice", J.Inst.F., 9, 287, (1936)
(c) "Aerodynamics of Domestic Open Fires", J.Inst.F., 12, 198, (1939)

3. CHESTERS J.H., PHILLIP A.R., HOWES R.S. and HALLIDAY I.M.D., "Open Hearth Furnace Models", J.I.S.I., 162, 385, (1949)

4. CHESTERS J.H. — "Flow Patterns in the Open Hearth Furnace", Open Hearth Proc. A.I.M.E., 34, 282, (1951)

5. CHESTERS J.H. — "The Growth of an Idea", Iron and Coal Trades Review, 166, 179, (1953)

6. CHESTERS J.H., BACON N.P. and HALLIDAY I.M.D., "Flow Patterns in three-dimensional shapes", J.I.S.I., 196, 286, (1960)

7. CHESTERS J.H. — "The Aerodynamic Approach to Furnace Design", J.Eng.Power, Trans. A.S.M.E., 361, October (1959)

8. WINTER E.F. and DETERDING J.H., "Apparatus and techniques for the application of a water flow system to the study of aerodynamic systems", B.J.App.Phys., 7, 247, (1956)

9. PUTNAM A.A. and UNGAR E.W., "The Basic Principles of Combustion-Model Research", J.Eng.Power, Trans. A.S.M.E., 388, October (1959)

10. CURTIS R.W. and JOHNSON L.E., "Use of Flow Models for Boiler-Furnace Design", J.Eng.Power, Trans. A.S.M.E., 371, October (1959)

11. JOHNSTONE R.E. and THRING M.W., "Pilot Plants, Models and Scale-up Methods in Chemical Engineering", McGraw-Hill, New York, (1957)

12. TOLLMIEN W. — "Berechnung turbulenter Ausbreitungsvorgänge", Z. angew Math.Mech., 6, 468, (1926), Translated, N.A.C.A., Tech. Memo 1085 (1945)

13. HOWARTH L. — "Concerning the Velocity and Temperature distributions in plane and axially symmetrical jets", Proc. Cambridge Phil. Soc., 34, 185, (1938)

14. TOMOTIKA S. "Application of the modified Vorticity-Transfer theory to the turbulent spreading of a jet of air", Proc. Roy. Soc., A165, 65, (1938)

15. ABRAMOVICH G. Central Aerohydrodynamical Inst. Rep. 377, Moscow, Translated N.A.C.A. Tech. Memo 1058 (1939)

16. PRANDIT H. (a) "The Essentials of Fluid Dynamics", Blackie & Sons, London, (1952)
(b) "Bericht über Untersuchungen zur ausgebildeten Turbulenz", Z. angew Math. Mech., 5, (2), 136, (1925)
(c) Bemerkungen zur Theorie der freien Turbulenz", Z. angew Math. Mech., 22, 241, (1942)

17. TAYLOR G.I. (a) "The Transport of Vorticity and Heat through Fluids in Turbulent Motion", Proc. Roy. Soc., 135A, 685, (1932)
(b) "Flow in Pipes and between Parallel Planes", Proc. Roy. Soc., 151A, 494, (1935)
(c) "The Distribution of Velocity and Temperature between Concentric Rotating Cylinders", Proc. Roy. Soc., 159A, 496, (1937)

18. REICHARDT H. (a) Z. angew Math. Mech. 21, (1941) Translated Roy. Aero Soc. J., 47, 167, (1943)
(b) V.D.I. Forschungsheft, 414, (1942)
(c) Z. angew Math. Mech. 24, 268, (1944)

19. BARON T. and ALEXANDER L.G., "Momentum, Mass and Heat Transfer in free jets", C.E.P., 47, 181, (1951)

20. RICOU F.P. "Measurement of the entrainment by turbulent jets", Ph.D. Thesis, Imperial College, London, January (1960)

21. THRING M.W. and NEWBY M.P., "Combustion Length of Enclosed Turbulent Jet Flames", 4th Symp. (International) on Combn., 789, Williams and Wilkins Co., Baltimore, U.S.A., (1953)

22. HINZE J.O. and VAN DER HEGGE ZIJNEN B.G., "Transfer of Heat and Matter in the Turbulent Mixing Zone of an Axially Symmetrical Jet", Appl.Sci.Res., The Hague, A1, 435, (1949)

23. SUNAVALA P.D., HULSE C. and THRING M.W., "Mixing and Combustion in Free and Enclosed Turbulent Jet Diffusion Flames", Combustion and Flame, 1, 179, (1957)

24. CRAYA A. and CURTET R., "Sur L'évolution d'un jet en espace confiné", C.R.A.Se, Paris T241, August (1955)

25. CURTET R.

(a) "Confined Jets and Recirculation Phenomena with Cold Air", Combustion and Flame, 2, 383, (1958)
(b) "Contribution à l'étude du melange des jets", 6th Congrès, A.I.R.H., La Haye, September (1955)
(c) "Sur L'écoulement d'un jet entre parois", Publications Scientifiques et Techniques du Ministère de L'Air, No.359, (1960)

26. COHEN de LARA G. et al.,

(a) "Étude sur le four expérimental d'IJmuiden de la diffusion des jets d'air schématisant les flammes de gaz et de combustibles liquid", I.F.R.F. Doc. No. F.17/b/1.
(b) "Étude aerodynamique des phenomènes de recirculation dans un modèle schématique de fours à flammes de diffusion de section circulaire", I.F.R.F. Doc. No. F.17/b/3
(c) "Essais préliminaires sur des modèles de sections de formes carrée et circulaire", I.F.R.F. Doc. No. F.17/b/2
(d) "Étude de la recirculation dans les modèles schématiques de fours à flammes de diffusion. Influence de la longeur du four et des modes d'alimentation en air de combustion". I.F.R.F. Doc. No. G.61/b/2
(e) "Étude de la recirculation dans les modèles schématiques de fours à flammes de diffusion. Influence du diametre du brûleur et de la conicité de la chambre de melange", I.F.R.F. Doc.No. G.61/b/3
(f) "Étude de la recirculation dans les modèles schématiques de fours à flammes de diffusion", Troisième Journée d'Étude sur les Flammes, Paris (1958)
(g) "Étude expérimentales des paramètres géométriques et dynamiques intervenant sur les phénomène de recirculation dans un modèle de four de section circulaire", Quatrième Journée d'Étude sur les Flammes, Paris (1961)

27. HUBBARD E.H. "Recirculation in cold models of Furnaces", A Review of work at SOGREAH, J.Inst.F., 35, 160, (1962)

28. IBIRICU M.M. "Recirculation", Ph.D. Thesis, University of Sheffield, (1962)

29. CHEMICAL ENGINEERS HANDBOOK, Editor J.H.Perry, McGraw-Hill, New York, 3rd Edition, (1950)

30. SQUIRE H.B. and TROUNCER J., "Round Jets in a General Stream", Aeronautical Research Council No. 1974 (1944)

31. FORSTALL W. and SHAPIRO A.H.,
(a) "Momentum and Mass Transfer in co-axial gas jets", J.Appl.Mech., 17, 399, (1950)
(b) "Momentum and Mass Transfer in co-axial gas jets", J.Appl.Mech., 18, 219, (1951)

32. CHIGIER N.A. and BEÉR J.M., "Velocity Fields in double concentric jets", I.F.R.F. Doc. No. G.02/a/1

33. CHIGIER N.A. and BEÉR J.M., "The Flow Region near the Nozzle in Double Concentric Jets", I.F.R.F. Doc. No. G.02/a/6

34. PATRICK M.A. Ph.D. Thesis, University of Sheffield (in course of preparation) 1965

35. WRIGHT F.H. "Multiple Flameholder Arrays: Flame Interactions", J.Amer.Rocket Soc., 29, 143, (1959)

36. CORRSIN S. "Investigation of the behaviour of parallel two-dimensional jets", N.A.C.A., A.C.R., 4H24, November,(1944)

37. GRAN OLLSEN R. "Geschwindigkerts - und Tempertur - hinter einem Gitter bei turbulenter veiteilung Strom̈ung Z. angew Math. Mech. 16, 257, (1936)

38. CORDES G. "Untersuchungen zur Stratischen Druckmessung in turbulenter strom̈ung", Ing. Archiv., 8, 245, (1937)

39. LAURENCE J.C. and BENNINGHOFF J.M., "Turbulence Measurements in Multiple Interfering Air Jets", N.A.C.A., T.N.4029, December (1957)

40. PENGELLY A.E.
(a) "The measurement of gas velocities in flames and furnaces", I.F.R.F. Doc. No. F.72/a/5, (1959)
(b) "Apparatus for the measurement of gas velocity in furnaces and models", J.Sci.Inst., 37, 339, (1960)
(c) "High Speed Instruments for Combustion Research", Sheffield University Fuel Soc.J., 11, 40, (1960)
(d) "New Equipment for Flame and Furnace Research", J.Inst.F., 35, 210, (1962)

41. COHEN L. and FRITZ W.A., Jr., "Heat Transfer Studies of Naval Boilers", Trans. A.S.M.E., 80, 683, (1958)

42. McADAMS W.H. "Heat Transmission", McGraw-Hill, New York, 3rd Edition, (1954)

43. BRITISH STANDARD SPECIFICATION 1042 "Flow Measurement", (1943)

44. TECHNICAL DATA ON FUEL, Editor, H.M. Spiers, British National Committee World Power Conference, London, 5th Edition, 63, (1955)

45. McNAIR E.J. Private Communication, 1961

46. CORRSIN S. "Investigation of the flow in an axially symmetrical heated jet of air", N.A.C.A., A.R.C. 3L23, Wartime Rep. W-94, (1943)

47. BEER J.M. and CHIGIER N.A., "Swirling Jet Flames issuing from an Annular Burner", I.F.R.F. Doc. No. K.20/a/9.

Fig. No. 1 - Comparison of Multiple Free Jet Data with Free Jet Data of Hinze

# $U_o/U_m$ VERSUS $X/d_e$ FOR VARIOUS NOZZLE ASSEMBLIES

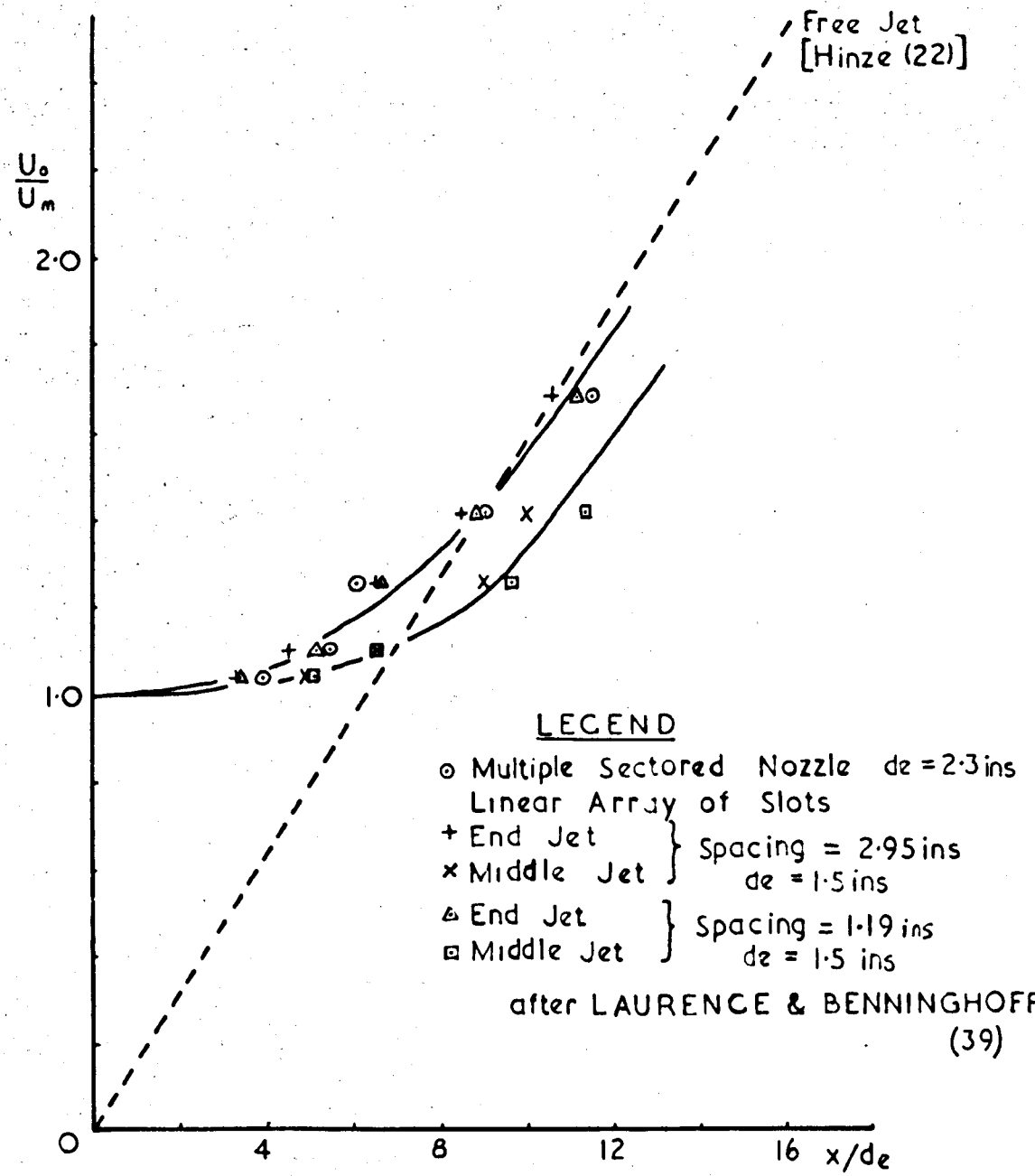


FIG. 1 COMPARISON OF MULTIPLE FREE JET DATA WITH THE FREE JET DATA OF HINZE

Fig. No. 2 - Diagram of Perspex Model used in Multiple Enclosed Jet Studies

FIG. 2 DIAGRAM OF THE PERSPEX MODEL

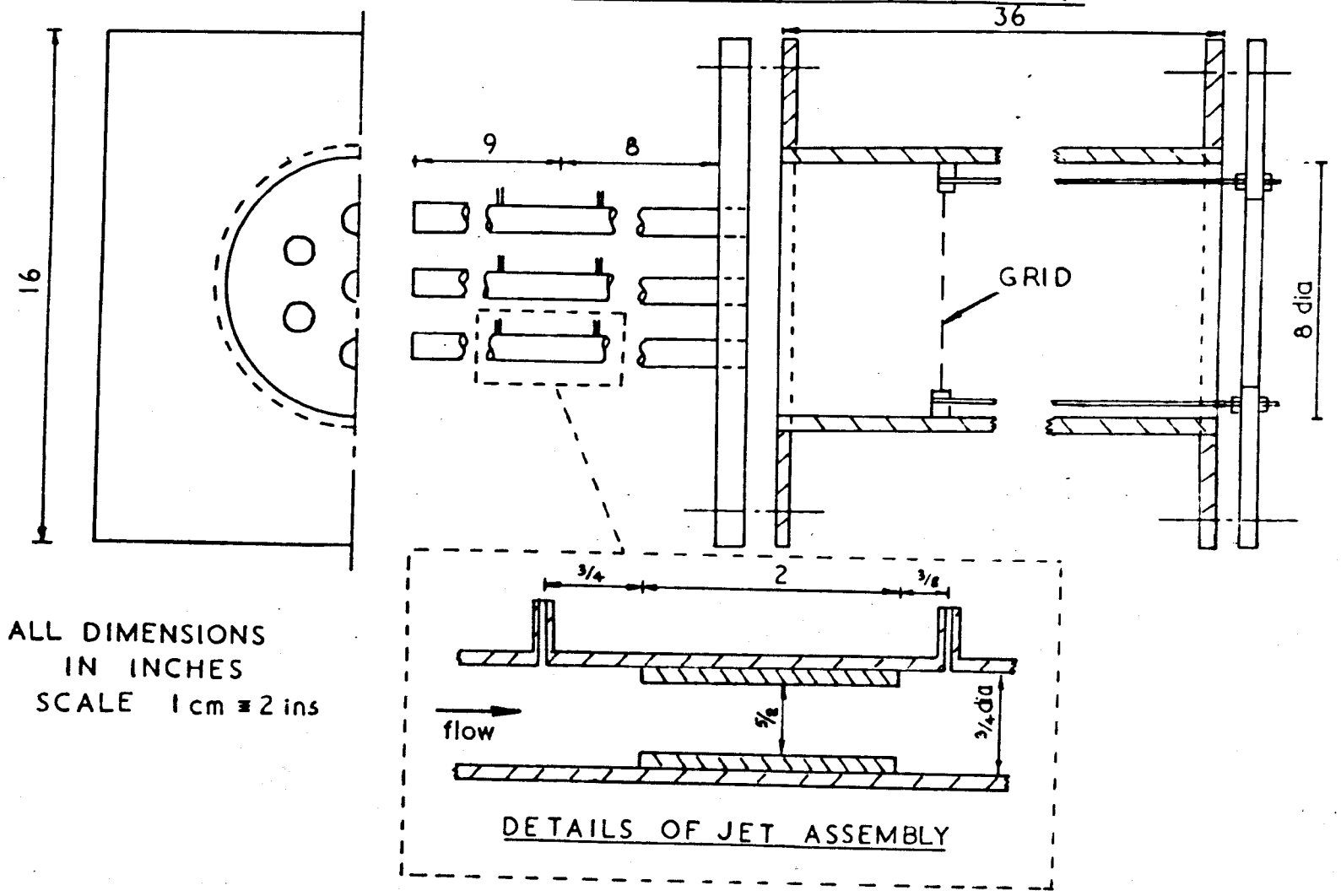


ALL DIMENSIONS
IN INCHES
SCALE 1 cm ≡ 2 ins

Fig. No. 3 - Axial Decay of Velocity in Single Enclosed Jets for $\Theta$ from 0.063 to 0.446

Fig. No. 4 - Axial Decay of Velocity in Single Enclosed Jets for $\Theta$ from 0.486 to 0.669

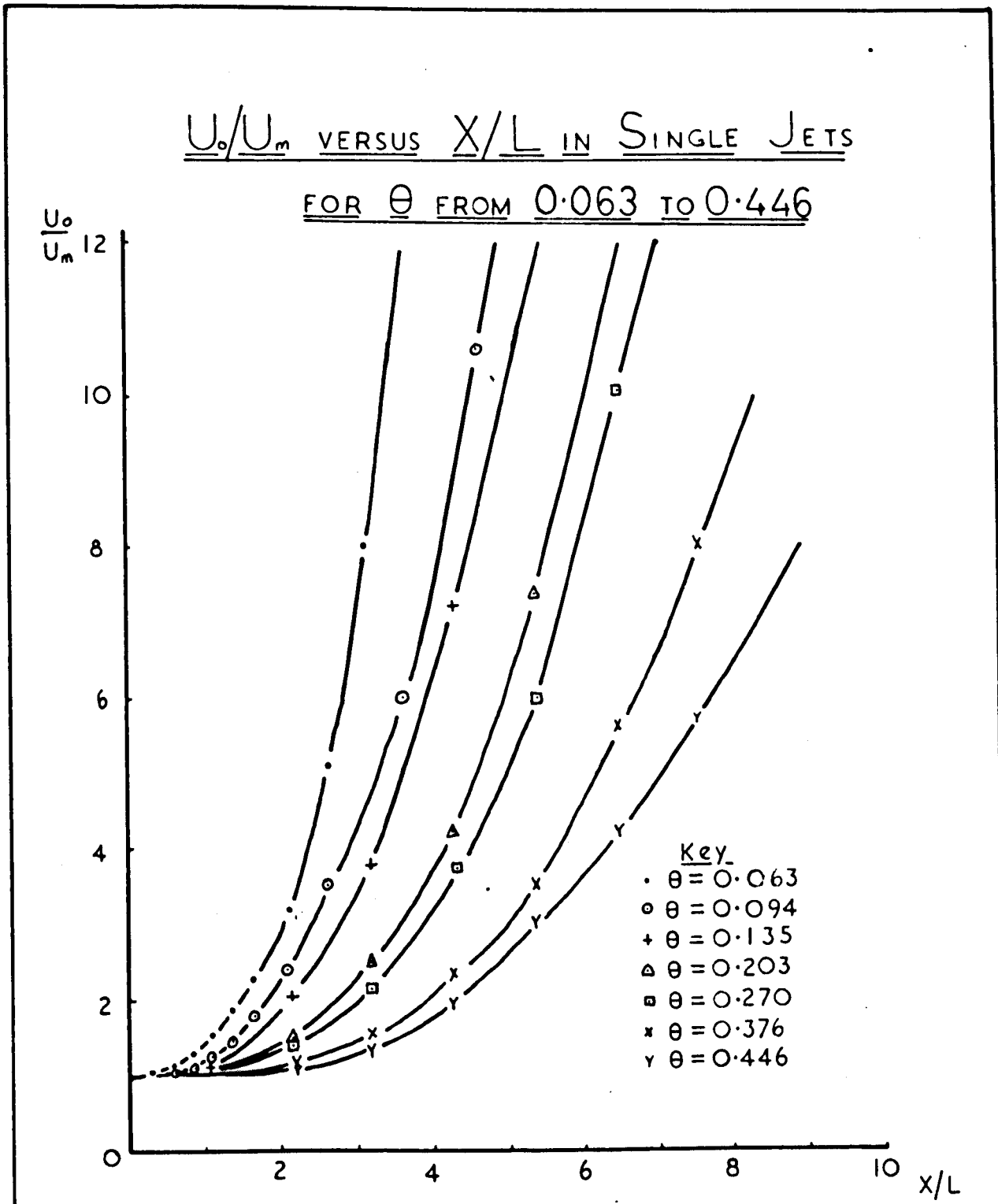


FIG. 3. AXIAL DECAY OF VELOCITY IN SINGLE JETS

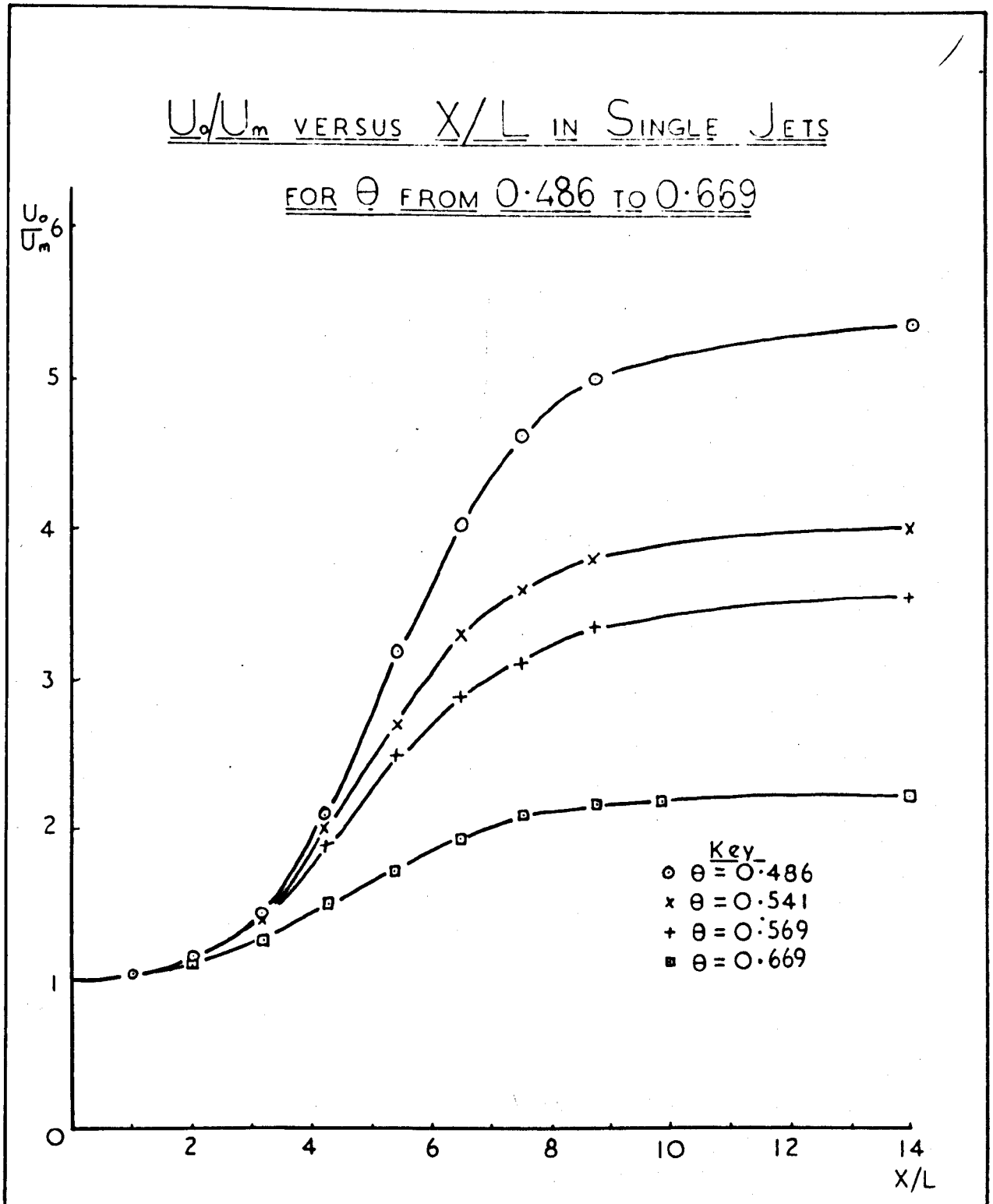


FIG. 4. AXIAL DECAY OF VELOCITY IN SINGLE JETS

Fig. No. 5 - Recirculation in Single Enclosed Jet Systems

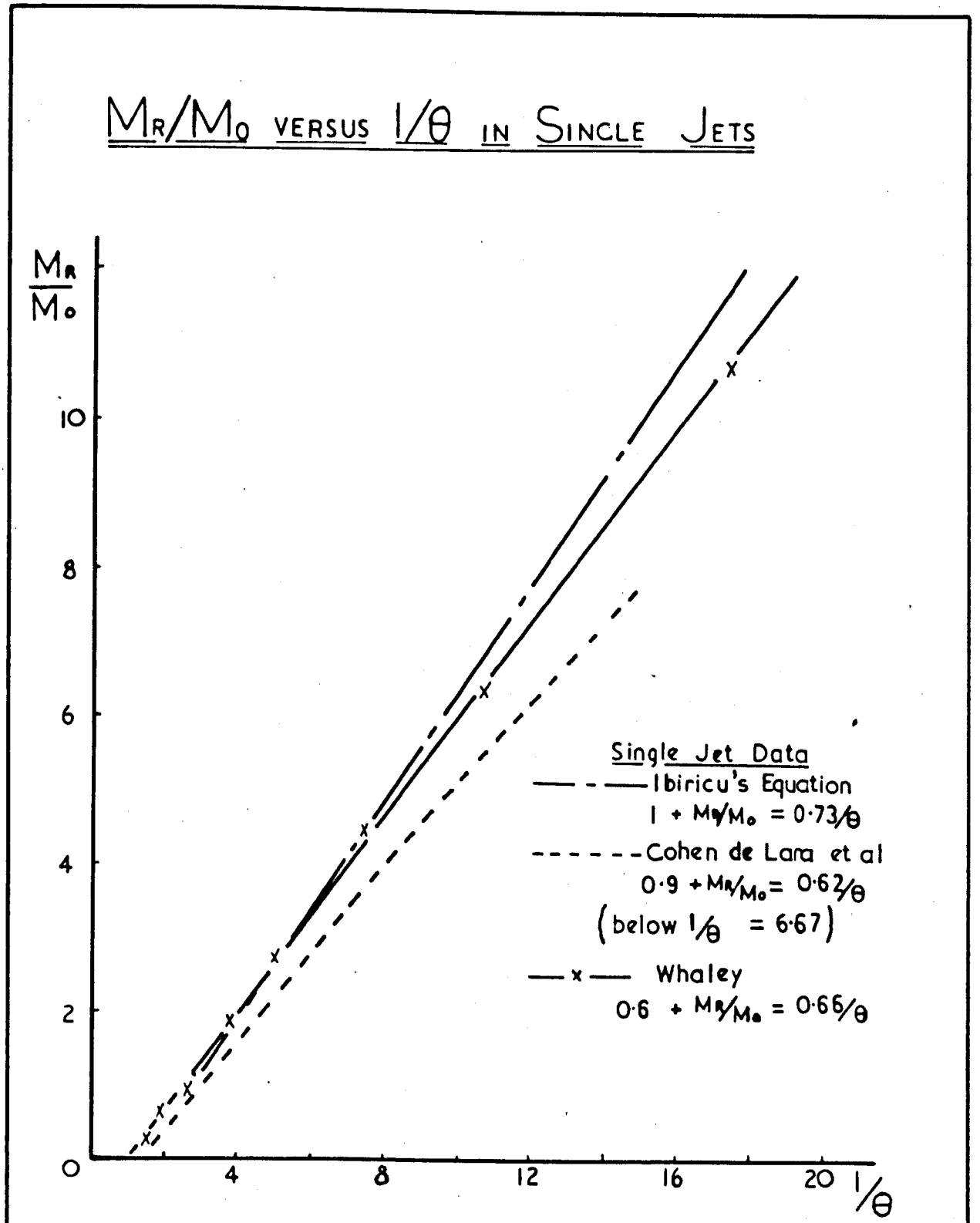


FIG. 5. RECIRCULATION IN SINGLE JET SYSTEMS

Fig. No. 6 - Variation of Nozzle Velocity in Multiple Enclosed Jets. Effect on axial velocity decay when $R = 2"$, $n = 6$, $r_o = 0.375"$

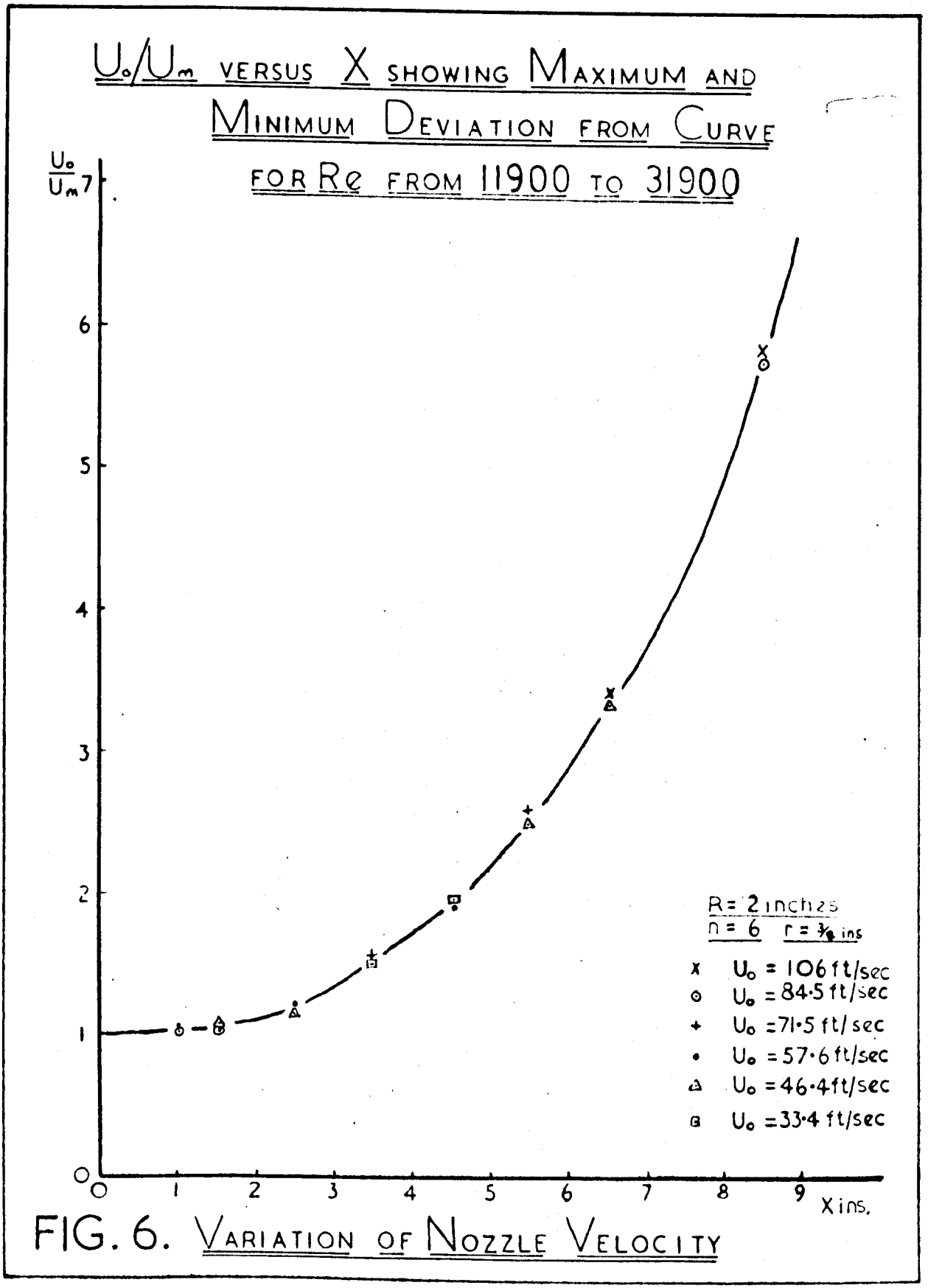


FIG. 6. VARIATION OF NOZZLE VELOCITY

Fig. No. 7 - Velocity Contours when R = 2", n = 6, $r_o$ = 0.375" for nozzle Reynolds Numbers from 11950 to 31900

Fig. No. 8 - Velocity Contours when R = 2", n = 6, $r_o$ = 0.25" for nozzle Reynolds Numbers from 10620 to 31900

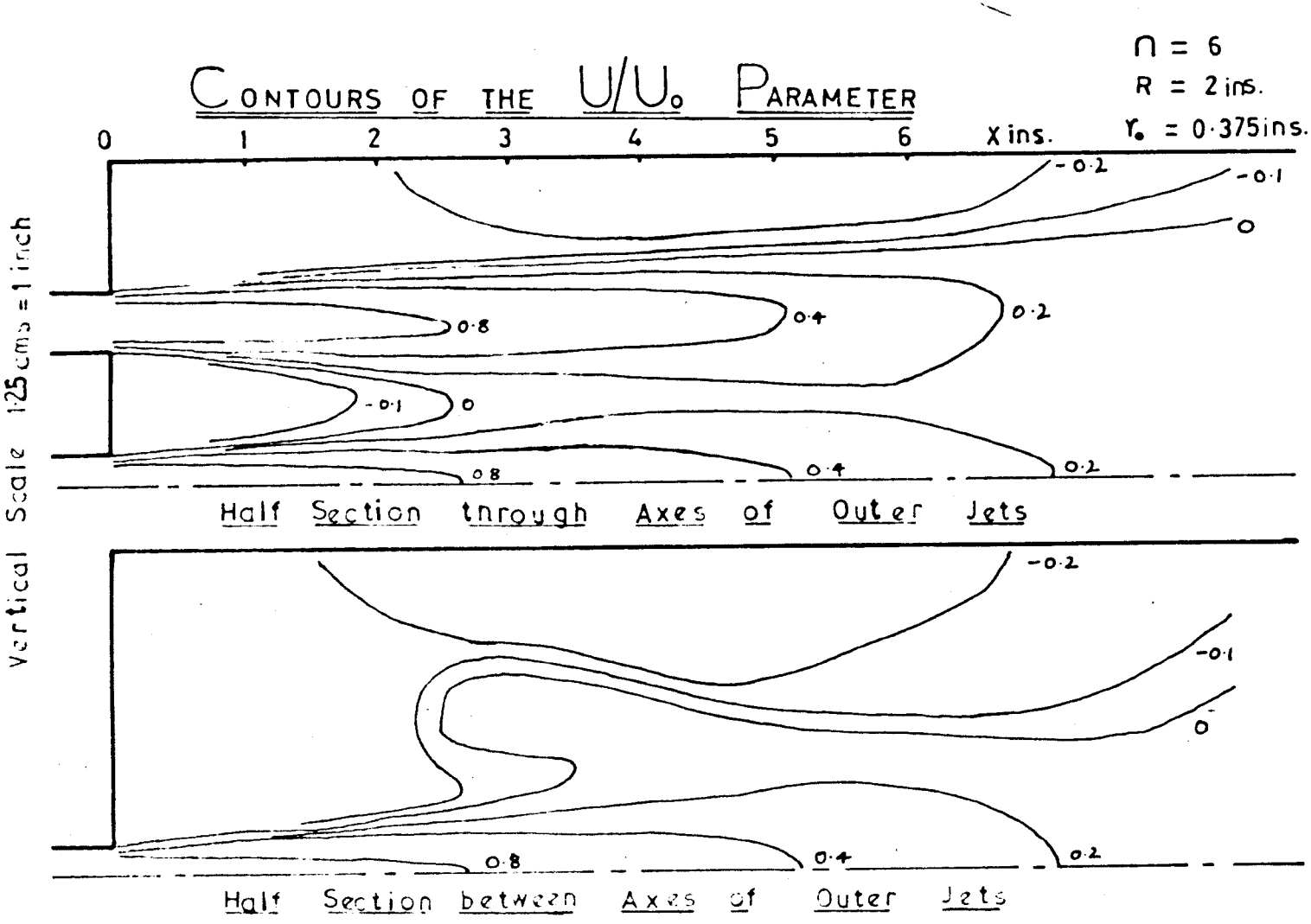


FIG. 7a PEAK VELOCITY IN JETS: 106 FT/SEC ($R_e$ = 31900)

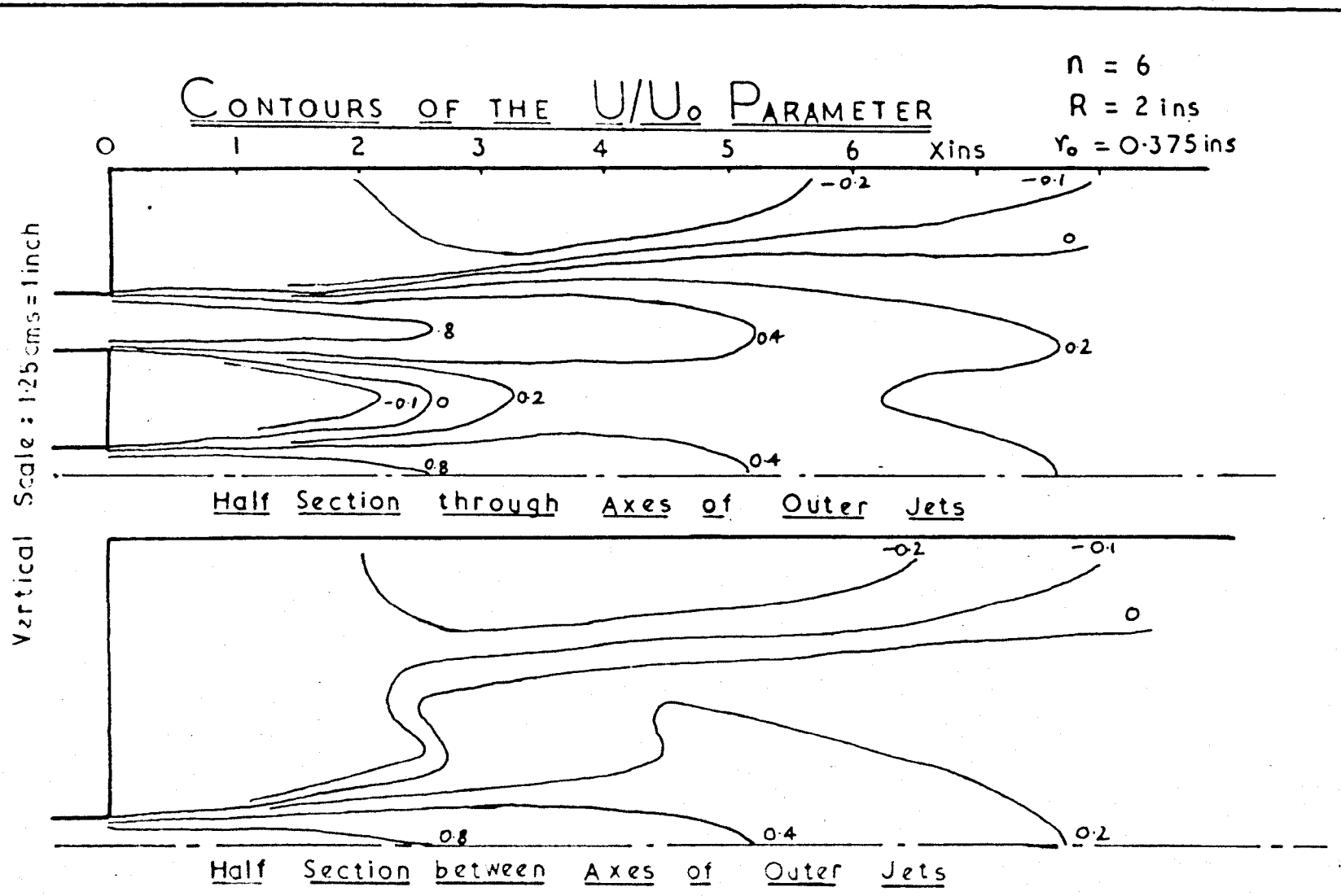


FIG. 7b PEAK VELOCITY IN JETS : 84·5 FT/SEC (Re = 27900)

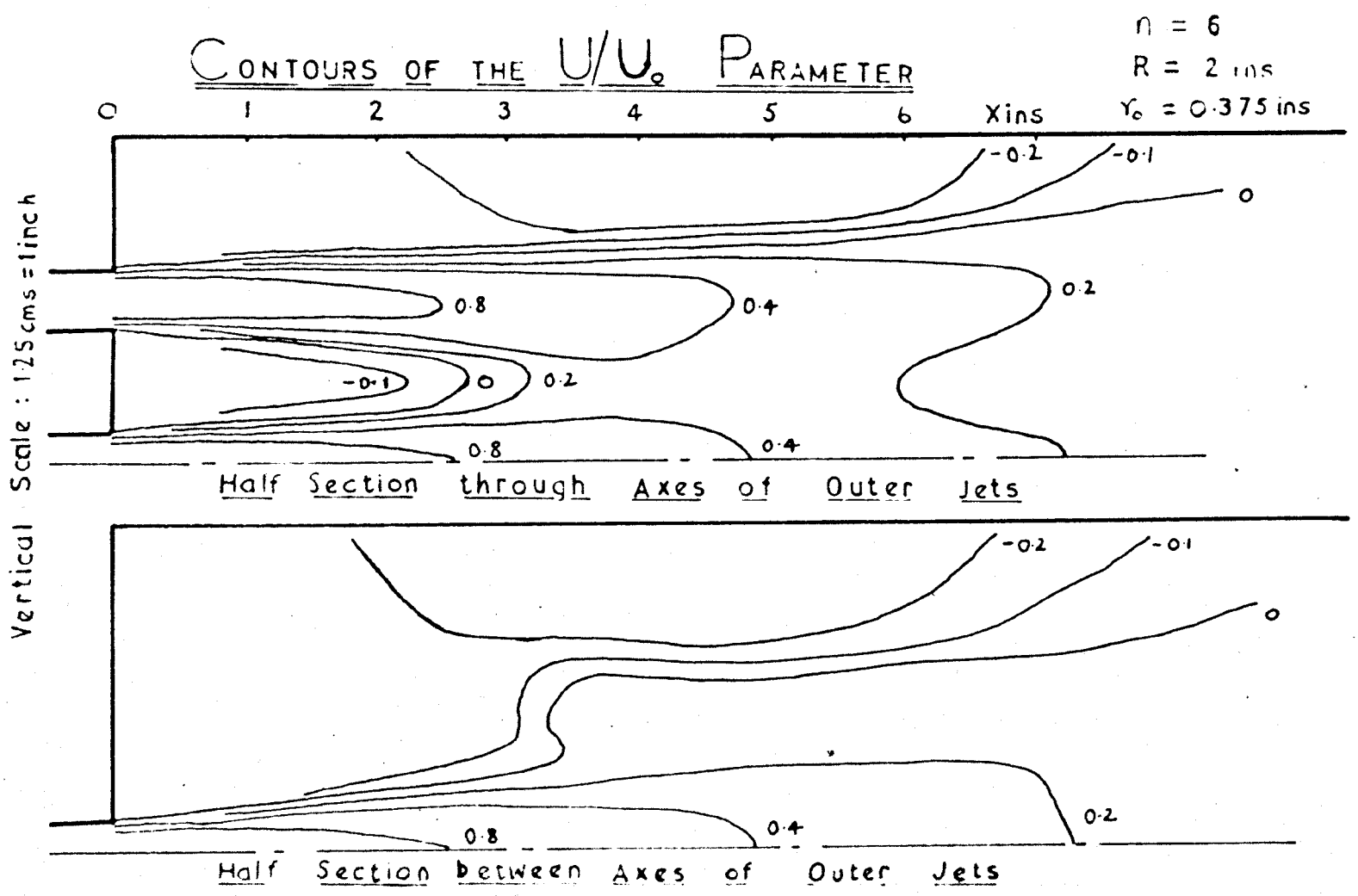


FIG. 7c PEAK VELOCITY IN JETS : 71·5 FT/SEC (Re = 23900)

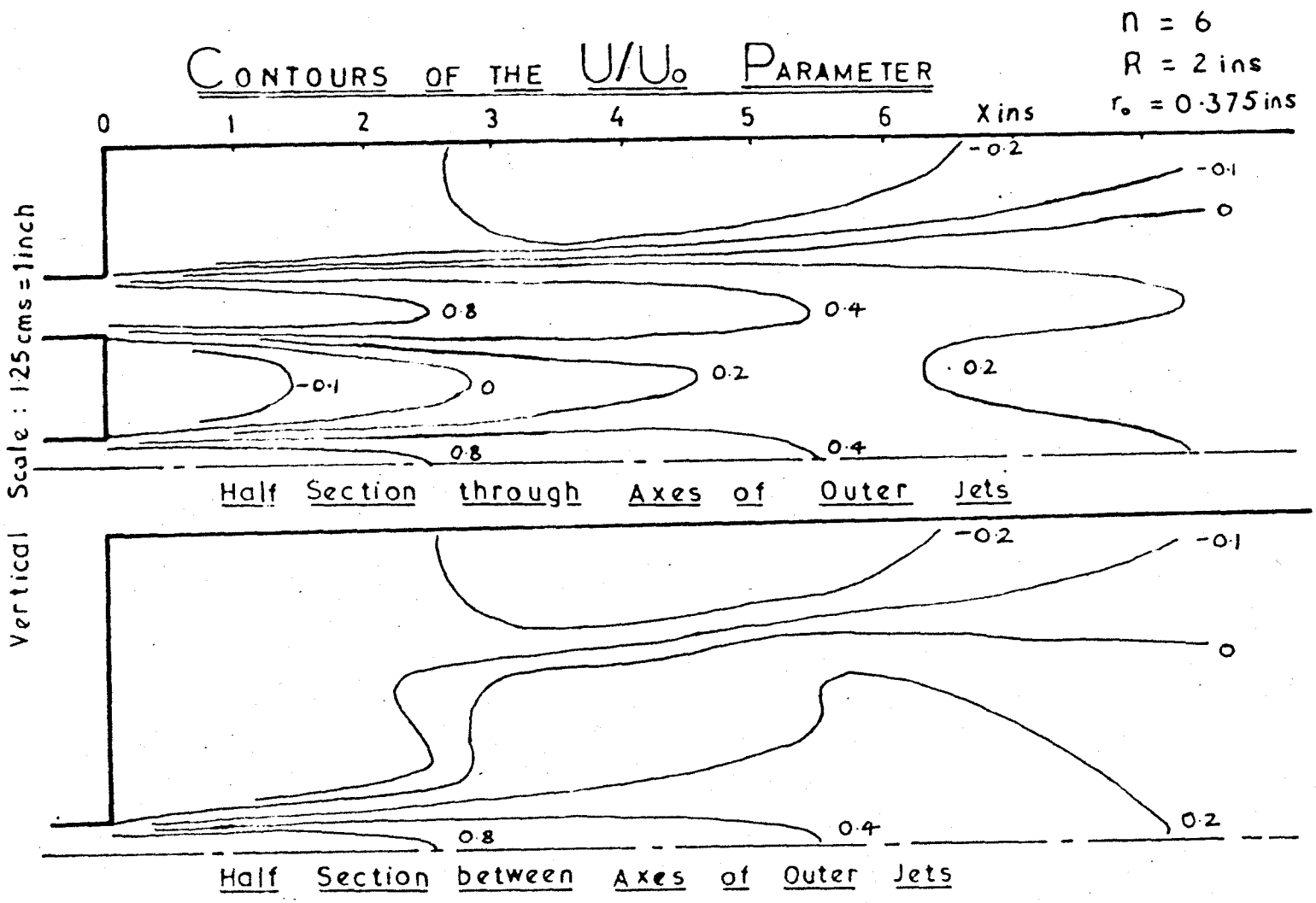


FIG. 7d PEAK VELOCITY IN JETS : 57·6 FT SEC (Re = 19900)

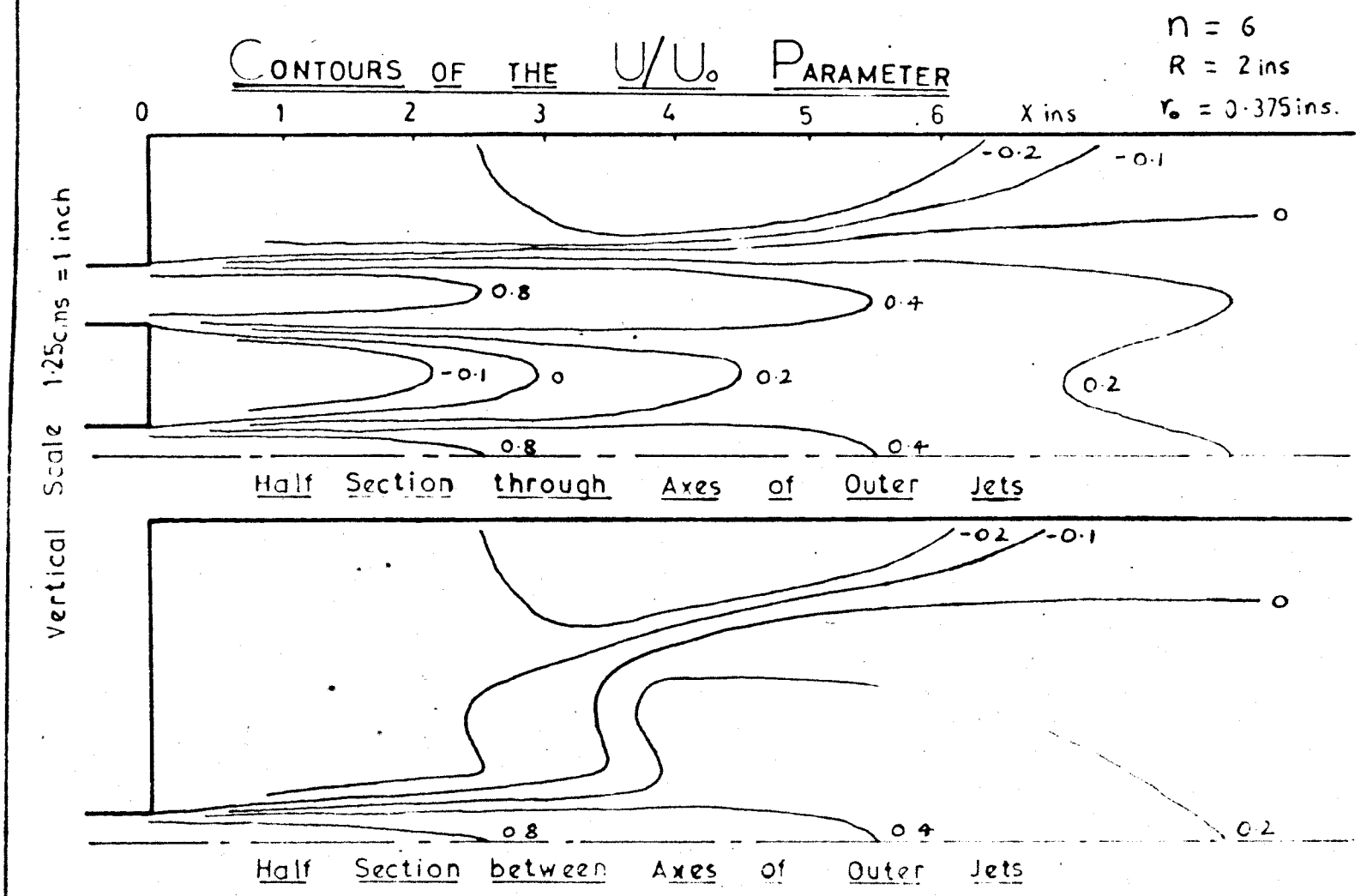


FIG. 7e PEAK VELOCITY IN JETS : 46·4 FT/SEC (Re = 15950)

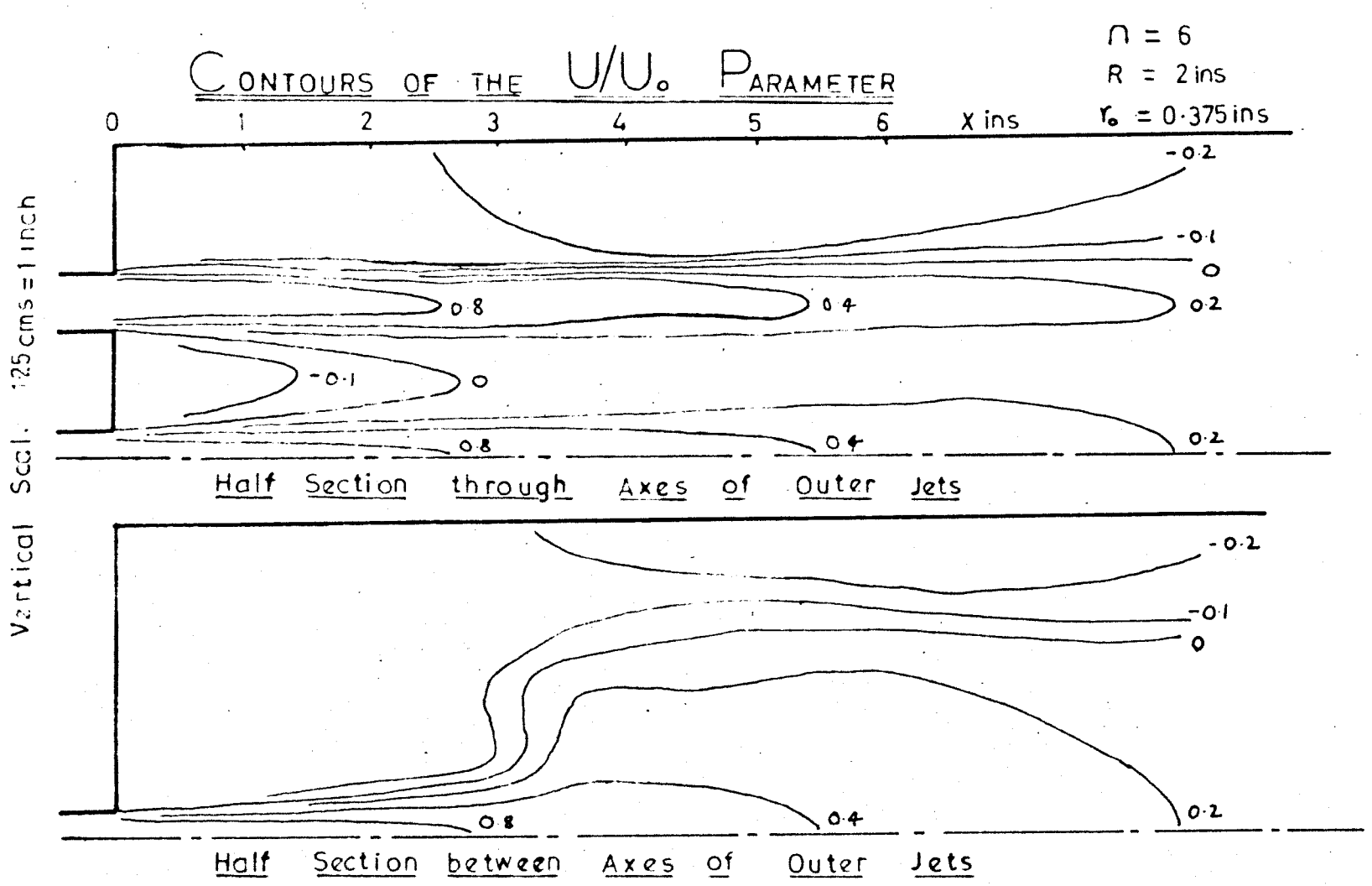


FIG. 7f PEAK VELOCITY IN JETS 33·4 FT/SEC (Re=11950)

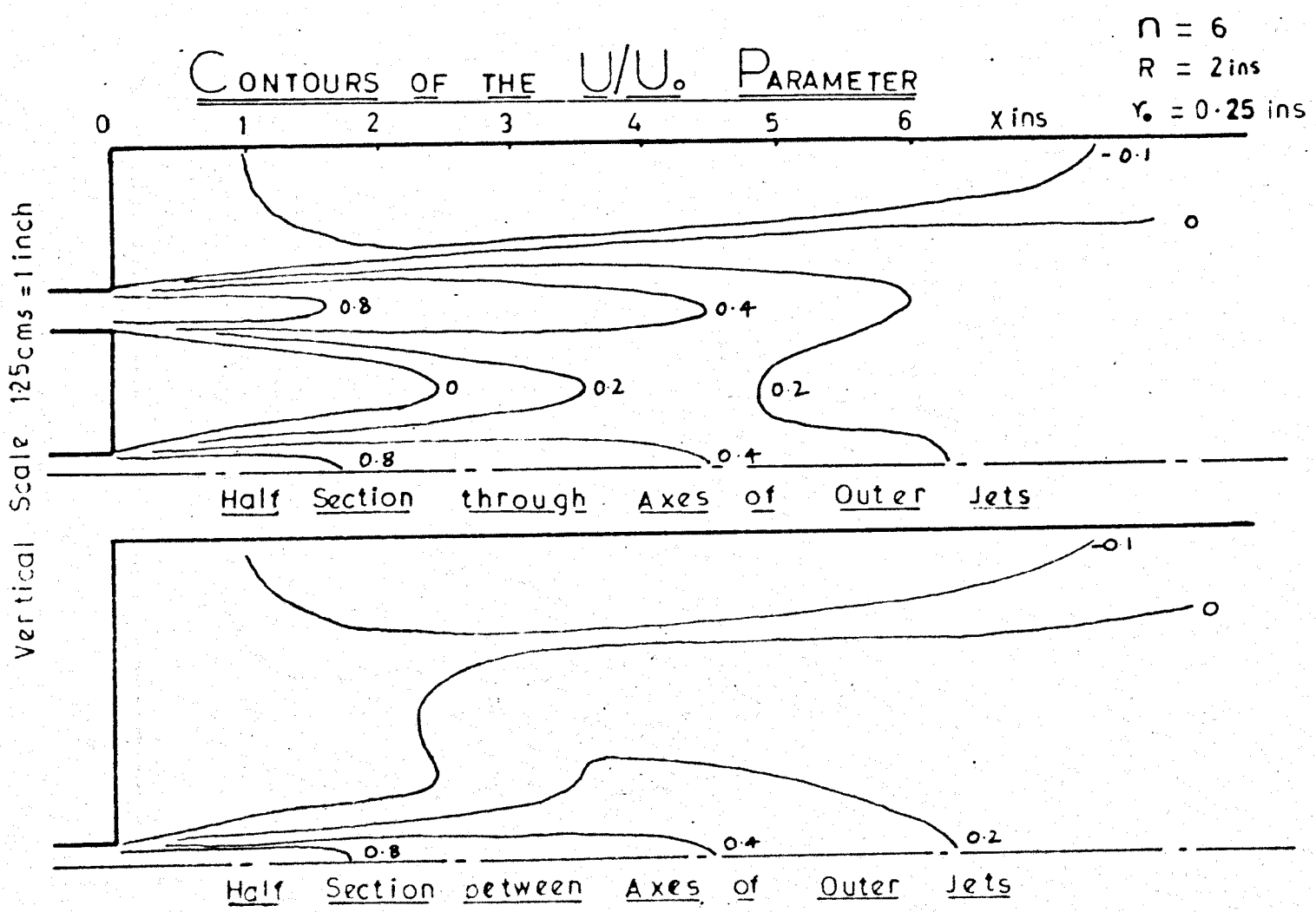


FIG. 8a PEAK VELOCITY IN JETS : 150 FT/SEC (Re = 31900)

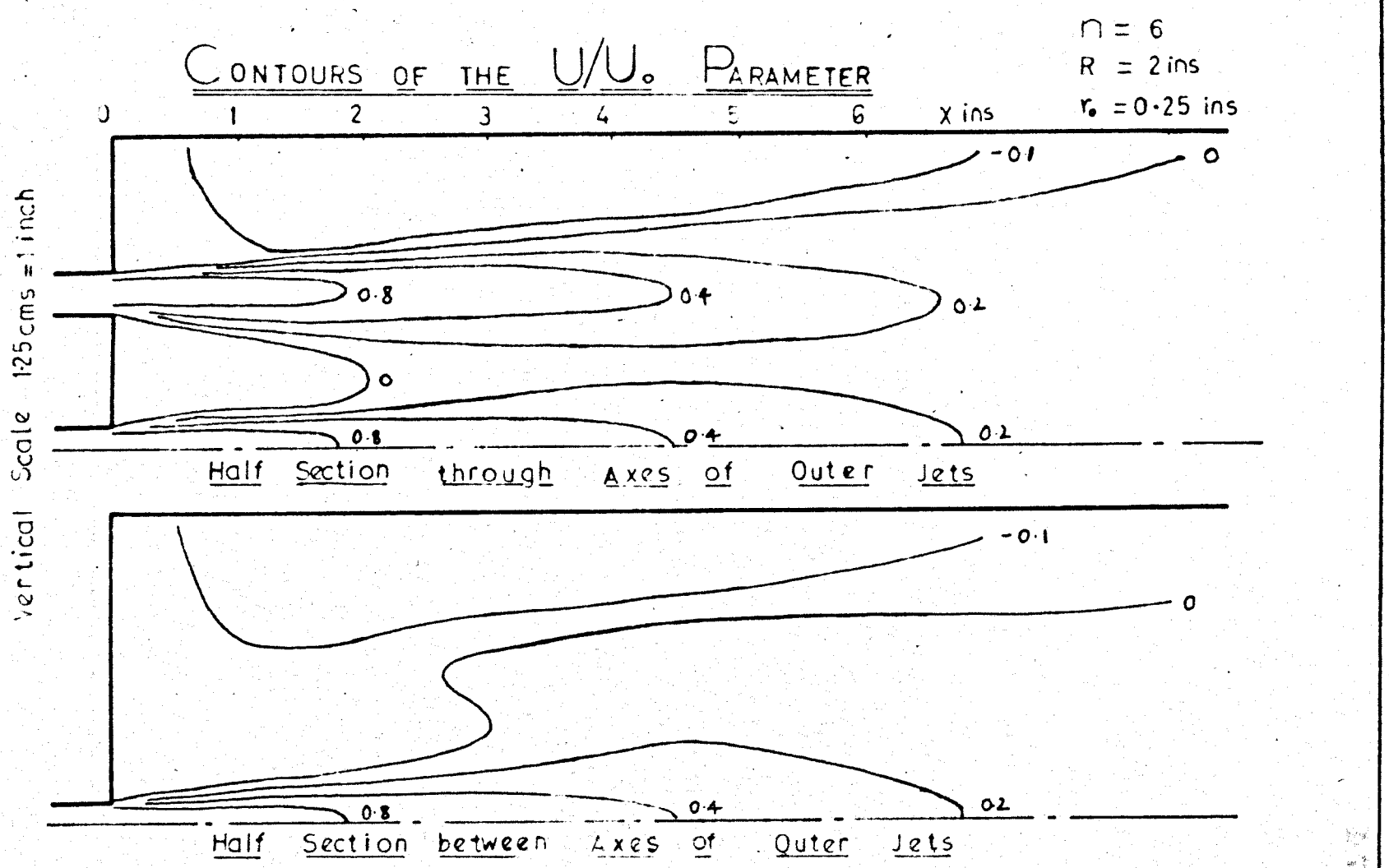


FIG. 8b PEAK VELOCITY IN JETS: 106 FT/SEC ($R_e$=21300)

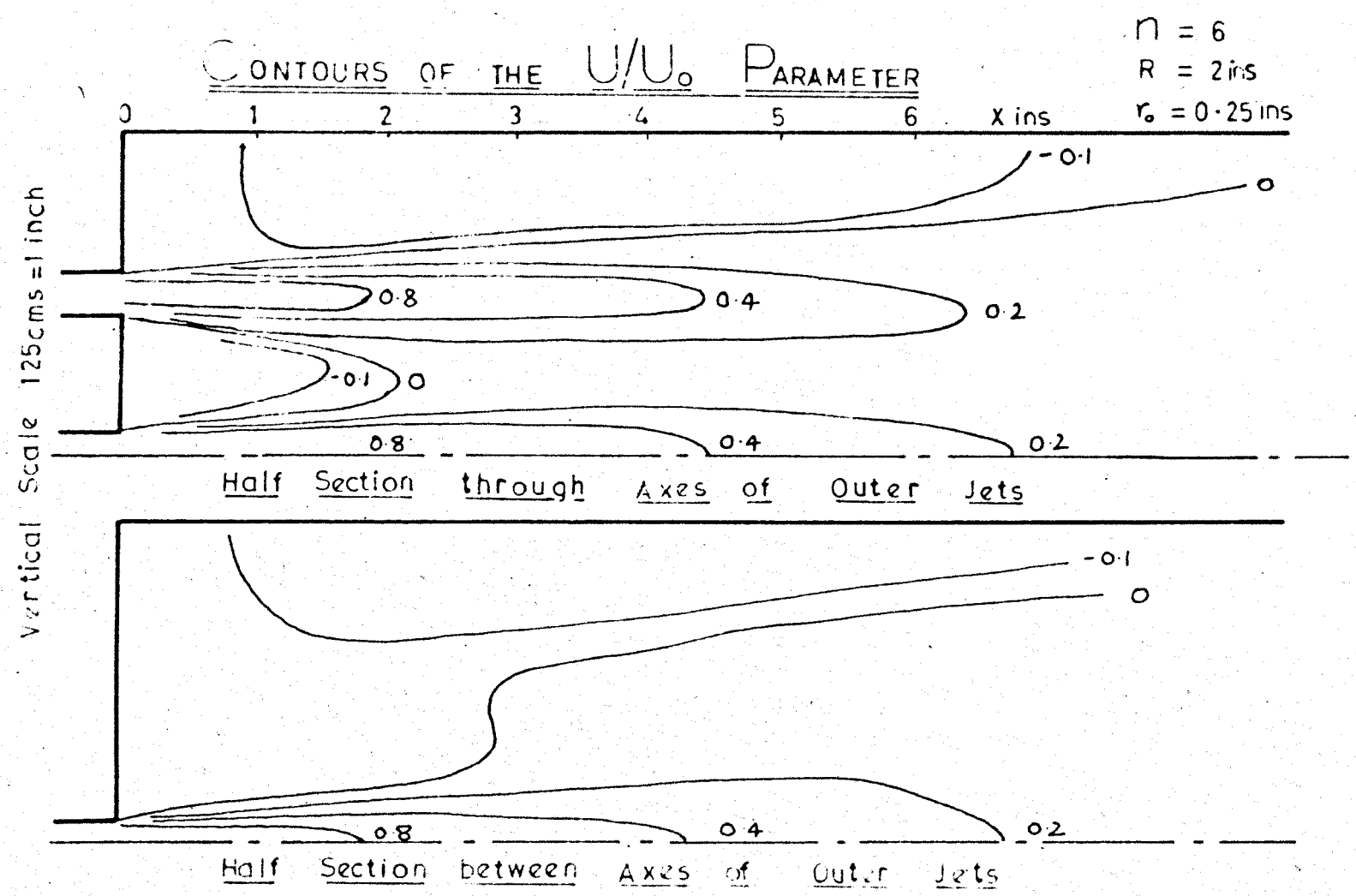


FIG. 8c PEAK VELOCITY IN JETS : 86 FT/SEC ($R_e$ = 18600)

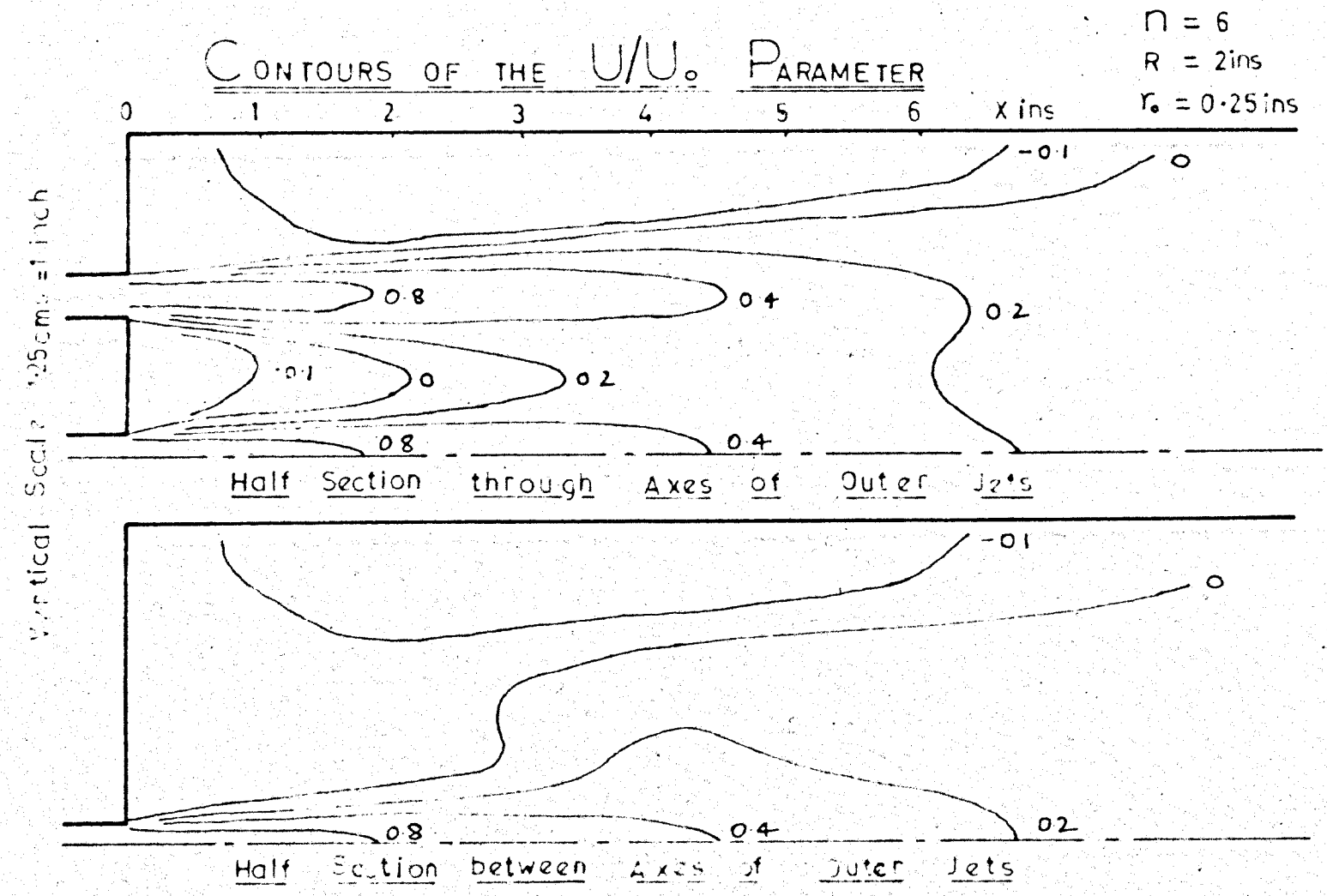


FIG. 8d PEAK VELOCITY IN JETS : 71 FT/SEC ($R_e$ = 15950)

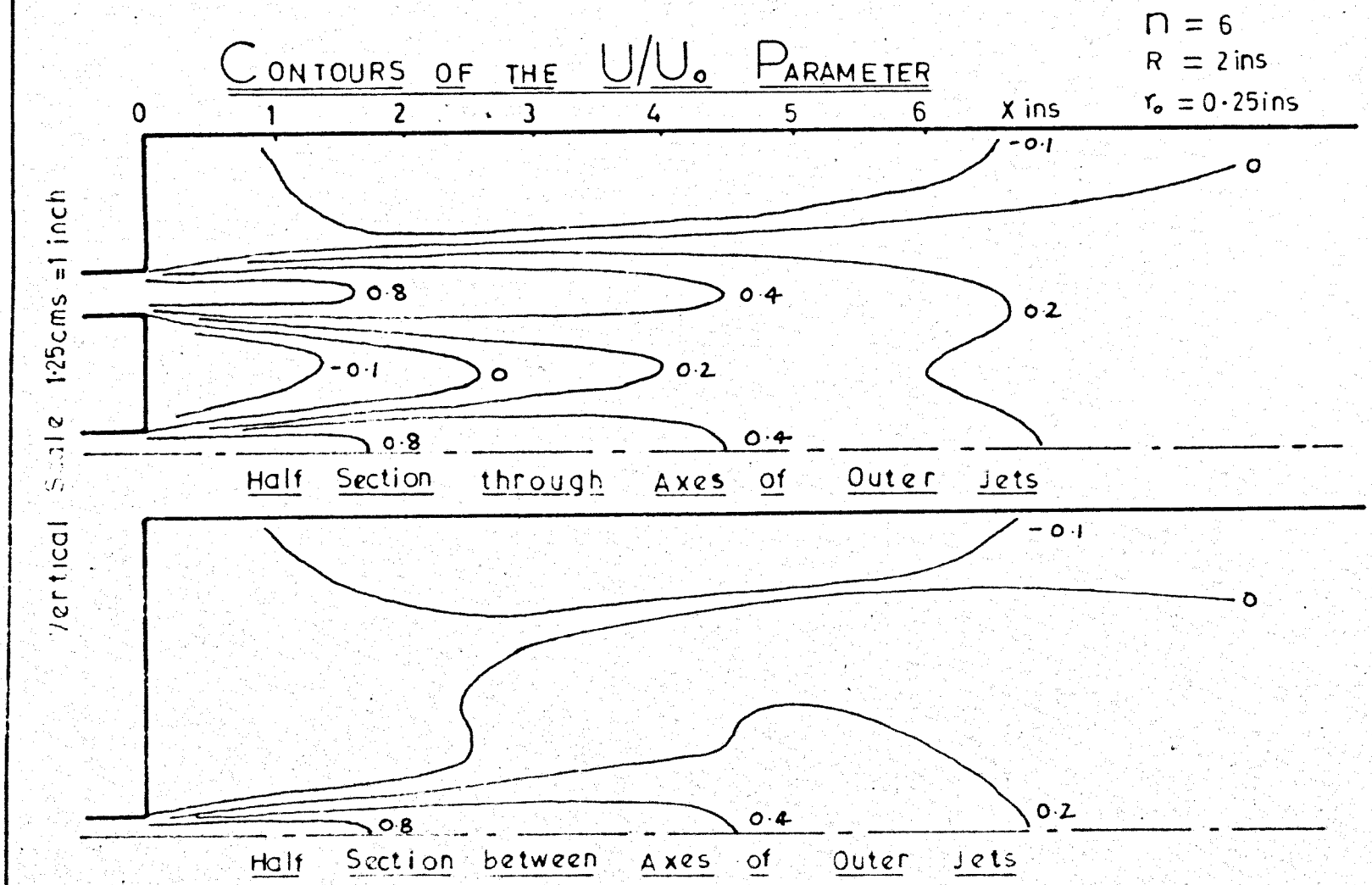


FIG. 8e PEAK VELOCITY IN JETS : 52 FT/SEC ( Re=13300)

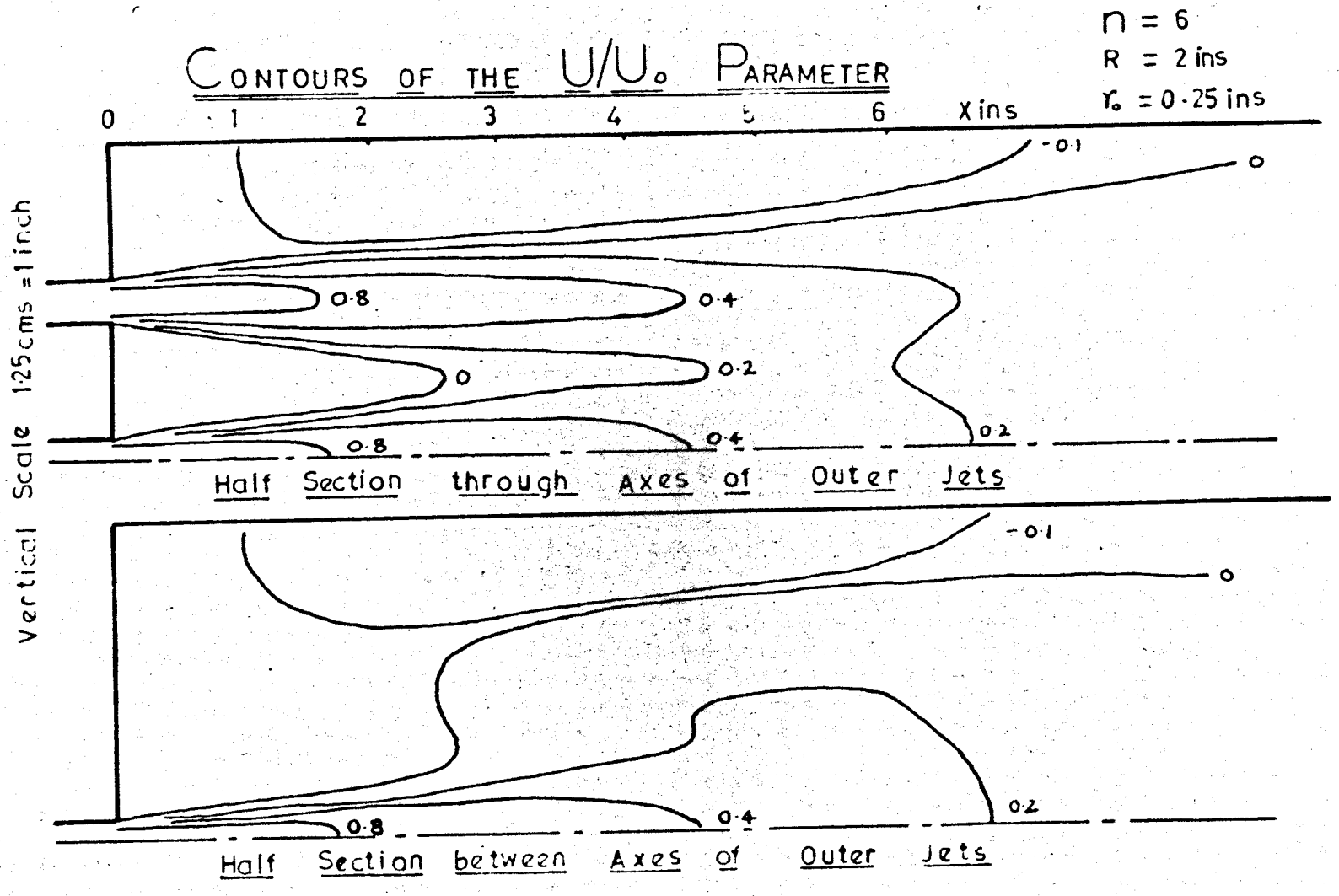


FIG. 8f PEAK VELOCITY IN JETS 42 FT/SEC (Re = 10620)

Fig. No. 9 - Effect of Pitch Circle Radius of Outer Nozzles when $n = 6$, $r_o = 0.375"$, $R/L$ from 0.375 to 0.656

Fig. No. 10 - Velocity Contours when $R/L = 0.656$, $n = 6$, $r_o = 0.25"$

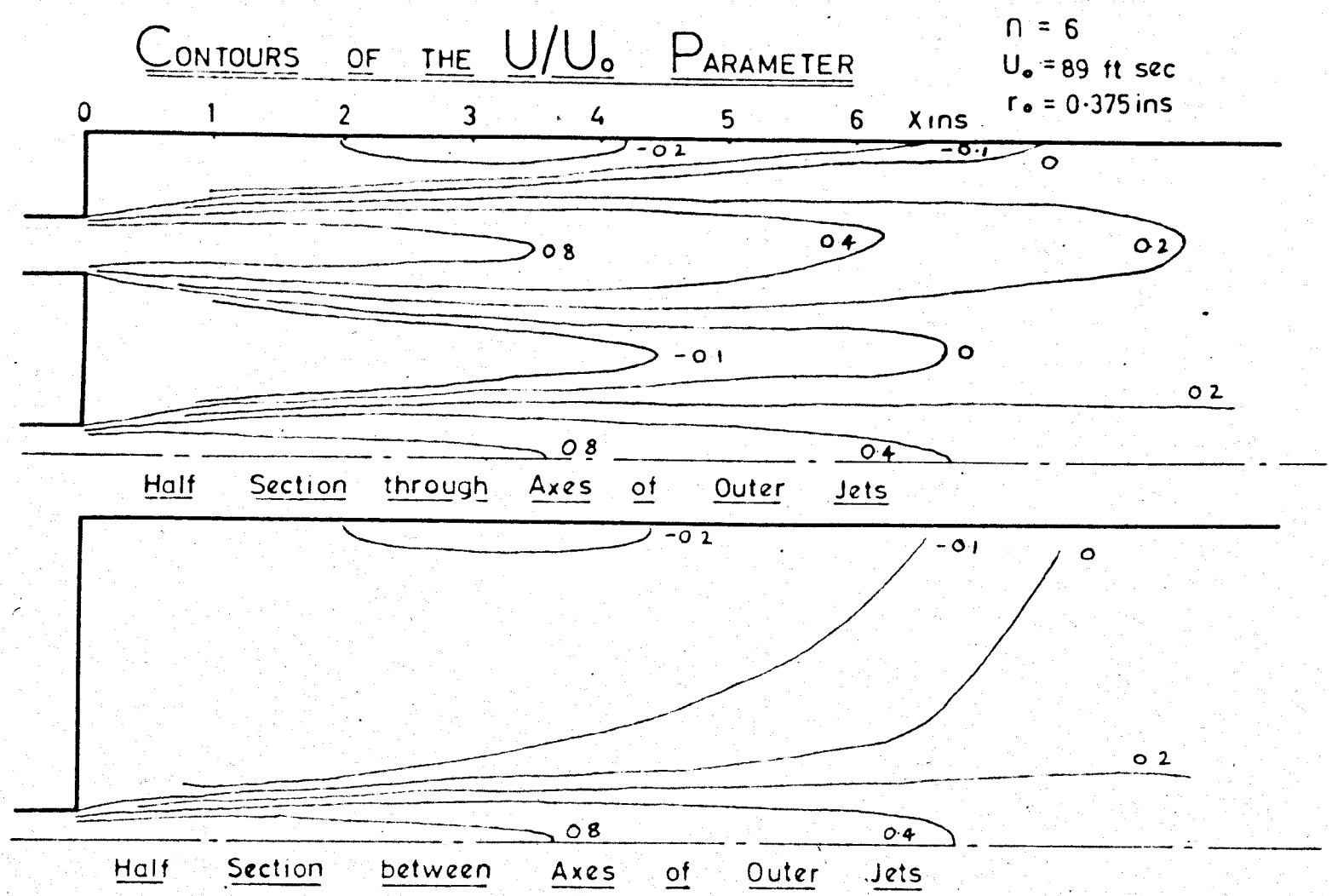


FIG. 9a PITCH RADIUS OF OUTER JETS : 2·625 INS

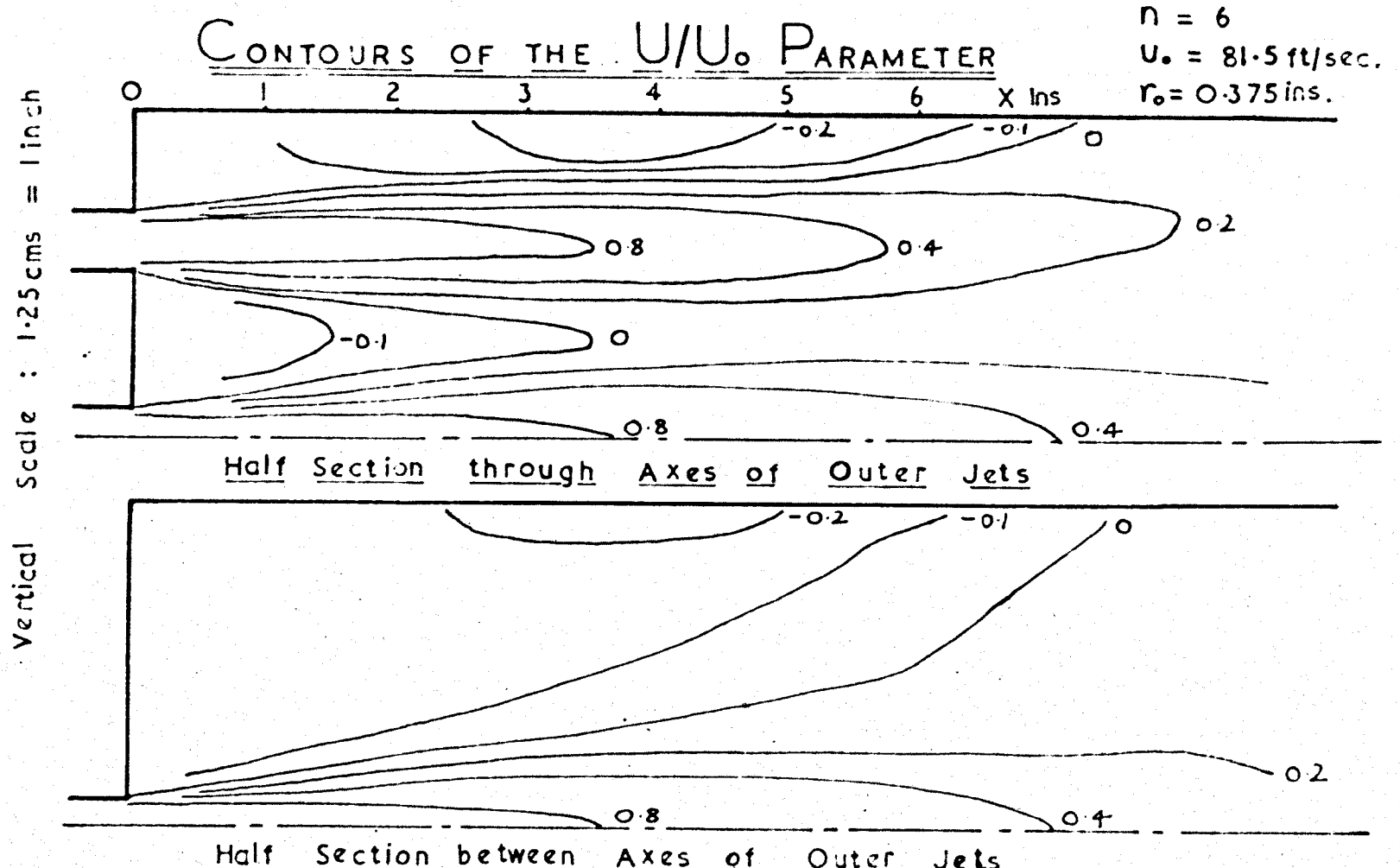


FIG. 9b PITCH RADIUS OF OUTER JETS : 2·375 INS.

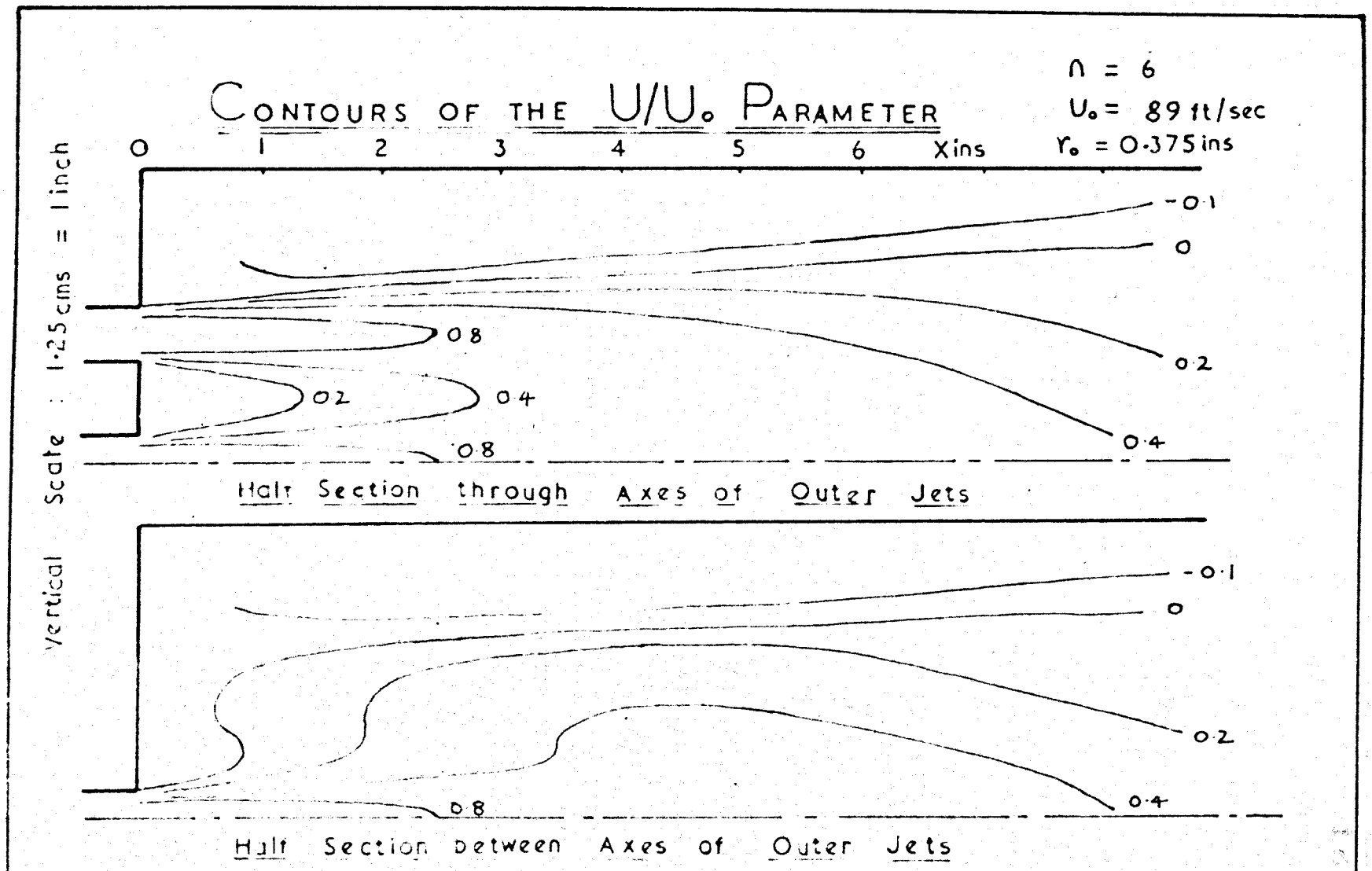


FIG. 9c PITCH RADIUS OF OUTER JETS: 1·75 INS.

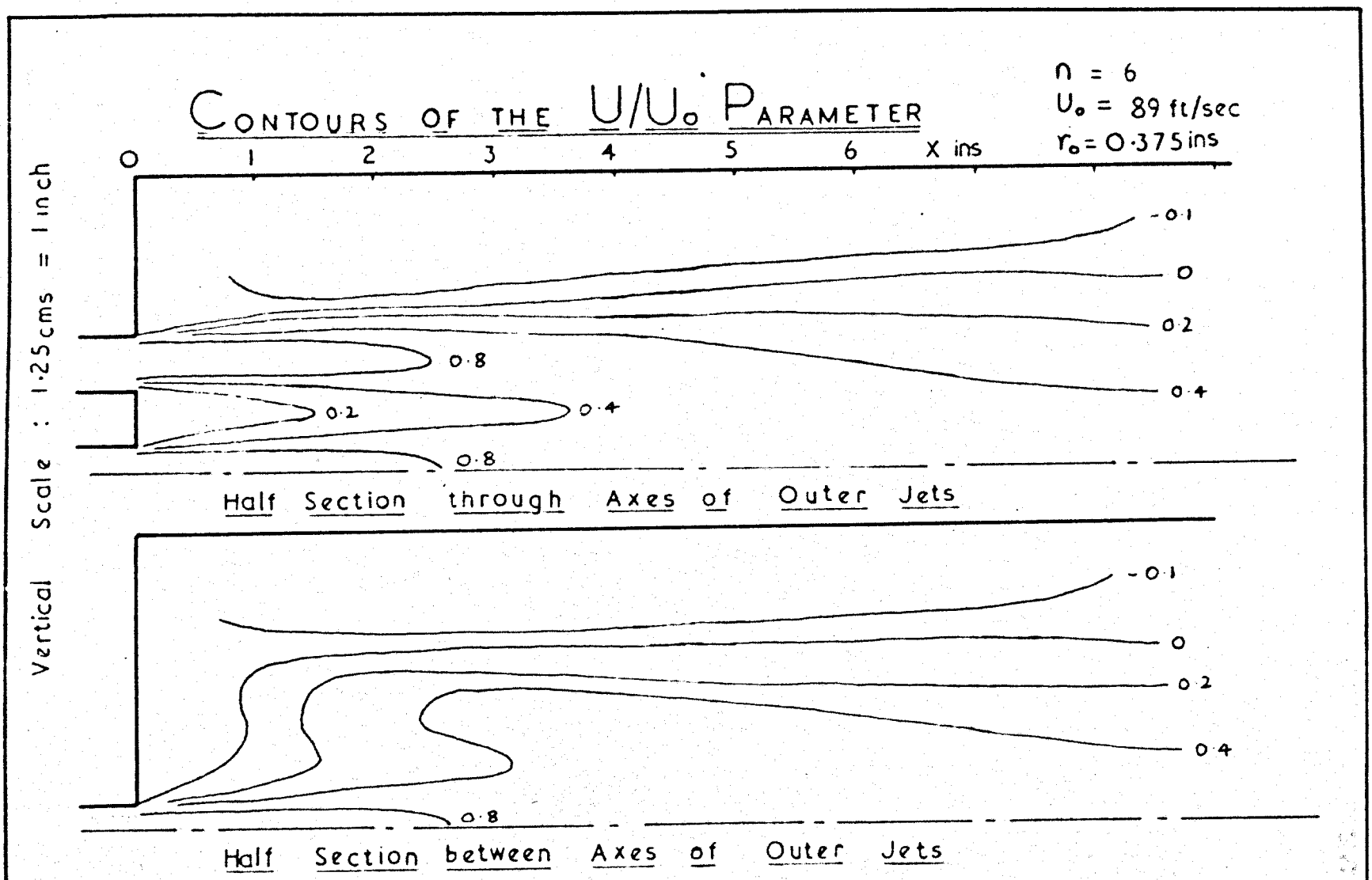


FIG. 9d PITCH RADIUS OF OUTER JETS : 1·5 INS

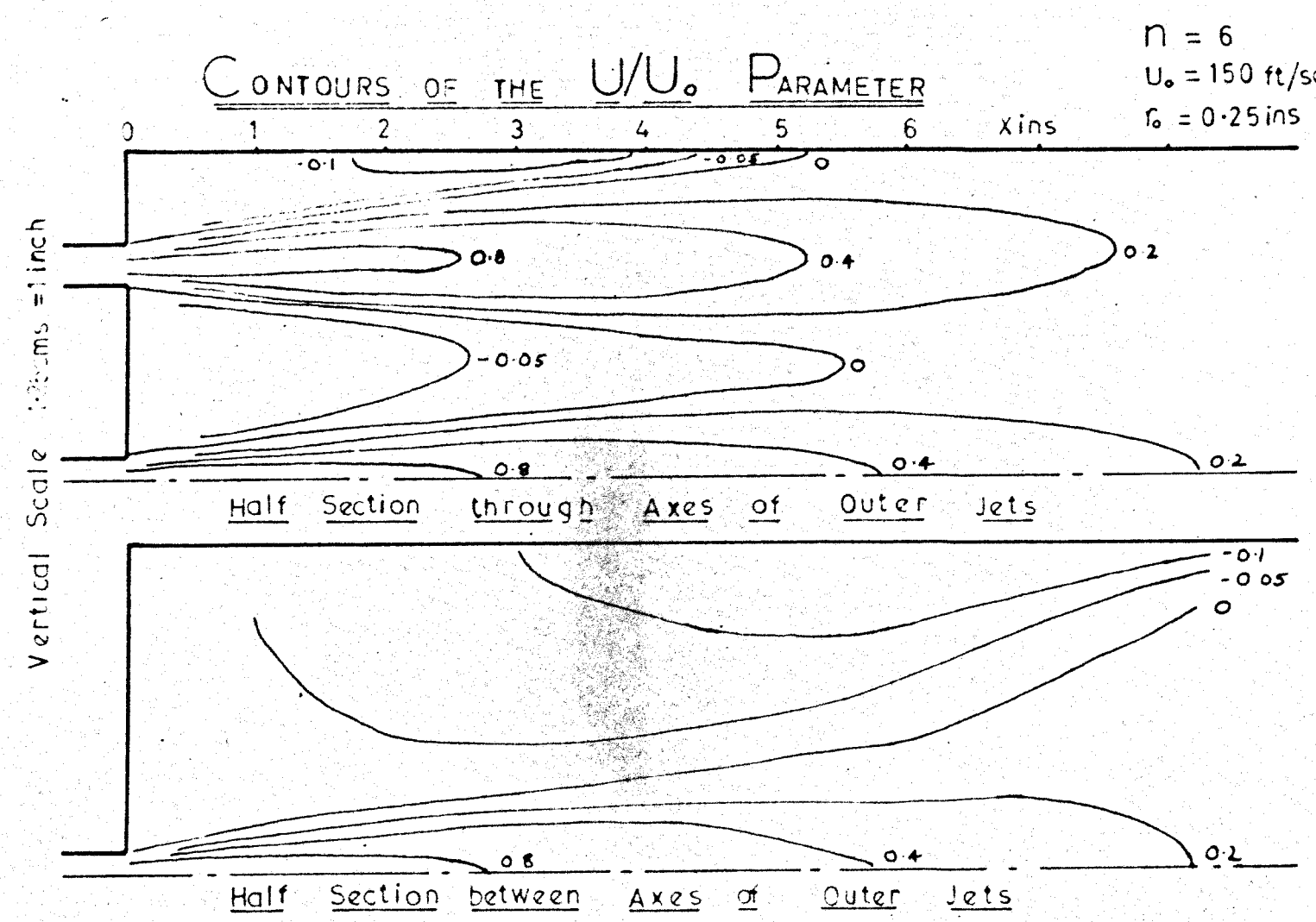


FIG. 10 PITCH RADIUS OF OUTER JETS : 2·625 INS.

Fig. No. 11 - Effect of reduction of number of outer nozzles, n = 3, for $R/L$ = 0.375 to 0.656, $r_o$ = 0.375", and $R/L$ = 0.656, $r_o$ = 0.25"

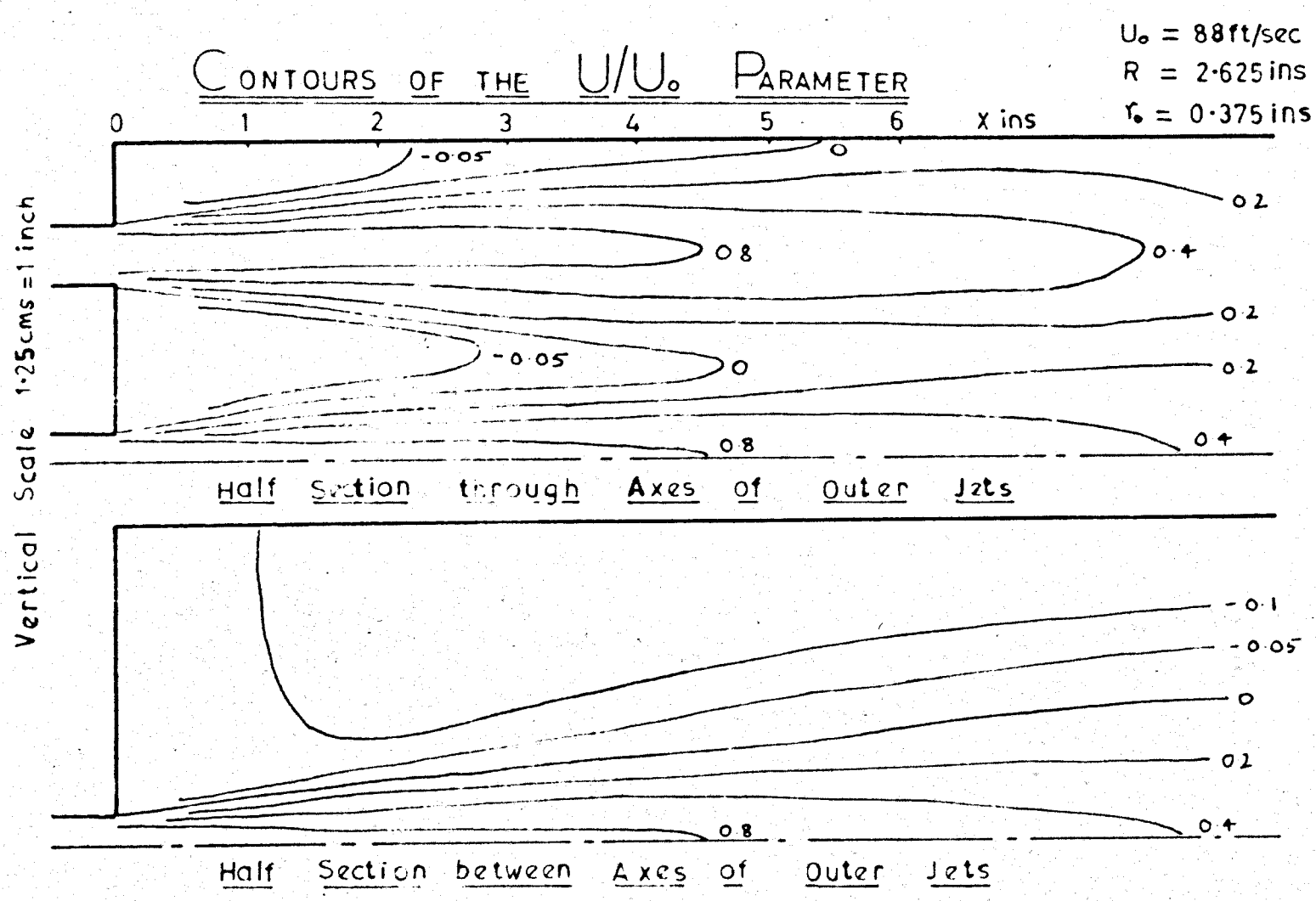


FIG. 11a NUMBER OF OUTER JETS : n = 3

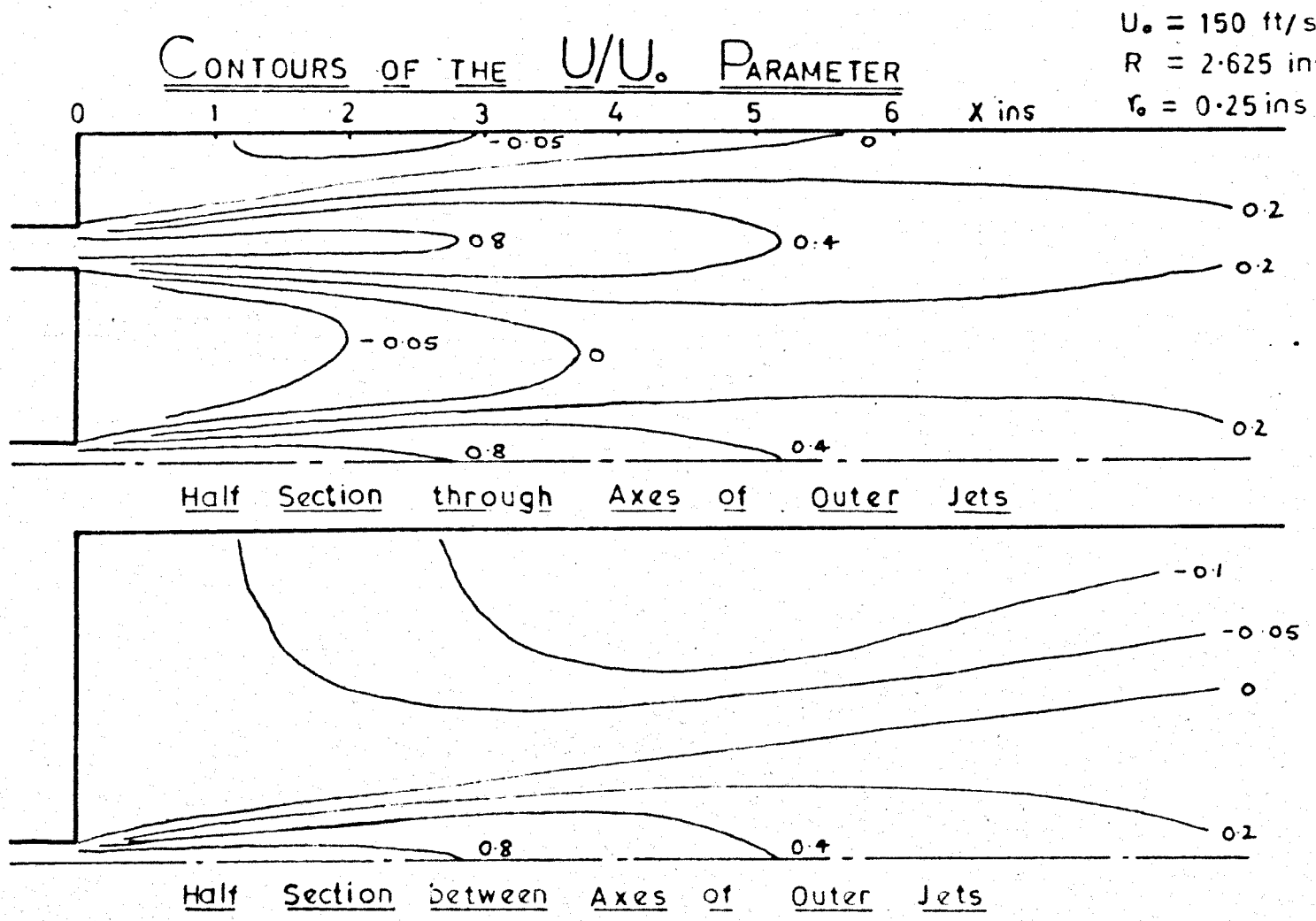


FIG. 11b NUMBER OF OUTER JETS : n = 3

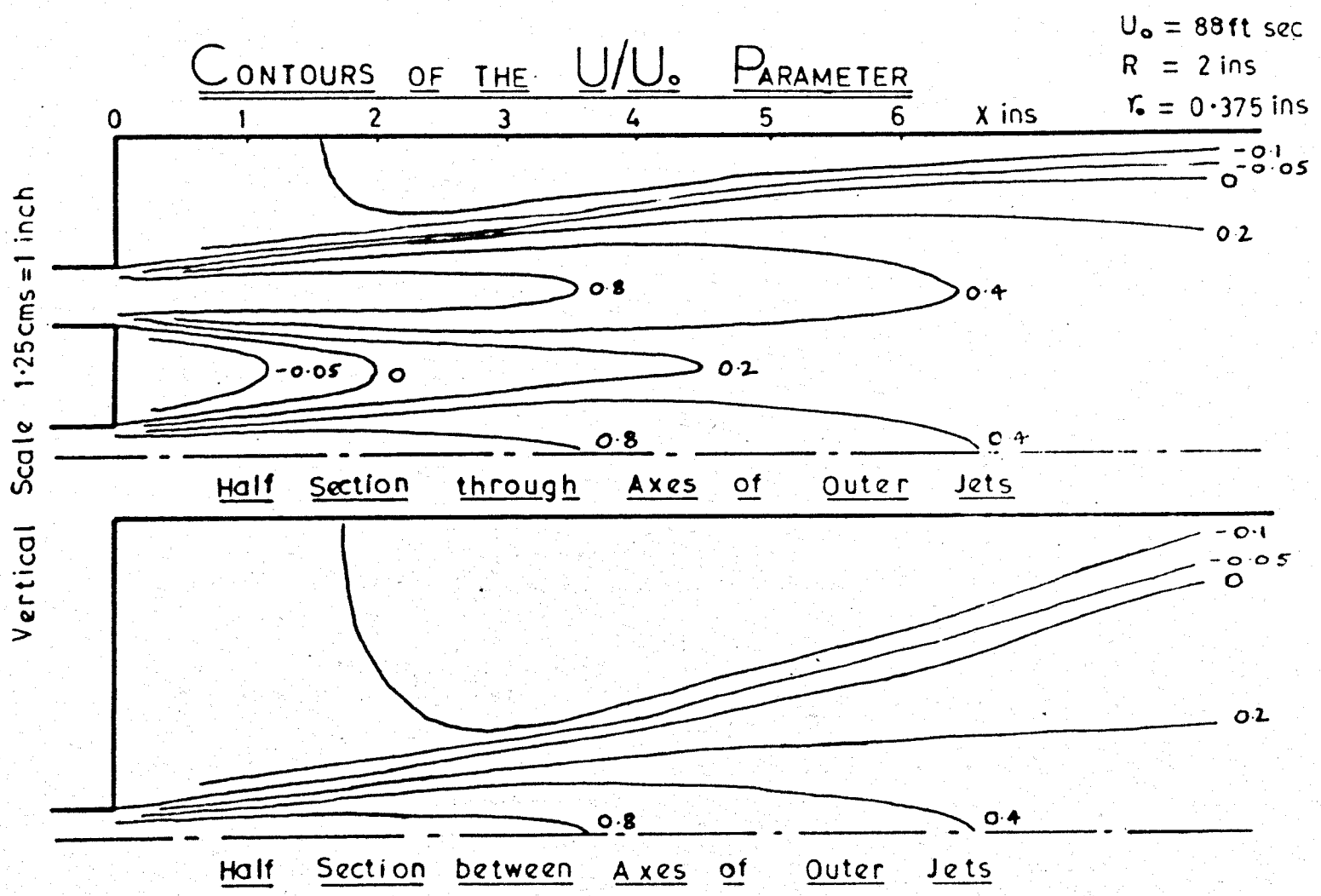


FIG. 11c NUMBER OF OUTER JETS : n = 3

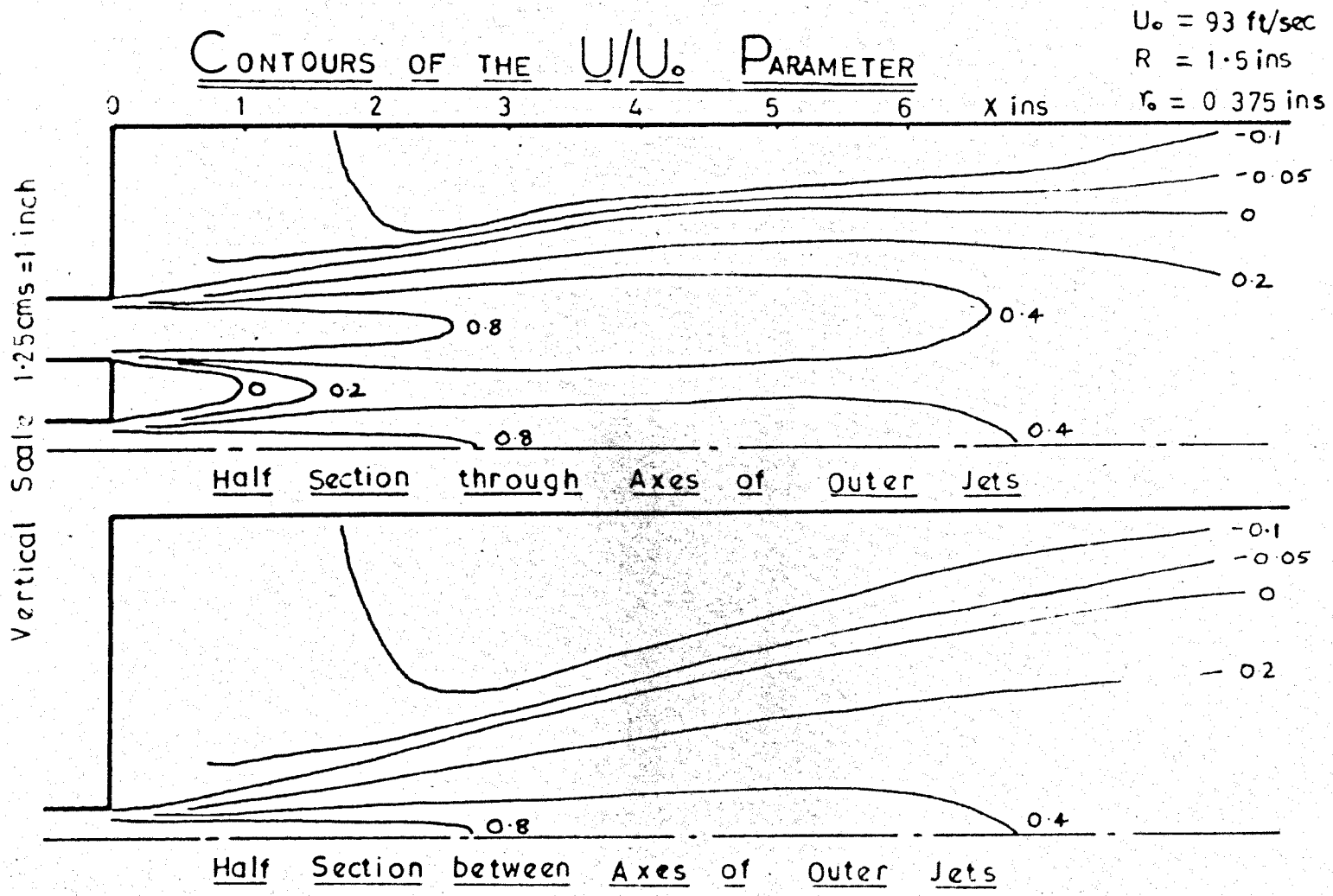


FIG. 11d NUMBER OF OUTER JETS : n = 3

Fig. No. 12 - Effect of Grid 1 on Flow Patterns when $R = 2"$, $r_o = 0.375"$, $n = 6$, $Re = 27900$ and $x/L$ from 0.5 to 1.75

Fig. No. 13 - Initial Effect of Grid 1 on Axial Velocity Decay, $Re = 27900$, $R = 2"$, $r_o = 0.375"$, $n = 6$, Grid Position $x/L = 1.75$

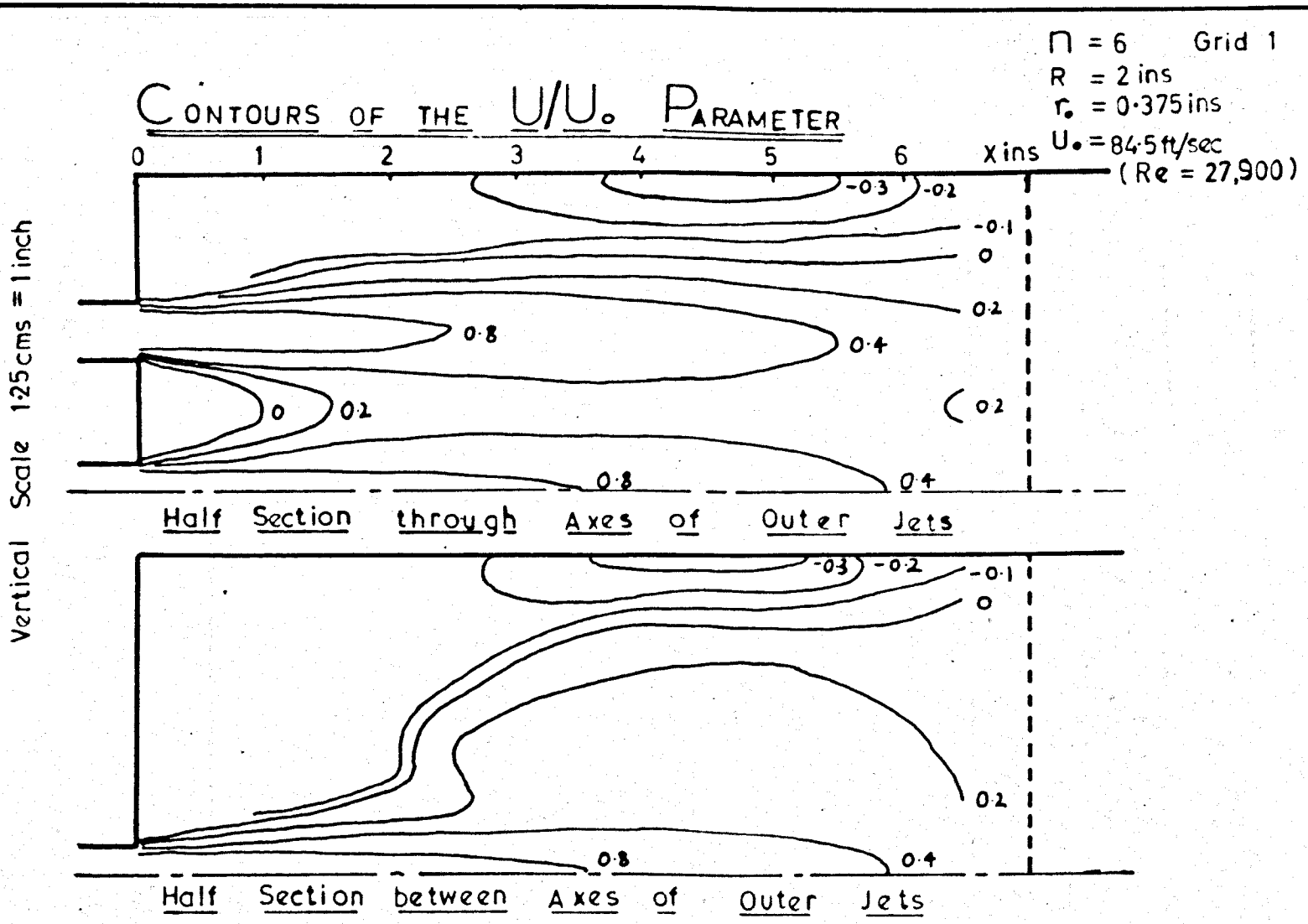


FIG. 12a GRID POSITION: X/L = 1·75

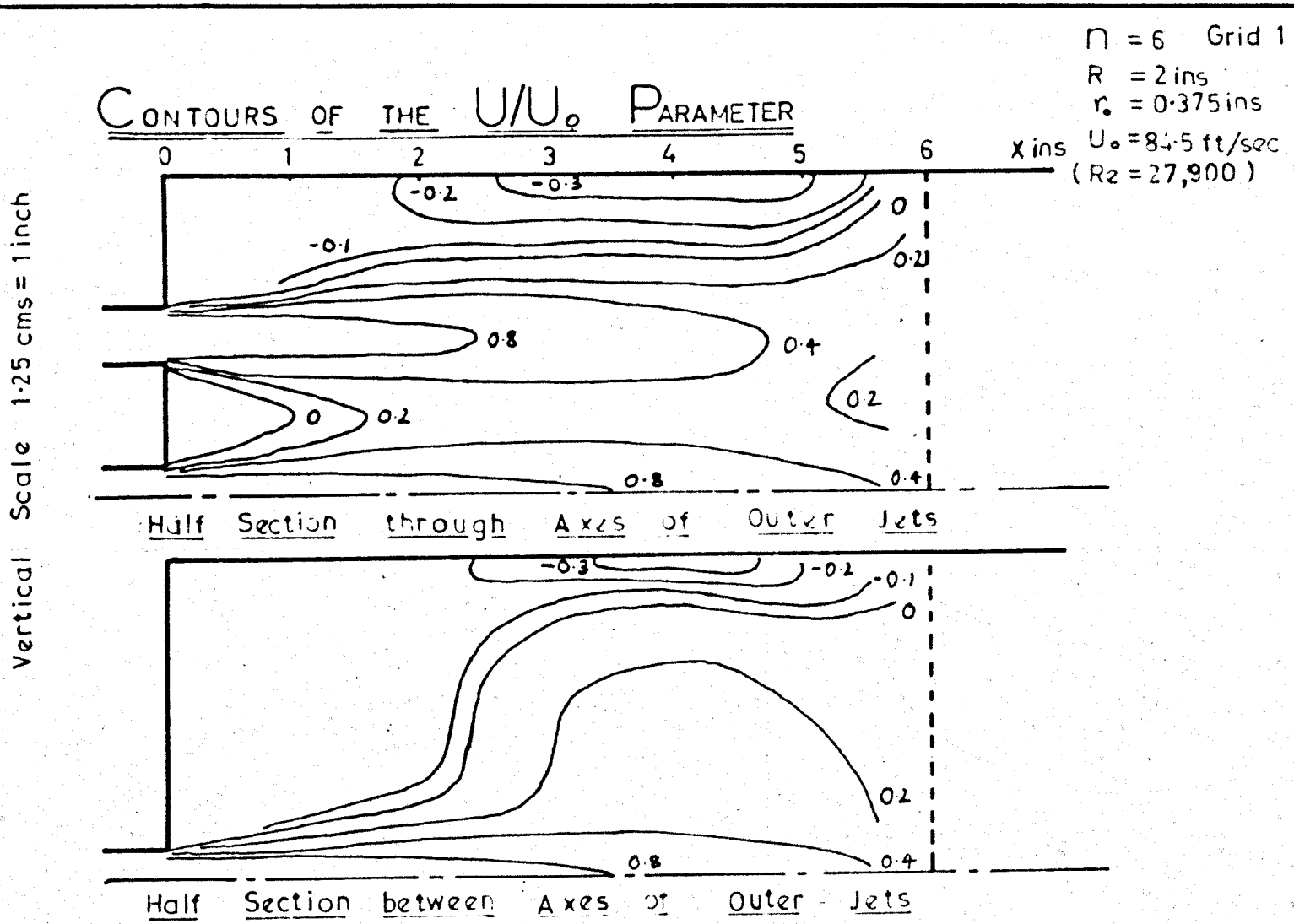


FIG. 12b GRID POSITION: X/L = 1·5

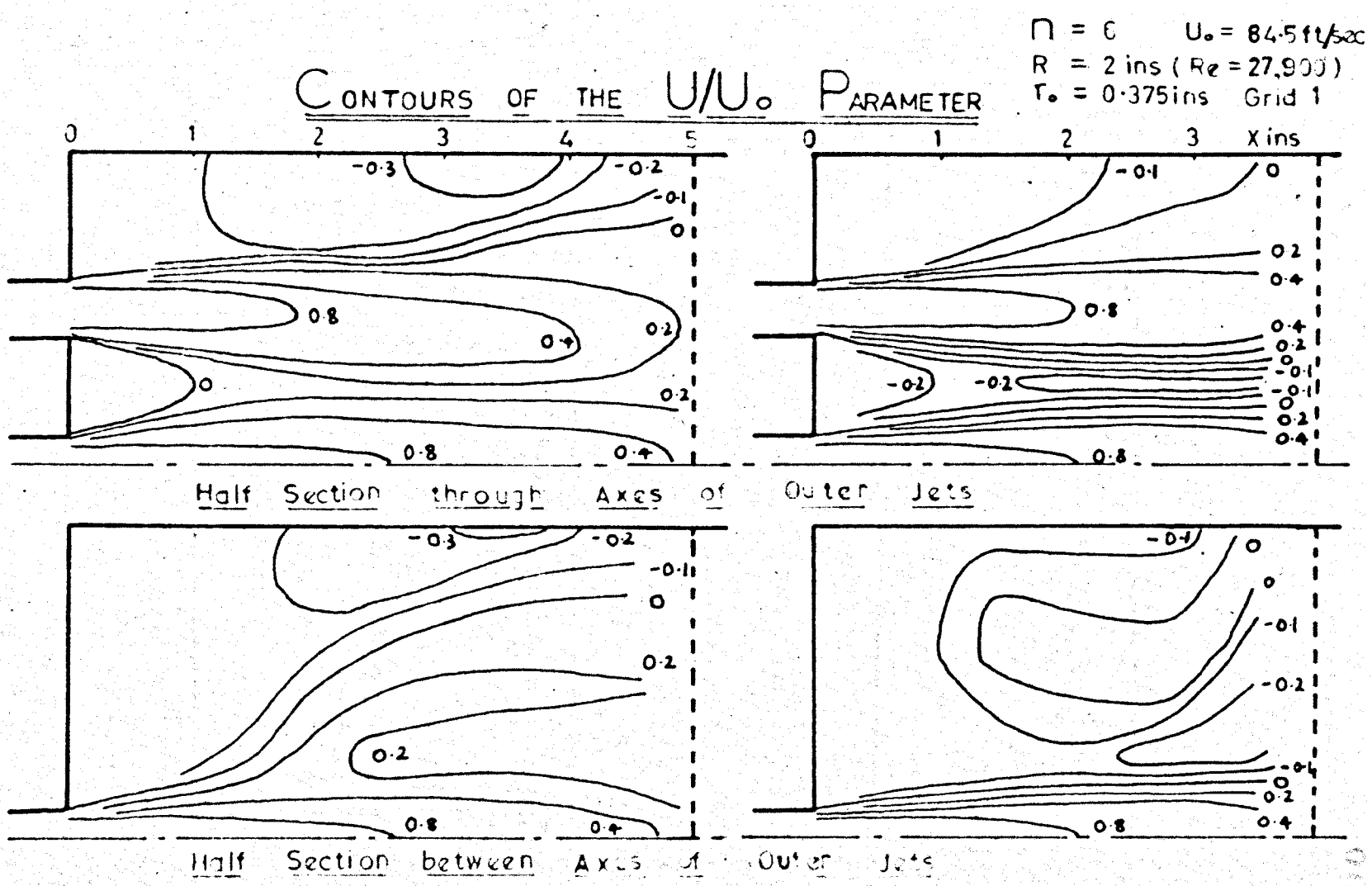


FIG. 12c GRID POSITION: X/L = 1·25 GRID POSITION: X/L = 1

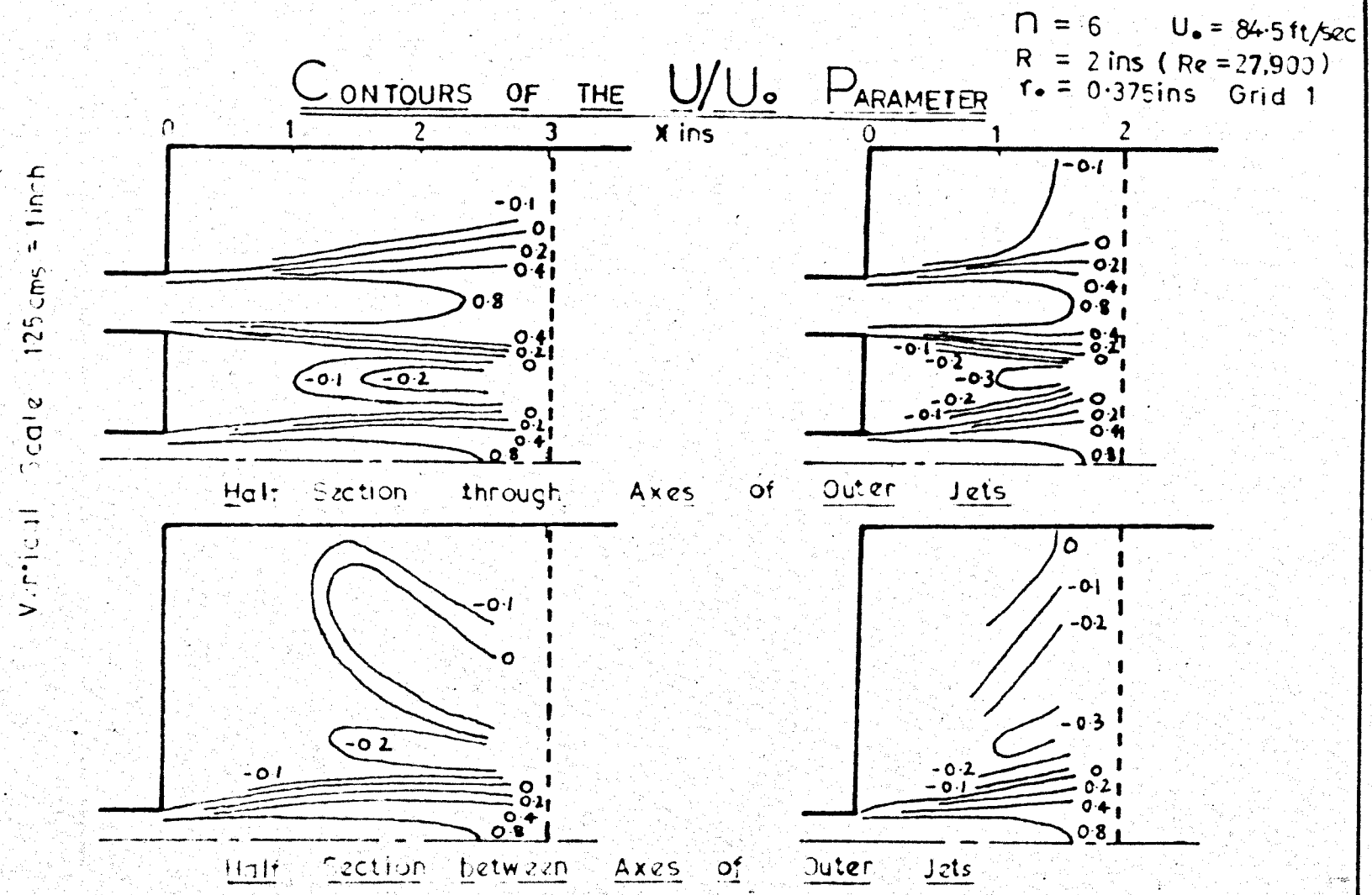


FIG. 12 d GRID POSITION : X/L = 0·75 GRID POSITION : X/L = 0·5

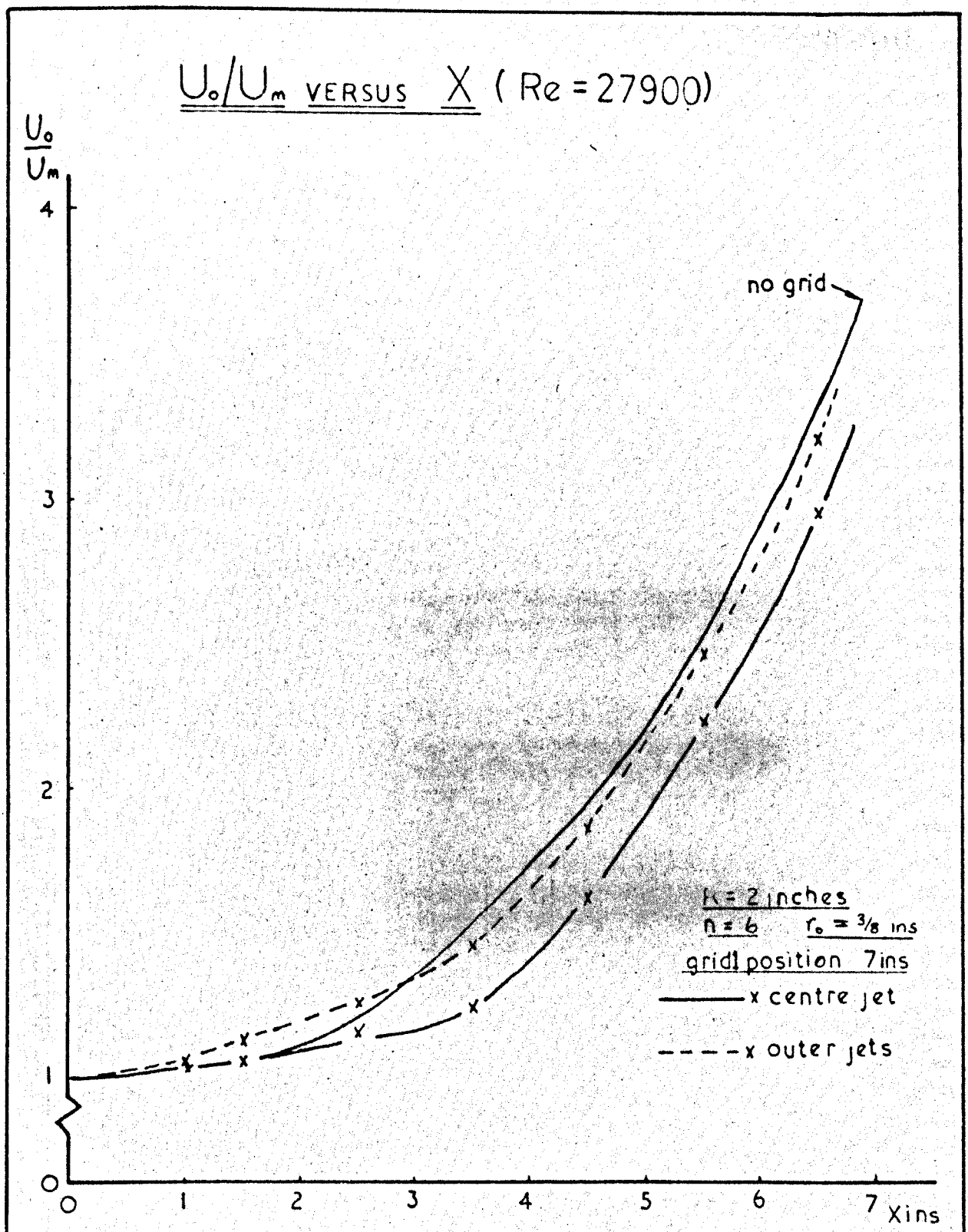


FIG. 13. INITIAL EFFECT OF GRID ON VELOCITY DECAY.

Fig. No. 14 - Effect of Increased Grid Resistance on Flow Patterns when $x/L = 1$ to 1.75, Re = 27900, R = 2", $r_o$ = 0.375", n = 6

Fig. No. 15 - Effect of decreased Grid Resistance on Flow Patterns $x/L = 0.75$ to 1.75, Re = 27900, R = 2", $r_o$ = 0.375", n = 6

Fig. No. 16 - Effect of Grid Resistance on Axial Velocity Decay when $x/L = 1.25$, Re = 27900, R = 2", $r_o$ = 0.375" n = 6

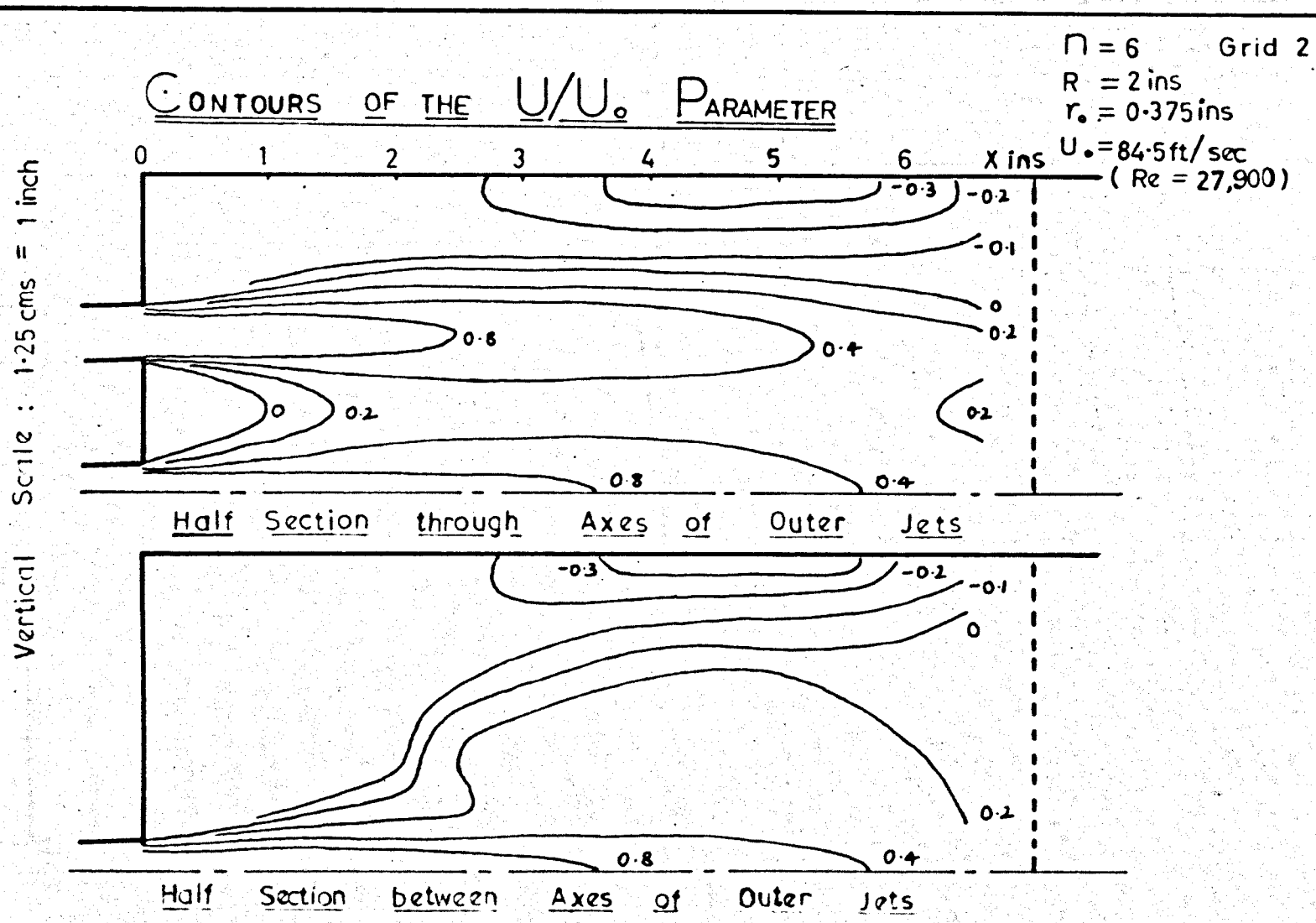


FIG. 14a EFFECT OF INCREASED GRID RESISTANCE WHEN X/L = 1·75

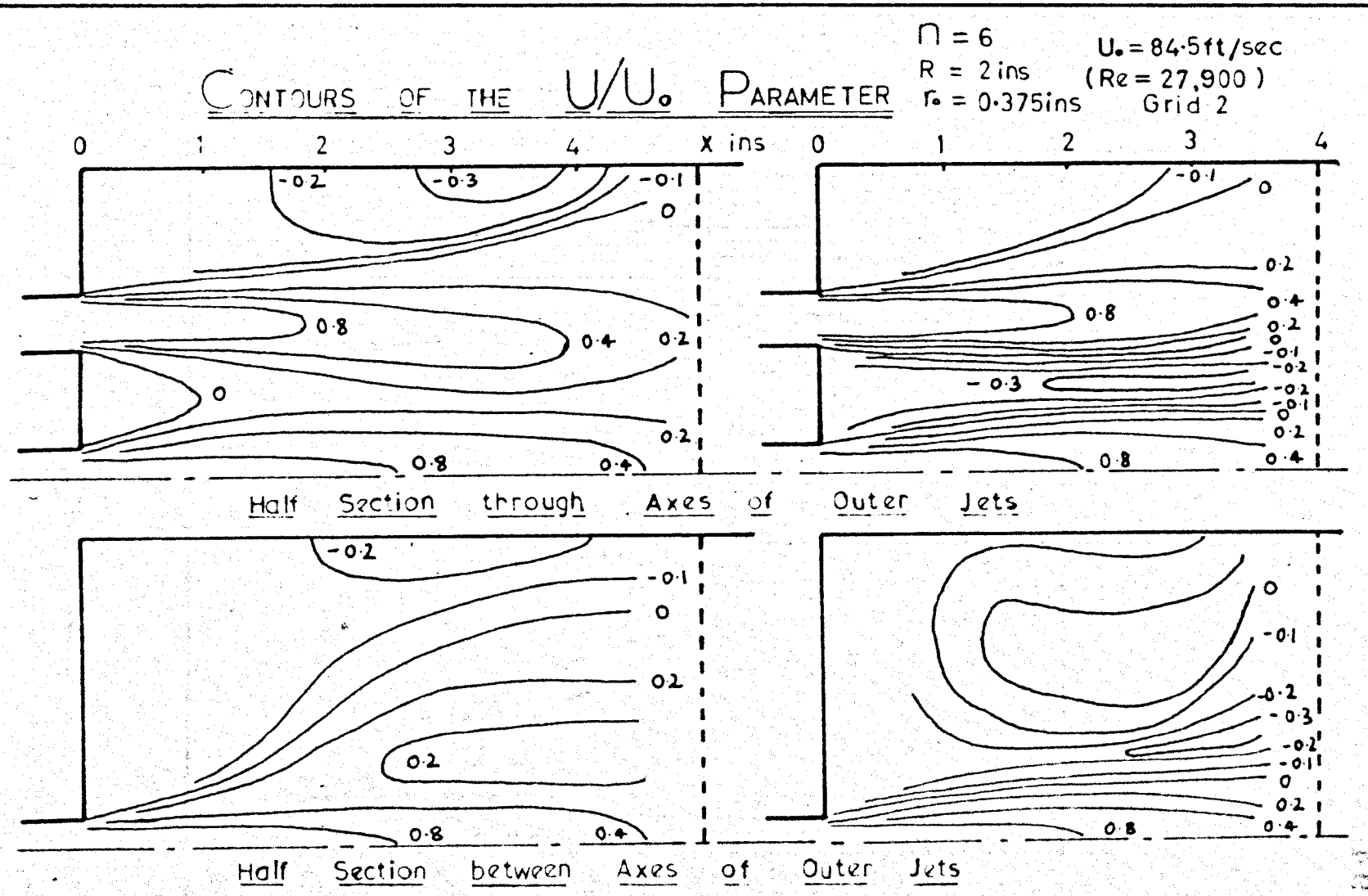


FIG. 14b EFFECT OF INCREASED GRID RESISTANCE WHEN X/L = 1·25 AND 1·0

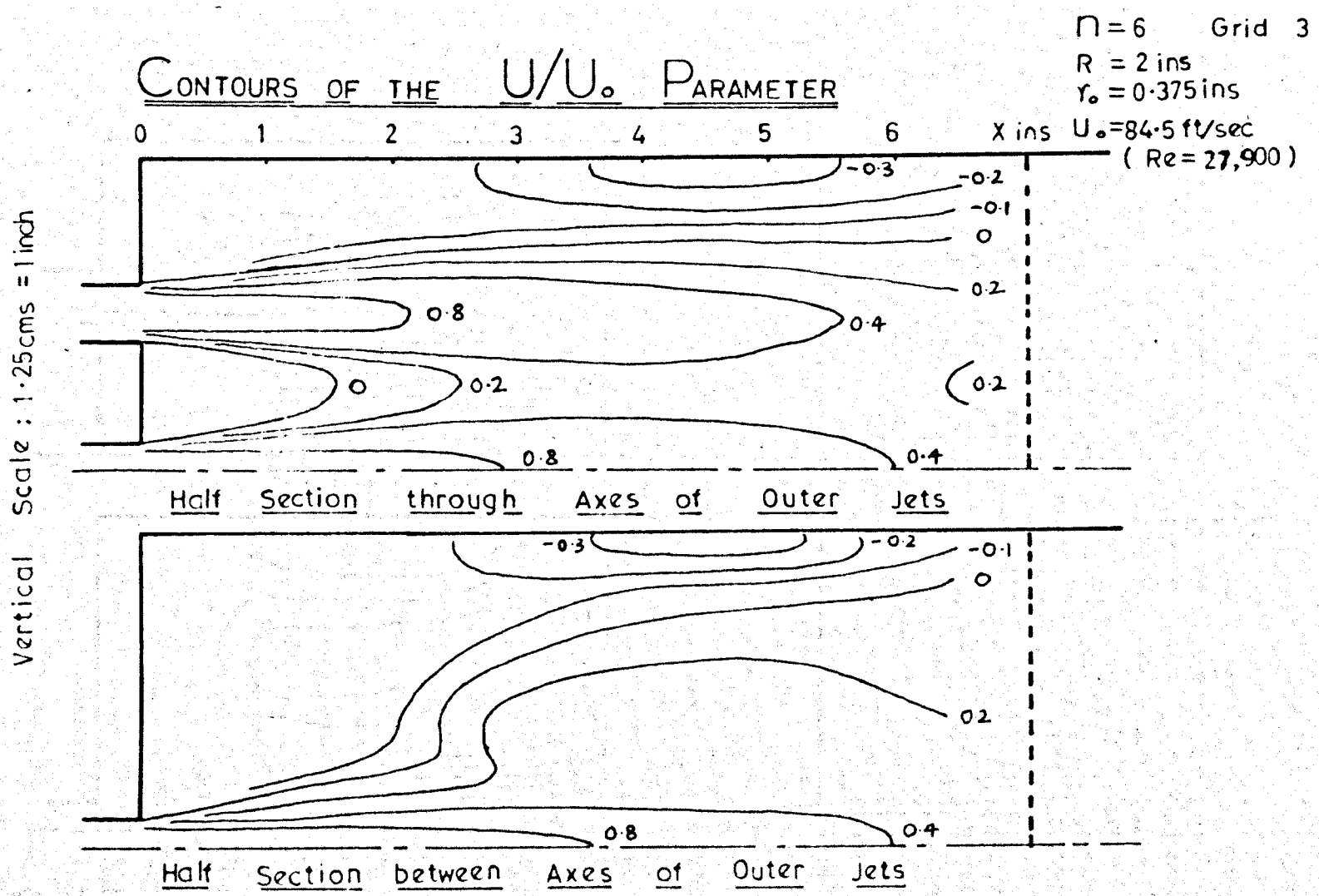


FIG. 15a EFFECT OF DECREASED GRID RESISTANCE WHEN X/L = 1·75

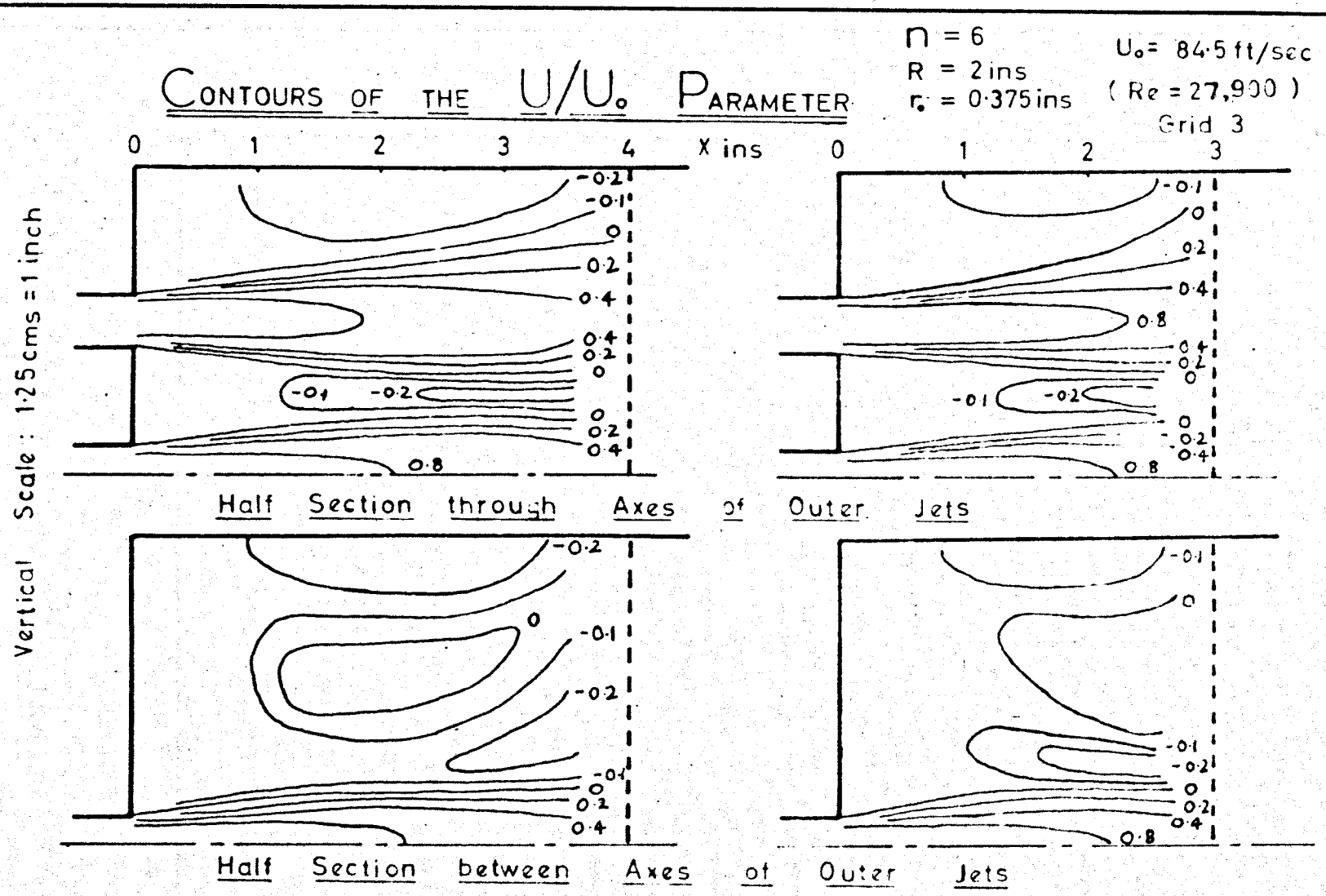


FIG. 15b EFFECT OF DECREASED GRID RESISTANCE WHEN X/L = 1 AND 0·75

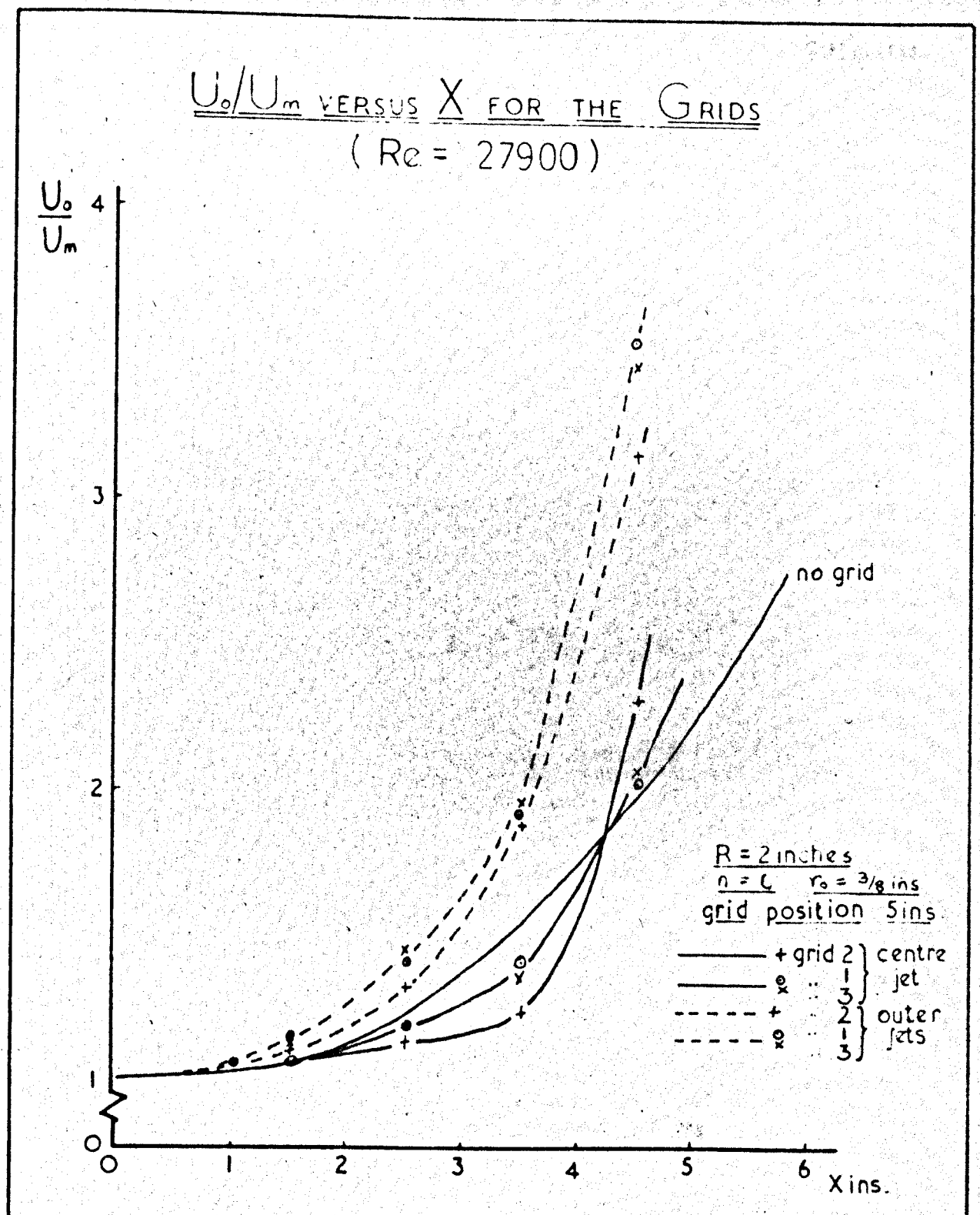


FIG.16. EFFECT OF GRID RESISTANCE

Fig. No. 17 - Effect of Grid 1 on Flow Patterns when $x/L$ = 1 to 1.75, Re = 31900, R = 2", $r_o$ = 0.25", n = 6

Fig. No. 18 - Effect of Grid 1 on Flow Patterns when $x/L$ = 1 to 1.75, Re = 28700, R = 2.625", $r_o$ = 0.375", n = 6

Fig. No. 19 - Effect of Grid 1 on axial velocity decay when $x/L$ = 1.25, Re = 28700, R = 2.625", $r_o$ = 0.375", n = 6

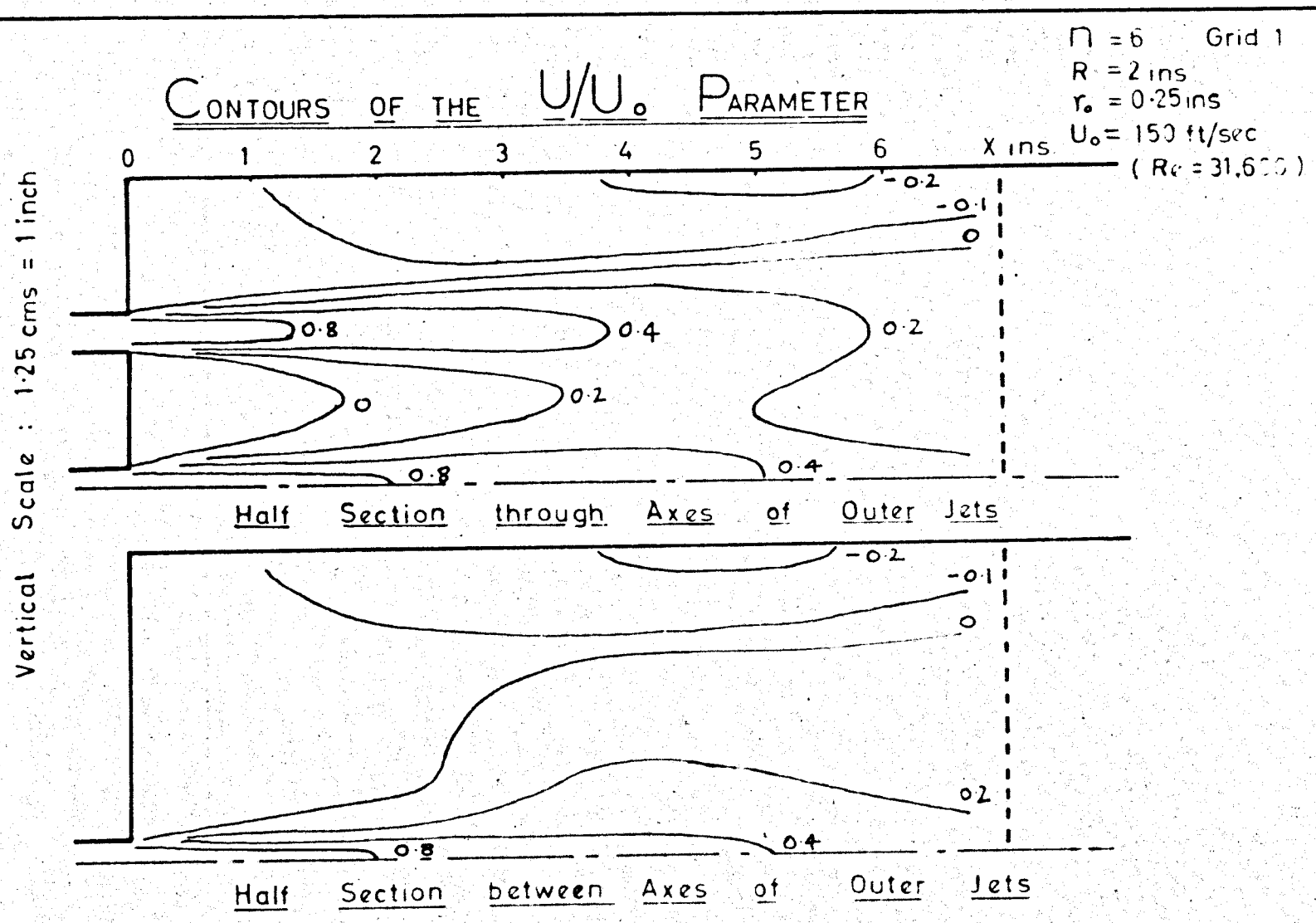


FIG. 17a GRID POSITION X/L = 1·75

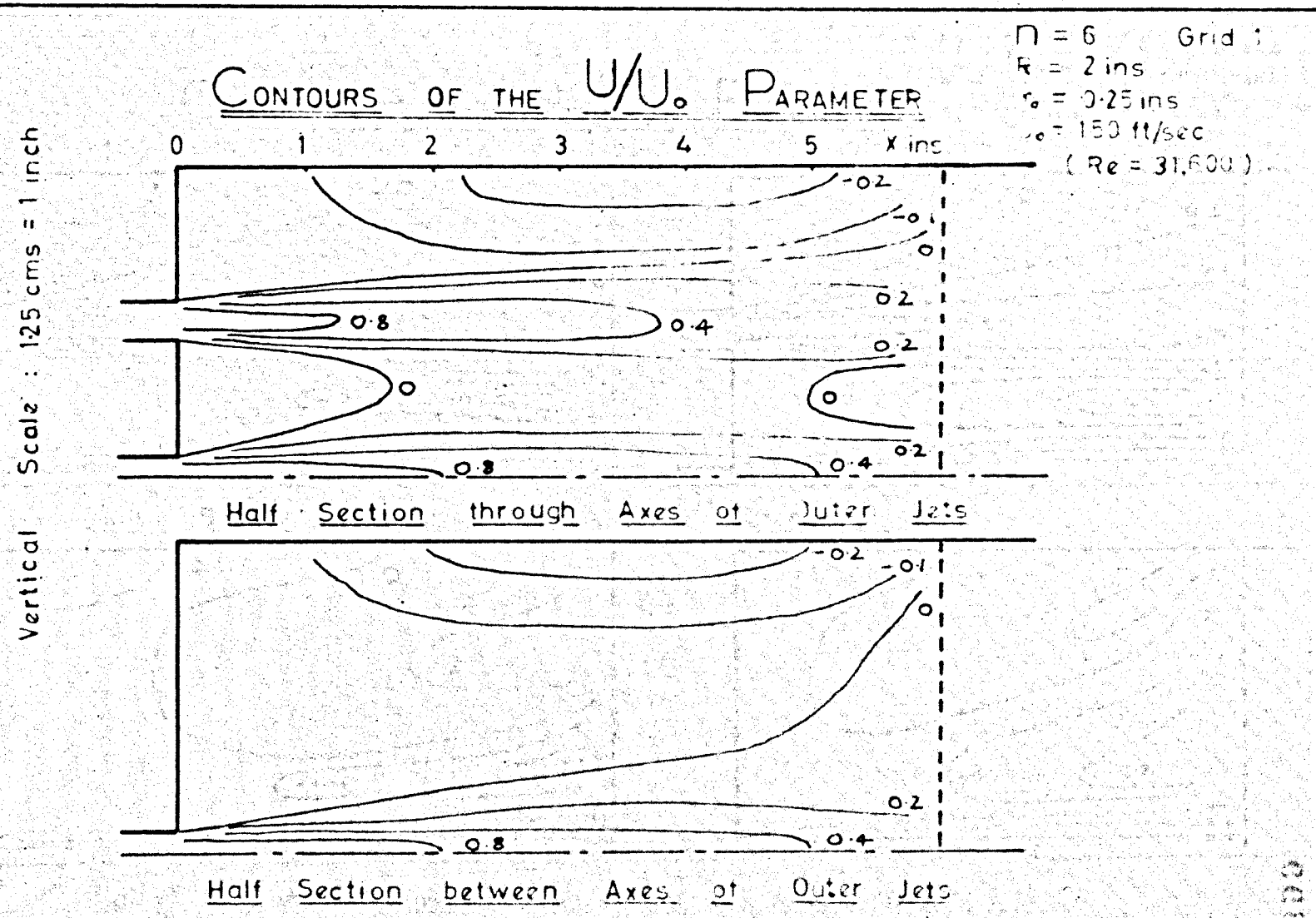


FIG. 17b GRID POSITION : X/L = 1·5

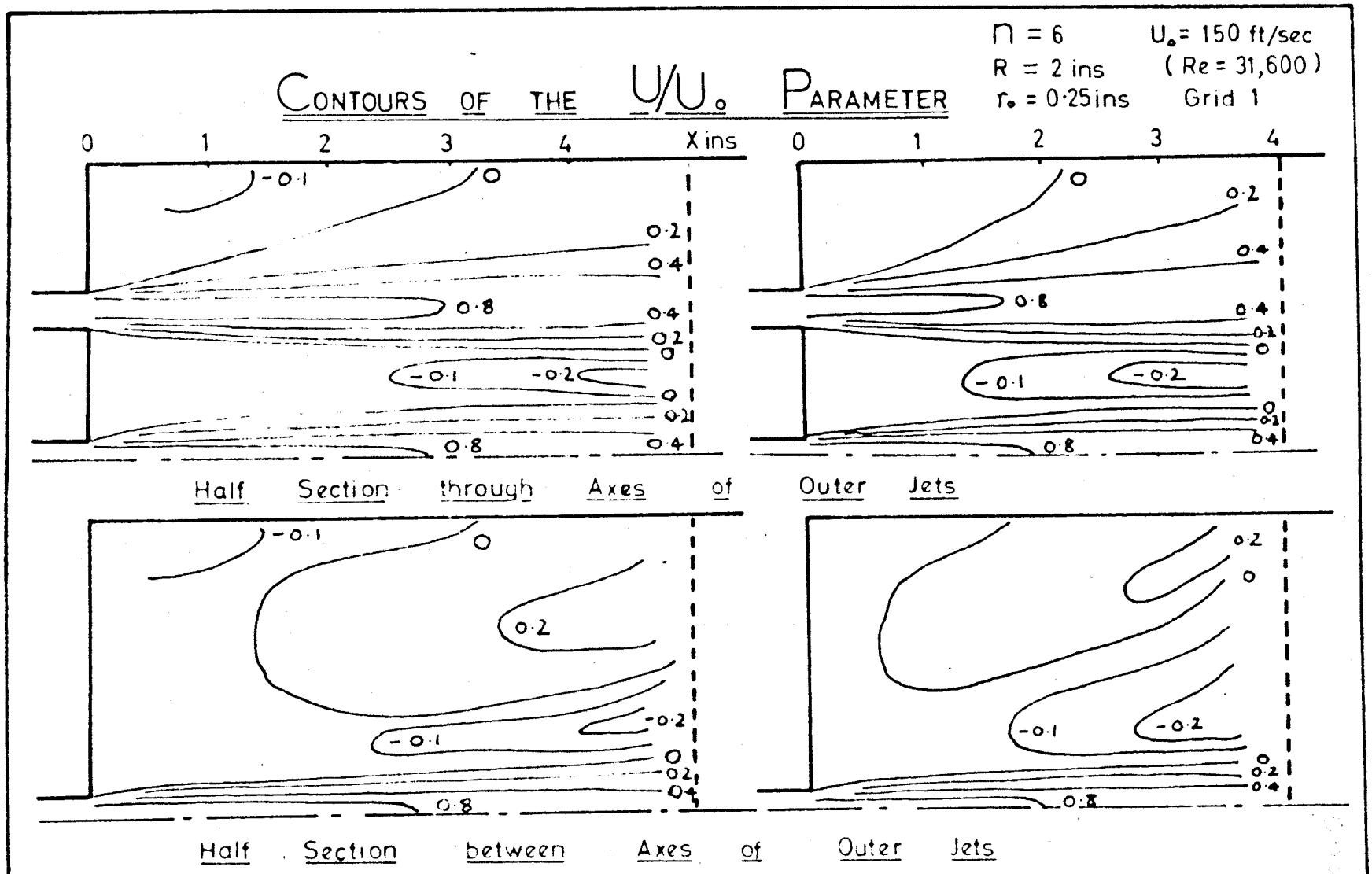


FIG. 17c GRID POSITIONS : X/L = 1·25 AND 1·0

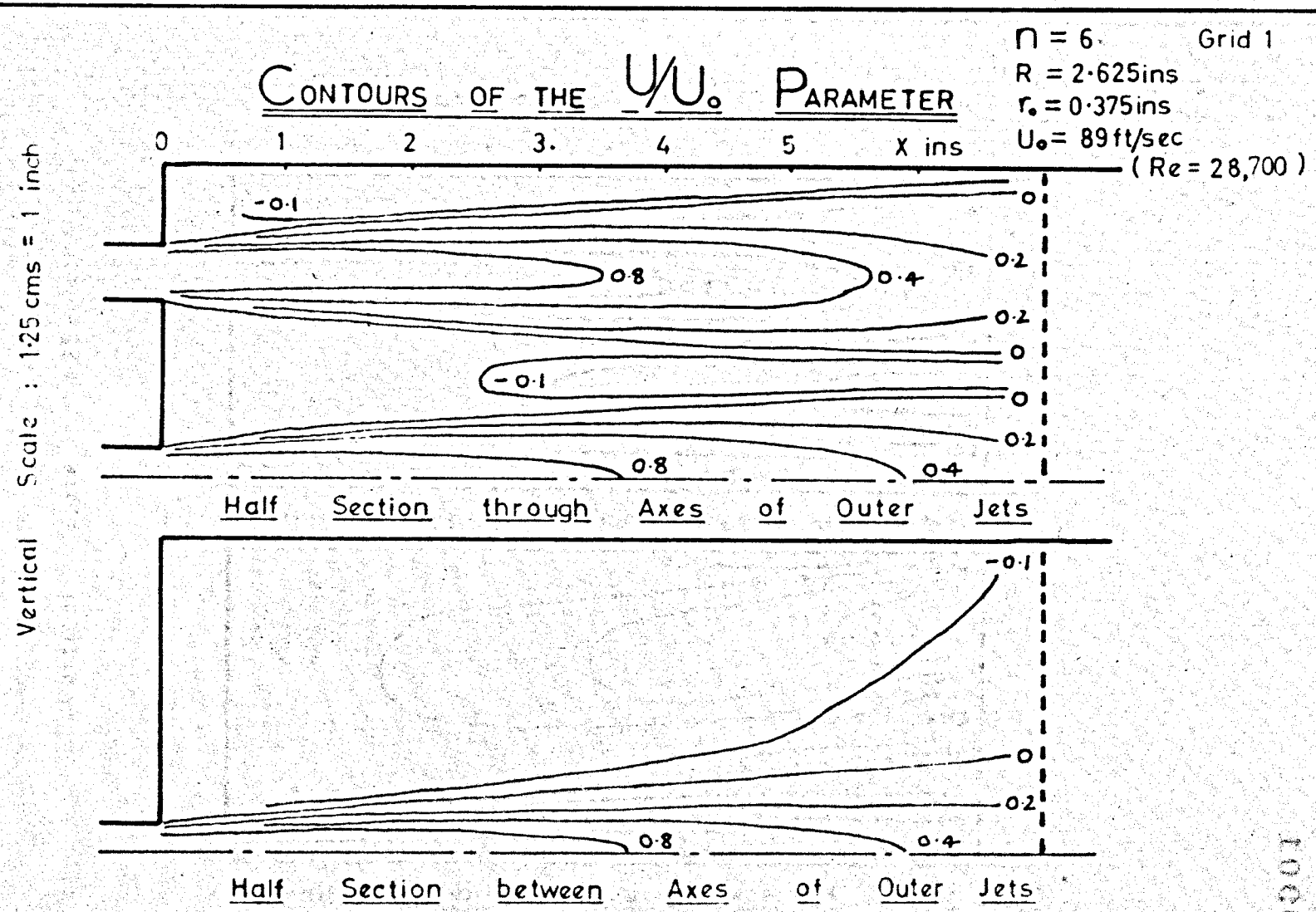


FIG. 18a GRID POSITION : X/L = 1·75

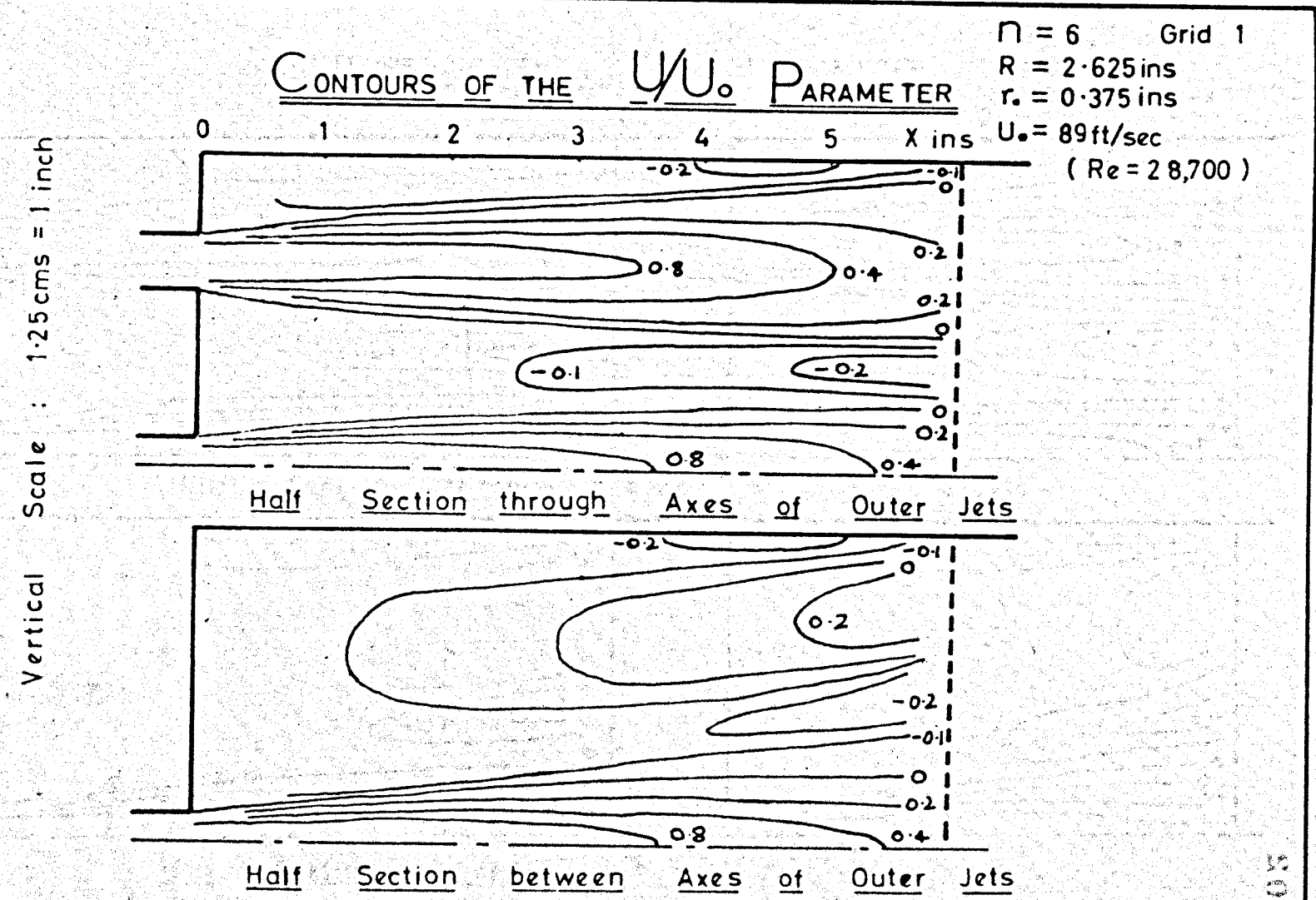


FIG. 18b GRID POSITION : X/L = 1·5

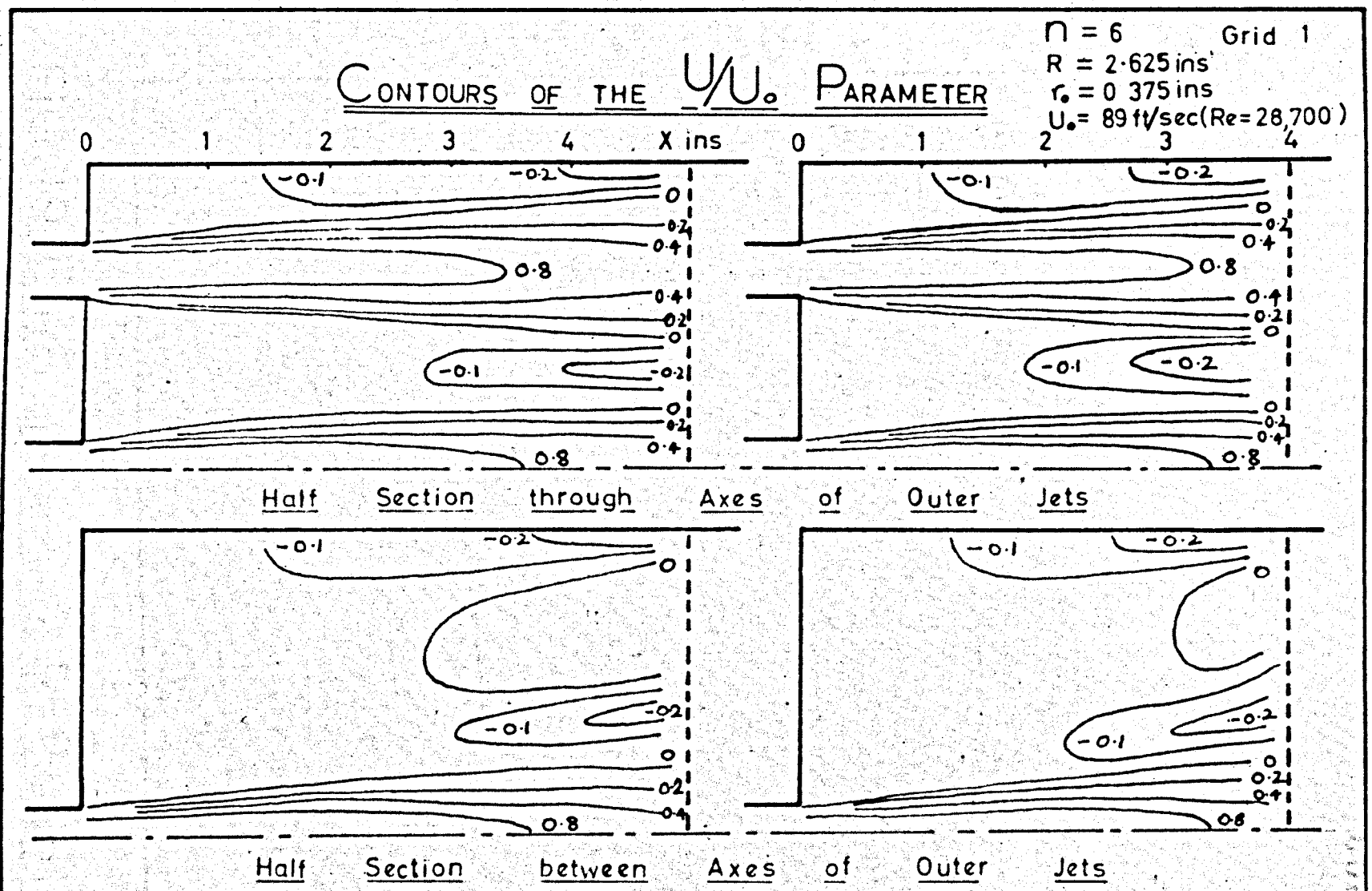


FIG. 18c GRID POSITIONS: X/L = 1·25 AND 1·0

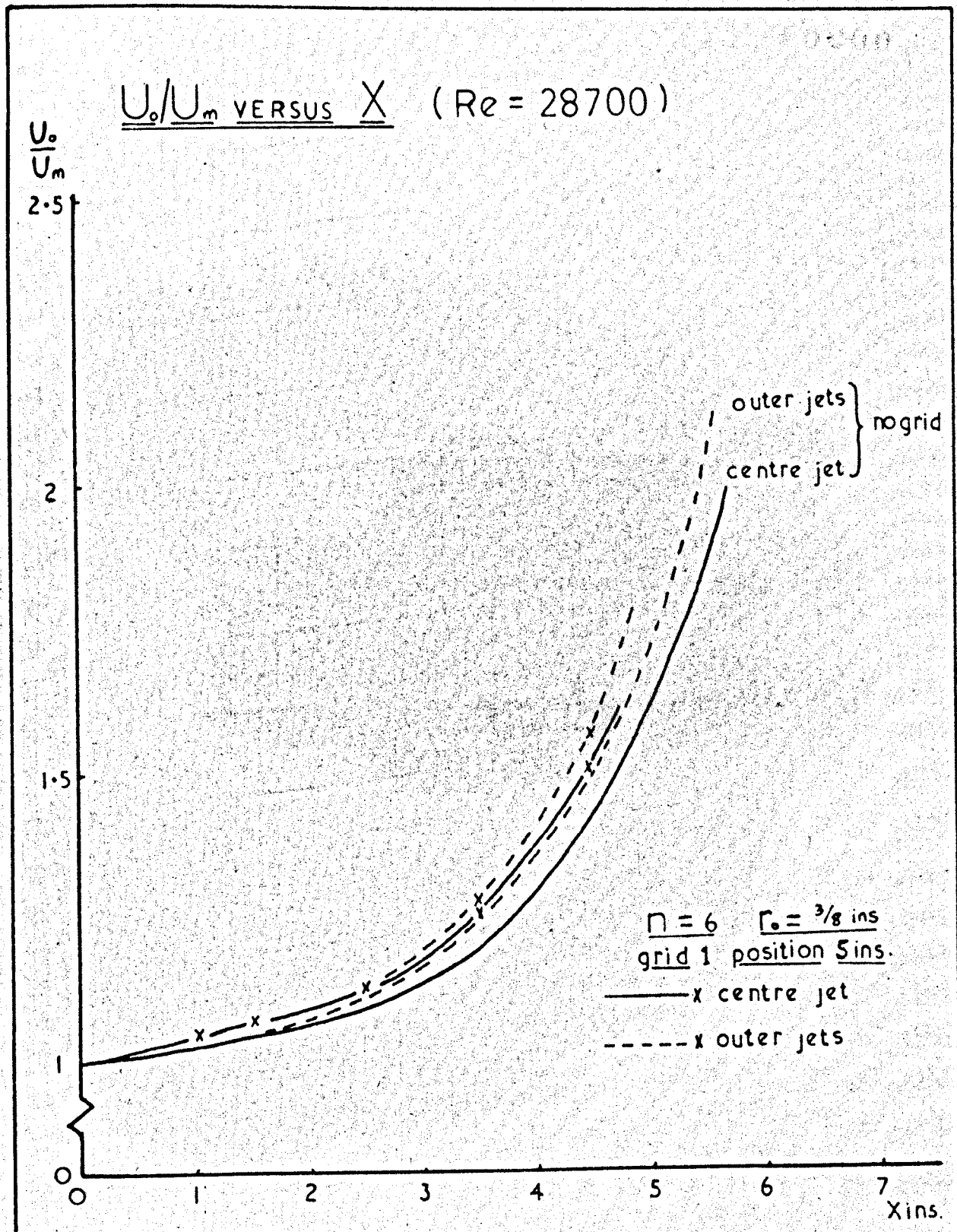


FIG. 19. EFFECT OF GRID WHEN R = 2·625 INCHES

Fig. No. 20 - Comparison of axial velocity decay of single and Multiple Jets, n = 6 and $\theta$ from 0.093 to 0.29

Fig. No. 21 - Comparison of axial velocity decay of single and multiple jets when n = 3, $\theta$ from 0.08 to 0.22

Fig. No. 22 - Comparison of axial velocity decay of single and multiple jets when n = 2, $\theta$ = 0.1 and 0.15

# $U_o/U_m$ VERSUS $X/L'$ FOR $\theta$ FROM 0·14 TO 0·23 AND $n = 6$

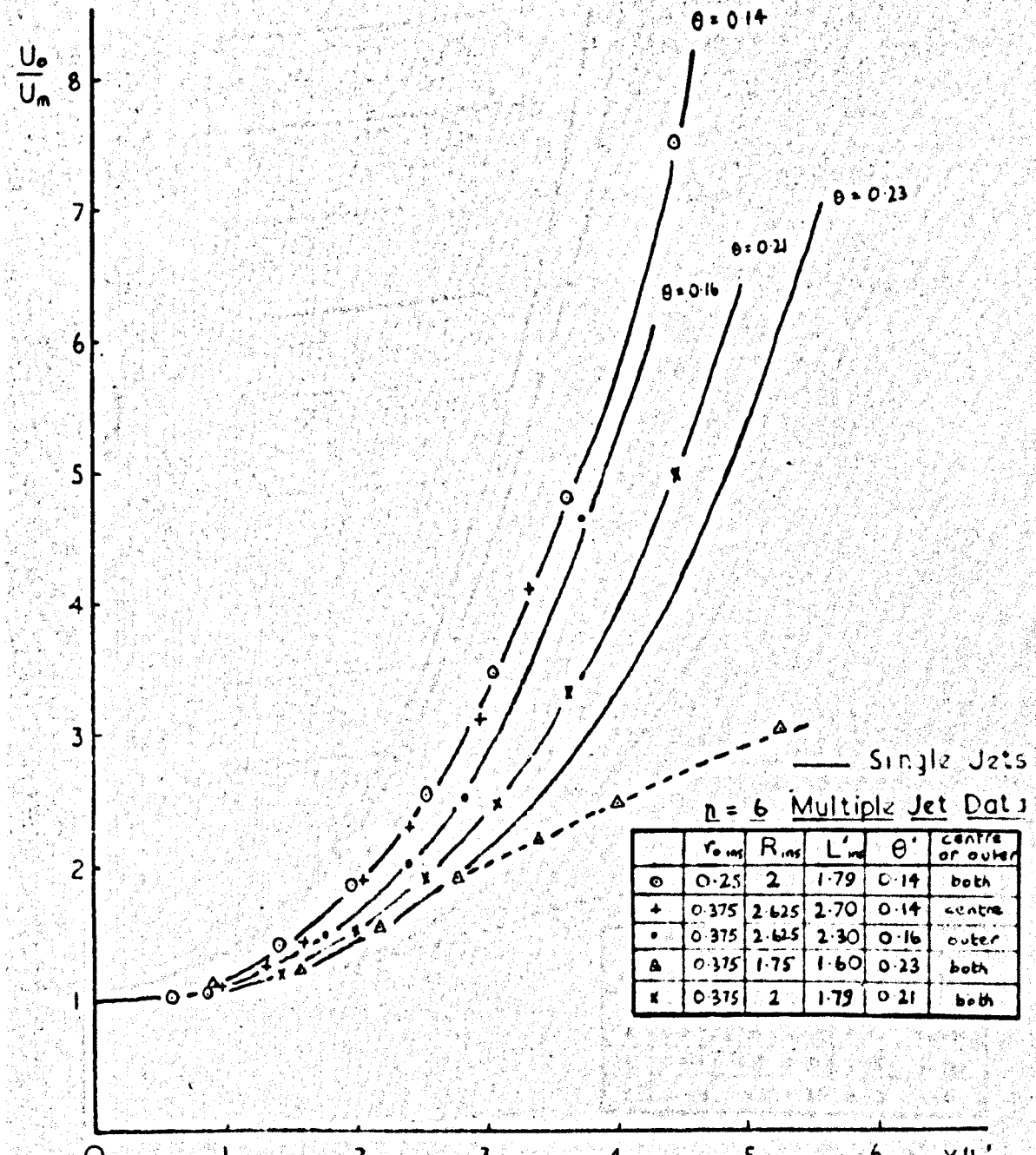


| | $r_{o\,ins}$ | $R_{ins}$ | $L'_{ins}$ | $\theta'$ | centre or outer |
|---|---|---|---|---|---|
| ⊙ | 0·25 | 2 | 1·79 | 0·14 | both |
| + | 0·375 | 2·625 | 2·70 | 0·14 | centre |
| • | 0·375 | 2·625 | 2·30 | 0·16 | outer |
| △ | 0·375 | 1·75 | 1·60 | 0·23 | both |
| × | 0·375 | 2 | 1·79 | 0·21 | both |

FIG. 20a. COMPARISON OF SINGLE AND MULTIPLE JETS

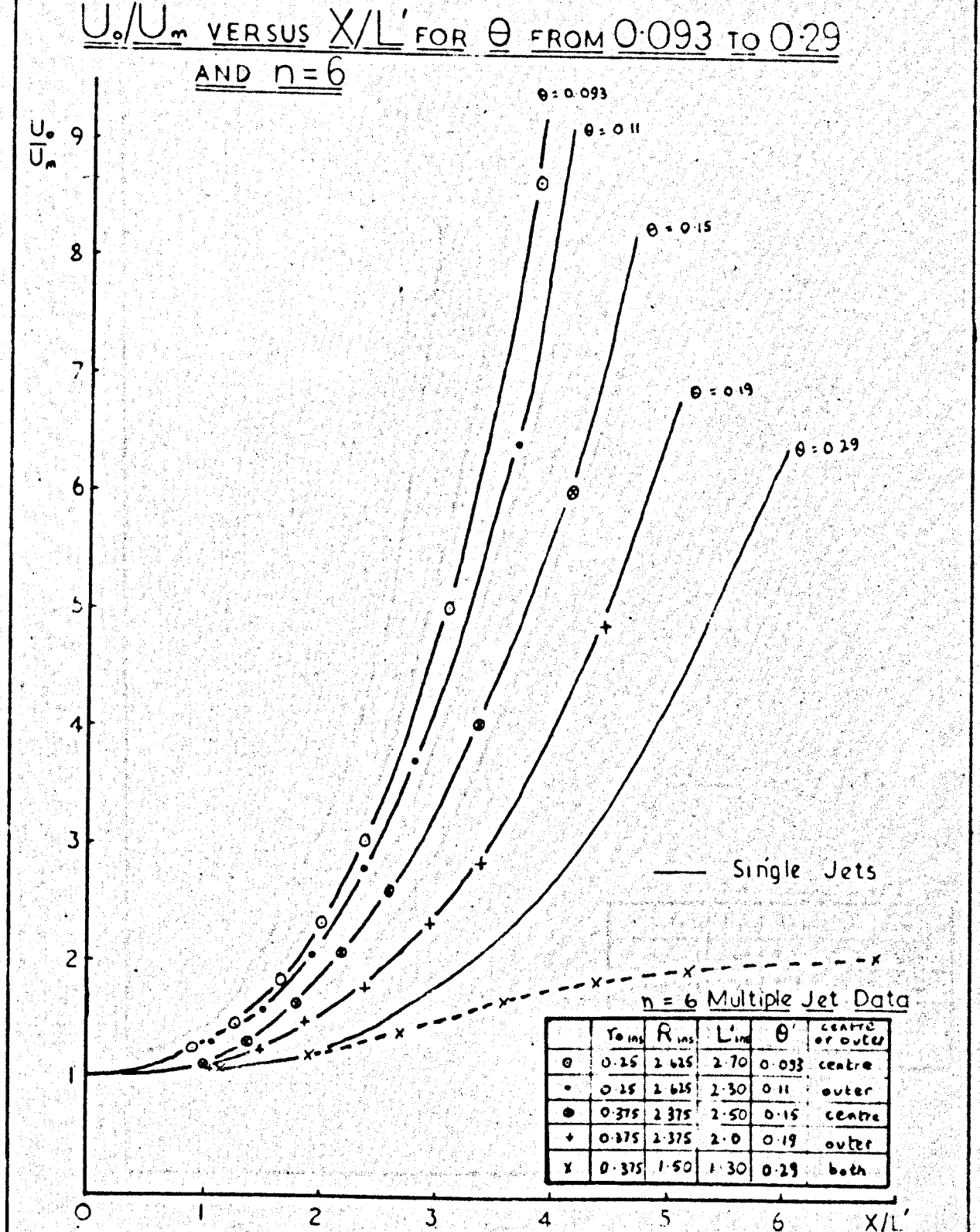


| | $r_{o\,ins}$ | $R_{ins}$ | $L'_{ins}$ | $\theta'$ | centre or outer |
|---|---|---|---|---|---|
| ⊙ | 0·25 | 2·625 | 2·70 | 0·093 | centre |
| • | 0·25 | 2·625 | 2·30 | 0·11 | outer |
| ⊗ | 0·375 | 2·375 | 2·50 | 0·15 | centre |
| + | 0·375 | 2·375 | 2·0 | 0·19 | outer |
| × | 0·375 | 1·50 | 1·30 | 0·29 | both |

FIG. 20b. COMPARISON OF SINGLE AND MULTIPLE JETS

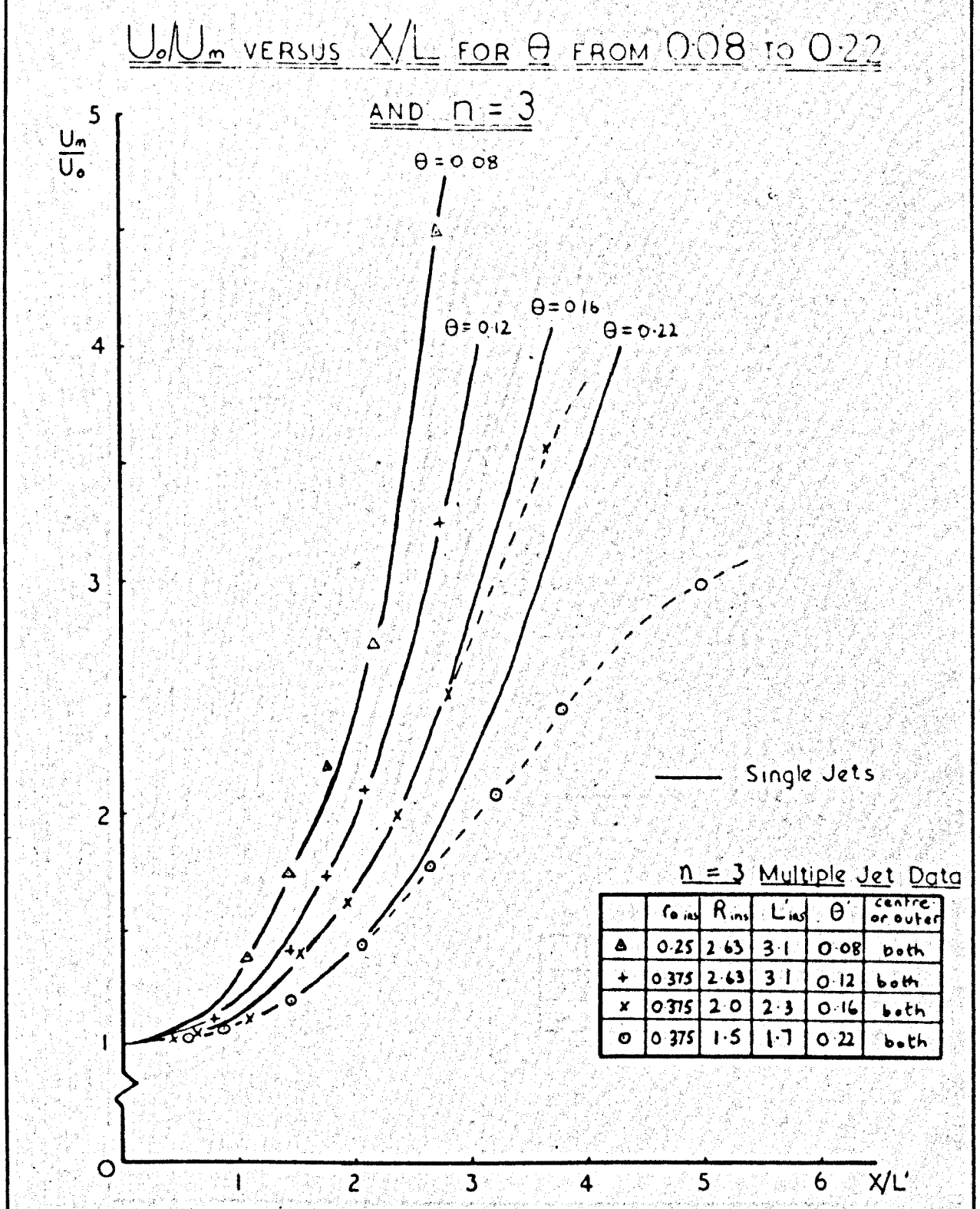


FIG. 21. COMPARISON OF SINGLE AND MULTIPLE JETS

# $U_o/U_m$ VERSUS $X/L$ FOR $\theta = 0.10$ AND $0.15$ AND $n = 2$

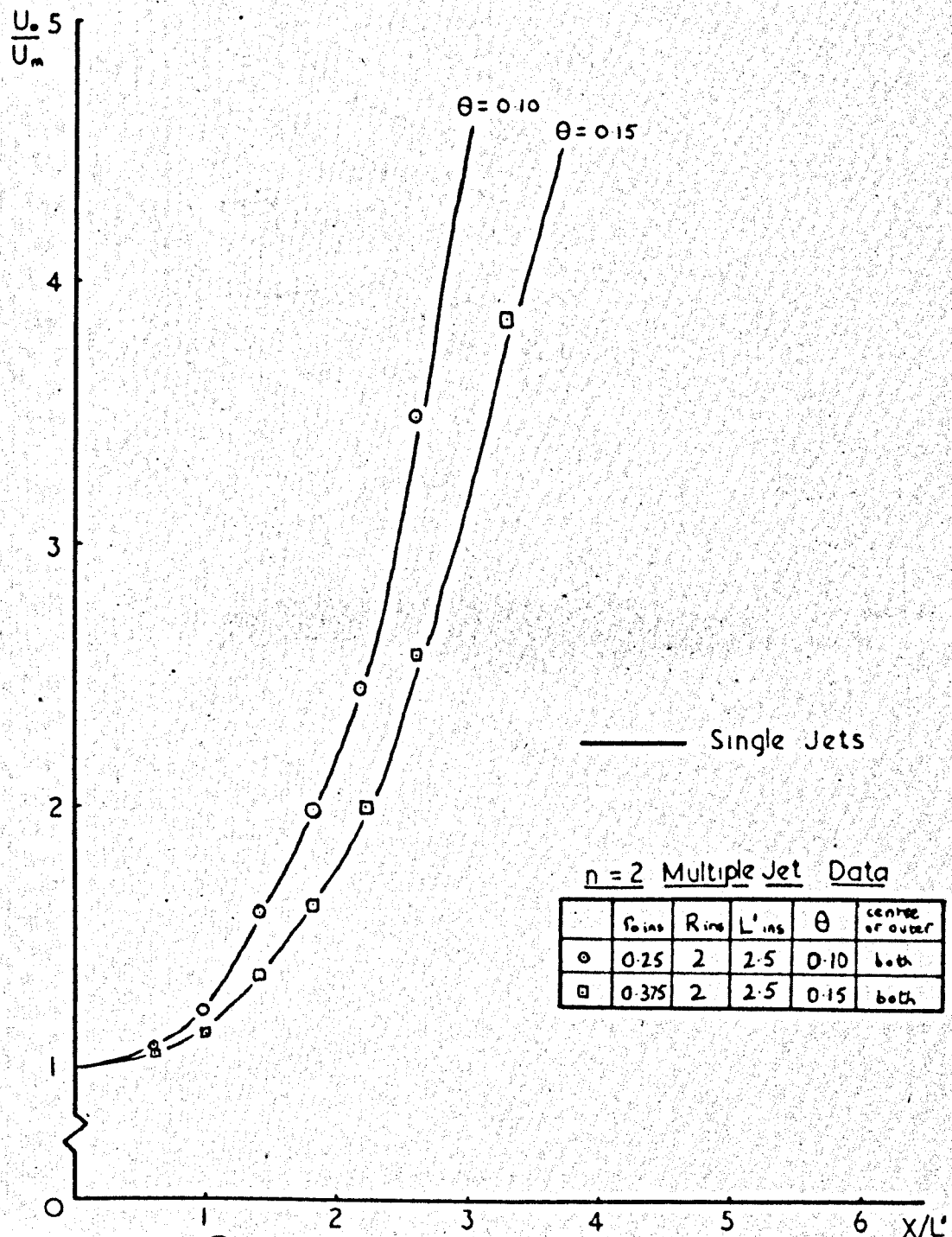


n = 2 Multiple Jet Data

| | $r_o$ ins | R ins | L' ins | θ | centre or outer |
|---|---|---|---|---|---|
| ⊙ | 0.25 | 2 | 2.5 | 0.10 | both |
| ⊡ | 0.375 | 2 | 2.5 | 0.15 | both |

FIG. 22. COMPARISON OF SINGLE AND MULTIPLE JETS

Fig. No. 23 - Comparison of Recirculation in Single and Multiple Enclosed Jet Systems

# $M_R/M_o$ versus $1/\theta$ in Single and Multiple Jet Systems

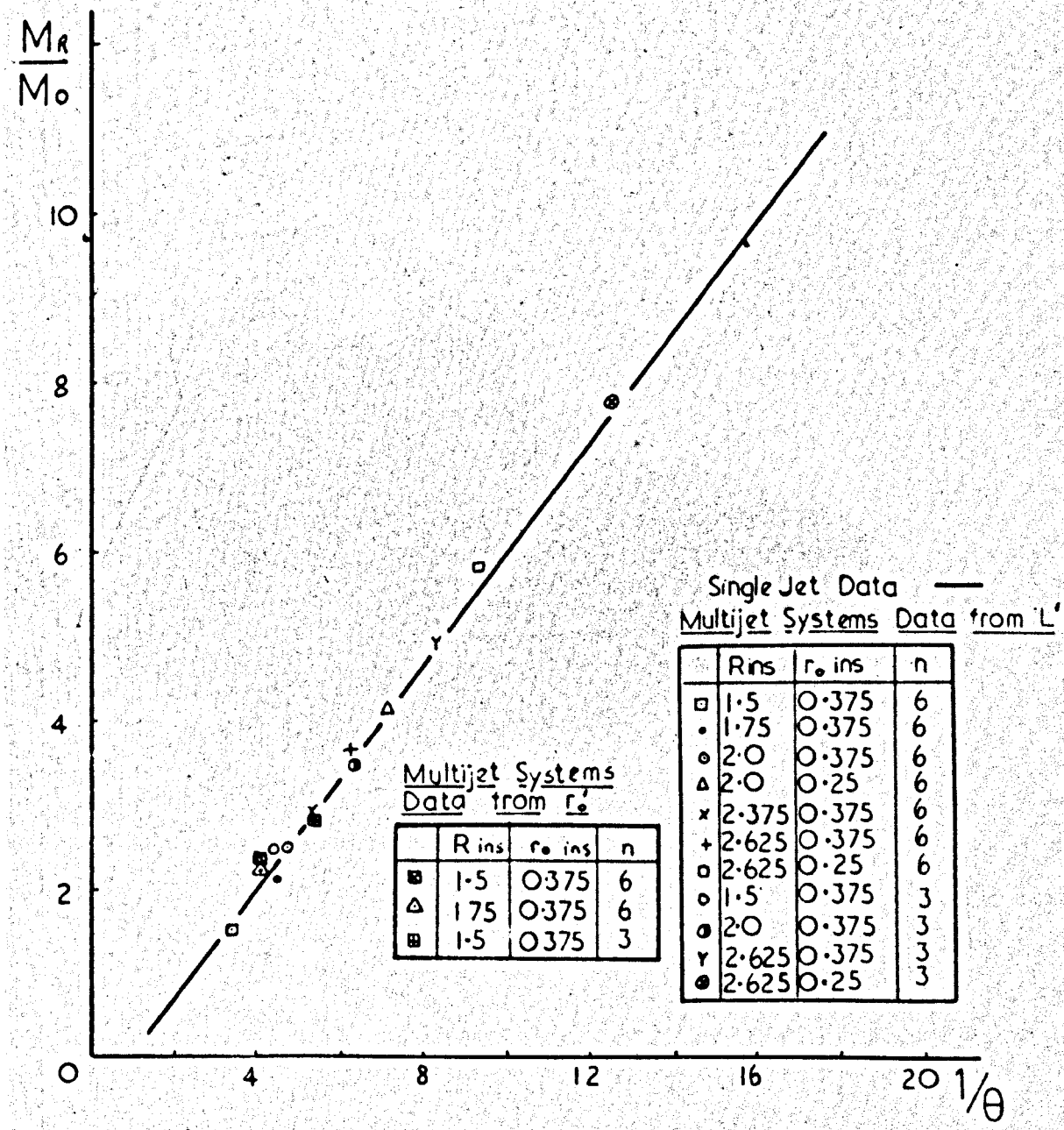


FIG. 23. Recirculation in Multiple Jet Systems

Fig. No. 24 - Water Model Flow Patterns when Re = 14700, $r_o$ = 0.375", n = 6, for $R/L$ from 0.375 to 0.656 and Grid 3 introduction at $x/L$ = 1 and 1.5 when $R/L$ = 0.5

VISUAL OBSERVATION OF WATER FLOW PATTERNS

n = 6
$U_o$ = 3·32 ft/sec
(Re = 14,700)
$r_o$ = 0·375 ins

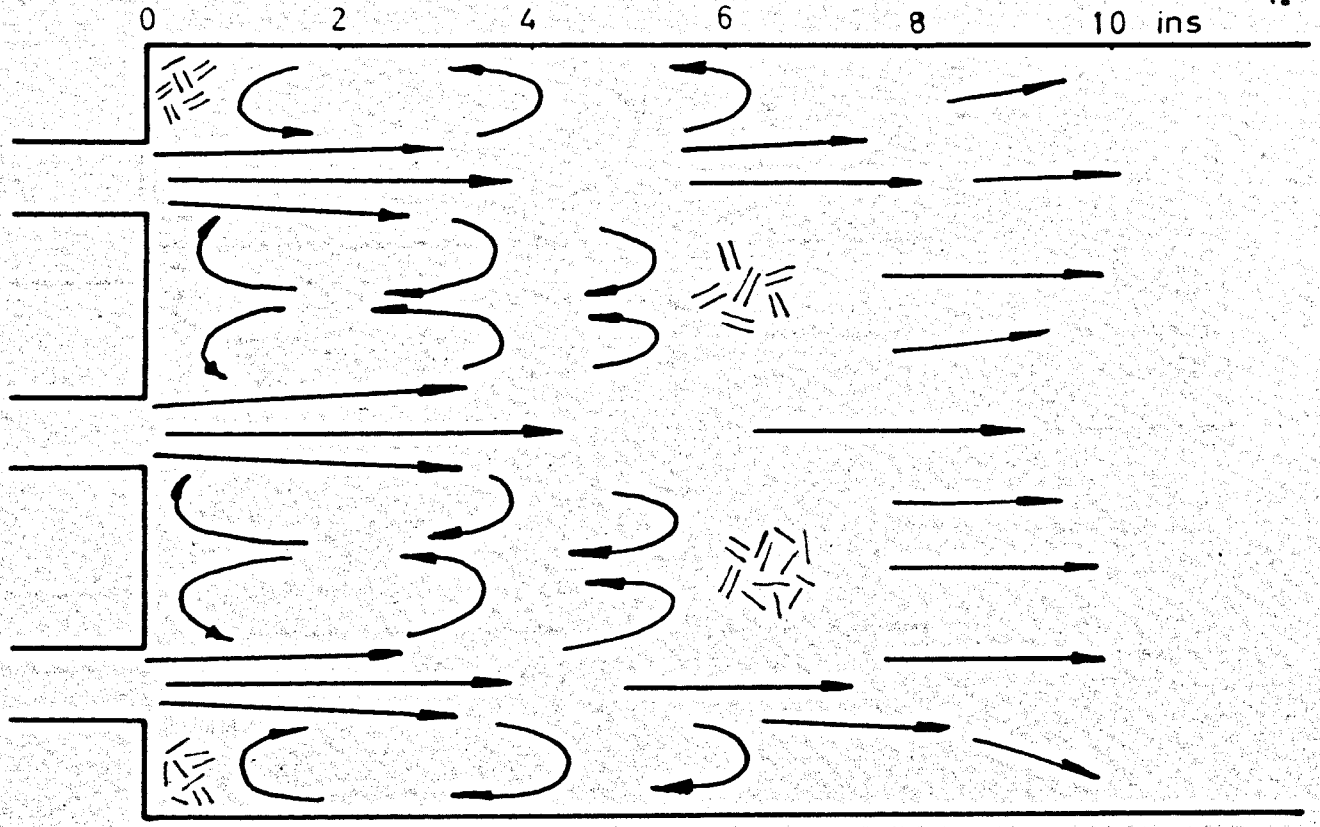


FIG. 24a PITCH DIAMETER OF OUTER JETS = 2·625 INS.

n = 6
$r_o$ = 0·375 ins
$U_o$ = 3·32 ft/sec
( Re = 14,700 )

# VISUAL OBSERVATION OF WATER FLOW PATTERNS

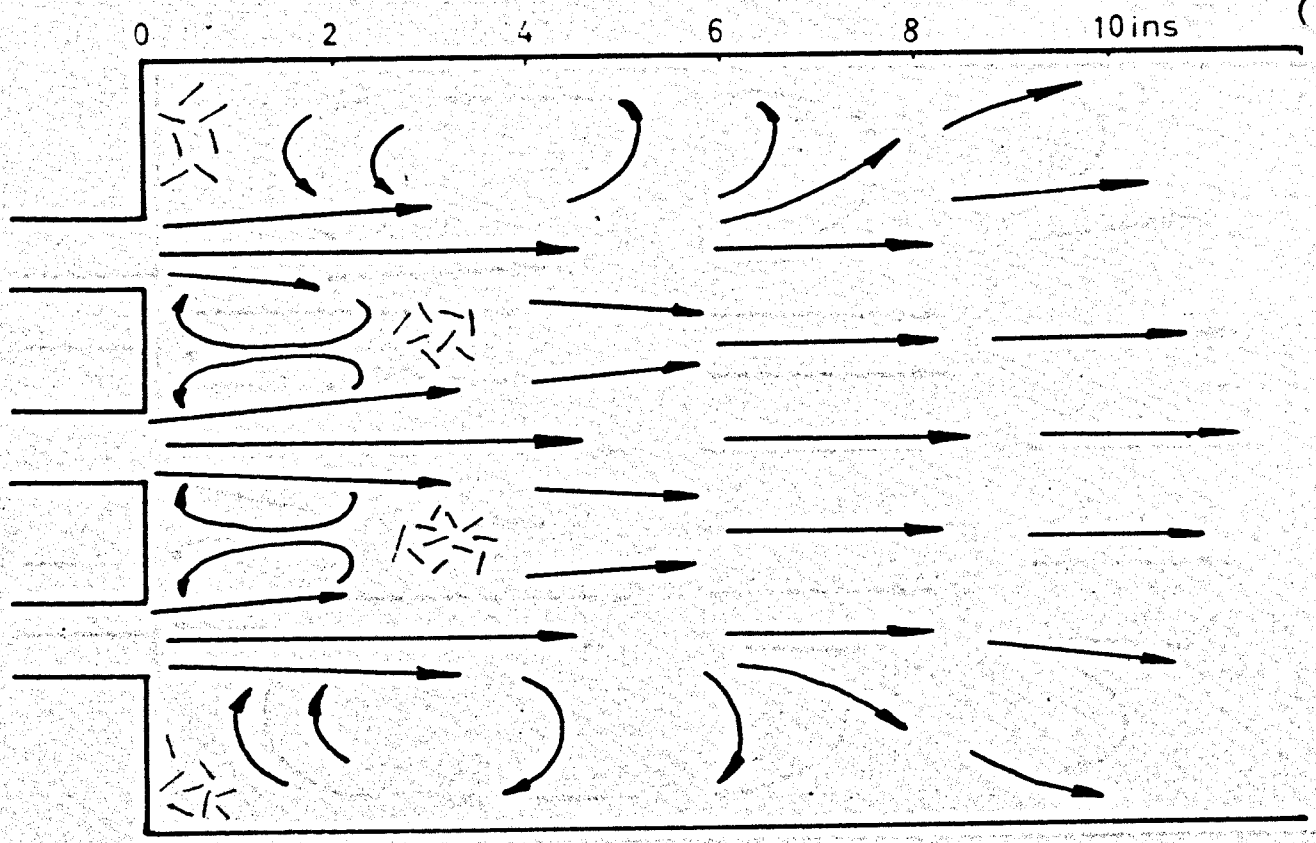


FIG. 24 b PITCH DIAMETER OF OUTER JETS = 2·0 INS.

n = 6
$U_o$ = 3·32 ft/sec
( Re = 14,700 )
$r_o$ = 0·375 ins

# Visual Observation of Water Flow Patterns

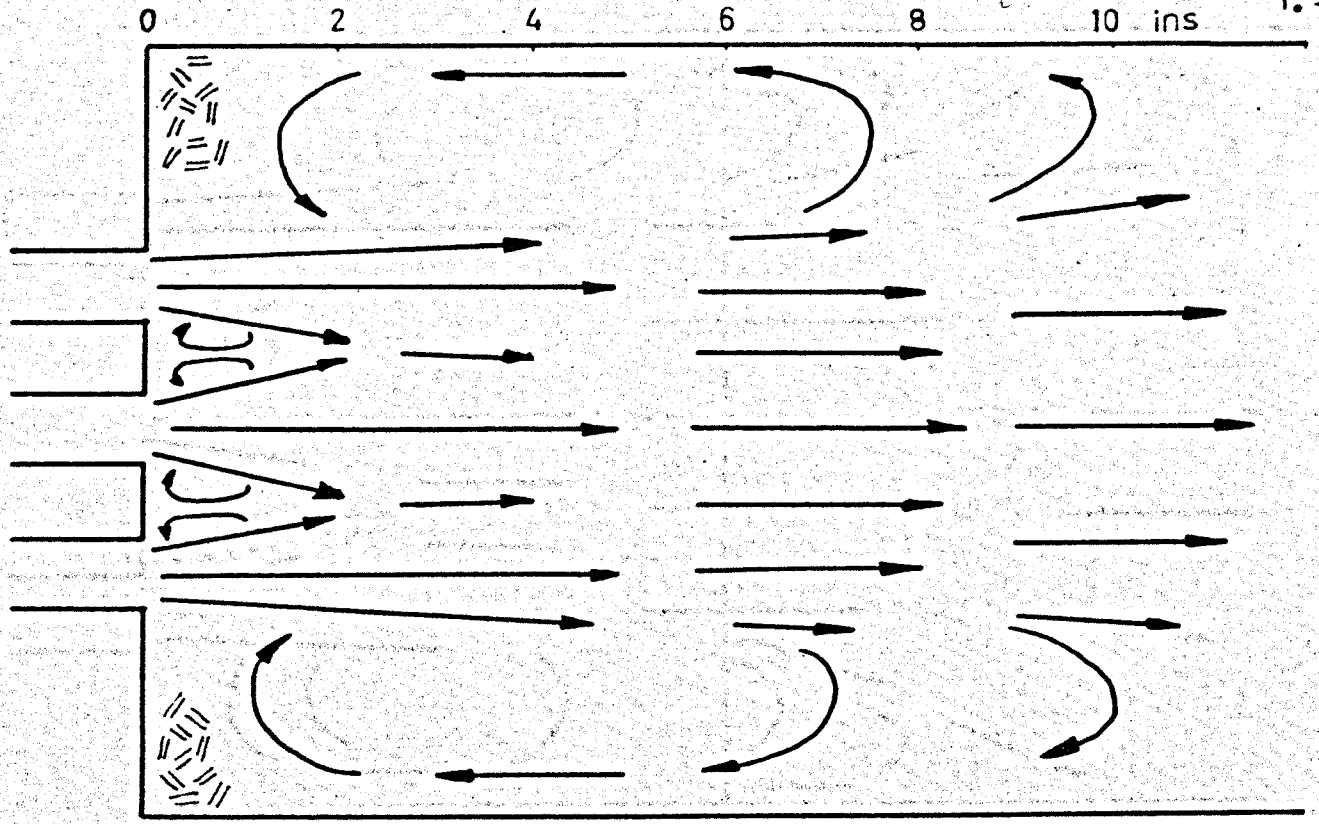


FIG. 24c Pitch Diameter of Outer Jets = 1·5 ins.

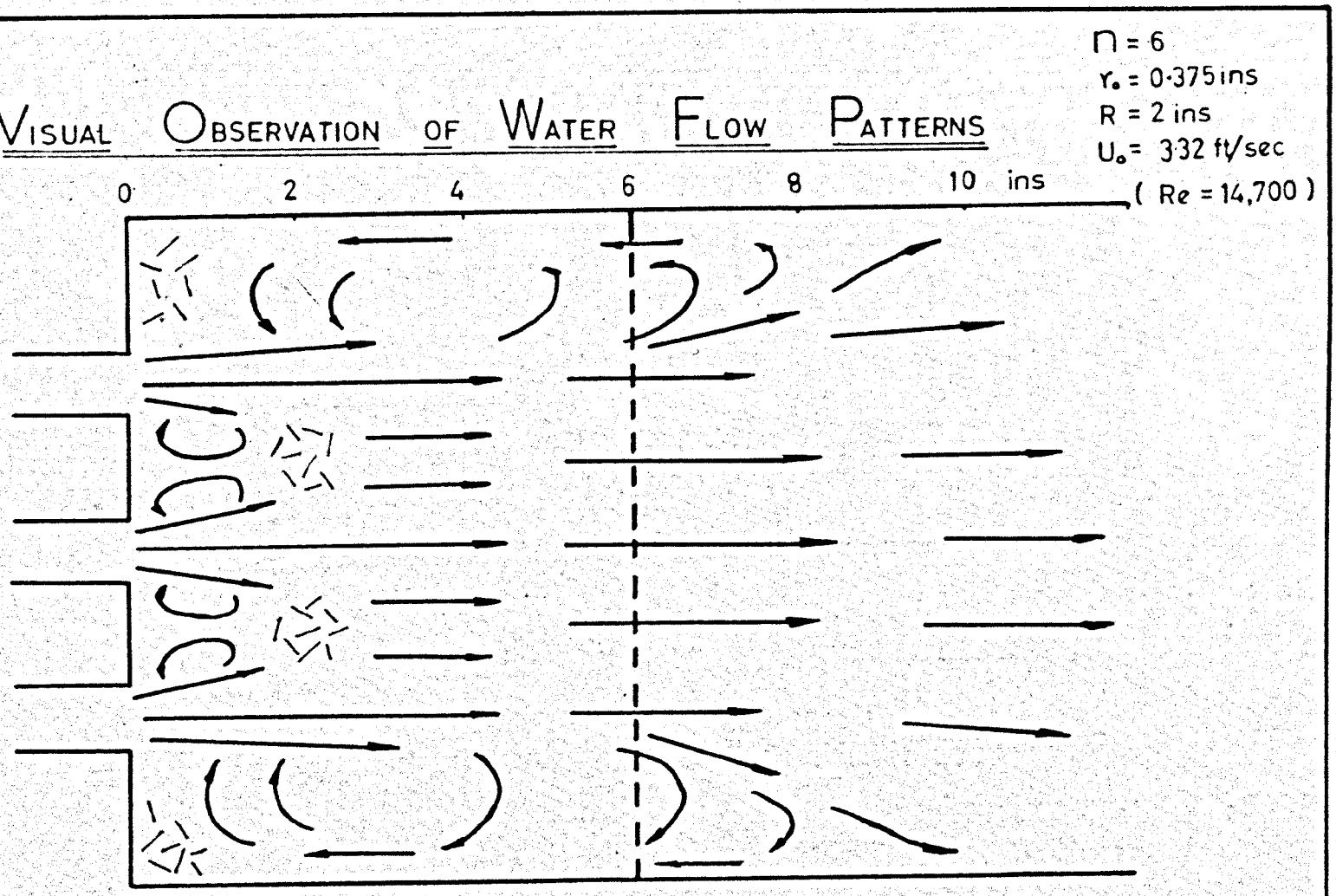


FIG. 24 d GRID 3 POSITION : X/L = 1·5

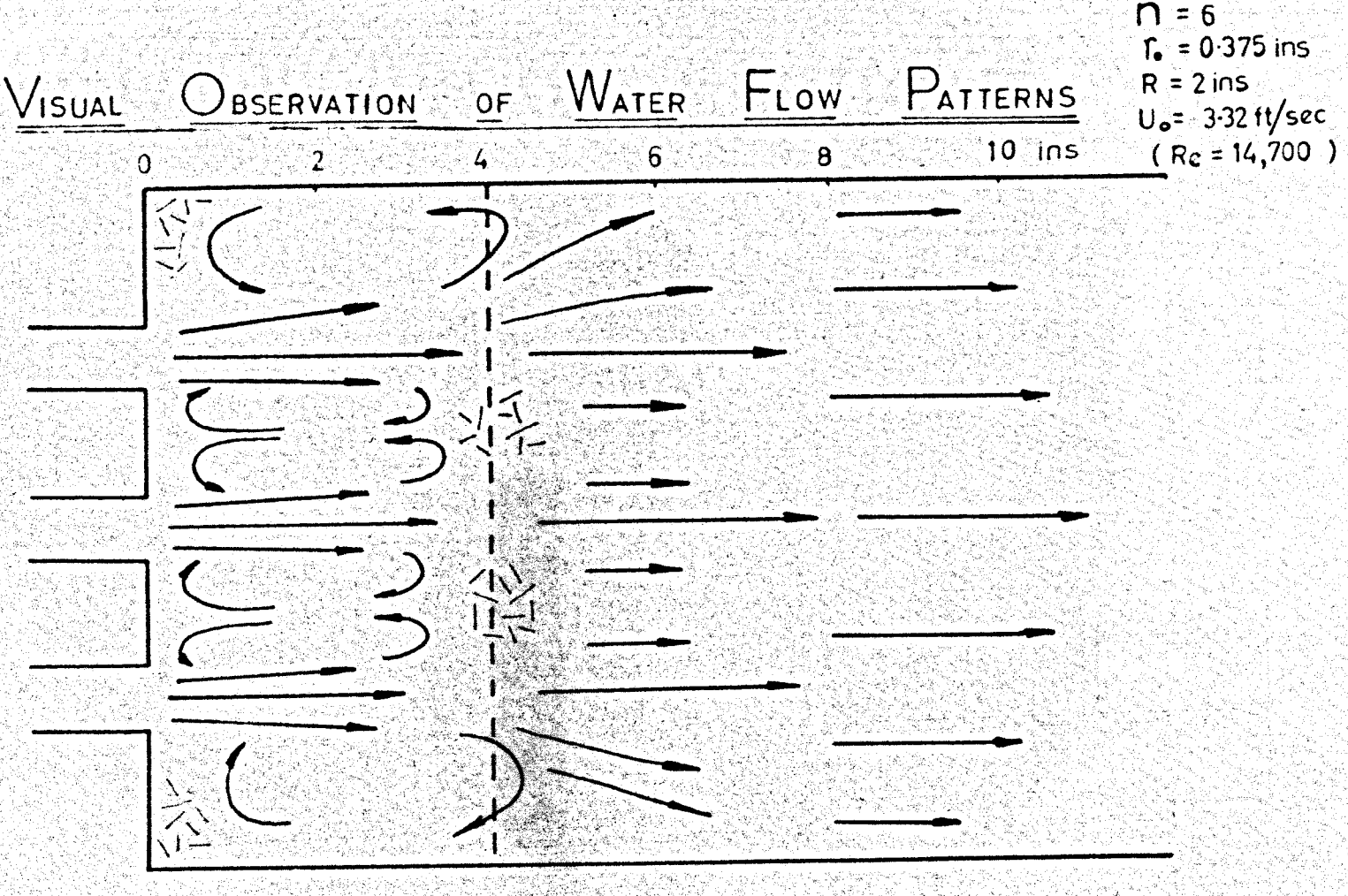


FIG. 24e GRID 3 POSITION : X/L = 1·0

Fig. No. 25 - Temperature Profiles at Exit from Tube Banks based on Flow Pattern Studies, $r_o/L = 0.094$ for $R/L = 0.375$ to $0.656$, $n = 3$ and $6$

# THEORETICAL ISOTHERMS AT EXIT FROM TUBE BANKS

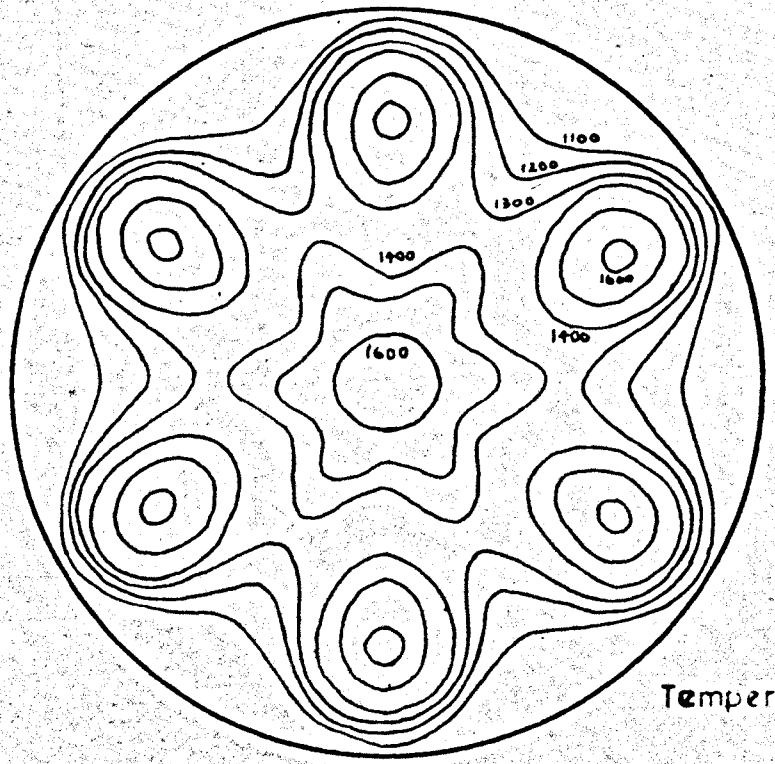


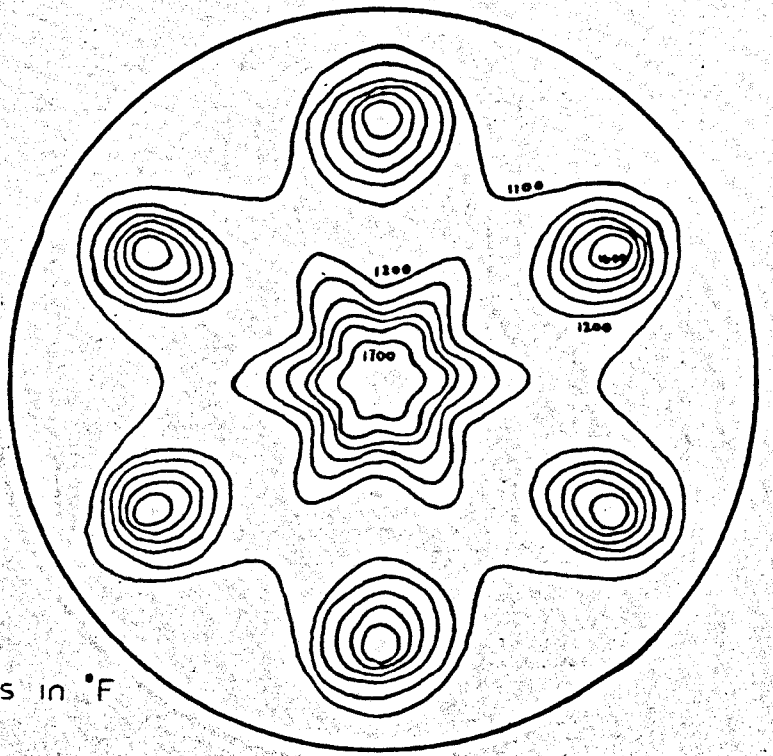


Temperatures in °F

Uniform Temperature at inlet to Tube Banks = 2600° F

Temperature proportional to Velocity at inlet to Tube Banks. Maximum Temperature = 2950°F

FIG. 25a BURNER CONFIGURATION : $R/L = 0{\cdot}656$, $r_o/L = 0{\cdot}094$, $n = 6$

# Theoretical Isotherms at Exit from Tube Banks

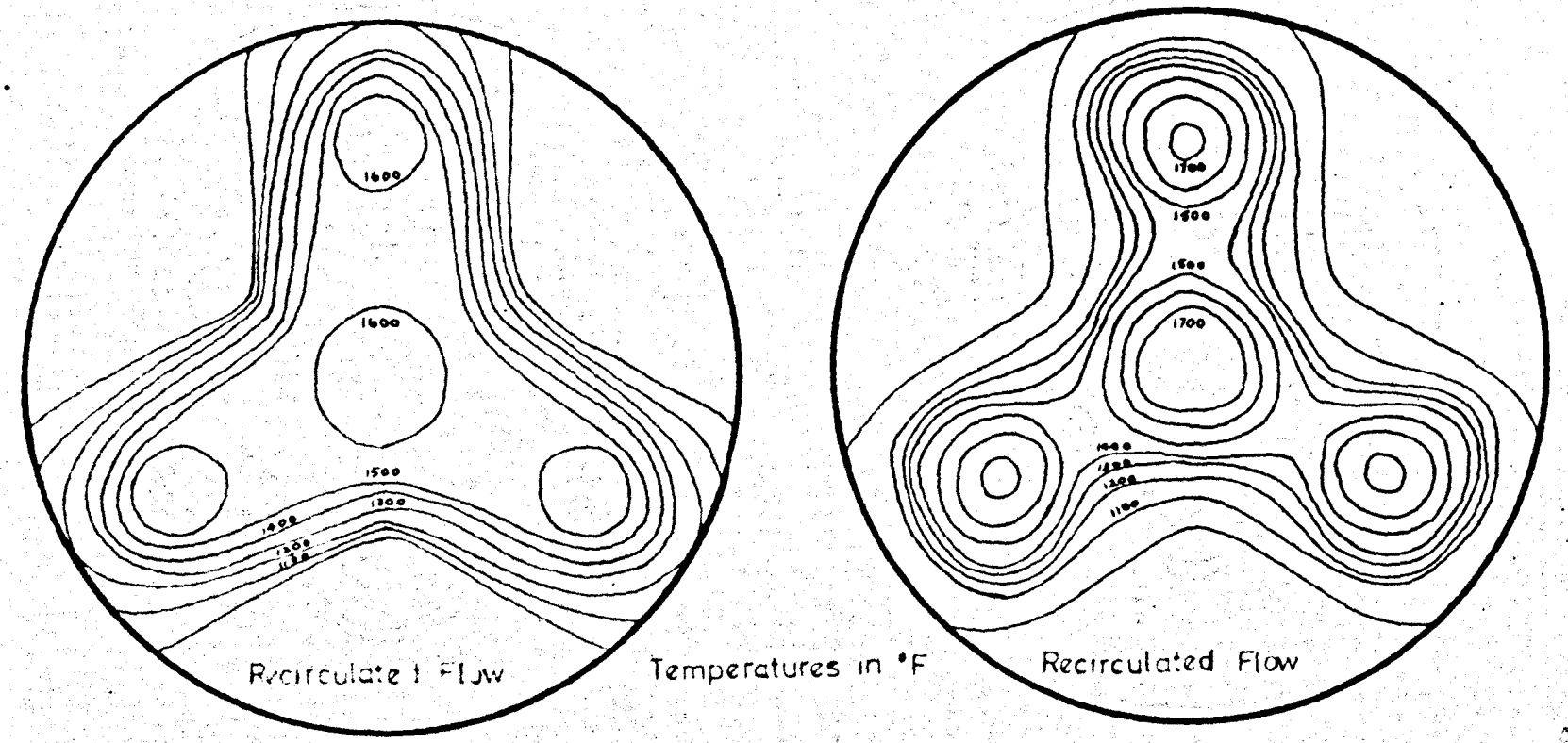


Uniform Temperature at inlet to Tube Banks = 2000 °F

Temperature proportional to Velocity at inlet to Tube Banks. Maximum Temperature = 2950 °F

FIG. 25 b Burner Configuration : $R/L = 0{\cdot}656$, $r_o/L = 0{\cdot}094$, $n = 3$

# THEORETICAL ISOTHERMS AT EXIT FROM TUBE BANKS

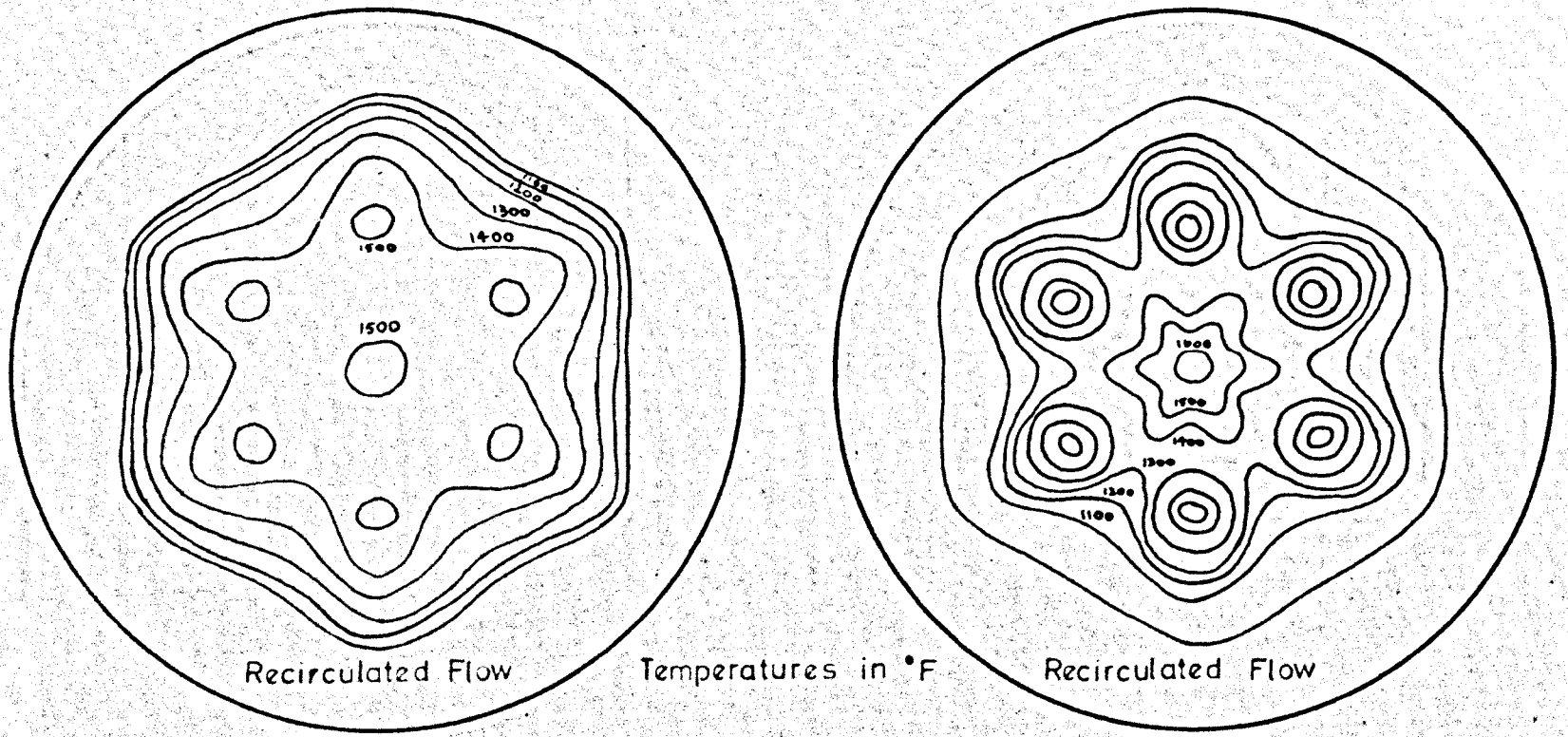


Uniform Temperature at inlet to Tube Banks = 2600°F

Temperature proportional to Velocity at Inlet to Tube Banks. Maximum Temperature = 2950°F

FIG. 25c BURNER CONFIGURATION : $R/L = 0.5$, $r_o/L = 0.094$, $n = 6$

# THEORETICAL ISOTHERMS AT EXIT FROM TUBE BANKS

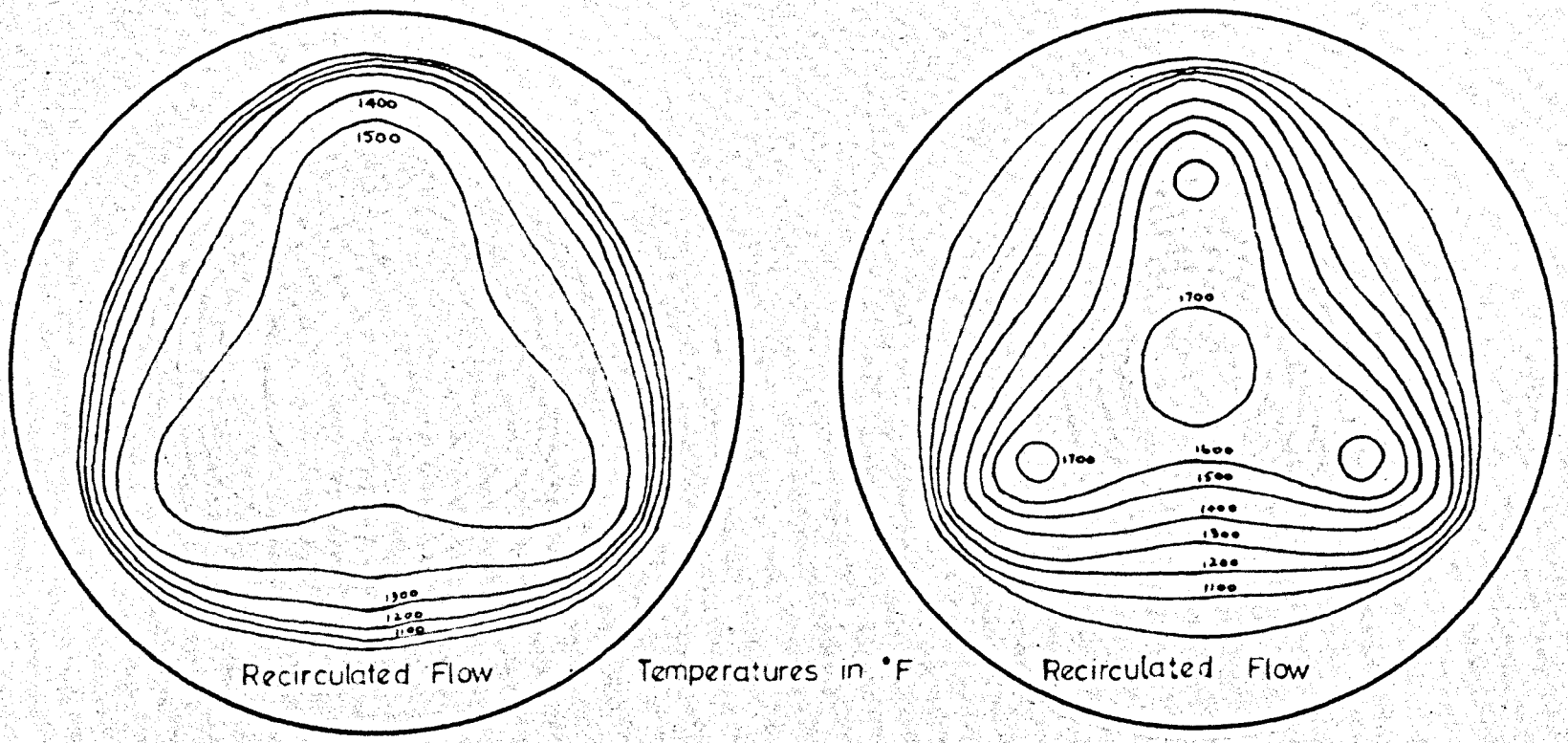


Uniform Temperature at inlet to Tube Banks = 2600°F

Temperature proportional to Velocity at inlet to Tube Banks. Maximum Temperature = 2950°F

FIG. 25d BURNER CONFIGURATION : $R/L = 0.5$, $r_o/L = 0.094$, $n = 3$

# THEORETICAL ISOTHERMS AT EXIT FROM TUBE BANKS

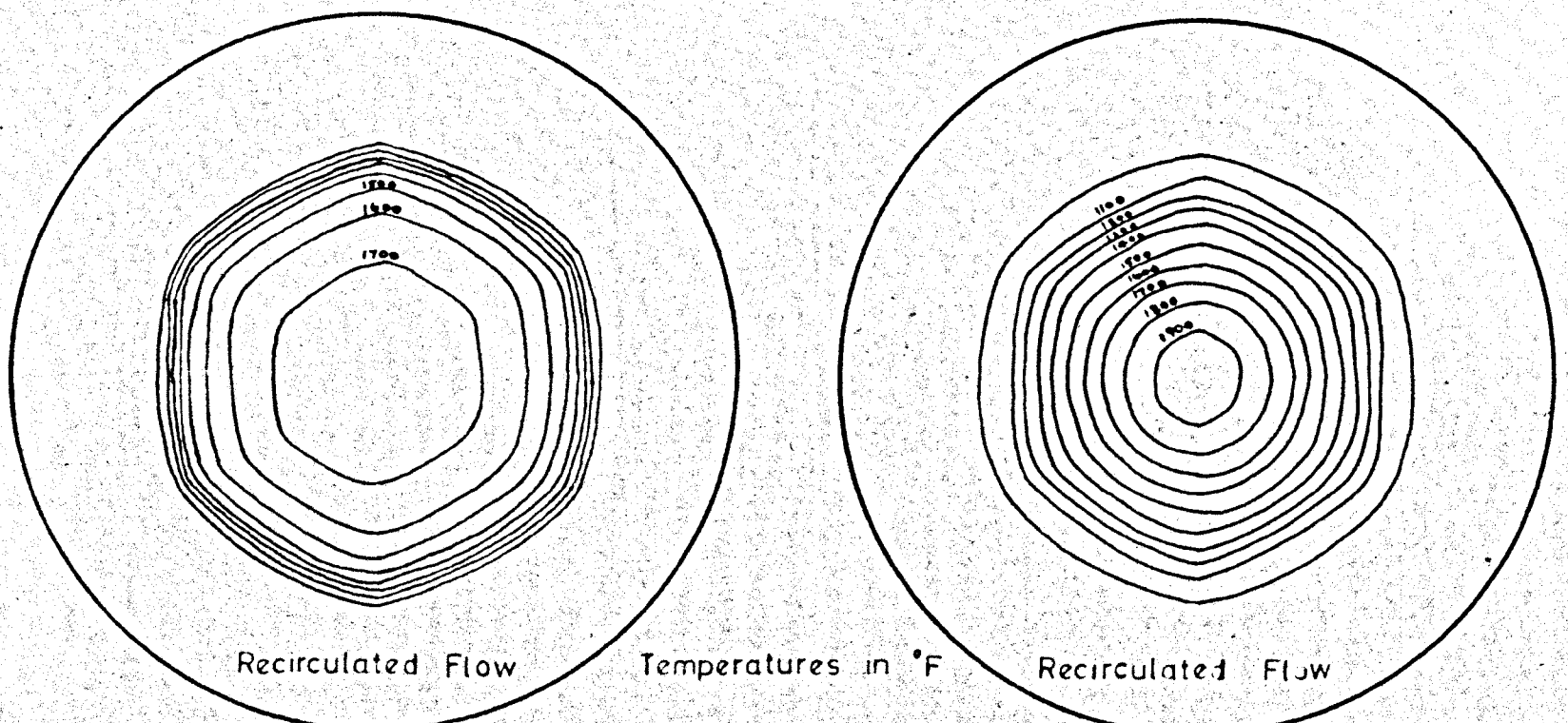


Uniform Temperature at inlet to Tube Banks = 2600°F

Temperature proportional to Velocity at inlet to Tube Banks. Maximum Temperature = 2950°F

FIG. 25e BURNER CONFIGURATION : $R/L = 0.375$, $r_o/L = 0.094$, $n = 6$

# THEORETICAL ISOTHERMS AT EXIT FROM TUBE BANKS

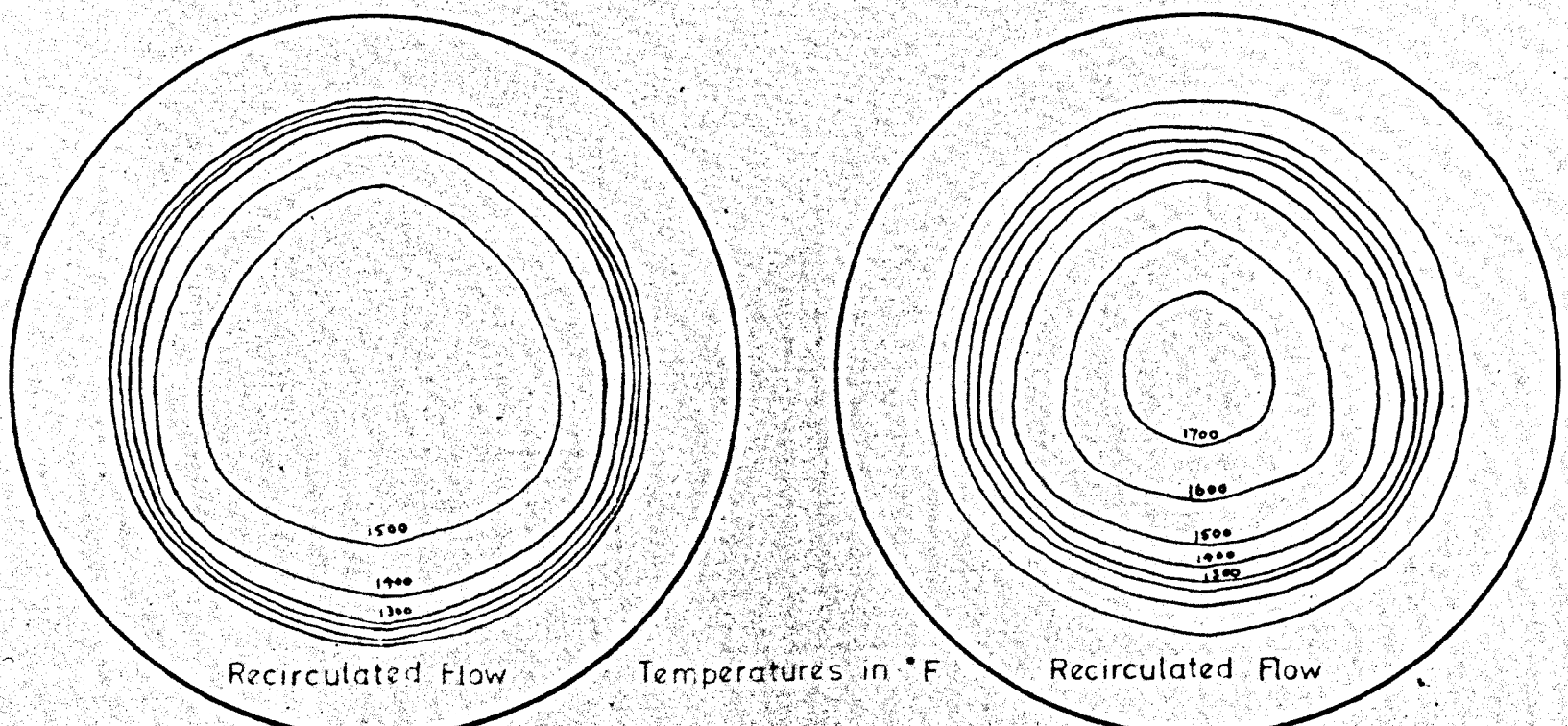


Uniform Temperature at inlet to Tube Banks = 2600°F

Temperature proportional to Velocity at inlet to Tube Banks, Maximum Temperature = 2950°F

FIG. 25f BURNER CONFIGURATION : $R/L = 0.375$, $r_0/L = 0.094$, $n = 3$

Fig. No. 26 - Effect of Increased Swirl on a Single Enclosed Jet Flow Pattern, $r_o$ = 0.375" and Tangential Air input is varied from to 45.1% of the total nozzle fluid

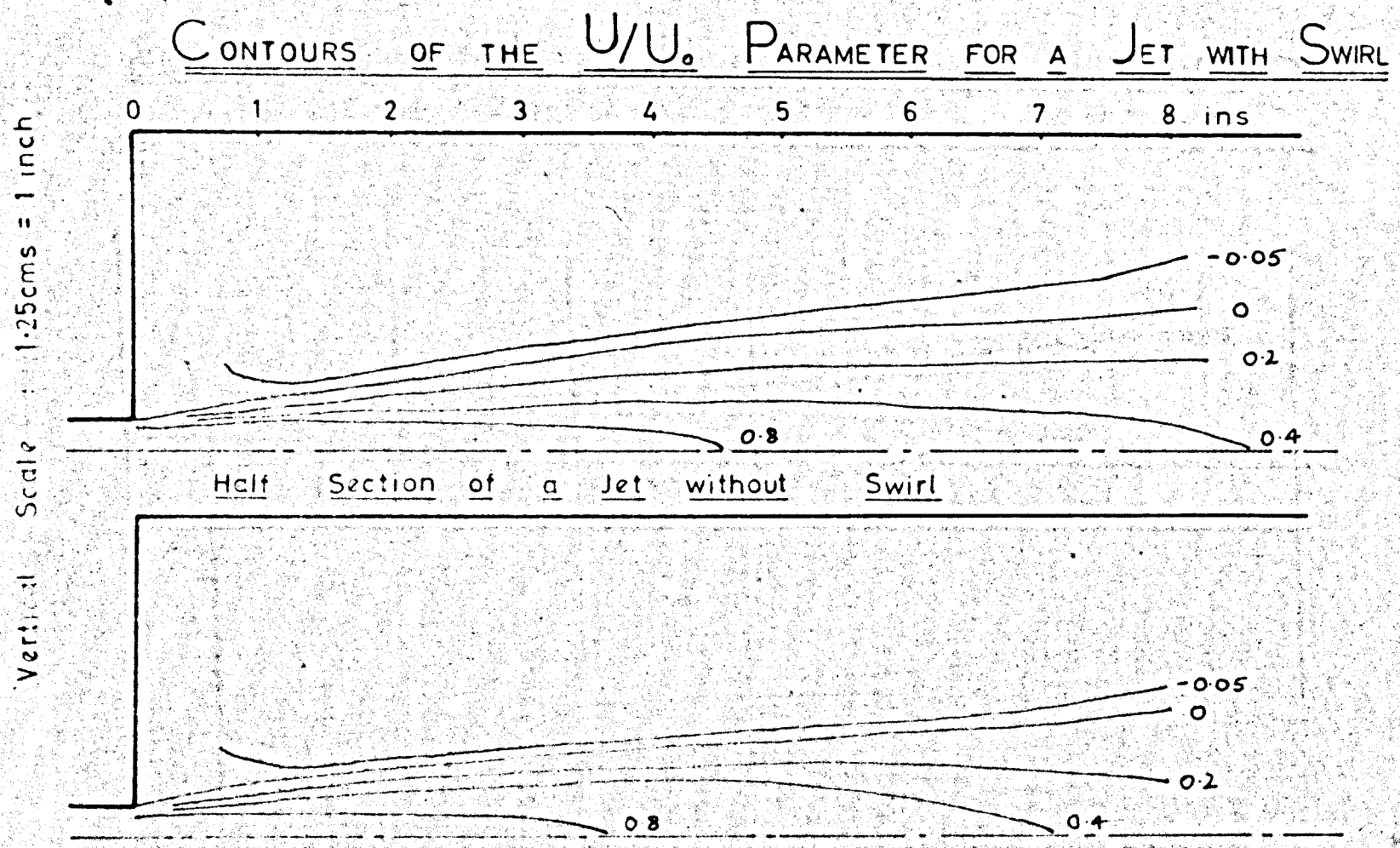


FIG. 26a EFFECT OF DEGREE OF SWIRL ON A 3/4" DIA. JET

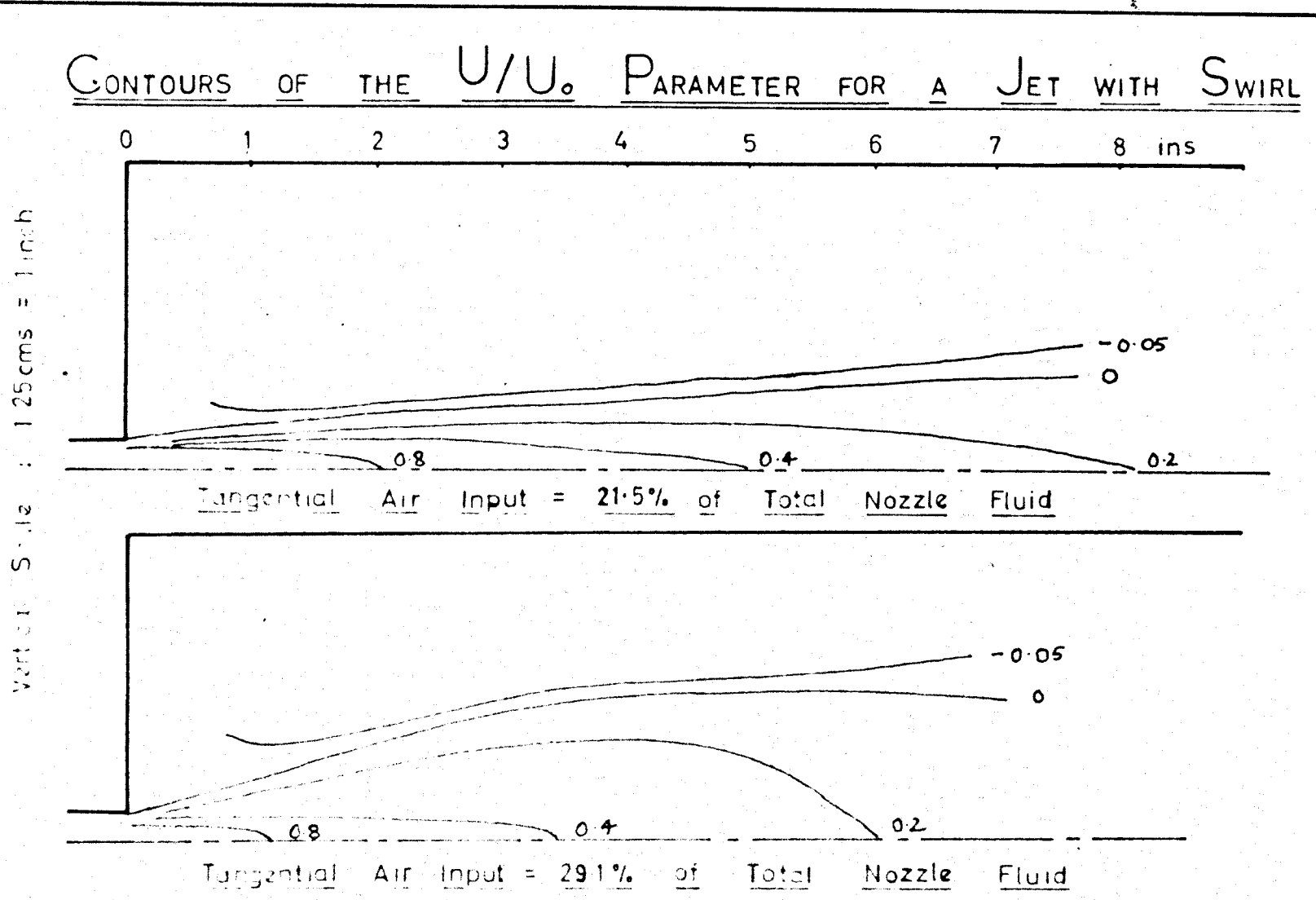


FIG. 26b EFFECT OF DEGREE OF SWIRL ON A 3/4" DIA. JET

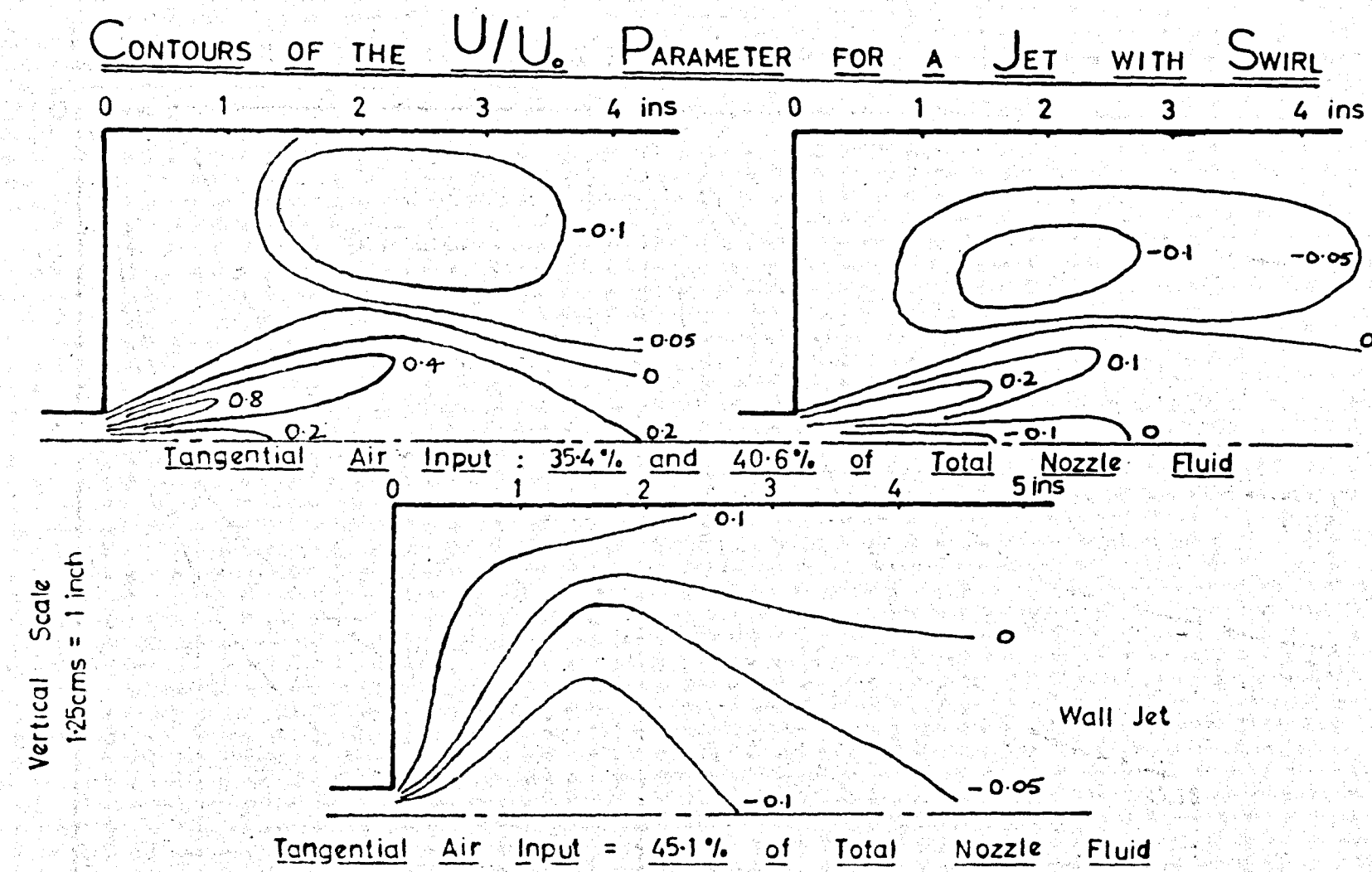


FIG. 26c EFFECT OF DEGREE OF SWIRL ON A 3/4" DIA. JET

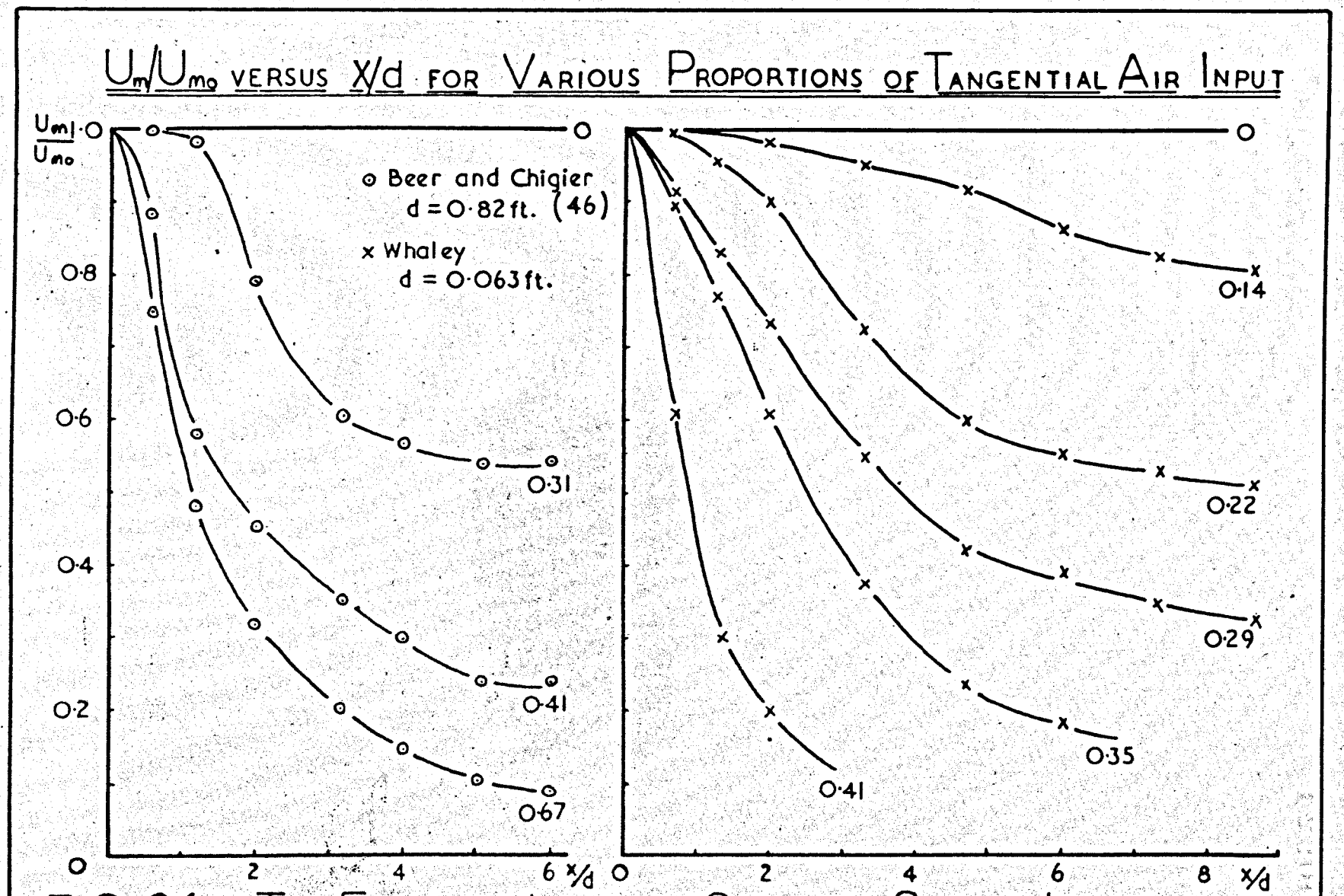


FIG. 26d THE EFFECT OF INCREASED SWIRL ON SINGLE JETS

Fig. No. 27 - Calibration Characteristics of the "T" shaped Probe. Comparison with standard pitot tube

Fig. No. 28 - Calibration Characteristics of the "T" shaped Probe. Pitching and Yawing Characteristics.

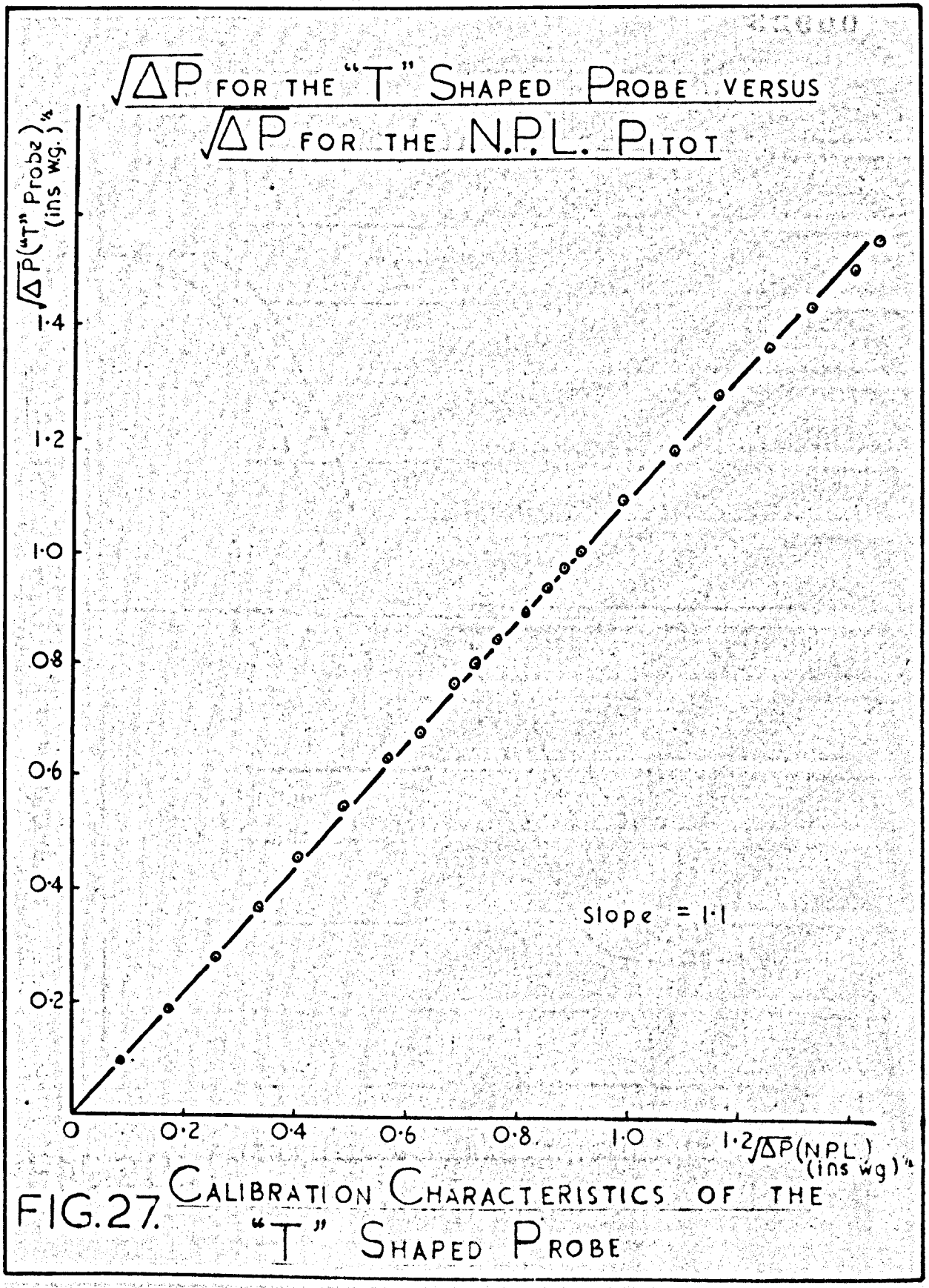


FIG.27. CALIBRATION CHARACTERISTICS OF THE "T" SHAPED PROBE

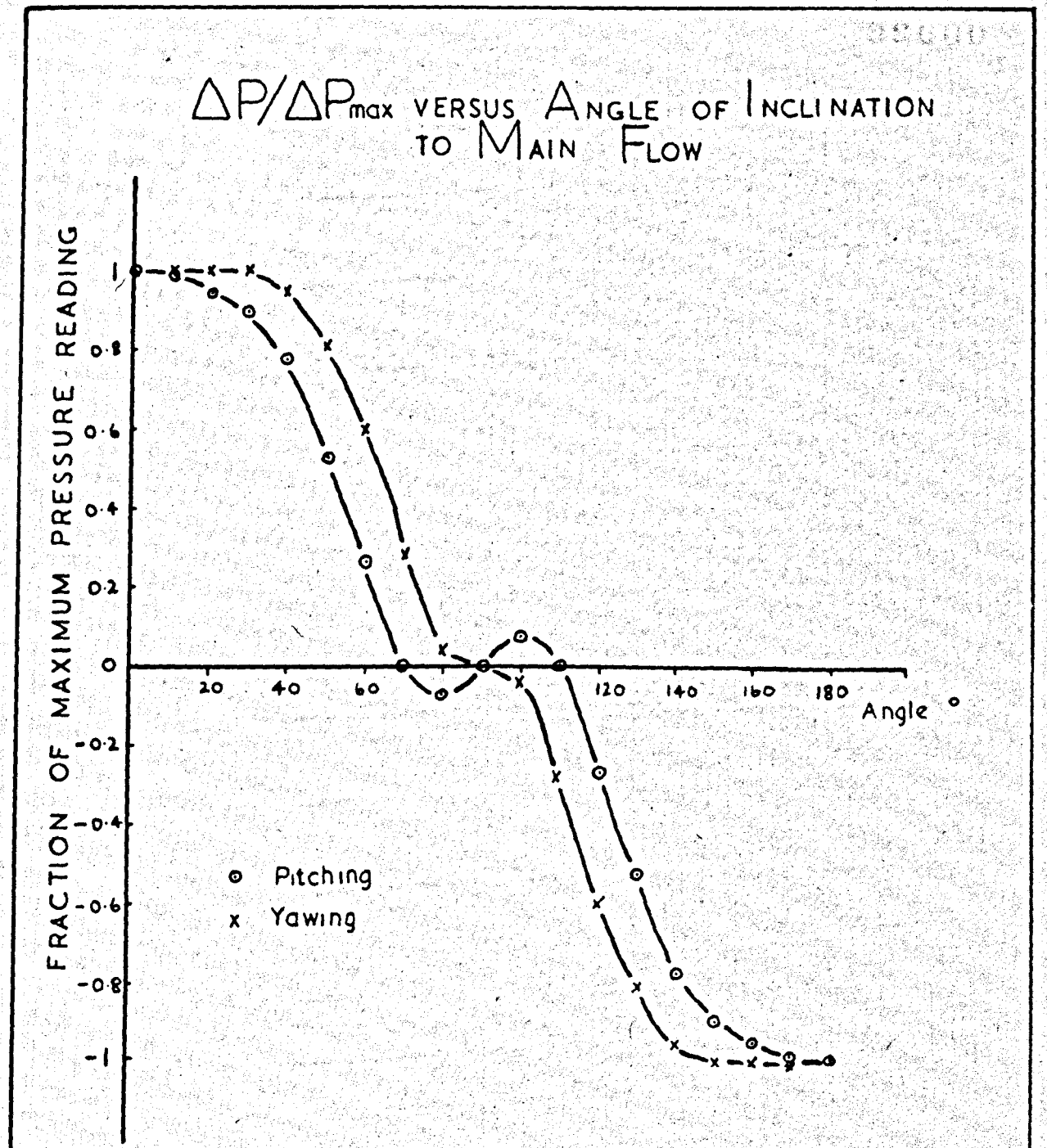


FIG.28. CALIBRATION CHARACTERISTICS OF THE "T" SHAPED PROBE

Fig. No. 29 - Calibration of Nozzles

# $\sqrt{\Delta H}$ versus Jet Flow Rate

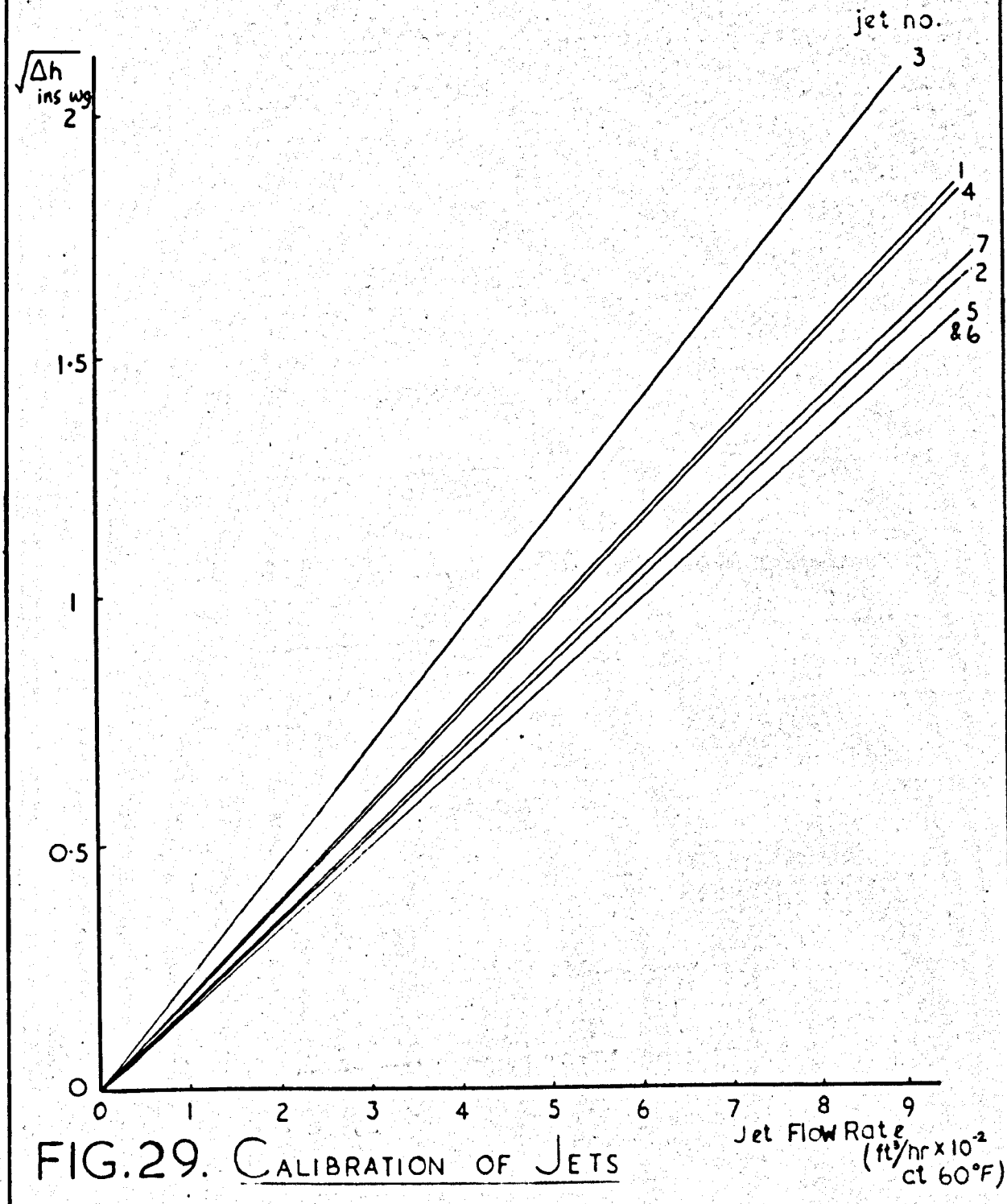


FIG.29. Calibration of Jets

Fig. No. 30 - Calibration of Pressure Transducer

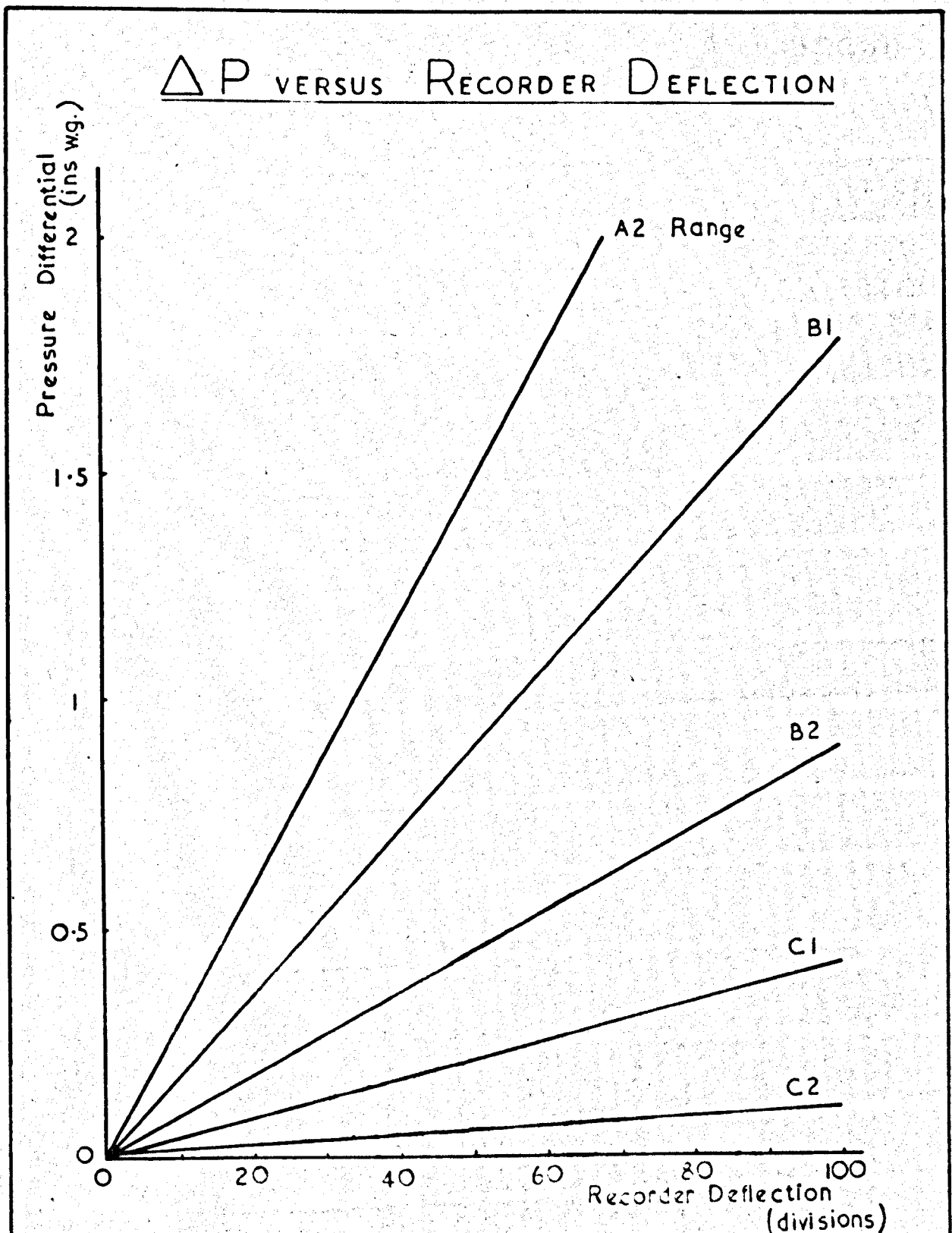


FIG.30. CALIBRATION OF PRESSURE TRANSDUCER

Fig. No. 31 - Comparison of Resistance Characteristics of the Grids with typical Marine Boiler tube banks

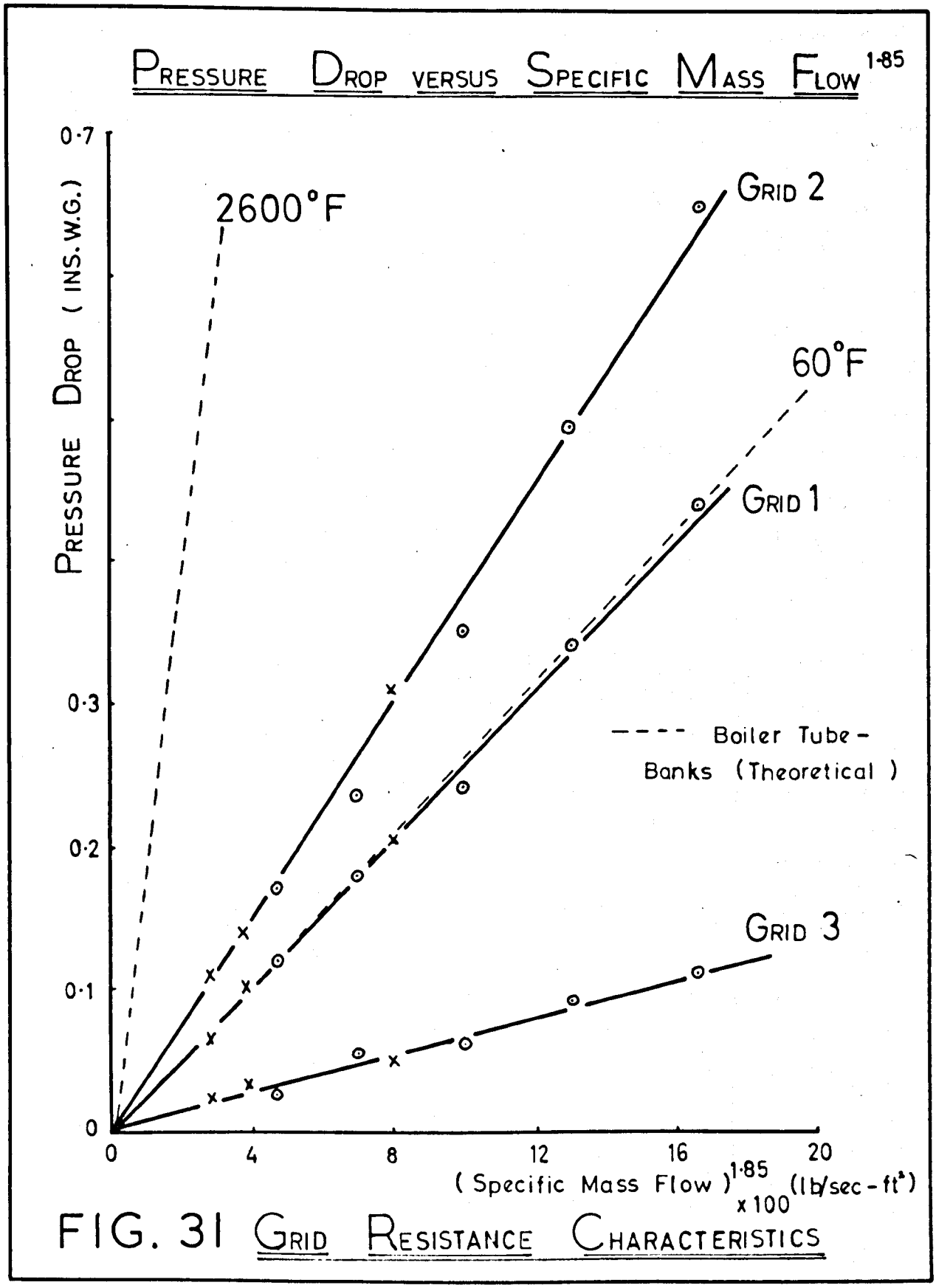


FIG. 31 GRID RESISTANCE CHARACTERISTICS

Fig. No. 32 - Simplified Diagram of Marine Boiler of the selectable Superheat type

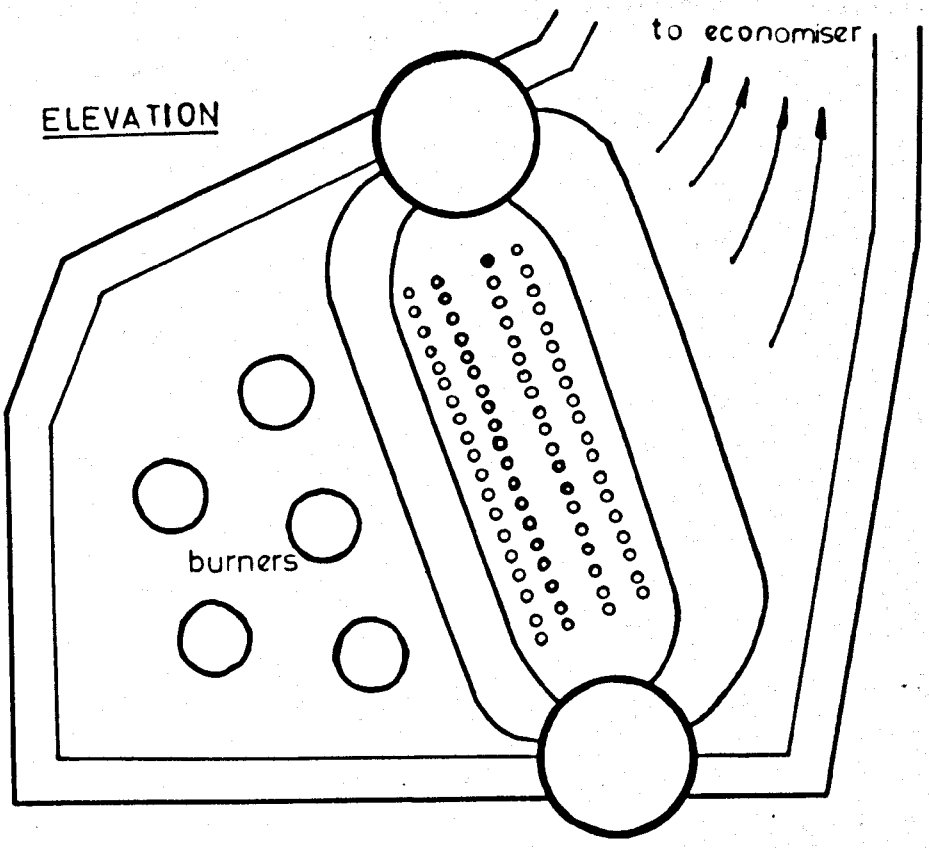


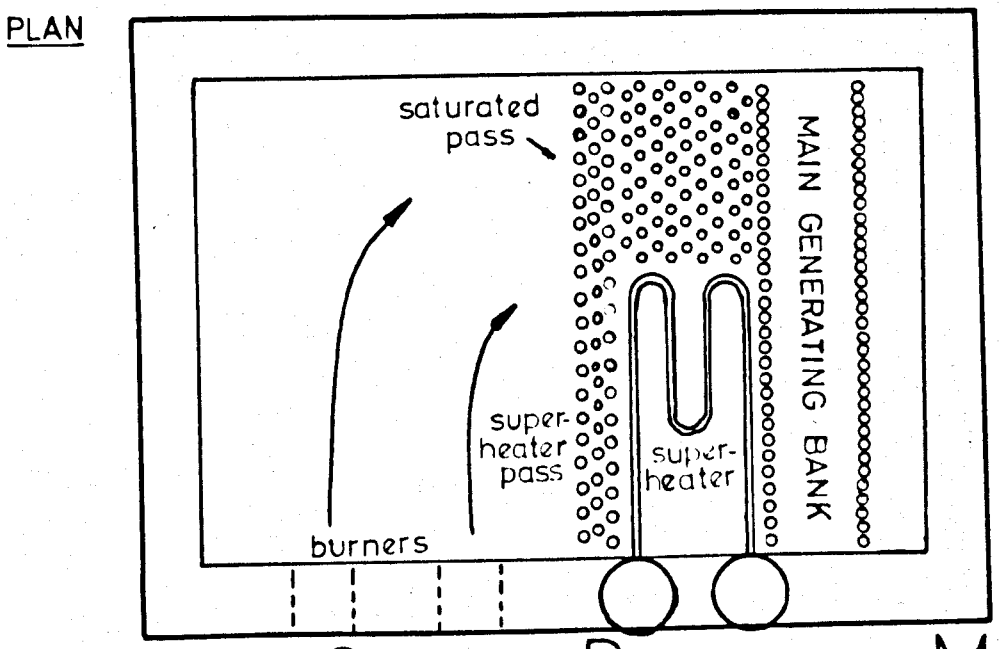


FIG. 32 SIMPLIFIED DIAGRAM OF A MARINE BOILER WITH SELECTABLE SUPERHEAT

Plate No. 1 - End View of Small Model assembled for calibration of probe

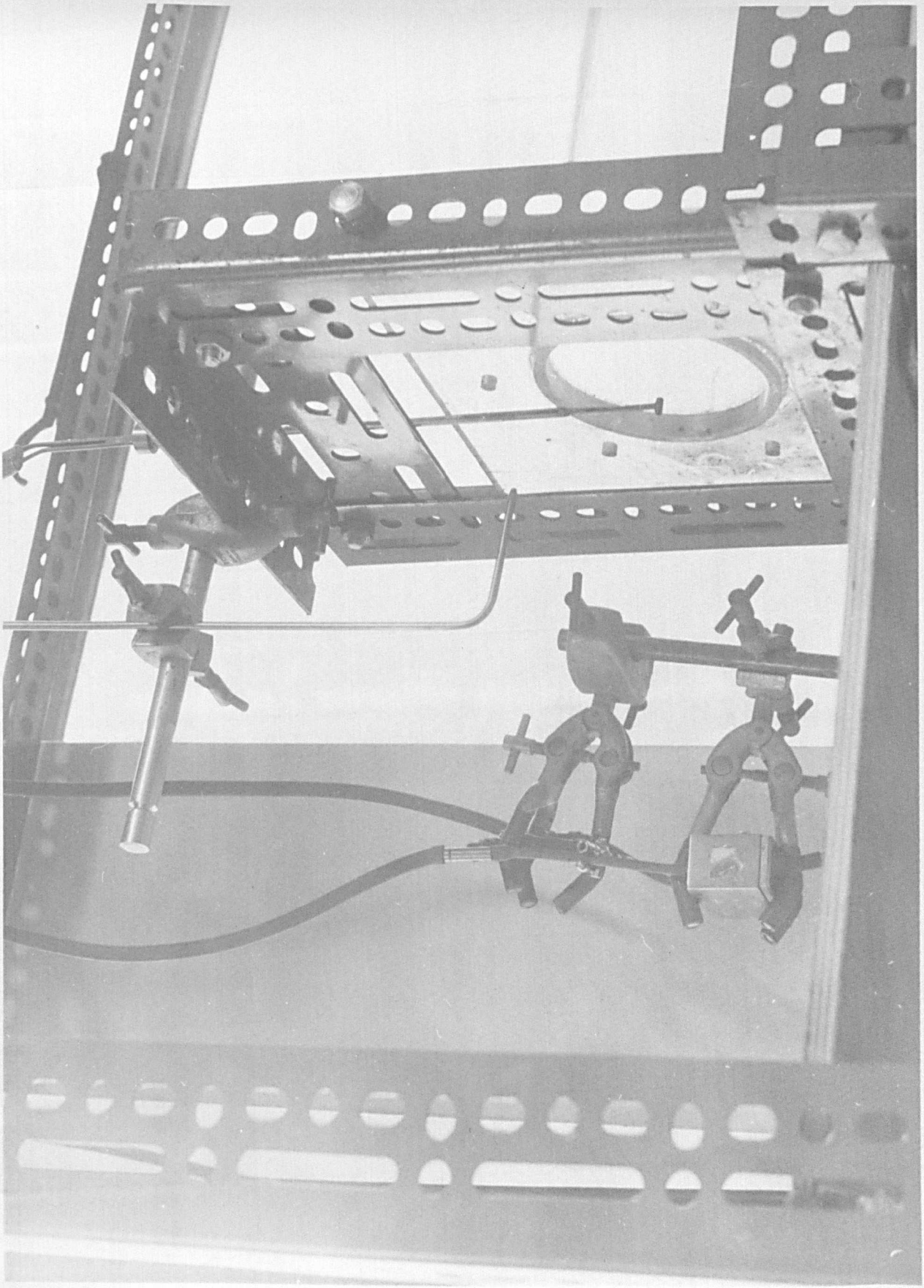

Plate No. 2a - General View of Large Perspex Model

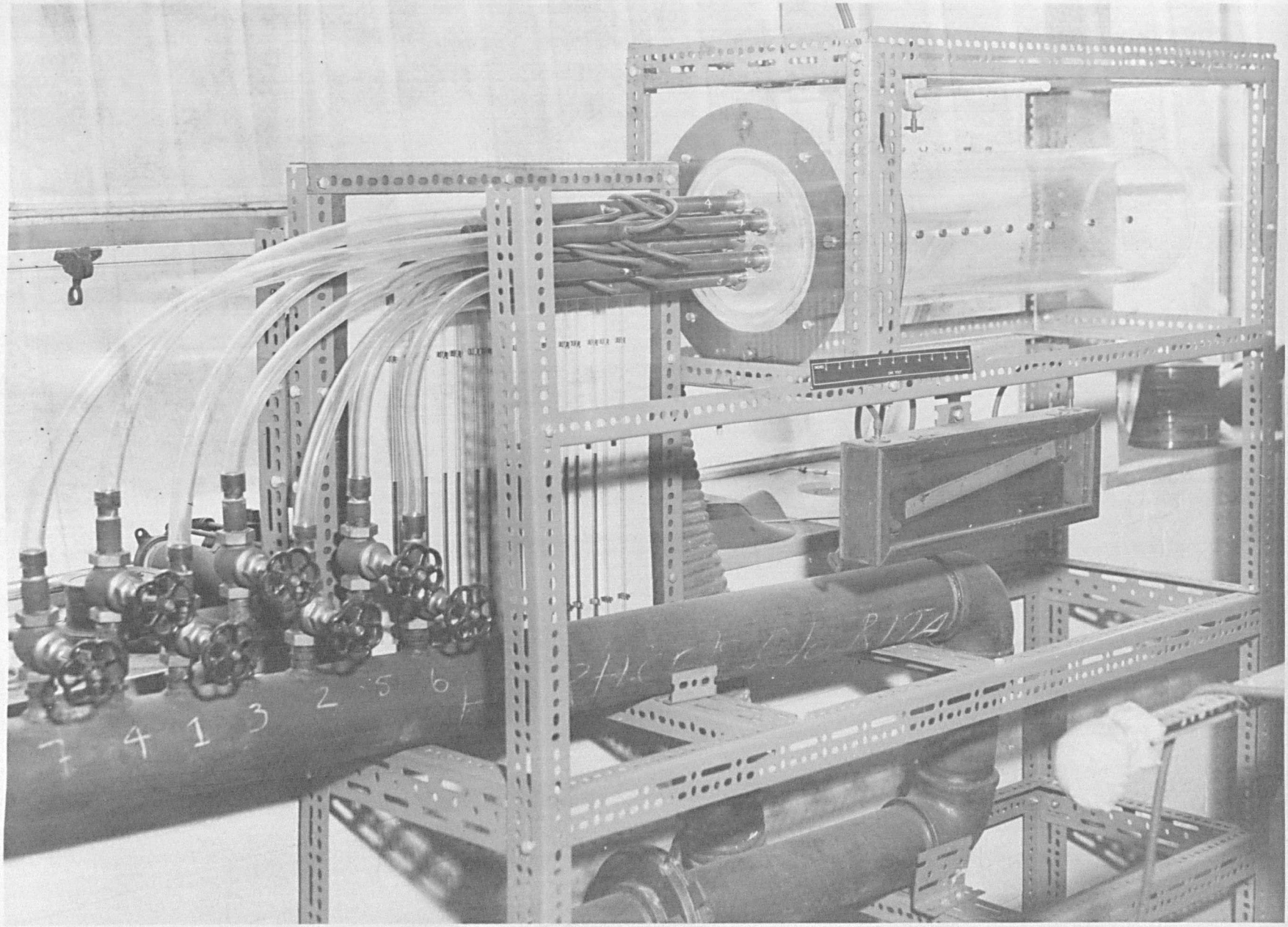
7 4 1 3 2 5 6

Plate No. 2b - View along axis of model

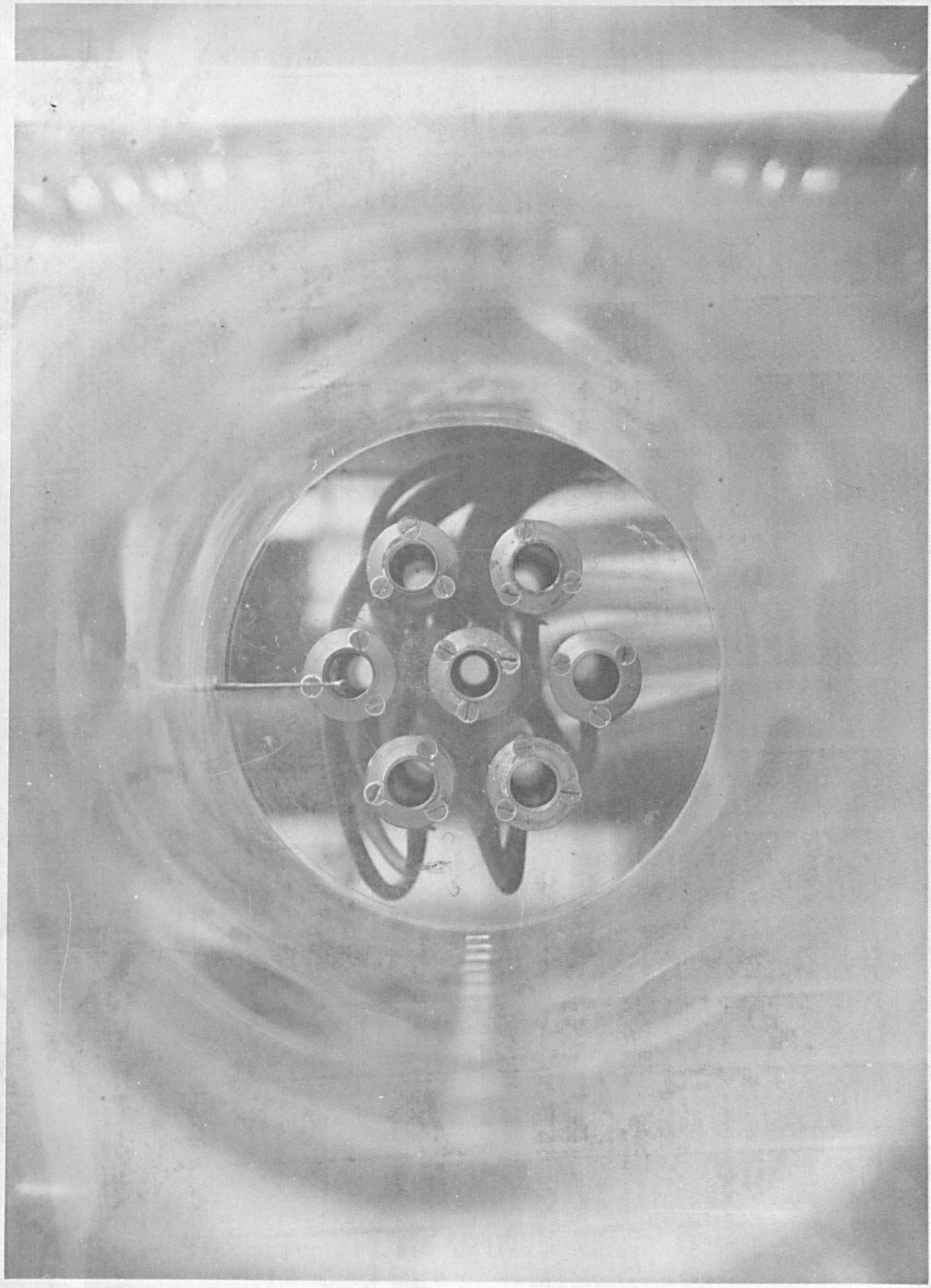

Plate No. 3a - Sleeves used for nozzle radius variation

Plate No. 3b - Modified central nozzle used for swirl studies showing tangential injection ports

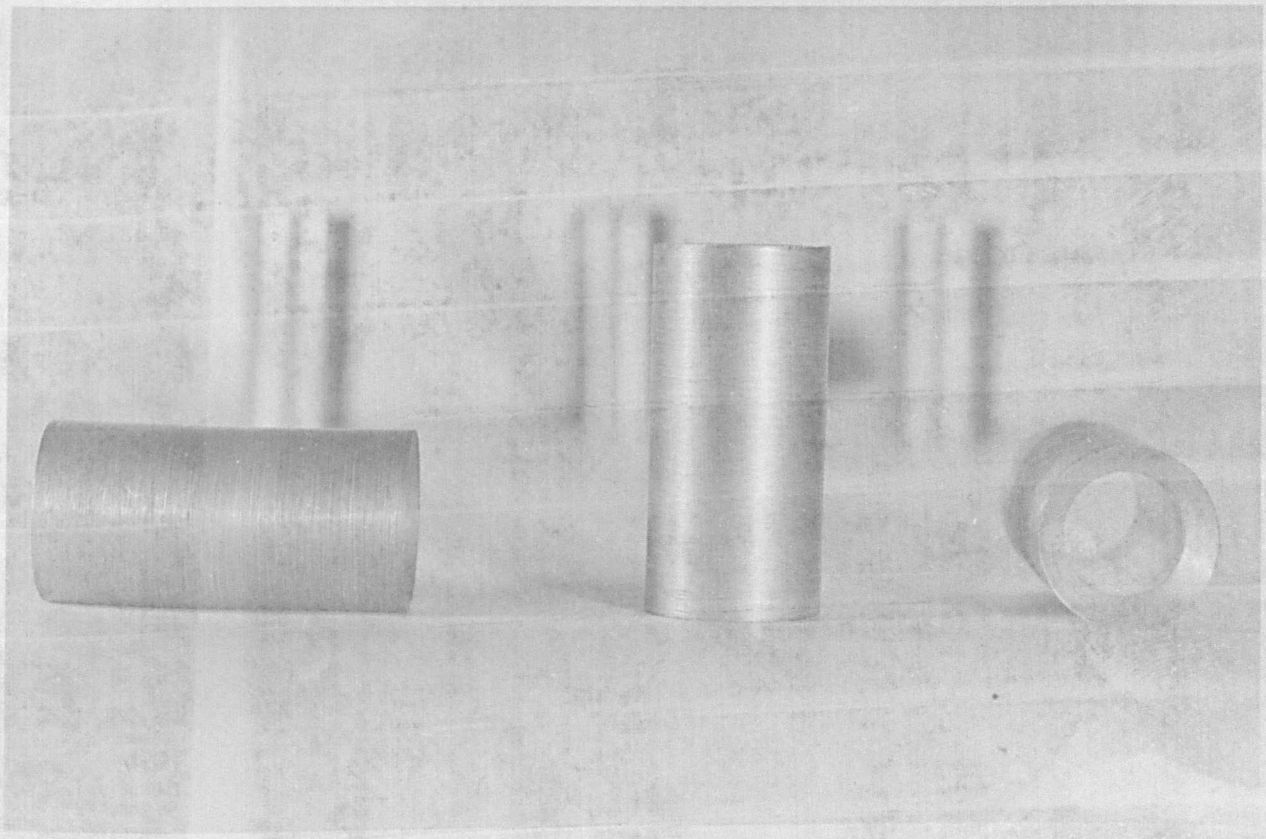

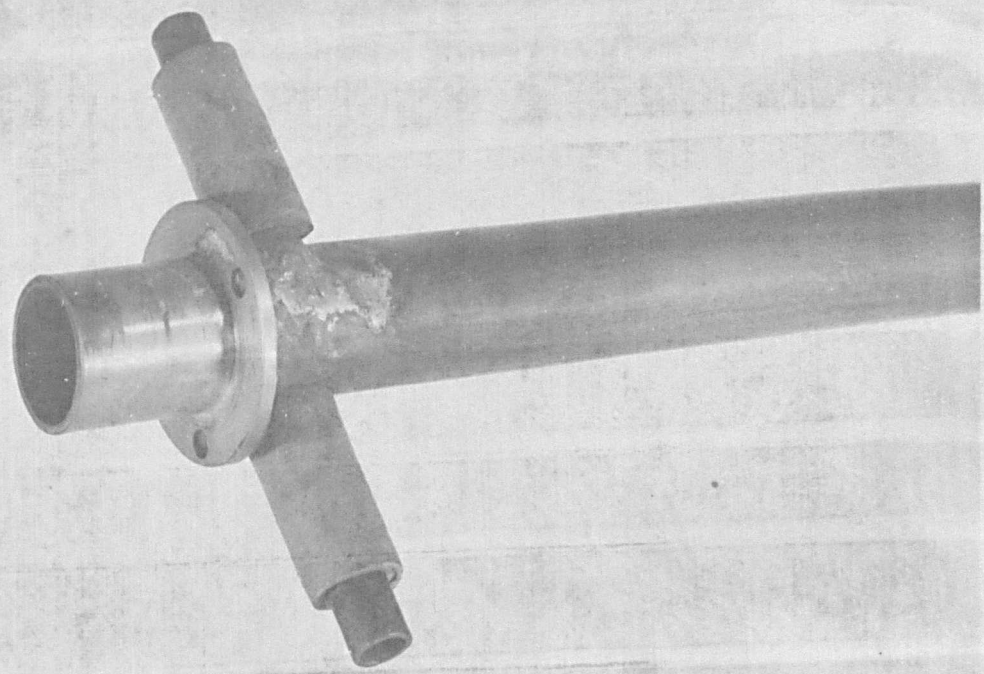

Plate No. 4 - Low Resistance Grid (Grid 3)

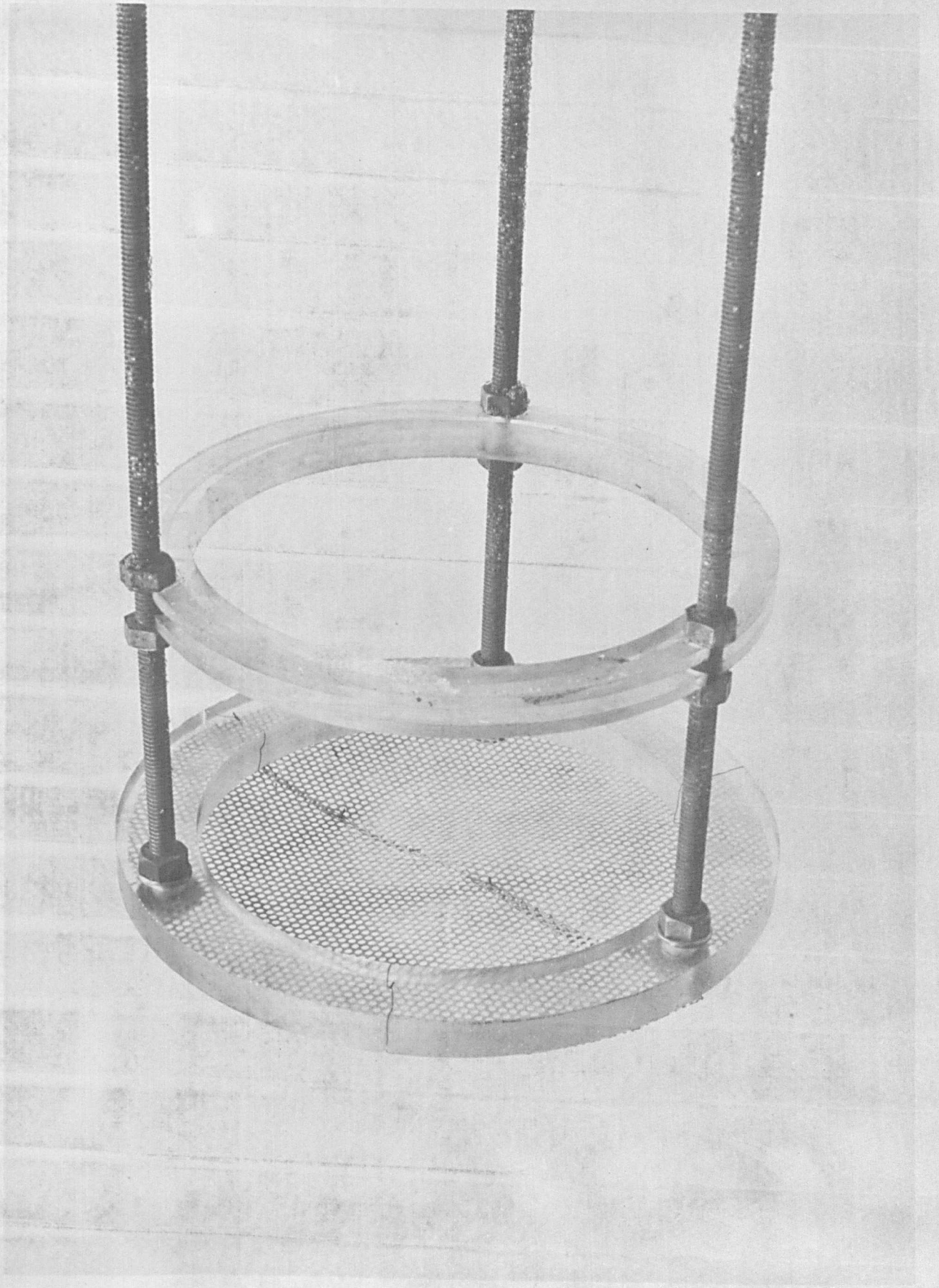

Plate No. 5 - Medium and High Resistance Grids
(Grids 1 and 2)

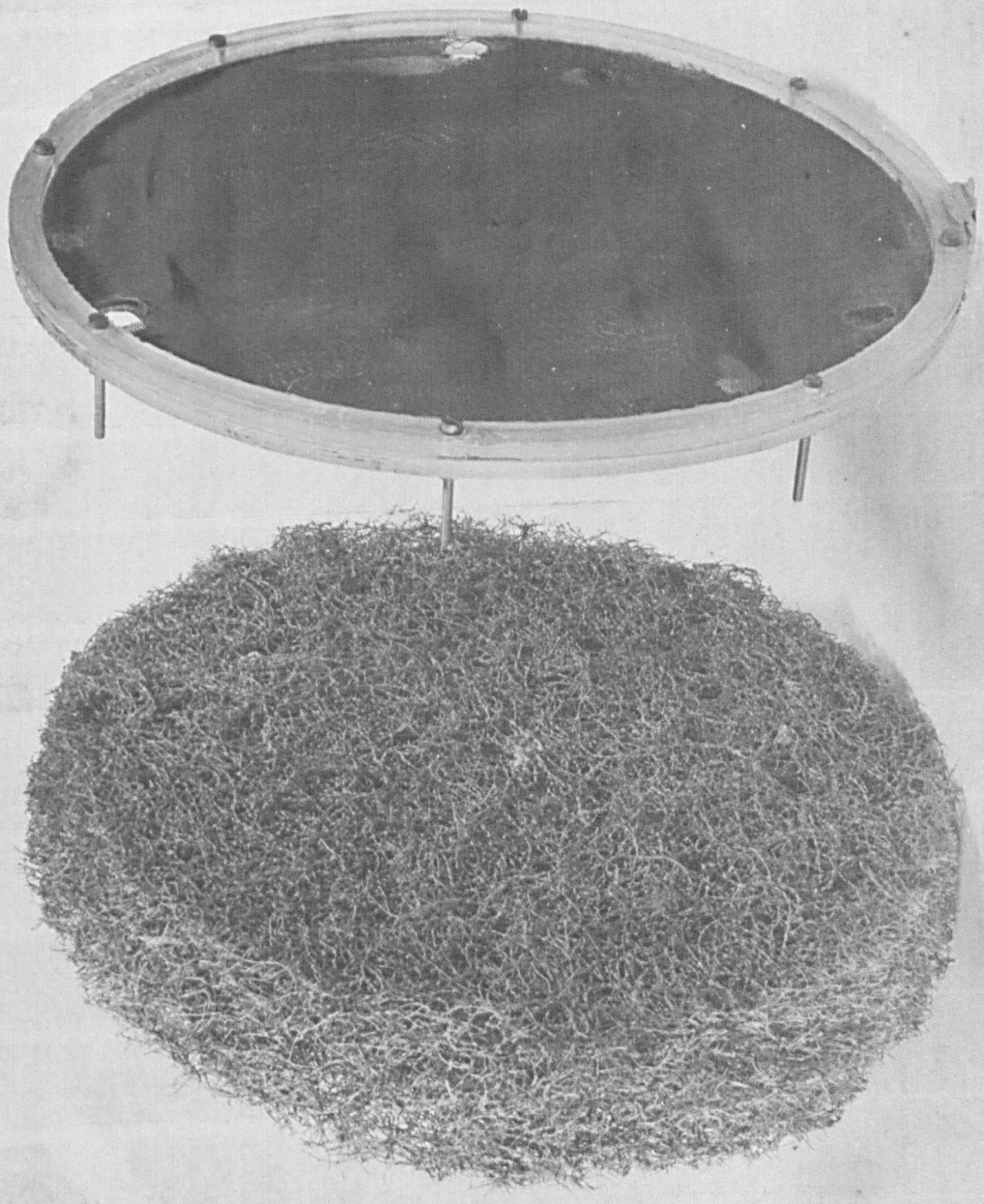

Plate No. 6 - Traversing Rig and Probe Assembly

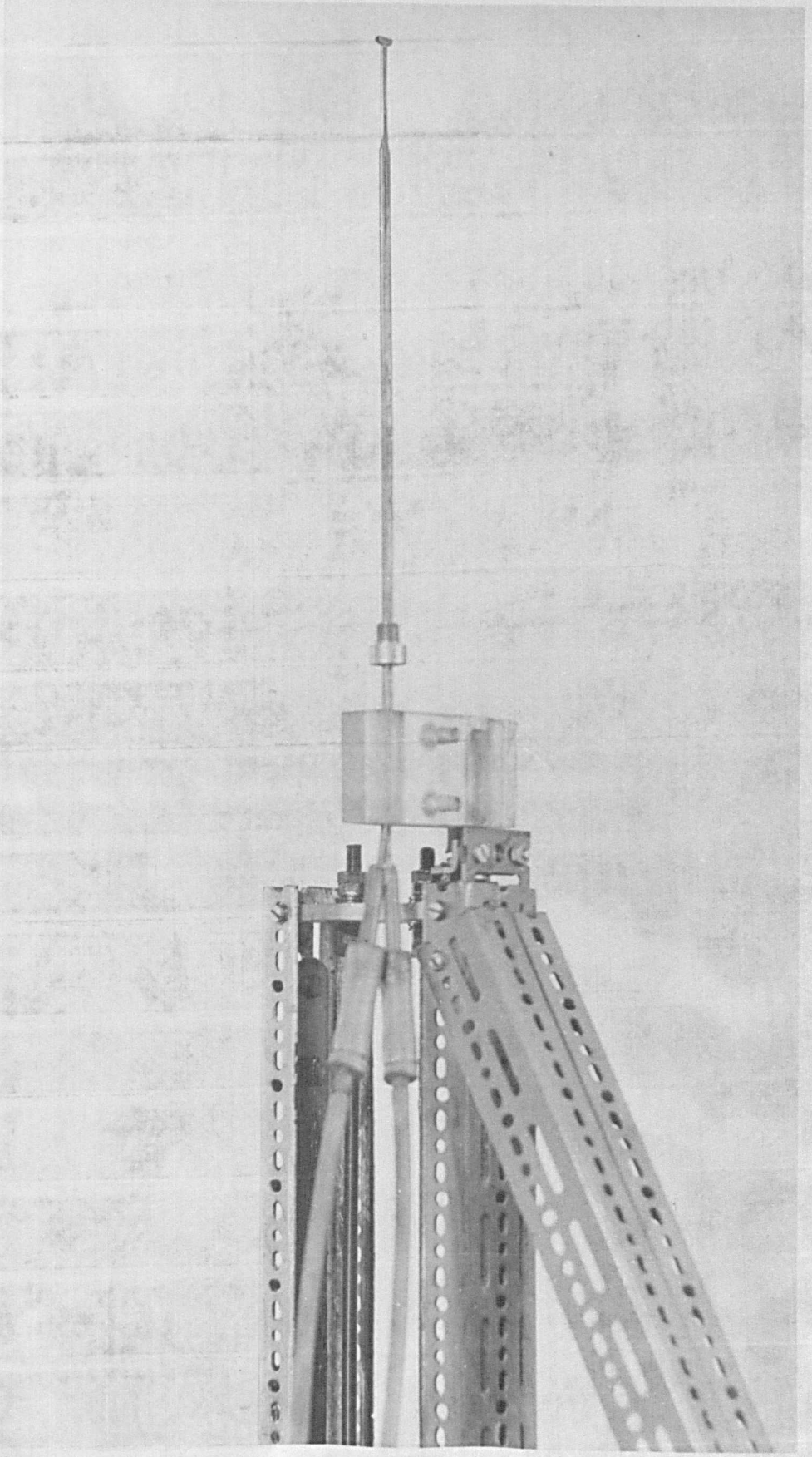

Plate No. 7,- Water Model Photograph illustrating flow patterns when
Re = 14700, R = 2", $r_o$ = 0.375", n = 6

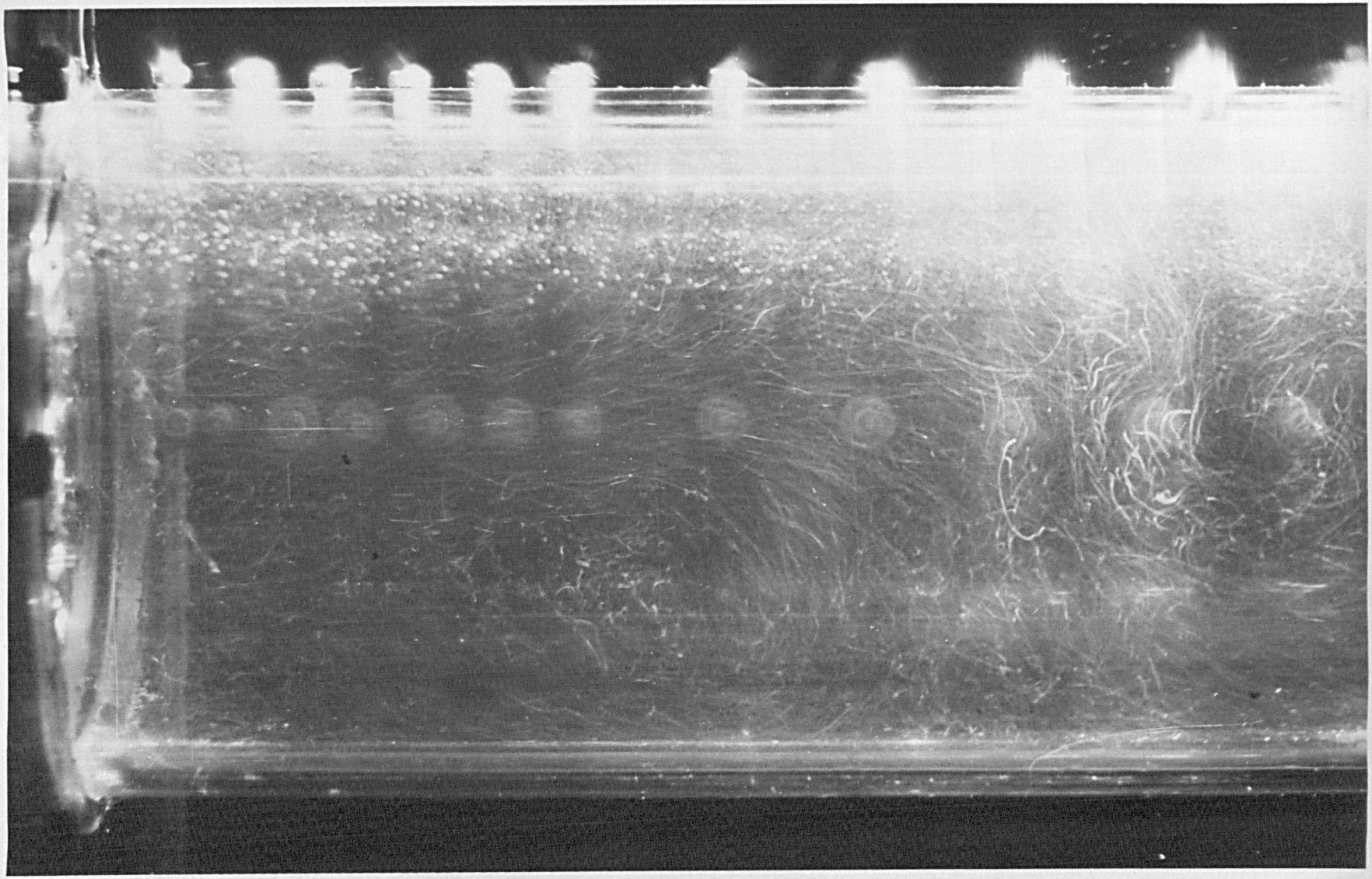

Plate No. 8 - Water Model Photograph illustrating flow patterns when $x/L = 1.5$, Re = 14700, R = 2", $r_o = 0.375"$, n = 6

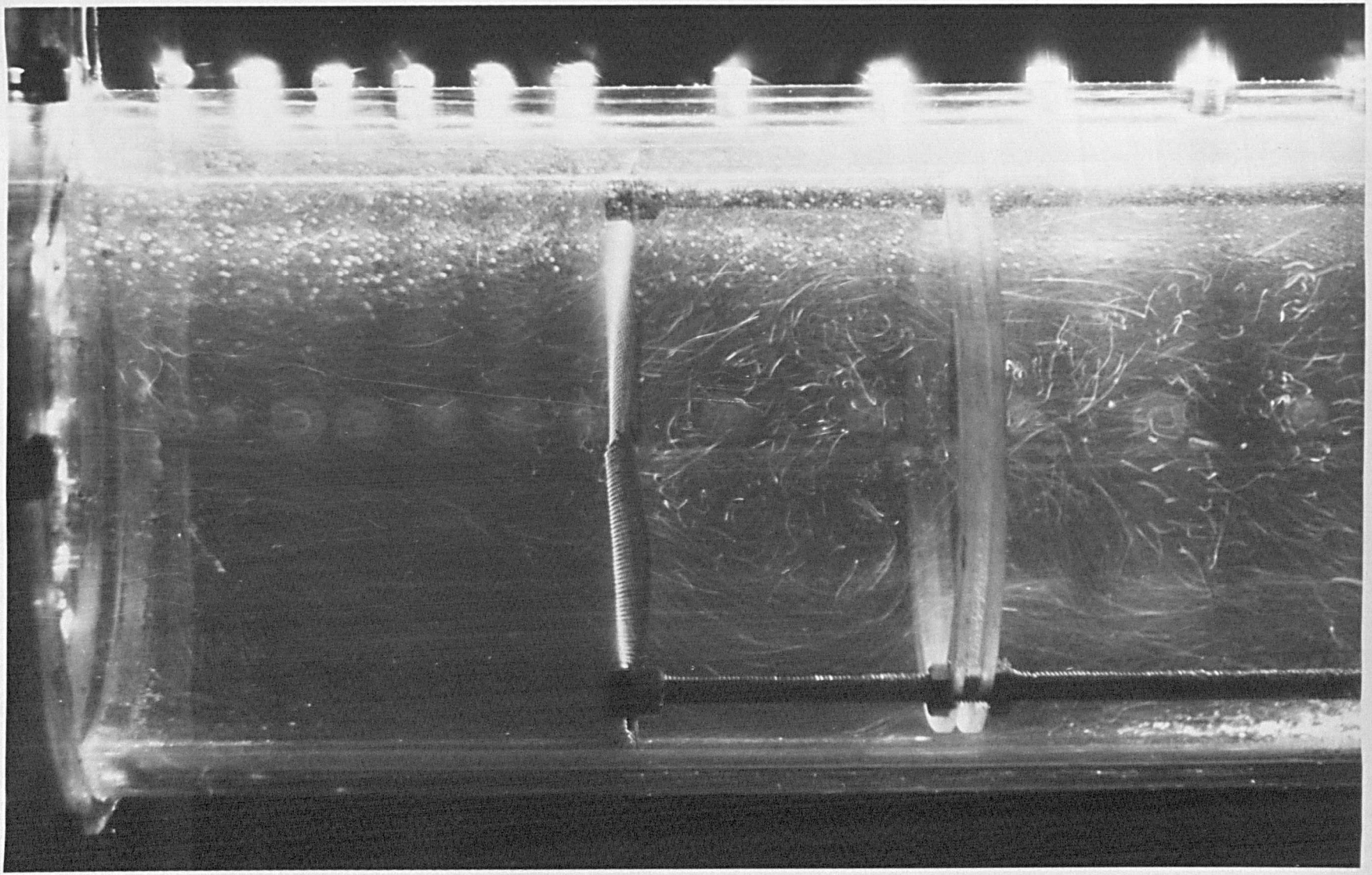

Plate No. 9 - Water Model Photograph illustrating flow patterns when
$x/L = 1.0$, Re = 14700, R = 2", $r_o = 0.375"$
n = 6

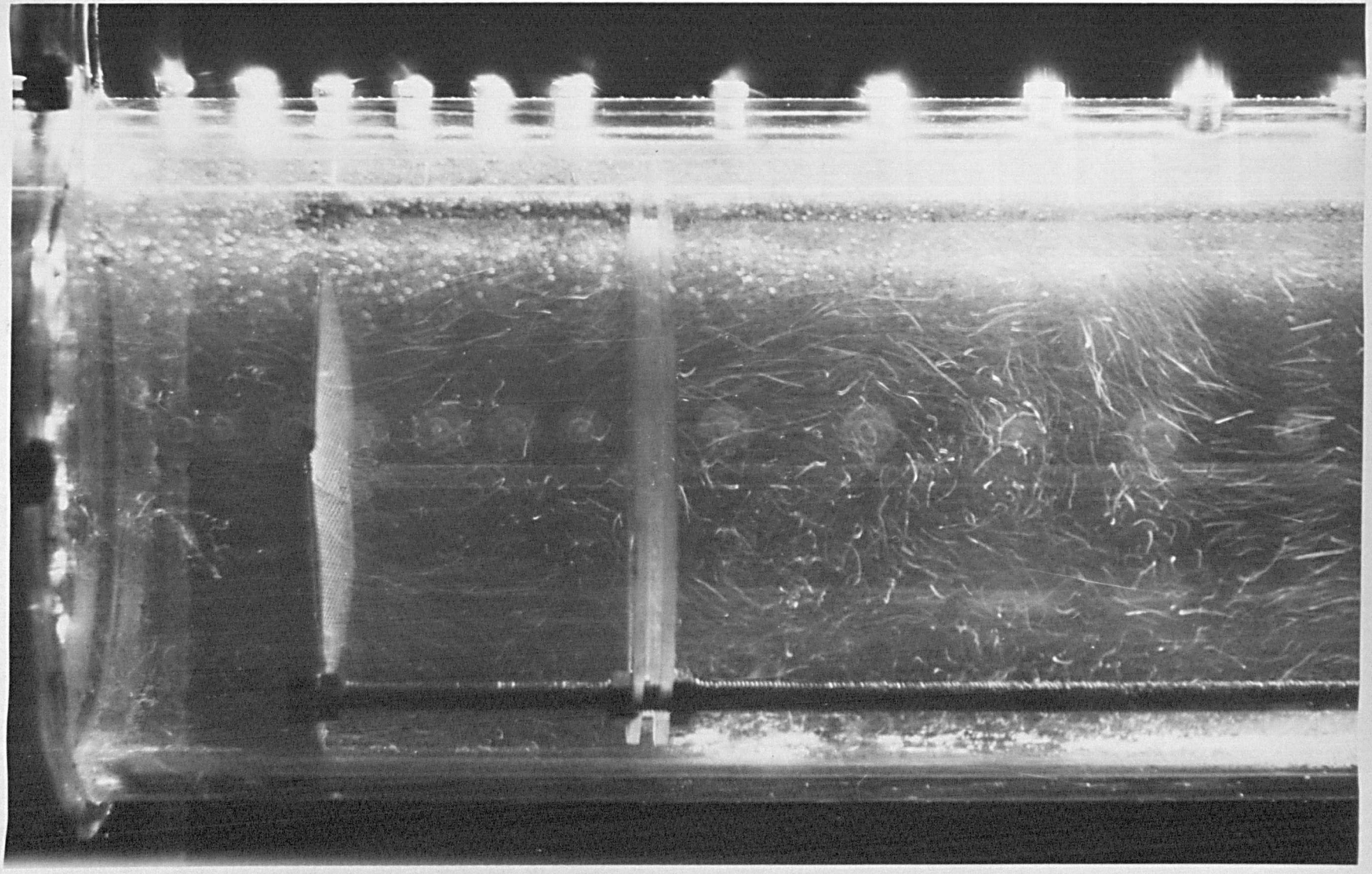

Plate No. 10 - Selectable Superheat type Marine Boiler

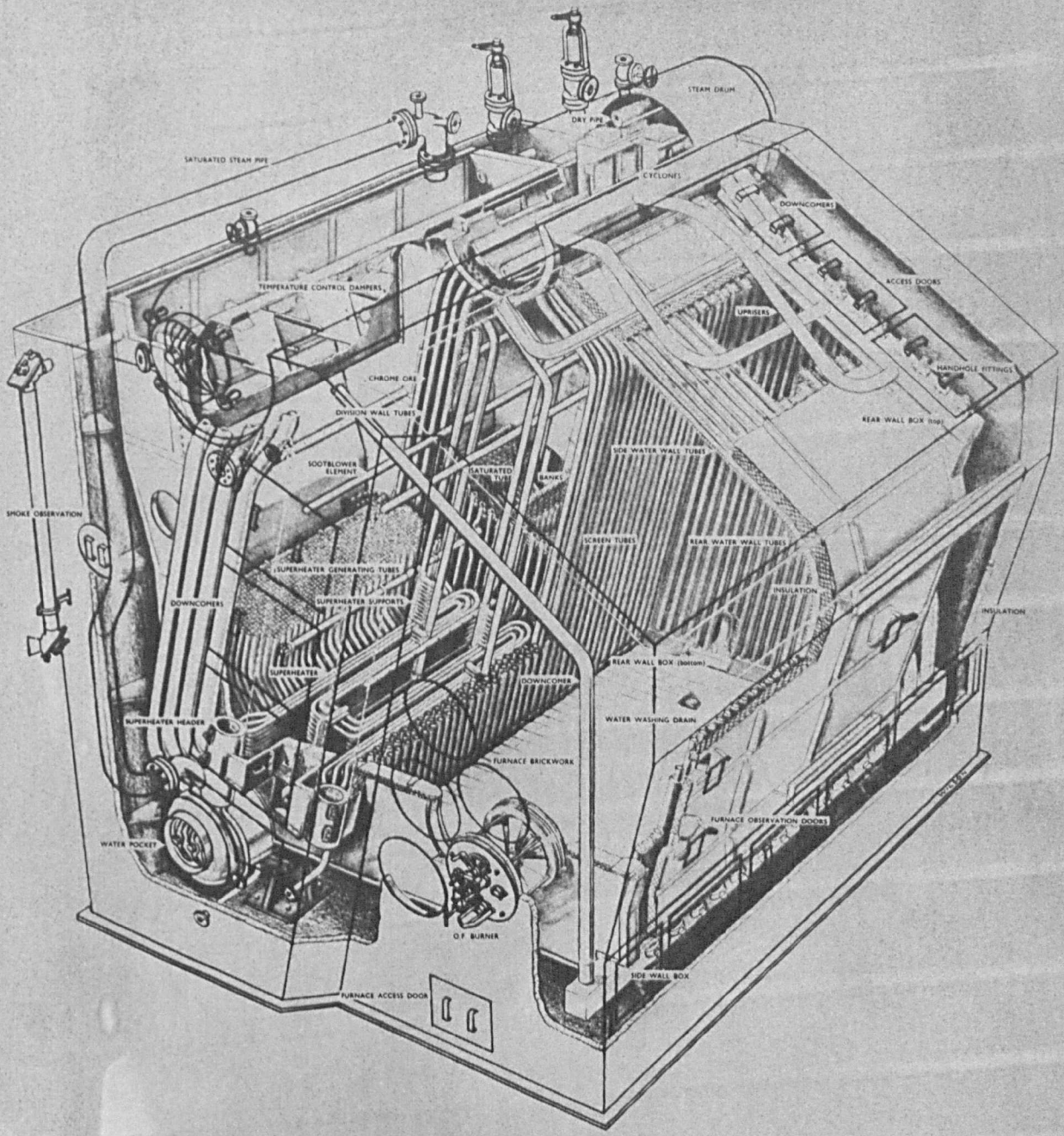


BABCOCK & WILCOX LIMITED TYPICAL MARINE SELECTABLE SUPERHEAT BOILER